A biodegradable and biobased intumescent flame-retardant for polylactic acid textiles and composites

A BIODEGRADABLE AND BIOBASED INTUMESCENT FLAME-RETARDANT FOR POLYLACTIC ACID TEXTILES AND COMPOSITES

MUHAMMAD MAQSOOD

A BIODEGRADABLE AND BIOBASED INTUMESCENT FLAME-RETARDANT FOR POLYLACTIC ACID TEXTILES AND COMPOSITES

by

Muhammad Maqsood

Printing: ProefschriftMaken || www.proefschriftmaken.nl

ISBN 978 94 6380 805 7

A BIODEGRADABLE AND BIOBASED INTUMESCENT FLAME-RETARDANT FOR POLYLACTIC ACID TEXTILES AND COMPOSITES

DISSERTATION

to obtain the degree of Doctor at the Maastricht University, on the authority of the Rector Magnificus, Prof.dr. Rianne M. Letschert in accordance with the decision of the Board of Deans, to be defended in public on Wednesday 10th of June 2020, at 14:00 hours

by

Muhammad Maqsood

Promotor:

Prof. Dr.-Ing. habil. Dipl.-Wirt. Ing. G.H. (Gunnar) Seide

Assessment committee:

Prof. Dr. Pamela Habibovic (Chair)

Dr. Jules Harings

Prof. Dr. Christian Hopmann, RWTH Aachen University, Germany

Prof. Dr. Robert Groten, University of Applied Sciences Niederrhein, Germany

The research for this work has received funding from project “BioTex Fieldlab” funded by Operational Programme South Netherlands (OP Zuid).

Glossary

AATCC	American association of textile chemists and colorists
APP	Ammonium polyphosphate
ASTM	American standards for testing and materials
ATH	Aluminum tri-hydroxide
$cN.tex^{-1}$	Centi-Newton per tex
CO_2	Carbon dioxide
DSC	Differential scanning calorimetry
dtex	Yarn linear density
DTY	Drawn textured yarn
EDS	Energy dispersive X-ray spectrometry
E&E	Electrical and electronic
EG	Expandable graphite
EHC	Effective heat of combustion
EXP	Halogen free flame-retardant
FDY	Fully drawn yarn
FR	Flame retardant
FTT	Fire testing technology
HCFR	Halogen containing flame-retardants
HFFR	Halogen free flame-retardants
HRR	Heat release rate
IDY	Industrially drawn yarn
IFR	Intumescent flame-retardant
ISO	International organization for standardization
KL	Kraft lignin
kWm^{-2}	Kilowatt per square meter
LDPE	Low density polyethylene
LOI	Limiting oxygen index
MC	Melamine cyanurate
MCC	Microscale combustion calorimeter

MDR	Melt draw ratio
MEL	Melamine
MFI	Melt flow index
$Mg(OH)_2$	Magnesium di-hydroxide
MJ	Mega-Joule
$MJ.m^{-2}$	Mega-Joule per square meter
m^2K/W	Square meter Kelvin per Watt
$mm.min^{-1}$	Millimeter per minute
MPa	Mega-Pascal
MWNT	Multi-walled nanotubes
OS	Oxidized starch
PA	Polyamide
PC	Polycarbonate
PCPP	Poly (1,2-propanediol 2-carboxyethyl phenyl-phosphinate)
PER	Pentaerythritol
PET	Polyethylene terephthalate
PHHR	Peak heat release rate
PLA	Polylactic acid
PPLA	Pre-polylactic acid
ppm	Parts per million
PU	Polyurethane
PVC	Polyvinyl chloride
PVDF	Poly(vinylidene fluoride)
RPM	Revolutions per minute
SEM	Scanning electron microscope
SPB	Sodium per borate
SSDR	Solid-state draw ratio
ST	Starch
Tcc	Cold crystallization temperature
TEM	Transmission electron microscope
Tg	Glass transition temperature
TGA	Thermogravimetric analysis

THR	Total heat release
Tm	Melting temperature
TSP	Total smoke production
TTI	Time to ignition
UL-94	Standard method released by underwriter's laboratories of United States
WAXD	Wide angle X-ray diffraction
W/mK	Watt per meter Kelvin
Xc	Crystallinity of fibers
Zn-Al-LDH	Zinc aluminum layered double hydroxide

Table of contents

Glossary **5**

Summary **15**

CHAPTER 1 General introduction, scope and objectives **21**

1.1. Introduction **23**

1.2. Polylactic acid (PLA) **25**

1.3. Flame retardants **27**

1.4. Action mechanism of flame retardants **31**

1.4.1. Dilution of volatile products **31**

1.4.2. Inhibition of vapor phase combustion **32**

1.4.3. Removing heat of combustion **32**

1.4.4. Smoke suppressants **33**

1.4.5. Char formation **33**

1.5. Intumescent flame retardants **34**

1.6. Testing methods **35**

1.7. Potential biobased and biodegradable carbonization agents **38**

1.7.1. Cellulose **38**

1.7.2. Starch **39**

1.7.3. Chitosan **40**

1.7.4. Alginates **40**

1.7.5. Lignin **41**

1.8. Approaches used to make PLA flame-retardant: state of the art **42**

1.9. Scope, objectives and outline of thesis **46**

1.9.1. Scope **46**

1.9.2. Aims and objectives **47**

1.9.3. Outline of thesis **48**

1.10. References **50**

CHAPTER 2 Investigation of the flammability and thermal stability of halogen-free intumescent system in biopolymer composites containing biobased carbonization agent and mechanism of their char formation **63**

Abstract **64**

2.1. Introduction **65**

2.2. Materials and methods **66**

2.2.1. Materials **66**

2.2.2. Preparation of PLA/IFR composites **67**

2.2.3. Mechanism of char formation 68
2.2.4. Limiting oxygen index and UL-94 vertical burning test 69
2.2.5. Cone calorimetry test 69
2.2.6. Thermogravimetric analysis 69
2.2.7. Scanning electron microscopy 69
2.2.8. Mechanical testing 70
2.3. Results and discussion 70
2.3.1. Determining the burning behavior of PLA/IFR samples 70
2.3.2. Measuring the heat release rate, total heat release and residual mass% 72
2.3.3. Investigating the thermal stability of PLA/IFR samples 79
2.3.4. Dispersion of the additives in PLA matrix 81
2.3.5. Determining the tensile strength, Young's modulus and elongation at break% 82
2.4. Conclusions 84
2.5. References 84

CHAPTER 3 The efficiency of biobased carbonization agent and intumescent flame retardant on flame retardancy of biopolymer composites and investigation of their melt-spinnability 91
Abstract 92
3.1. Introduction 93
3.2. Materials and methods 94
3.2.1. Materials 94
3.2.2. Preparation of PLA/IFR composites 95
3.2.3. Thermogravimetric analysis 95
3.2.4. Scanning electron microscopy 95
3.2.5. Limiting oxygen index and UL-94 vertical burning tests 96
3.2.6. Cone calorimetry test 96
3.2.7. Mechanical testing of multifilament yarns 96
3.2.8. Melt spinning of IFR composites 96
3.3. Results 98
3.3.1. Mechanism of intumescence 98
3.3.2. Measuring the flammability and dripping behavior of composites 100
3.3.3. Time to ignition, heat release rate, total heat release and residual mass% 102
3.3.4. Energy dispersive X-ray spectrometry 109
3.3.5. Investigating the dispersion of additives in PLA matrix 109
3.3.6. Assessment of thermal stability of composites 110
3.4. Discussion 113

3.5. Conclusions **115**

3.6. References **115**

CHAPTER 4 Investigation of melt-spinnability of plasticized polylactic acid biocomposites containing intumescent flame retardant **121**

Abstract **122**

4.1. Introduction **123**

4.2. Materials and methods **124**

4.2.1. Materials **124**

4.2.2. Preparation of composites **124**

4.2.3. Yarn manufacturing **125**

4.2.4. Fabric manufacturing **128**

4.2.5. Thermogravimetric analysis **128**

4.2.6. Scanning electron microscopy **128**

4.2.7. Mechanical testing **128**

4.2.8. Limiting oxygen index and UL-94 vertical burning test **129**

4.2.9. Cone calorimetry **129**

4.3. Results and discussion **130**

4.3.1. Mechanism of intumescence **130**

4.3.2. Dispersion of additives in composites and multifilament yarns **131**

4.3.3. Measuring the fire retardancy and dripping behavior of composites **133**

4.3.4. Thermal stability measurement by thermogravimetric analysis **135**

4.3.5. Measuring the tensile strength, elongation at break and Young's modulus **138**

4.3.6. Mechanical properties of multifilament yarns **139**

4.3.7. Heat release rate, total heat release, time to ignition and residual mass% **140**

4.4. Conclusions **145**

4.5. References **146**

CHAPTER 5 Novel bicomponent functional fibers with sheath/core configuration containing intumescent flame-retardants for textile applications **153**

Abstract **154**

5.1. Introduction **155**

5.2. Materials and methods **157**

5.2.1. Materials **157**

5.2.2. Preparation of IFR composites **158**

5.2.3. Bicomponent spinning **158**

5.2.4. Mechanical testing **161**

5.2.5.Thermogravimetric analysis **161**

5.2.6. Scanning electron microscopy 162
5.2.7. Differential scanning calorimetry 162
5.2.8. Thermally bonded nonwoven as carpet backing 162
5.2.9. Fire testing 163
5.3. Results and discussion 164
5.3.1. Melt spinning and mechanical properties of bicomponent fibers 164
5.3.2. Thermal stability of bicomponent fibers 167
5.3.3. Surface morphology and cross sectional images of bicomponent fibers 169
5.3.4. Differential scanning calorimetry 171
5.3.5. Cone calorimetry measurements and ignitability by single flame source test ... 174
5.4. Conclusions 178
5.5. References 179

CHAPTER 6 Improved thermal processing of polylactic acid/oxidized starch composites and flame-retardant behavior of intumescent nonwovens 185
Abstract 186
6.1. Introduction 187
6.2. Materials and methods 189
6.2.1. Materials 189
6.2.2. Preparation of composites 189
6.2.3. Melt spinning of composites 190
6.2.4. Scanning electron microscopy 191
6.2.5. Apparent viscosity measurement 191
6.2.6. Mechanical testing 192
6.2.7. Thermogravimetric analysis 192
6.2.8. Differential scanning calorimetry 192
6.2.9. Needlepunched nonwovens 193
6.2.10. Fire testing 193
6.3. Results and discussion 194
6.3.1. Measuring the apparent viscosity of composites as a function of shear rate 194
6.3.2. Multifilament fibers and their mechanical properties 195
6.3.3. Thermal stability of multifilament fibers 197
6.3.4. Thermal properties and crystallinity of multifilament fibers 199
6.3.5. Surface morphology and diameter of multifilament fibers 200
6.3.6. Burning behavior of nonwovens by cone calorimetry 202
6.4. Conclusions 208
6.5. References 208

CHAPTER 7 Development of biobased socks from sustainable polymer and statistical modeling of their thermo-physiological properties 215

Abstract 216

7.1. Introduction 217

7.2. Materials and methods 218

7.3. Cost analysis 223

7.4. Methodology 224

7.5. Results and discussion 226

7.5.1. Thermal conductivity 227

7.5.2. Thermal resistance 229

7.5.3. Relative water vapour permeability 230

7.5.4. Air permeability 232

7.5.5. Vertical wicking 233

7.6. Conclusion 234

7.7. References 235

CHAPTER 8 General discussion and opportunities for industrial scale up 239

8.1. Prospects of biobased flame-retardants for the industrial scale-up 241

8.1.1. Health and environmental impact 242

8.1.2. Fire performance 242

8.1.3. Economic efficiency 242

8.2. Future work and opportunities for industrial scale up 243

8.3. References 244

CHAPTER 9 Valorization addendum 247

Acknowledgements 253

Biography 257

List of publications 261

Summary

Polymeric materials play an important role in our daily life due to their vast application range and several other benefits such as, ease of processing, thermal stability, low cost and adaptable mechanical properties. However, to improve the sustainability of polymers and to reduce carbon footprint, polymers from renewable resources are given much attention due to the developing concern over environmental protection. These renewable materials are progressively used nowadays in many technical applications instead of short-term use products. However, among other applications, flame retardancy of such polymers needs to be improved for technical applications due to potential fire risk they possess and their involvement in our daily life. To overcome this potential risk, various flame-retardant compounds based on conventional and non-conventional approaches such as inorganic FR's, nitrogen-based FR's, halogenated FR's and nanofillers were synthesized. However, most of the conventional FR's are non-biodegradable and if disposed in the landfill, microorganisms in the soil or water cannot degrade them. Hence, they remain in the environment for long time and may find their way not only in the food chain but can also easily attach to any airborne particle and can travel distances and may end-up in freshwater, food products, ecosystems or even can be inhaled by breathing if they are present in the air. Therefore, the goal of this research work is to promote the use of biodegradable and biobased compounds for flame-retardants used in polymeric materials. The most effective method to enhance the flame-retardant behavior of polymers is to build a char layer at the surface of burning material because it reduces the polymer's pyrolysis rate by condensed phase mechanism and bring it below to a level where self-sustained combustion is not possible. It reduces the free escape of volatile compounds that are formed after combustion by locking them in the charred structure and restricts the dripping of molten polymeric materials, which sometimes is a major reason of flame propagation. The system in which this phenomenon is obtained is known as intumescent flame-retardant (IFR) system. However, in conventional IFR systems, the components used are mainly non-biodegradable and obtained from non-biobased resources such as pentaerythritol (PER). PER is a polyol obtained from petrochemicals and has higher water solubility, which makes it not feasible for polymer thermal processing, melt spinning to produce fibers for textile applications and several other engineering applications. Furthermore, it is not a good choice to use non-biodegradable PER in biodegradable materials such as Polylactic acid (PLA). Thus, it is necessary

to test biodegradable and biobased flame-retardants to substitute PER in intumescent formulations for biodegradable polymer PLA. In this way, the whole IFR system can be made biodegradable if all of its components are biodegradable. Hence, it is necessary to propose more environmental friendly approach in IFR system. We therefore, in this dissertation, have developed a biobased and biodegradable intumescent flame-retardant for PLA based textiles and composites. The goal of this dissertation is not only to use biodegradable and biobased flame-retardants in polymeric materials but also to measure the effectiveness and efficiency of the developed products by comparing the FR properties with the standard benchmark properties, defined for the targeted products. Therefore, flame-retardancy of PLA composites and PLA textile products developed in this dissertation is tested with ISO standard testing methods. To achieve these goals, additives composition, temperature profiles and processing conditions of PLA/IFR compounds are optimized to obtain the desired functional and mechanical properties. The melt-spinnability of the developed PLA/IFR formulation is up-scaled from lab to pilot-scale by optimizing the spinning process parameters. IFR multifilaments, based on mono-component and bi-component fibers are developed to produce nonwoven FR carpet backing by thermal bonding and needle-punching techniques. A remarkable increase in flame-retardancy (higher limiting oxygen index values and V-0 ratings in UL-94 vertical burning tests) and a significant decrease in heat release rate, total smoke production and effective heat of combustion were observed. The ignitability test showed none of the fabric sample produced from IFR fibers was ignited after 15 (s) of flame exposure and therefore, achieved E and Efl classification, as per EN ISO 11925-2 standard testing method, which certifies that this product can be used commercially for FR floor coverings. Hence, the results in this dissertation confirmed that biodegradable and biobased additives can be used in IFR's to produce PLA based textiles and composites with comparable FR properties to conventional FR's.

CHAPTER 1

General introduction, scope and objectives

1.1. Introduction

The fire hazard has become quite severe due to the invasion of polymers in our daily life [1]. Undeniably, majority of the frequently used polymers not only burn quite briskly and release large amounts of smoke and heat but also melts vigorously that promotes further fire propagation [2]. Numerous financial losses and personal deaths have been reported every year due to fire propagation and the smoke thus produced contains toxic substances causing severe health problems to the society [3]. According to International Association of Fire and Rescue Services (CTIF), approximately 2.0 – 2.5 million fire accidents were reported in Europe in 2018 resulting in 20,000 – 25,000 fire deaths, while 60% of the deaths were caused by smoke inhalation [4]. Therefore, in developed countries, fire regulations are becoming more stringent and generally operated by using two different approaches; firstly by implementing the safety measures such as the use of smoke detectors and fire protective equipment and secondly by using those materials, which contribute to fire as little as possible [5].

Generally, flame-retardant additives are used in polymers to improve their flame-retardancy against fire hazards [6]. The fire hazards from a particular polymer can be judged by certain predefined parameters, such as time to ignition, heat release rate, fire propagation rate, amount of smoke and CO_2 release and the toxicity of the byproducts. Flame-retardants are of different types and they are generally classified based on their mode of action, chemical nature, working and protection mechanism [7]. Halogen containing flame retardants generally operate in the gaseous phase by terminating the free radicals involved in the combustion process. They are found to be very effective at very low additive concentration in the polymer but at the same time, release toxic substances during emission hence, are abandoned in most of the developed countries. Halogen containing flame-retardants have been gradually replaced with other type of flame-retardants in the last couple of decades [8].

As a replacement of halogen containing flame-retardants, mineral hydrated fillers such as aluminum tri-hydroxide (ATH) and magnesium hydroxide ($Mg(OH)_2$) were used as halogen free

flame-retardants [9]. However, their effectiveness is mainly dependent on higher loading concentration in the polymer, as quite often the loading concentration of such additives exceeds 40-50 wt% in the polymer to achieve a certain level of flame retardancy. On the one hand, such a high loading concentration of these mineral hydrated fillers can increase the flame retardancy up to the required level, on the other hand their mechanical properties also gets affected due to which sometimes it becomes difficult to further process them [10]. Nanoparticles have been found very effective in flame retardant formulations but they are seldom used alone. They are always used in combination with other materials and act as an efficient synergist. If they are well dispersed in the matrix, even very low loading concentration (1–5 wt%) can be very effective [11]. They have been found very efficient in lowering the peak heat release rate measured by cone calorimetry. Nanoparticles are of various types but mostly carbon nanotubes and clays are the most studied ones in flame retardancy [12]. Phosphorous based flame-retardants mostly promote char formation but they are also known as flame inhibitors [13]. Charring on the polymer surface not only reduces the quantity of fuel required to sustain flame, but also acts as physical barrier, which restricts the polymer from further burning and from external heat flux. When the char layer swells, it becomes even more effective in restricting the passage of heat through the underlying material [14]. Such systems are known as intumescent and they are based on halogen free flame-retardants. The loading concentration of phosphorous based flame-retardants in intumescent system lies in the range of 15- 25 wt%, and they are not only effective but at the same time non-toxic to the environment [15].

Textile is one of the world's largest market mainly based on synthetic fibres used in consumer products [16]. Many textiles are subjected to flame-retardant requirements, which need to be taken into account during product development. For example, blankets, carpets and seat covers in airplanes need to observe specific flame-retardant regulations [17]. Textiles cause overall 50% of all accidental fires in the world, 25% of fires from textiles are fatal and the other 75% can result in severe injury [18]. That is why regulations are put in place regarding the flame-retardant properties of certain textile in specific applications. However, in textiles mostly fire retardancy is achieved by coating the surface of the fabric with FR concentrated solution by pad-dry-cure method [19]. Flame-retardant textiles developed by this approach (coating on surface) can resist fire up to a certain limit, but once ignited cannot be protected from further burning as there is no

protection mechanism, which can stop fire propagation. Thus, intumescent flame-retardant system is an approach that can protect the ignited textile from further burning as it builds a charred layer on the burning material, which cuts the fuel supply and reduces the concentration of oxygen that helps in fire extinguishing.

Most of the flame-retardants used in polymers are non-biodegradable and therefore, tend to accumulate in the environment and are persistent [20]. Due to this non-biodegradability of halogenated FRs, certain biotic or abiotic processes can occur in specific environmental conditions. Biotic processes are the processes where bioaccumulation of the toxic substances and entrance into the food chain may occur and consequently may affect the plants, humans and wildlife [21]. While abiotic is a chemical process where photo-degradation and decomposition of the material at elevated temperatures and reactions with other compounds may occur which can change the materials intrinsic properties [22]. Moreover, non-biodegradable halogenated FRs may find their way in the environment through wastewater streams of the industries that produce them or through adsorption onto the dust particles at the manufacturing facilities where they are incorporated directly to various products [23]. Once these FRs come into the environment, they can easily attach to any airborne particle and can travel distances far from emission or production sites. Hence, traces of such non-biodegradable FRs can be found in freshwater, food products, ecosystems or even can be inhaled by breathing if they are present in the air [24]. On the other hand, biodegradable FRs are the one that can be degraded by microorganisms in the soil or water and results in mineralization. Therefore, one solution of this problem is to use halogen free flame-retardants in FR applications and the other is to use those flame-retardants, which are biodegradable. This chapter covers four main aspects. The first portion of this chapter is covering conventional approaches to improve the flame retardancy of polymers. In the second portion, different types of flame-retardants and their mechanism of actions are discussed. In the third portion, potential of biobased and biodegradable additives in flame retardant applications are highlighted. Finally the scope, objectives and outline of the thesis will be discussed.

1.2. Polylactic acid (PLA)

Polylactic acid (PLA) is a biobased polymer derived from renewable resources and can be degraded in the soil by microorganisms under certain conditions of temperature and humidity [25].

The feedstock for PLA is obtained from natural and sustainable resources such as corn-starch [26]. The main producers of PLA are NatureWorks LLC (Minnetonka, United States), WeforYou GmbH (Graz, Austria), Evonik Industries AG (Essen, Germany) and Total-Corbion NV (Gorinchem, The Netherlands) and the global PLA market is expected to become more than US$ 5bn by 2020 [27]. The global production volume of bioplastics in 2019 was 2.11 million tonnes according to the latest market data collected by European Bioplastics e.V. (Berlin, Germany) and Nova Research Institute GmbH (Hurth, Germany), out of which biodegradable plastics such as PLA and starch blends accounts for over 1 million tonnes [28]. PLA is recognized to be the first melt process-able synthetic fiber that has been derived from 100% natural resources, hence can be degraded under suitable conditions [29]. In addition to eco-friendly benefits, PLA also offers decent performance in technical application owing to its comparable mechanical properties to that of petroleum based polyethylene terephthalate (PET) [30]. However, PLA is less flammable than other synthetic thermoplastics such as PET, with less visible smoke on burning and a lower peak heat release rate (PHHR) [31]. The physical and fire related properties of PLA polymer are compared with other commercial polymers such as PET, Polyamide 6 (PA6) and Polypropylene (PP) in Table 1.1.

Table 1.1. Physical and fire related properties of some commercial polymers [32]

Properties	Unit	PLA	PET	PA6	PP
Density	g/cm^3	1.24	1.38	1.14	0.92
Melting temperature	°C	170-180	255-260	210-220	155-165
Glass transition temperature	°C	55-60	70-80	57-65	-10
Time to ignition	s	58	46	48	42
Smoke generation	m^2/kg	63	394	195	142
Limiting oxygen index	%	24	19	18	20
Peak heat release rate	kW/m^2	425-450	625-640	575-590	495-510
Effective heat of combustion	kJ/g	18	24	19	21

PLA is aliphatic polyester synthesized from lactic acid building blocks [34]. In 1932, low molecular weight PLA was developed by Carothers and coworkers [35]. Traditionally PLA is known for biomedical applications due to its biocompatibility, however in the recent past the

innovation of some novel polymerization techniques led to the manufacturing of high molecular weight PLA that broadened the scope of PLA applications ranging from packaging to high-tech applications [36]. Melt processing is considered to be the most economically viable option for filament production [37]. In this technique, polymer is heated above its melting point and filaments are formed followed by hot drawing to attain the desired mechanical properties [38]. For optimization and smooth running of the process, the understanding of rheological behavior, crystallization and thermal properties of the polymer is mandatory.

Lactic acid is the basic building block for polylactic acid, which is manufactured by transforming starch or sugar through bacterial fermentation or by petrochemical route. By poly-condensation reaction, lactic acid can be transformed directly to polyesters due to the presence of carboxyl and hydroxyl groups. However, conventional poly-condensation reaction results in lower molecular weight of this polymer, unless organic solvents are involved in the process. Though by ring opening polymerization technique, high molecular weight of polylactic acid can be achieved [39]. The production route of polylactic acid by ring opening polymerization is shown in Figure 1.1.

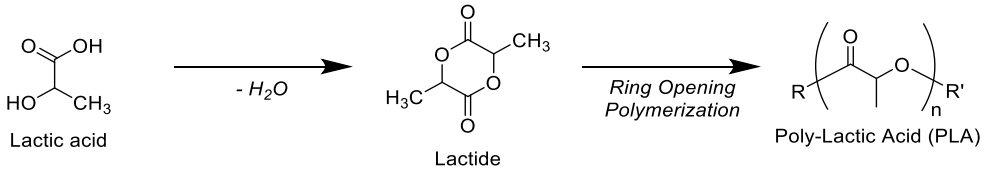

Figure 1.1. Ring opening polymerization route for the production of polylactic acid

1.3. Flame retardants

Carbon is the fundamental element in all types of organic polymers [33]. Carbon-Carbon bonds are the backbones of each polymer, whereas some polymers also contain Carbon-Oxygen and Carbon-Nitrogen bonds depending on the presence of heteroatoms in the main chains. Upon exposure to adequate amount of heat, all type of organic polymers can be thermally decomposed. The heat supplied is absorbed as long as the Carbon-Carbon, Carbon-Oxygen and Carbon-Nitrogen bonds stay in contact but, after the bonds are broken, volatile gases are emitted that acts as a fuel to the fire [40]. The thermal decomposition of a polymer is dependent on various factors such as, the composition of a polymer, conditions at which the polymer is degraded and presence of

additives in the polymer. Although the degradation and stability of each polymer is dependent on the factors discussed above but, approximately all polymers, tend to decompose within the temperature range of 250˚- 450˚C [41]. Therefore, flame retardant additives are incorporated in a polymer to improve its flame retardancy.

The task of a flame-retardant is to interfere with polymer ignition and to make it less flammable by intervening in a process, by which burning phenomenon takes place [42]. Their role is to prolong the resistance to burning, rather than entirely eradicating the flammability of the polymers, as all polymers are prone to ignition at extreme temperature conditions. However, by right additives composition, a polymer can become flame-retardant and ignition of a polymer can be prolonged. There is no universal flame retardant available that can be used for all types of polymers due to their different chemical compositions and different requirements for each targeted application [43]. Definitely, the requirements for a foam application will be different to the requirements for molding sheets or for the textiles. In short, each flame-retardant is designed for a particular end use and their selection is dependent on the type of fire hazards. Flame-retardants are generally assessed by considering their performance against (a) heat release rate (b) flame spread rate (c) ignition of a polymer and (d) formation of smoke, toxic gases [44]. Therefore, to get the desired results a careful selection of a flame-retardant is necessary. Sometimes more thermally stable polymer together with a flame-retardant is preferred to control fire hazards however, this approach is not so convincing because, thermally stable polymers usually contain high fluorine content (which is toxic) and are somewhat difficult to process and more costly as well [45].

Fire propagation can be inhibited/suppressed by any of the following four approaches, i.e. (a) by using inherently flame retardant polymers (high performance polymers); (b) by chemically modifying the polymer structure; (c) by a surface treatment to the polymer; (d) by integrating fire-retardants in the polymers by compounding. These approaches are discussed briefly.

High performance or inherently flame retardant polymers such as PBO (Polyphenylene-Benzobisoxazole) also known as Zylon (commercial name) or PBZT (Polyphenylene-Benzobisthiazole) possess excellent flame retardant properties but they are not suitable for every application due to higher cost and aging problems [46]. The chemical structures of PBO and PBZT are shown in Figure 1.2.

Figure 1.2. Chemical structures of inherently flame-retardant polymers (PBO and PBZT)

In the second approach, the monomer of a polymer is chemically modified to get flame-retardant polymer, such as Trevira CS [47]. It is a chemically modified PET fiber, which possess intrinsic flame-retardant properties and therefore do not require external treatment to impart flame-retardancy. A typical example of Trevira CS fiber is shown in Figure 1.3.

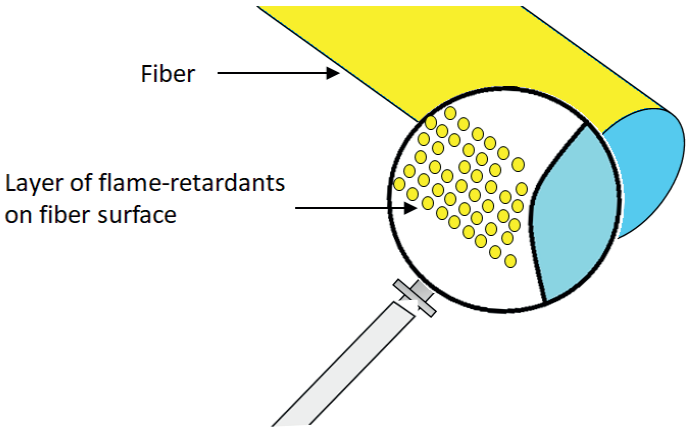

Figure 1.3. A typical example of Trevira CS fiber

In the third approach, a polymer surface is coated to make it flame-retardant. This method is easy to implement and offers quite a few benefits. The biggest advantage of using this method is that, flame-retardancy can be imparted to a polymer without altering its intrinsic mechanical characteristics. This method can be implemented in various types of materials such as, polymers, metals, wood and textiles. There are various technologies that are used to modify the surface of a polymer and cold plasma is one of them. The surface of a material is treated to achieve desired functional properties without altering its intrinsic properties. Surface functionalization reactions are stimulated on the surface of a material by using cold plasma technology or tiny layers of organic or inorganic materials are deposited by combining the molecular fragments on materials

surface by reactive species of cold plasma technology [48]. A typical example of cold plasma coating is shown in Figure 1.4, where powder additives are streamlined by the force of the plasma gas, which is governed by an electric field towards the target. The streamlined additives are bombarded towards the target and are collected by the stream collector.

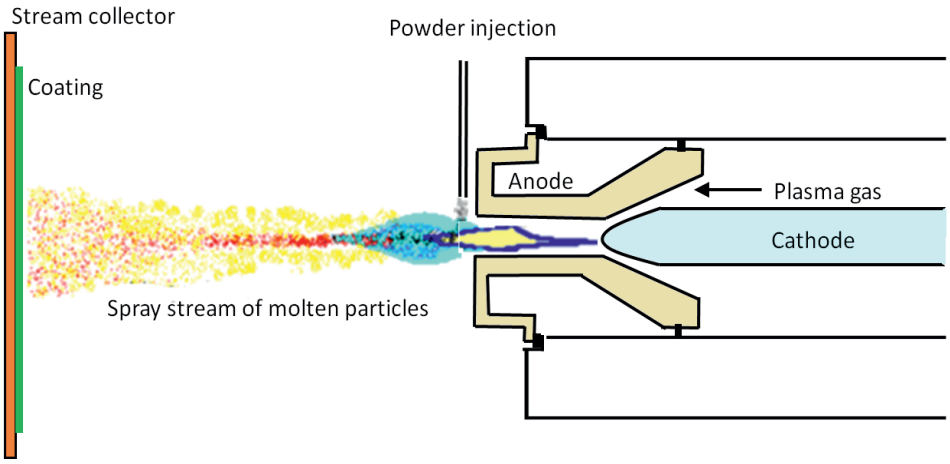

Figure 1.4. A typical example of cold plasma coating

In the fourth approach, flame-retardant additives are directly incorporated to the polymers, by melting and adding the required percentage of additives, to form FR composites. This approach is generally favored because it provides a balance between the required flame-retardant properties and the cost occurred in the process [49]. Moreover, this approach is quite flexible in order to design polymers with desired multifunctional properties and can be used at the industrial scale as well. A typical example of a compounder is shown in Figure 1.5. The polymer is fed in one of the hoppers and additives in the other. The polymer and the additives are heated by heating elements and homogeneous polymer melt comes out of the nozzle in the form of a strand. This compounded strand is passed through water tub to normalize its temperature before being passed through the cutter that cuts the compounded strand into small granules, which are ready to be used for subsequent processing.

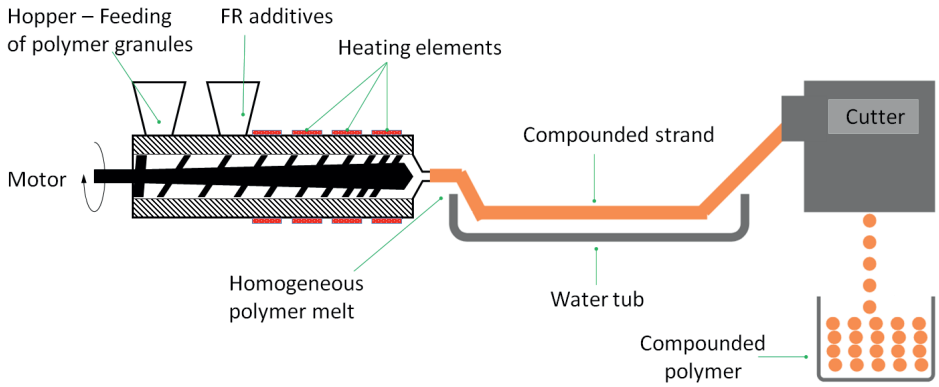

Figure 1.5. A typical example of a compounder

Flame-retardant additives depending on their type and composition, behave differently with the polymer as most of them interact chemically with the polymer while some interact physically as well to interfere the combustion process. There are different stages of a combustion process, starting from heating the polymer, its decomposition, ignition and flame spreading in the polymer. Not all FR additives interfere the combustion process at same stage; some are designed to interfere before polymer decomposition and some are intended to suppress the combustion before ignition, while some are aimed to prevent the flame spreading in the polymer [50].

1.4. Action mechanism of flame retardants

Since flame-retardants interfere in more than one stage of combustion process therefore, their action mechanism is mainly dependent at which stage of combustion they interfere in [51]. The action mechanisms of different types of flame-retardants are discussed below.

1.4.1. Dilution of volatile products

Alumina trihydrate ($Al_2O_3.3H_2O$) is a compound used for dilution of volatile products since it starts breaking down to water molecules and aluminum oxide at 175-210˚C [52]. Moreover, this compound is environmentally safe and also not very expensive, hence overall decreases the production cost [53]. However, the drawback of this compound is very low decomposition temperature and requires relatively higher loading concentration (wt%) in the polymer to induce fire retardancy. To overcome these drawbacks, recently magnesium hydroxide $Mg(OH)_2$ has been

used for the dilution of volatile products since it operates in a similar way to alumina trihydrate but with higher decomposition temperature (280-340°C). Hence, $Mg(OH)_2$ can be used for polymers that are processed above 250˚C without the problem of early decomposition during melt processing [54]. However, still relatively higher loading concentration (40-50,wt%) of the compound is required to impart acceptable degree of flame retardancy in the polymer.

1.4.2. Inhibition of vapor phase combustion

For vapor phase combustion to take place, volatile products are required that are produced by oxidative thermal decomposition of a polymer. Vapor phase combustion can be controlled by using flame-retardants designed for such purposes that decompose at similar temperature range at which the polymer starts to decompose and those radicals are formed, which are less reactive also known as free radicals. These radicals do not react anymore with the volatile products in the vapor phase hence, slows down the combustion process [55]. These free radicals have very low energy and do not have the capability to further prolong the oxidation process. Once the oxidation process is slowed down, the transfer of heat back to the polymer is reduced, which slows down the combustion process hence, eventually the flame is extinguished. Typical example of such cases is the application of organo-bromine and organo-chlorine based flame-retardants [56].

1.4.3. Removing heat of combustion

Due to the burning of volatile compounds in the polymer, heat is generated and if sufficient heat flows back to the polymer, its thermal decomposition is continued due to self-sustaining of burning cycle. The schematic diagram of burning cycle is shown in Figure 1.6.

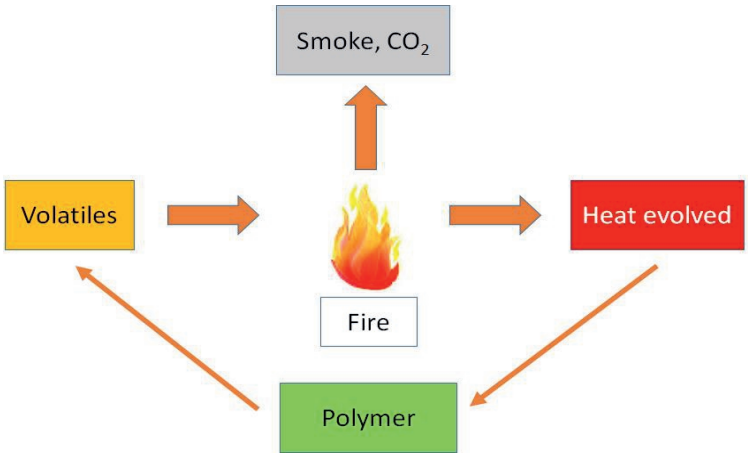

Figure 1.6. Schematic diagram of a burning cycle

This burning cycle can be broken and combustion of the polymer can be stopped if some portion of the heat is eliminated from the burning cycle. By removing heat from the burning cycle, the pyrolysis rate of the polymer is slowed down and eventually the combustion process will be stopped [57].

1.4.4. Smoke suppressants

Due to the burning of some polymeric materials, smoke is generated which can be very harmful and sometimes can be a cause of death. Polyvinyl chloride (PVC) is one of the polymers, which burns with significant amount of smoke and to reduce its thermal decomposition and smoke emission, smoke suppressants are necessary. Compounds based on zinc, iron, tin and molybdenum can be used as smoke suppressants in PVC products such as ammonium octamolybdate and molybdenum trioxide can be used as smoke suppressants in PVC cabling [58].

1.4.5. Char formation

Volatile products are emitted from the polymer as it is ignited by thermal oxidative reaction, which actually is the main reason for the burning of a polymer. However, this mechanism can be changed to produce less volatile products and more char on the surface of a polymer [59]. The formation of char on polymer surface not only act as smoke suppressant but also removes heat of combustion therefore, this action mechanism is considered far superior than the mechanisms discussed earlier

[60]. The type of flame-retardants generally preferred for char formation are halogen free flame-retardants and the system in which they are used is known as intumescent flame retardant system [61].

1.5. Intumescent flame retardants

Intumescence is originated from a Latin word "intumescere" which means to swell up [62]. The intumescent material if heated above a certain temperature starts to expand and swell up resulting in the formation of a charred layer on the exterior of the material [63]. This charred layer restricts the diffusion of oxygen to the site of combustion and protects the underlying material from exposure to fire and heat flux [64]. IFR's offer a highly effective strategy to enhance the fire retardancy of polymers as a charred layer is developed that acts as a shield between the polymer and heat source and protects the polymer material from further burning and dripping. Modern IFR systems are based on halogen-free flame-retardants (HFFR's) which, unlike their halogen-containing counterparts, are environmentally safe as they do not degrade into dioxins whereas halogenated compounds with aromatic rings can degrade into dioxins and dioxin-like compounds [65]. Chlorinated dioxins are among the highly toxic compounds listed by the Stockholm Convention on Persistent Organic Pollutants [66]. The action mechanism of IFR's is shown in Figure 1.7.

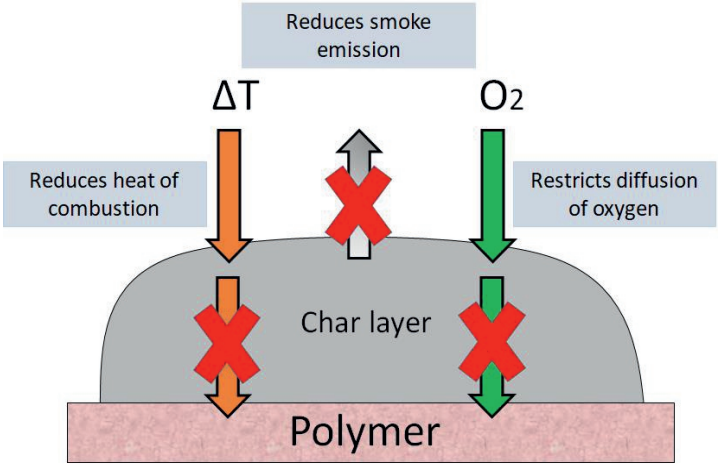

Figure 1.7. Action mechanism of intumescent flame-retardants

Formation of char takes place mostly in the condensed phase and other than creating a physical barrier, it also has several other benefits such as, it does not allow the passage of decomposed volatile products to the place of fire and provides insulation to the underlying material against thermal degradation [67][68]. Since the char forming systems tend to interrupt the burning cycle rather than working on flame poisoning mechanism therefore, regarded as more effective and less hazardous to the environment [69].

Chars normally have broad continuous crust on the outer surface and inner surface have a resemblance to closed foam cell like structure [70]. In an ideal case, the char should be thick and have large volume in order to provide better thermal insulation to the underlying material [71]. In case of intumescent flame-retardants better flame retardancy can be achieved at lower loading concentrations (wt%) compared to flame-retardants based on magnesium hydroxide and alumina trihydrate [72]. For example, a loading concentration of 15-20 wt% in case of intumescent flame retardants can generate the same level of flame retardancy, what can be achieved with 40-50 wt% of magnesium hydroxide and alumina trihydrate [73]. The intumescent system mainly consists of an acid source, which releases acidic species upon heating, a carbonization agent, which acts as a char former on the material's surface [74]. Inorganic acids, phosphates and ammonium salts are used as an acidic source, whereas compounds containing hydroxyl groups such as polyols are used as char formers [75].

1.6. Testing methods

The fire hazards of a material can be assessed by various standard testing methods as each fire regulation defines a particular fire test for its assessment. The fire performance of a material is generally assessed by the following three methods, i.e. limiting oxygen index (LOI), UL-94 vertical burning test and cone calorimetry [76]. LOI measures the minimum concentration of oxygen required to ensure a self-sustained flame. In this test, the specimen is placed vertically in a glass column and is ignited from the top with flame progressing downwards. A material with a very low LOI (i.e. around 20%), generally burns quite easily therefore, higher LOI values corresponds better flame retardancy of a material [77]. This test is performed under ISO 4589 standard testing method. A schematic diagram for the LOI test is shown in Figure 1.8.

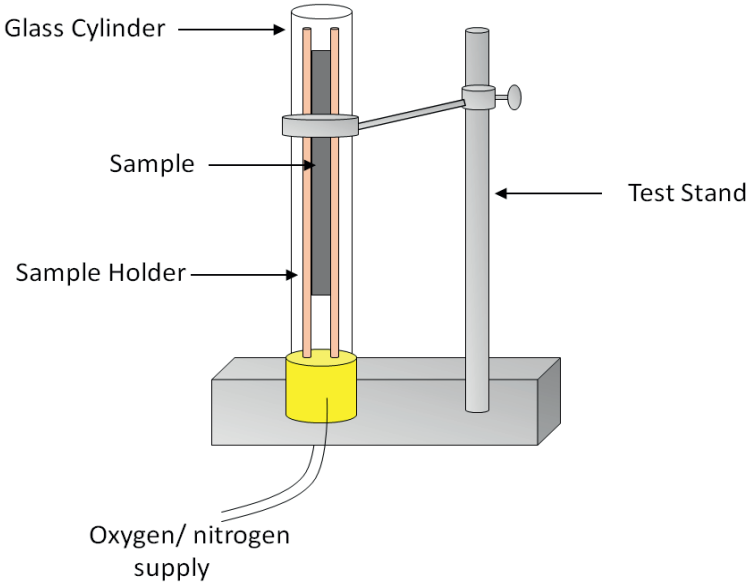

Figure 1.8. Schematic diagram of limiting oxygen index equipment

The second commonly used test method in flame retardancy is UL-94 vertical burning test [78]. In this test, the specimen is positioned vertically and is ignited from the bottom end. The specimens are exposed to flame for 10 s twice, their flaming time is noted and are classified based on three different ratings according to ISO 9773 standard testing method. V-0 is considered the best rating, and it corresponds to a specimen that does not drip and flame out in less than 10 s. V-1 rating corresponds to the specimen, which takes more than 10 s and less than 30 s to flame out and does not drip. V-2 rating is given to those specimens, which drip after flaming and takes even more time to flame out. No ratings are given to those specimen which does not flame out [64]. The schematic diagram of UL-94 vertical burning test is shown in Figure 1.9.

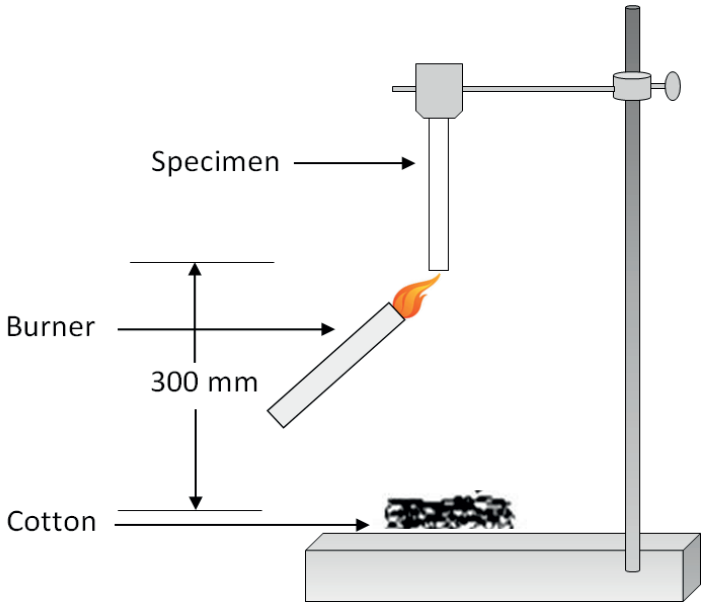

Figure 1.9. Schematic diagram of UL-94 vertical burning test

Cone calorimeter is an equipment that gives useful insights about the burning behavior of a material by reporting, time to ignition, peak heat release rate, total heat release and residual mass% of the sample [62]. A specimen in the form of 3-4 mm thick molded sheet is placed horizontally in a controlled heat flux, and is ignited with a spark igniter according to ISO 5660 standard testing method. Heat flux can be varied between 10 to 100 kWm^{-2} but mostly it is used in the range of 35 to 50 kWm^{-2}. During this test the ventilation of air flow is well maintained and the concentration of oxygen in the air flow is constantly monitored. The intensity of burning is then assessed by measuring the concentration of oxygen in the air flow, as combustion is directly linked to the oxygen consumption. Moreover, irrespective of the material, 1 kg consumption of oxygen is equivalent to heat release of 13.1 MJ according to empirical Huggett relation [79]. The main outcome of this test is the determination of peak heat release rate of a material, which is a very important parameter to estimate the fire hazards. The schematic diagram of cone calorimetry test is shown in Figure 1.10.

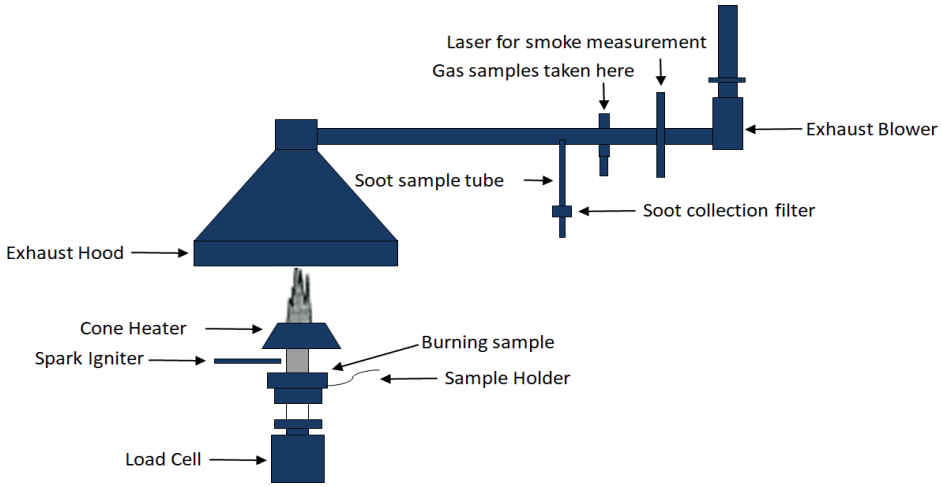

Figure 1.10. Schematic diagram of cone calorimetry equipment

1.7. Potential biobased and biodegradable carbonization agents

The researcher's community in the recent past has shifted their focus towards the development of flame-retardants, which are based on biodegradable resources [80]. Carbon is the major element present in the biomass and according to a study, the entire biomass available on earth represents approximately 560 billion tons of carbon [81]. Therefore, carbon element present in natural compounds can be used as carbonization agent in intumescent flame-retardants [82]. In the following section, biodegradable compounds that have the potential to be used as biobased carbonization agents in intumescent formulations are discussed briefly.

1.7.1. Cellulose

Cellulose is the most abundant natural source of organic compound on earth and is the core component of the cell walls in the plants. It is estimated that each year on this planet, different plants synthesize approximately 100 billion tons of cellulose, which is a linear homopolymer compound, consisting of D-glucose units connected by β 1-4 glycosidic bonds with polymerization degree ranging between 1000 to 30,000 [83]. During decomposition of cellulose, aliphatic groups start to disappear and benzene rings and furan compounds start to increase quite significantly in the condensed phase. At elevated temperatures such as at 800°C, a char layer is developed. It

should be noted that the decomposition route of cellulose can be modified, which is dependent on the presence of other components in cellulose and on the heating conditions [84].

1.7.2. Starch

The chemical formula of starch is similar to cellulose as starch also contains D-glucose units. Plants synthesize this polymer as energy storage material and after processing; it takes the form of small granules with a diameter ranging between 1–200 µm. Two different types of macromolecules are present in starch polymer: the one is amylose, which is a linear polymer that contains glucose units connected through α 1-4 linkage whereas, the other one is amylopectin, which is a branched polymer connected through α 1-6 linkage [85]. The chemical structures of starch and its derivatives are shown in Figure 1.11.

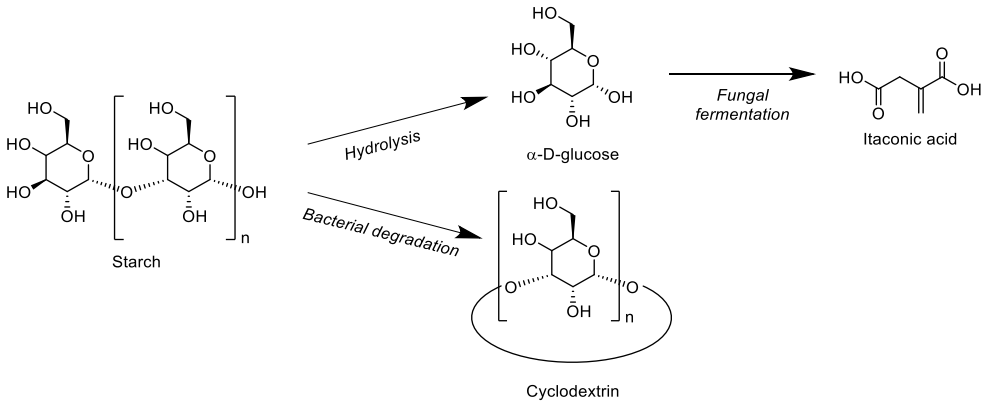

Figure 1.11. Starch and its derivatives used as flame-retardants

The production of starch worldwide is approximately 70 million tons per year. By acid or enzyme treatments, native starch can be hydrolyzed into non-complex carbohydrates such as dextrins. Cyclodextrin is one such example, which is obtained by starch degradation by the bacillus amylobacter bacteria [86]. Starch can also be converted into its derivatives by a process called fermentation. For example, glucose or molasses can be converted into itaconic acid by using fungi such as aspergillus terreus. Similarly, tartaric acid can be produced by the fermentation of grape stock to make wine. Both itaconic acid and tartaric acid are used as a raw material for the development of flame-retardants [87].

1.7.3. Chitosan

Chitosan is a copolymer consisting of D-glucosamine and N-acetyl-D-glucosamine units connected through β 1-4 linkage. Chitosan is formed by the enzymatic deacetylation of chitin (Figure 1.12), which is found in shrimp shells [88].

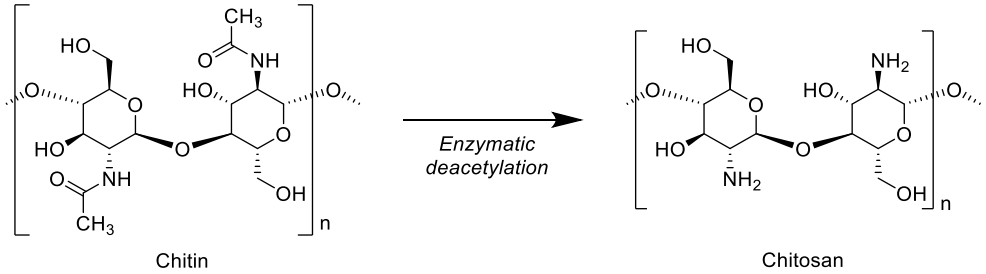

Chitin Chitosan

Figure 1.12. Enzymatic deacetylation of chitin to chitosan

The acetylation degree of chitosan varies from 60 to 100% depending upon the commercial application. The production capacity of chitosan worldwide is approximately 20×10^{3} tons annually and its market is growing especially in North America and Asia. The thermal decomposition of chitosan takes place in three steps. The first weight loss occurs in between 130-140°C, which corresponds to dehydration of loosely bonded molecules. The second degradation step, which occurs between 260-360°C, corresponds to de-polymerization and deacetylation of chitosan. In the third step, due to residual decomposition reaction, a very low weight loss rate occurs above 400°C, and char residue up to 30 wt% is formed at 500°C [89].

1.7.4. Alginates

Alginates are derived from alginic acid (Figure 1.13) and are found in the cell walls of brown algae as salts of alginic acid, which is a copolymer of guluronic acid and mannuronic acid with repeating units connected through β 1-4 linkages [90]. The chemical and physical properties of this polymer are dependent on the fraction and distribution of co-monomers present in it. Alginates are considered as anionic polysaccharides. The thermal decomposition of alginates occurs in two main steps under nitrogen atmosphere. In the first step, they undergo dehydration at very low temperatures (100-120°C) as they contain very high moisture content, i.e. sodium alginate contains about 15-wt% and that of alginic acid about 10-wt%. In the second step, the major decomposition

of the polymer starts between 150-300°C, which leads to char residues of up to 21-25 wt% at maximum temperature of 800°C [51].

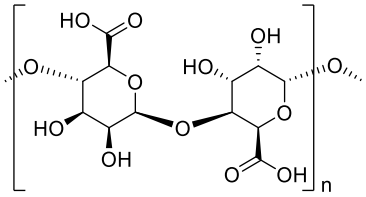

Alginic acid

Figure 1.13. Chemical structure of alginic acid

1.7.5. Lignin

Lignin is an aromatic polymer (Figure 1.14) and after cellulose is the second most abundant natural polymer. Lignin is present in plants and in algae and their role is quite significant in strengthening the cell walls of plants by providing protection and rigidity. They also give waterproofness to the cell walls of plants [91]. The thermal decomposition of lignin occurs over a broad range of temperature (200-500°C) in two main steps. The decomposition mechanism of lignin is somewhat different compared to other components of biomass. Generally, the first weight loss of lignin occurs between 100-180°C, which corresponds to the dehydration of water molecules connected to the raw matter [92]. However, the main decomposition starts from 200°C, and low molecular weight molecules are released by the cleavage from the propanoid side chain. From 275-450°C, further degradation of lignin takes place due to the cleavage in the main chain either by β-scission, C-C bond or aryl ether cleavage, which leads to release in large quantity of methane. The condensation of the aromatic structure takes place above 500°C, which results in the development of a substantial char yield and dihydrogen is released in the gas phase [93].

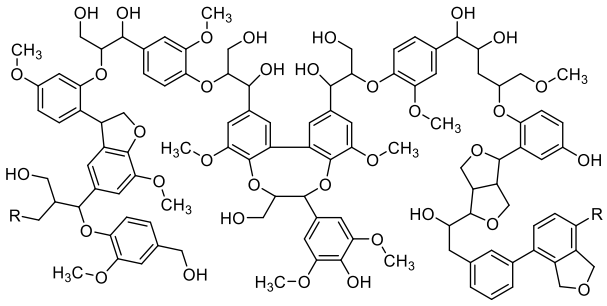

Figure 1.14. Lignin chemical structure

To conclude above discussion, the following key-points are the main indicators for the application of biobased carbonization agents in intumescent flame-retardants [94].

- The thermal stability of biobased carbonization agents should be sufficiently high to enable polymer processing
- Biobased carbonization agents should contain functional groups such as hydroxyl and carboxyl groups, which are responsible for char formation by reacting with acid sources in intumescent formulations.

1.8. Approaches used to make PLA flame-retardant: state of the art

Flame retardancy of PLA can be improved by various techniques such as, by blending with more thermally stable polymers, by compounding inorganic FR's, nitrogen-based FR's, halogenated FR's and nanofillers in PLA matrix. Researchers have tried various techniques to improve flame retardancy of PLA, while some are reported in Table 1.2.

Table 1.2. Approaches used to make PLA flame-retardant

Source	Authors	Short description	Findings
[95]	Kimura and Horikoshi	Tried to improve flame retardancy of PLA by blending with virgin polycarbonate (PC) but results showed not very significant improvement in flame retardancy of the blend.	To achieve better results, silicon-comprising PC was blended with PLA, but still only V-2 rating could be achieved in UL-94 vertical burning test.
[96]	Nishida et al.	Studied flame retardant properties of PLA by compounding ATH in the polymer.	However, they found that in order to get superior results; a relatively higher amount of ATH (about 40 to 50%) needs to be added in PLA matrix.
[97]	Yanagisawa et al.	Incorporated ATH together with phenolic resins in PLA matrix to improve its flame retardancy for electronic applications. A significant char formation during combustion on the surface of the composite was observed.	The addition of phenolic resin not only resulted in improved flame retardancy, reinforced by alumina from ATH on the surface of composite, but also reduced the loading content of ATH to 35% (w/w).
[98]	Kubokawa et al.	Determined flame retardancy of PLA based fabrics by using bromine containing additives, and tri-phenyl phosphates and tested LOI of the fabrics.	LOI of untreated fabrics was 24%, however after treatment with FR additives, LOI of the fabrics increased to 28% with tri-phenyl phosphate and to 26% with bromine- containing FR additives.
[99]	Wang et al.	Prepared composites containing pentaerythritol (PER) and melamine cyanurate (MC) by controlling the weight ratio (2:2:1) and organo-modified zinc aluminum layered double hydroxide (Zn-Al-LDH).	Microscale combustion calorimeter (MCC) and cone calorimetry results revealed substantial progresses in flame retardancy of the nanocomposites. A significant reduction in heat release rate and total heat release was observed.

[100]	Wei et al.	Investigated the effect of aryl poly-phenyl phosphonate together with PLA. LOI, UL-94 vertical burning and cone calorimetry tests were carried out together with the investigation of thermal and mechanical behavior of the composites.	PLA composites containing 7 and 10 wt% of poly phenyl phosphonate achieved V-0 rating in UL-94 vertical burning test. However, not much improvement in HRR and THR of the FR composites were observed in comparison to neat PLA.
[101]	Bourbigot et al.	Studied flame-retardancy of different polymer nanocomposites such as polylactides, polyurethane and polyamides. Different nano-fillers such as carbon nanotubes and organoclay were incorporated in these polymers and their flame retardancy was investigated.	Found that nano-dispersion play a vital role in improving flame retardancy of nanocomposites and nano-fillers give better results when they are used in combination with inorganic flame-retardants due to better synergistic effects.
[102]	Solarski et al.	Developed PLA/clay nanocomposites and studied their thermal and fire properties. Four different formulations ranging from 1 to 4 wt% of the organo clay (C30B) were prepared. The nanocomposites were melt spun to produce multifilament yarns.	Yarns with better mechanical properties were used to produce knitted structures. The fire properties of the knitted fabrics were tested by cone calorimetry. It was observed that PHHR of the fabrics containing only 2 wt% of the clay were reduced up to 38%.
[21]	Suardana et al.	Prepared bio-composites containing natural fibers together with di-ammonium phosphate and investigated their mechanical and fire related properties.	By increasing wt% of di-ammonium phosphate fire properties, flexural modulus and weight loss rate of the composites were improved however, tensile and flexural strengths of the composites were reduced.
[63]	Qian et al.	Prepared aluminated mesoporous silica, and used it as an FR additive in PLA resin. Different formulations of fumed silica and aluminated mesoporous silica were compounded in PLA resin.	Achieved UL-94 V-0 rating and LOI value also increased quite significantly. PHHR of FR composites decreased to about 15% compared to neat PLA by the addition of only 0.5 wt% of aluminated mesoporous silica.

[103]	Wang et al.	Developed an inherently fire-resistant PLA polymer by using chain-extending procedure of pre-polylactic acid (PPLA). PPLA was produced by direct condensation reaction of L-lactic acid and its fire properties were tested.	5-wt% of PPLA in PLA polymer would be sufficient to achieve remarkable FR properties as LOI value of 35% and UL-94 V-0 rating was achieved with delayed ignition time compared to pure PLA.
[104]	Mngomezulu et al.	Investigated FR properties of PLA and expandable graphite (PLA/EG) composites. EG was compounded in PLA with different wt% to produce PLA/EG composites and their surface morphology, filler dispersion, dynamic mechanical behavior and crystallization rate were studied.	The presence of graphite layers with not so good filler dispersion resulted in poor bonding between PLA resin and EG. The crystallization rate of PLA was increased with an increase in the glass transition temperature. Furthermore, lower modulus of the composites with higher wt% of EG was observed.
[105]	Shumao et al	Used ramie fibers together with PLA to reinforce the polymer and to enhance the mechanical properties. Used different formulations together with ramie fibers.	At 40 wt% loading the LOI value could only be reached at 30%. Resulted phosphoric acid contributed in intermolecular dehydration of ramie fibers followed by dehydrogenation.
[67]	Zhan et al.	Investigated the combustion and thermal degradation behavior of PLA with a special flame-retardant consisting of spirocyclic-pentaerythritol bisphosphorate disphosphoryl melamine (SPDPM) and melt compounded with different wt% in PLA.	Attained UL-94 V-0 rating at 25 wt% loading and LOI value was 38%. A significant reduction in weight loss rate of PLA was observed after addition of SPDPM in PLA as confirmed by thermogravimetric analysis.
[106]	Fox et al.	POSS modified cellulose was melt blended with PLA to prepare PLA/POSS composites. Thermal and fire related properties of as prepared composites were tested by thermogravimetric analysis, dynamic mechanical analysis and cone calorimetry.	PHHR of the composites was reduced to 45% by the introduction of 15 wt% of modified cellulose in comparison to PHHR of neat PLA. THR was also reduced to 20% and lesser smoke generation was observed in comparison to non-modified cellulose.

From state of the art we found that, most of the conventional flame-retardants, i.e. inorganic FR's, nitrogen-containing FR's, silicon based FR's, nano-fillers and halogenated flame-retardants are non-biodegradable and if disposed in the landfill, microorganisms in the soil or water cannot degrade them. Hence, they remain in the environment for long time, and may find their way not only in the food chain but can also migrate from the products in which they are directly incorporated to the surroundings, and can cause serious health problem if inhaled in human body. Moreover, non-biodegradable halogenated FRs may find their way in the environment through wastewater streams of the industries that produce them or through adsorption onto the dust particles at the manufacturing facilities where they are incorporated directly to various products. Once these FR's go to the environment, they can easily attach to any airborne particle and can travel distances far from emission or production sites. Hence, traces of such non-biodegradable FRs can be found in freshwater, food products, ecosystems or even can be inhaled by breathing if they are present in the air [24]. Therefore, it is very important that the flame-retardants used in technical applications not only need to be effective but at the same time should be biodegradable and safe to the environment and microorganisms in the soil or water can degrade them and result in mineralization.

1.9. Scope, objectives and outline of thesis

1.9.1. Scope

In conventional IFR's, the components used are mainly non-biodegradable and obtained from non-biobased resources such as pentaerythritol (PER). PER is a polyol obtained from petrochemicals and has higher water solubility, which makes it not feasible for polymer thermal processing, melt spinning to produce fibers for textile applications and several other engineering applications. Furthermore, it is not a good choice to use non-biodegradable PER in biodegradable materials such as PLA. Mostly in technical textiles, non-biodegradable halogenated flame-retardants are used with aromatic rings such as brominated and chlorinated compounds that convert into dioxins and dioxin-like compounds, which are of course among the highly toxic compounds listed by the Stockholm Convention on Persistent Organic Pollutants. Thus, it is necessary to test biodegradable and biobased flame-retardants to substitute PER in intumescent formulations for biodegradable polymer PLA. In this way, the whole IFR system can be made biodegradable if all of its components are biodegradable. We therefore, in this dissertation have used biodegradable acid

donors that breaks down into naturally occurring phosphates and biobased carbonization agents in intumescent formulations developed for PLA based textiles and composites. The carbonization agents used in this dissertation are carbohydrates (corn-starch) and natural aromatic phenolic compounds (kraft lignin) obtained from renewable resources. They contain the necessary carboxyl and hydroxyl functional groups that are responsible for charring effect in IFR's and their thermal stability is sufficiently high to enable thermal processing and to produce melt-spinnable multifilament fibers.

1.9.2. Aims and objectives

The goal of this dissertation is not only to use biodegradable and biobased flame-retardants in polymeric materials but also to achieve flame retardancy of PLA based composites and textiles as per the requirements defined by the standard fire testing methods for the targeted applications. The other goal is to produce FR products for technical applications whose flame-retardancy is comparable to the standard benchmark properties, defined for those targeted applications. In order to investigate the efficiency and effectiveness of the developed technical products the following objectives should be accomplished.

- To attain limiting oxygen index (LOI) value of the FR products equal to or above 28% as per the ISO 4589 standard testing method.
- To achieve V-0 or at least V-1 rating of the FR products in UL-94 vertical burning test as per the ISO 9773 standard testing method.
- To accomplish peak heat release rate (PHHR) value of the FR products not more than 400 kW/m^2 as per the ISO 5660 standard testing method
- To attain effective heat of combustion (EHC) value of the FR products not more than 15 kJ/g as per the ISO 5660 standard testing method
- To achieve total smoke production (TSP) value of the FR products not more than 300 m^2/m^2 as per the ISO 5660 standard testing method
- To accomplish E and Efl rating in ignitability test of the nonwoven carpet backing as per the ISO 11925 standard testing method.
- To optimize the additives compositions in the FR compounds to improve the spinnability of IFR composites

- To upscale the melt-spinnability of the developed PLA-IFR formulation from lab to pilot-scale by optimizing the spinning process parameters and to develop IFR multifilaments based on mono and bi-component flame-retardant fibers.

1.9.3. Outline of thesis

The approaches used, to achieve above defined objectives are described in the following chapters. The work presented hereafter is intended to deliver a small library based on potential strategies to develop intumescent flame-retardants for PLA based textiles and composites, established on biodegradable and biobased resources. The process parameters involved at different stages of the product development are optimized and thermal, mechanical, functional and fire-related properties of the developed products are characterized in order to meet the defined benchmark properties. The schematic overview of different chapters in this dissertation is shown in Figure 1.15.

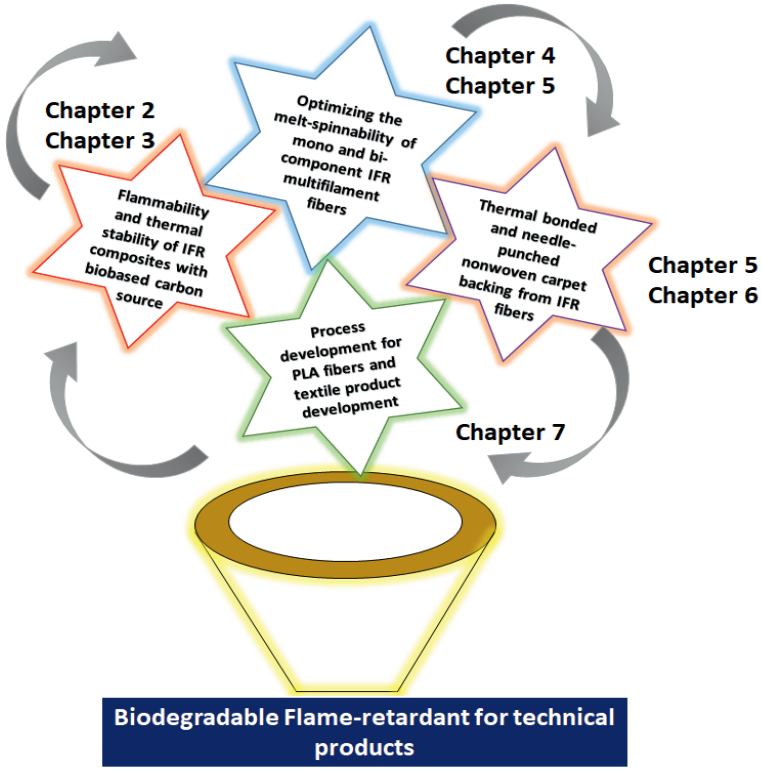

Figure 1.15. Schematic overview of the thesis

In **Chapter 2**, the effect of cornstarch as a carbonization agent in intumescent formulations is investigated as a potential biobased substitute for PER together with biodegradable halogen free flame-retardant, and PLA/APP/ST composites are prepared. The mechanism of intumescence indicating catalytic phosphorylation to produce phosphate esters, which eventually dehydrated the starch and formed char structure containing residue up to 43% is discussed.

Chapter 3 describes the efficiency of kraft lignin (KL) as a biobased carbonization agent in intumescent formulations and their FR properties are assessed and compared with conventional carbonization agent (PER) by preparing PLA/APP/KL and PLA/APP/PER composites. IFR composites comprising different formulations are produced with and without carbonization agents (KL and PER) by melt extrusion and their flammability is assessed by UL-94, LOI and cone calorimetry tests.

Chapter 4 investigates, melt spinnability, thermal stability, mechanical and fire-related properties of PLA composites prepared by melt blending on twin-screw extruder comprising phosphorous–nitrogen-based flame retardant (EXP), kraft lignin (KL) and plasticizer (PES). In this chapter, different process parameters such as, solid-state draw ratio, temperature of the godets and melt-throughput are optimized to upscale the spinnability of PLA/IFR composites from lab to pilot scale. Mono-component multifilament fibers are prepared on pilot scale melt-spinning machine and single jersey knitted fabrics are produced from these fibers to test their fire properties.

Chapter 5 describes the development of melt-spun bicomponent multifilament functional fibers from single polymer, with sheath/core configuration, by using highly-crystalline PLA with IFR's in the core component, while amorphous PLA is in the sheath component. The changes in fiber mechanical properties and crystallinity were recorded in response to varying process parameters. Cone calorimetry showed a 46% decline in the heat release rate of nonwovens, produced from FR PLA bicomponent fibers, compared to pure PLA nonwovens. This indicated the development of an intumescent char by leaving a residual mass of 34% relative to the initial mass of the sample.

Thermoplastic processing and melt spinning of native starch is very challenging due to (a) the linear and branched polymers (amylose and amylopectin) present in its structure and (b) the presence of inter-and-intramolecular hydrogen bond linkages in its macromolecules that restrict the molecular chain mobility. Therefore, in **Chapter 6**, oxidized starch (OS) (obtained after oxidation of native starch with sodium perborate) is melt-blended with PLA polymer to improve

thermal processing of the composites to produce multifilaments. These multifilament are cut into short fibers, carded to form fibrous web and needle-punched together to form nonwoven fabrics. The fire related properties of these nonwoven fabrics are tested.

In this dissertation, other than flame-retardancy, textile apparel applications of PLA are also investigated, since this polymer has comparable mechanical and physical properties to polyethylene terephthalate (PET) - a fiber mostly used in textile applications. Therefore, a process development for PLA fiber production is optimized, and socks from pure PLA draw textured melt spun yarns are produced in **Chapter 7**. The effect of yarn linear density, fabric structure and fabric stitch density on thermo-physiological characteristics of PLA socks are investigated.

Chapter 8 gives an overview of the opportunities and requirements for industrial scale up of biobased and biodegradable flame-retardants and their future perspectives. Some important factors such as fire performance criteria, environmental and health criteria and economic criteria for industrial scale up are discussed.

Finally, **Chapter 9** discuss the valorization potential of the research presented in this dissertation.

1.10. References

1. Liu, Y.; Mo, X.; Pang, J.; Yang, F. Effects of silica on the morphology, structure, and properties of thermoplastic cassava starch/poly(vinyl alcohol) blends. *J Appl Polym Sci* **2016**, *44020*, 1–9, doi:10.1002/app.44020.
2. Vothi, H.; Nguyen, C.; Lee, K.; Kim, J. Thermal stability and flame retardancy of novel phloroglucinol based organo phosphorus compound. *Polym Degrad Stab* **2010**, *95*, 1092–1098, doi:10.1016/j.polymdegradstab.2010.02.024.
3. Song, K.; Wang, Y.; Ruan, F.; Liu, J.; Li, N.; Li, X. Effects of a Macromolecule Spirocyclic Inflatable Flame Retardant on the Thermal and Flame Retardant Properties of Epoxy Resin. *Polymers (Basel)* **2020**, *12*, 1–16.
4. Zhang, W.; Wu, W.; Meng, W.; Xie, W.; Cui, Y.; Xu, J. Core-Shell Graphitic Carbon Nitride/Zinc Phytate as a Novel Efficient Flame Retardant for Fire Safety and Smoke

Suppression in Epoxy Resin. *Polymers (Basel)* **2020**, *12*, 1–12.

5. Zhang, J.; Ji, Q.; Shen, X.; Xia, Y.; Tan, L.; Kong, Q. Pyrolysis products and thermal degradation mechanism of intrinsically flame-retardant calcium alginate fibre. *Polym Degrad Stab* **2011**, *96*, 936–942, doi:10.1016/j.polymdegradstab.2011.01.029.
6. Menard, R.; Negrell, C.; Ferry, L.; Sonnier, R.; David, G. Synthesis of biobased phosphorus-containing flame retardants for epoxy thermosets comparison of additive and reactive approaches. *Polym Degrad Stab* **2015**, *120*, 300–312, doi:10.1016/j.polymdegradstab.2015.07.015.
7. Menard, R.; Negrell, C.; Fache, M.; Ferry, L.; Sonnier, R.; David, G. From a bio-based phosphorus-containing epoxy monomer to fully bio-based flame-retardant thermosets. *RSC Adv* **2015**, *5*, 70856–70867, doi:10.1039/C5RA12859E.
8. Liu, Y.; Wang, J.; Zhu, P.; Zhao, J.; Zhang, C.; Guo, Y.; Cui, L. Thermal degradation properties of biobased iron alginate film. *J Anal Appl Pyrolysis* **2016**, 1–10, doi:10.1016/j.jaap.2016.03.014.
9. Laachachi, A.; Cochez, M.; Leroy, E.; Gaudon, P.; Ferriol, M.; Cuesta, J.M.L. Effect of Al2O3 and TiO2 nanoparticles and APP on thermal stability and flame retardance of PMMA. *Polym Adv Technol* **2006**, *17*, 327–334, doi:10.1002/pat.690.
10. Bourbigot, S.; Fontaine, G. Flame retardancy of polylactide: An overview. *Polym Chem* **2010**, *1*, 1413–1422, doi:10.1039/c0py00106f.
11. Murariu, M.; Bonnaud, L.; Yoann, P.; Fontaine, G.; Bourbigot, S.; Dubois, P. New trends in polylactide (PLA)-based materials: “Green” PLA-Calcium sulfate (nano)composites tailored with flame retardant properties. *Polym Degrad Stab* **2010**, *95*, 374–381, doi:10.1016/j.polymdegradstab.2009.11.032.
12. Chapple, S.; Anandjiwala, R.; Ray, S.S. Mechanical, thermal, and fire properties of polylactide/starch blend/clay composites. *J Therm Anal Calorim* **2013**, *113*, 703–712, doi:10.1007/s10973-012-2776-6.
13. Gui, H.; Xu, P.; Hu, Y.; Wang, J.; Yang, X.; Bahader, A.; Ding, Y. Synergistic effect of graphene and an ionic liquid containing phosphonium on the thermal stability and flame retardancy of polylactide. *RSC Adv* **2015**, *5*, 27814–27822, doi:10.1039/C4RA16393A.
14. Zhou, R.; Ming, Z.; He, J.; Ding, Y.; Jiang, J. Effect of Magnesium Hydroxide and Aluminum Hydroxide on the Thermal Stability, Latent Heat and Flammability Properties

of Paraffin/ HDPE Phase. *Polymers (Basel)* **2020**, *12*, 1–14.

15. Karim, M.N.; Rigout, M.; Yeates, S.G.; Carr, C. Surface chemical analysis of the effect of curing conditions on the properties of thermally-cured pigment printed poly (lactic acid) fabrics. *Dye Pigment* **2014**, *103*, 168–174, doi:10.1016/j.dyepig.2013.12.010.
16. Cayuela, D.; Montero, L.; Díaz, J.; Algaba, I.; Manich, A.M. Microstructure variations of polylactide fibres with texturing conditions. *Text Res J* **2012**, *82*, 1996–2005, doi:10.1177/0040517512438122.
17. Parmar, M.S.; Singh, M.; Tiwari, R.K.; Saran, S. Study on flame retardant properties of poly(lactic acid) fibre fabrics. *Indian J Fibre Text Res* **2014**, *39*, 268–273.
18. Duquesne, S.; Samyn, F.; Ouagne, P.; Bourbigot, S. Flame retardancy and mechanical properties of flax reinforced woven for composite applications. *J Ind Text* **2015**, *44*, 665–681, doi:10.1177/1528083713505633.
19. Cheng, X.-W.; Guan, J.-P.; Tang, R.-C.; Liu, K.-Q. Improvement of flame retardancy of poly(lactic acid) nonwoven fabric with a phosphorus- containing flame retardant. *J Ind Text* **2016**, *46*, 914–928, doi:10.1177/1528083715606105.
20. Yuan, Y.; Yu, B.; Shi, Y.; Mao, L.; Xie, J.; Pan, H.; Liu, Y. Insight into Hyper-Branched Aluminum Phosphonate in Combination with Multiple Phosphorus Synergies for Fire-Safe Epoxy Resin Composites. *Polymers (Basel)* **2020**, *12*, 1–15.
21. Suardana, N.; Kyoo, M. Effects of diammonium phosphate on the flammability and mechanical properties of bio-composites. *Mater Des* **2011**, *32*, 1990–1999, doi:10.1016/j.matdes.2010.11.069.
22. Teoh, E.L.; Mariatti, M.; Chow, W.S. Thermal and Flame Resistant Properties of Poly (Lactic Acid)/Poly (Methyl Methacrylate) Blends Containing Halogen-free Flame Retardant. *Procedia Chem* **2016**, *19*, 795–802, doi:10.1016/j.proche.2016.03.087.
23. Wu, X.; Jiang, G.; Zhang, Y.; Wu, L.; Jia, Y.; Tan, Y.; Liu, J. Enhancement of Flame Retardancy of Colorless and Transparent Semi-Alicyclic Polyimide Film from. *Polymers (Basel)* **2020**, *12*, 1–16.
24. Huang, R.; Guo, X.; Ma, S.; Xie, J.; Xu, J.; Ma, J. Novel Phosphorus-Nitrogen-Containing Ionic Liquid Modified Metal-Organic Framework as an Effective Flame Retardant for Epoxy Resin. *Polymers (Basel)* **2020**, *12*, 1–16.
25. Lim, L.; Auras, R.; Rubino, M. Processing technologies for poly (lactic acid). *Prog Polym*

Sci **2008**, *33*, 820–852, doi:10.1016/j.progpolymsci.2008.05.004.

26. Pla, P.; Raquez, J.; Habibi, Y.; Murariu, M.; Dubois, P. Polylactide (PLA) based nanocomposites. *Prog Polym Sci* **2013**, *38*, 1504–1542, doi:10.1016/j.progpolymsci.2013.05.014.
27. Lee, J.H.; Park, S.H.; Kim, S.H. Surface Alkylation of Cellulose Nanocrystals to Enhance Their Compatibility with Polylactide. *Polymers (Basel)* **2020**, *12*, 1–16, doi:10.3390/polym12010178.
28. Praglowska, J.; Janus, L.; Piatkowski, M.; Bogdal, D.; Matysek, D. Hybrid Bilayer PLA/Chitosan Nanofibrous Scaffolds Doped with ZnO, Fe3O4, and Au Nanoparticles with Bioactive Properties for Skin Tissue Engineering. *Polymers (Basel)* **2020**, *12*, 1–19.
29. Nampoothiri, K.M.; Nair, N.R.; John, R.P. An overview of the recent developments in polylactide (PLA) research. *Bioresour Technol* **2010**, *101*, 8493–8501, doi:10.1016/j.biortech.2010.05.092.
30. Pilla, S.; Kramschuster, A. Microcellular processing of polylactide – hyperbranched polyester – nanoclay composites. *J Mater Sci* **2010**, *45*, 2732–2746, doi:10.1007/s10853-010-4261-6.
31. Gupta, B.; Revagade, N.; Anjum, N. Preparation of Poly (lactic acid) Fiber by Dry – Jet – Wet Spinning . II . Effect of Process Parameters on Fiber Properties. *J Appl Polym Sci* **2006**, *101*, 3774–3780, doi:10.1002/app.23543.
32. Maqsood, M.; Seide, G. Development of biobased socks from sustainable polymer and statistical modeling of their thermo-physiological properties. *J Clean Prod* **2018**, *197*, 170–177, doi:10.1016/j.jclepro.2018.06.191.
33. Gan, L.; Geng, A.; Wu, Y.; Wang, L.; Fang, X.; Xu, L. Antibacterial, Flexible, and Conductive Membrane Based on MWCNTs/Ag Coated Electro-Spun PLA Nanofibrous Scaffolds as Wearable Fabric for Body Motion Sensing. *Polymers (Basel)* **2020**, *12*, 1–11.
34. Rasal, R.M.; Janorkar, A. V; Hirt, D.E. Poly (lactic acid) modifications. *Prog Polym Sci* **2010**, *35*, 338–356, doi:10.1016/j.progpolymsci.2009.12.003.
35. Liu, H.; Xie, F.; Yu, L.; Chen, L.; Li, L. Thermal processing of starch-based polymers. *Prog Polym Sci* **2009**, *34*, 1348–1368, doi:10.1016/j.progpolymsci.2009.07.001.
36. Maqsood, M.; Seide, G. Statistical modeling of thermal properties of biobased compostable gloves developed from sustainable polymer. *Fibers Polym* **2018**, *19*, 1094–1101,

doi:10.1007/s12221-018-1126-0.

37. Cheng, Y.; Deng, S.; Chen, P.; Ruan, R. Polylactic acid (PLA) synthesis and modi fi cations : a review. *Front Chem China* **2009**, *4*, 259–264, doi:10.1007/s11458-009-0092-x.
38. Gupta, B.; Revagade, N. Poly (lactic acid) fiber : An overview. *Prog Polym Sci* **2007**, *32*, 455–482, doi:10.1016/j.progpolymsci.2007.01.005.
39. Wischke, C.; Schwendeman, S.P. Principles of encapsulating hydrophobic drugs in PLA / PLGA microparticles. *Int J Pharm* **2008**, *364*, 298–327, doi:10.1016/j.ijpharm.2008.04.042.
40. Alongi, J.; Andrea, R.; Bosco, F.; Carosio, F.; Di, A.; Cuttica, F.; Antonucci, V.; Giordano, M.; Malucelli, G. Caseins and hydrophobins as novel green flame retardants for cotton fabrics. *Polym Degrad Stab* **2014**, *99*, 111–117, doi:10.1016/j.polymdegradstab.2013.11.016.
41. Anastasakis, K.; Ross, A.B.; Jones, J.M. Pyrolysis behaviour of the main carbohydrates of brown macro-algae. *Fuel* **2011**, *90*, 598–607, doi:10.1016/j.fuel.2010.09.023.
42. Dorez, G.; Ferry, L.; Sonnier, R.; Taguet, A. Effect of cellulose , hemicellulose and lignin contents on pyrolysis and combustion of natural fibers. *J Anal Appl Pyrolysis* **2014**, *107*, 323–331, doi:10.1016/j.jaap.2014.03.017.
43. Chirico, A. De; Armanini, M.; Chini, P.; Cioccolo, G. Flame retardants for polypropylene based on lignin. *Polym Degrad Stab* **2003**, *79*, 139–145.
44. Carosio, F.; Fontaine, G.; Alongi, J.; Bourbigot, S. Starch-Based Layer by Layer Assembly: Efficient and Sustainable Approach to Cotton Fire Protection. *Appl Mater Interfaces* **2015**, doi:10.1021/acsami.5b02507.
45. Carosio, F.; Alongi, J.; Malucelli, G. Layer by Layer ammonium polyphosphate-based coatings for flame retardancy of polyester – cotton blends. *Carbohydr Polym* **2012**, *88*, 1460–1469, doi:10.1016/j.carbpol.2012.02.049.
46. Camino, G.; Costa, L.; Cortemiglia, M. Overview of Fire Retardant Mechanisms. *Polym Degrad Stab* **1991**, *33*, 131–154.
47. Alongi, J.; Cuttica, F.; Bourbigot, S.; Malucelli, G. Thermal and flame retardant properties of ethylene vinyl acetate copolymers containing deoxyribose nucleic acid or ammonium polyphosphate. *J Therm Anal Calorim* **2015**, doi:10.1007/s10973-015-4808-5.
48. Qian, W.; Li, X.; Wu, Z.; Liu, Y.; Fang, C.; Meng, W. Formulation of Intumescent Flame Retardant Coatings Containing Natural-Based Tea Saponin. *J Agric Food Chem* **2015**,

doi:10.1021/jf505898d.

49. Tondi, G.; Wieland, S.; Wimmer, T. Tannin-boron preservatives for wood buildings : mechanical and fire properties. *Eur J Wood Prod Prod* **2012**, *70*, 689–696, doi:10.1007/s00107-012-0603-1.
50. Pan, Y.; Zhan, J.; Pan, H.; Wang, W.; Tang, G.; Song, L.; Hu, Y. Effect of Fully Biobased Coatings Constructed via Layer-by-Layer Assembly of Chitosan and Lignosulfonate on the Thermal, Flame Retardant, and Mechanical Properties of Flexible Polyurethane Foam. *Sustain Chem Eng* **2015**, 4–11, doi:10.1021/acssuschemeng.5b01423.
51. Soares, J.P.; Santos, J.E.; Chierice, G.O.; Cavalheiro, E.T.G. Thermal behavior of alginic acid and its sodium salt. *Eclet Quim* **2004**, *29*, 53–56.
52. Mihaela, A.; Moldoveanu, C.; Odochian, L.; Maria, C.; Apostolescu, N.; Neculau, R. Study on the thermal behavior of casein under nitrogen and air atmosphere by means of the TG-FTIR technique. *Thermochim Acta* **2012**, *546*, 120–126, doi:10.1016/j.tca.2012.07.031.
53. Laoutid, F.; Bonnaud, L.; Alexandre, M.; Lopez-cuesta, J.; Dubois, P. New prospects in flame retardant polymer materials: From fundamentals to nanocomposites. *Mater Sci Eng R* **2009**, *63*, 100–125, doi:10.1016/j.mser.2008.09.002.
54. Illy, N.; Fache, M.; Menard, R.; Negrell, C.; Caillol, S.; David, G. Phosphorylation of bio-based compounds: state of the art. *Polym Chem* **2015**, 1–32, doi:10.1039/C5PY00812C.
55. Enescu, D.; Alongi, J.; Frache, A.; Chimica, I.; Torino, P.; Branch, A.; Michel, V.T. Evaluation of Nonconventional Additives as Fire Retardants on Polyamide 6,6: Phosphorous-Based Master Batch , a-Zirconium Dihydrogen Phosphate ,and b-Cyclodextrin Based Nanosponges. *J Appl Polym Sci* **2011**, *123*, 3545–3555, doi:10.1002/app.
56. Carosio, F.; Laufer, G.; Alongi, J.; Camino, G.; Grunlan, J.C. Layer-by-layer assembly of silica-based flame retardant thin film on PET fabric. *Polym Degrad Stab* **2011**, *96*, 745–750, doi:10.1016/j.polymdegradstab.2011.02.019.
57. Braun, U.; Schartel, B.; Fichera, M.A.; Ja, C. Flame retardancy mechanisms of aluminium phosphinate in combination with melamine polyphosphate and zinc borate in glass-fibre reinforced polyamide 6 , 6. *Polym Degrad Stab* **2007**, *92*, 1528–1545, doi:10.1016/j.polymdegradstab.2007.05.007.
58. Bocz, K.; Domonkos, M.; Igricz, T.; Kmetty, Á.; Bárány, T.; Marosi, G. Flame retarded

self-reinforced poly (lactic acid) composites of outstanding impact resistance. *Compos PART A* **2015**, *70*, 27–34, doi:10.1016/j.compositesa.2014.12.005.

59. Jimenez, M.; Guin, T.; Bellayer, S.; Dupretz, R.; Bourbigot, S.; Grunlan, J.C. Microintumescent mechanism of flame-retardant water-based chitosan–ammonium polyphosphate multilayer nanocoating on cotton fabric. *J Appl Polym Sci* **2016**, *43783*, 1–12, doi:10.1002/app.43783.
60. Maqsood, M.; Seide, G. Investigation of the Flammability and Thermal Stability of Halogen-Free Intumescent System in Biopolymer Composites Containing Biobased Carbonization Agent and Mechanism of Their Char Formation. *Polymers (Basel)* **2018**, *11*, 1–16, doi:10.3390/polym11010048.
61. Zhu, H.; Zhu, Q.; Li, J.; Tao, K.; Xue, L.; Yan, Q. Synergistic effect between expandable graphite and ammonium polyphosphate on flame retarded polylactide. *Polym Degrad Stab* **2011**, *96*, 183–189, doi:10.1016/j.polymdegradstab.2010.11.017.
62. Kotresh, T.M.; Indushekar, R.; Subbulakshmi, M.S.; Vijayalakshmi, S.N.; Prasad, A.S.K.; Agrawal, A.K. Evaluation of commercial flame retardant polyester curtain fabrics in the cone calorimeter. *J Ind Text* **2006**, *36*, 47–58, doi:10.1177/1528083706064379.
63. Qian, Y.; Wei, P.; Jiang, P.; Li, Z.; Yan, Y.; Ji, K. Aluminated mesoporous silica as novel high-effective flame retardant in polylactide. *Compos Sci Technol* **2013**, *82*, 1–7, doi:10.1016/j.compscitech.2013.03.019.
64. Wang, K.; Wang, J.; Zhao, D.; Zhai, W. Preparation of microcellular poly(lactic acid) composites foams with improved flame retardancy. *J Cell Plast* **2017**, *53*, 45–63, doi:10.1177/0021955X16633644.
65. Depeng, L.; Chixiang, L.; Xiulei, J.; Tao, L.; Ling, Z. Synergistic effects of intumescent flame retardant and nano-CaCO 3 on foamability and flame-retardant property of polypropylene composites foams. *J Cell Plast* **2017**, 1–17, doi:10.1177/0021955X17720157.
66. Vahabi, H.; Ferry, L.; Longuet, C.; Otazaghine, B.; Negrell-guirao, C.; David, G.; Lopez-cuesta, J. Combination effect of polyhedral oligomeric silsesquioxane (POSS) and a phosphorus modified PMMA , flammability and thermal stability properties. *Mater Chem Phys* **2012**, *136*, 762–770, doi:10.1016/j.matchemphys.2012.07.053.
67. Zhan, J.; Song, L.; Nie, S.; Hu, Y. Combustion properties and thermal degradation behavior

of polylactide with an effective intumescent flame retardant. *Polym Degrad Stab* **2009**, *94*, 291–296, doi:10.1016/j.polymdegradstab.2008.12.015.

68. Maqsood, M.; Langensiepen, F.; Seide, G. The Efficiency of Biobased Carbonization Agent and Intumescent Flame Retardant on Flame Retardancy of Biopolymer Composites and Investigation of their melt spinnability. *Molecules* **2019**, *24*, 1–18.
69. Yuan, X.; Wang, D.; Chen, L.; Wang, X.; Wang, Y. Inherent flame retardation of bio-based poly (lactic acid) by incorporating phosphorus linked pendent group into the backbone. *Polym Degrad Stab* **2011**, *96*, 1669–1675, doi:10.1016/j.polymdegradstab.2011.06.012.
70. Tang, G.; Wang, X.; Zhang, R.; Wang, B.; Hong, N.; Hu, Y.; Song, L.; Gong, X. Effect of rare earth hypophosphite salts on the fire performance of biobased polylactide composites. *Ind Eng Chimestry Res* **2013**, 1–10.
71. Tang, G.; Wang, X.; Xing, W.; Zhang, P.; Wang, B.; Hong, N.; Yang, W.; Hu, Y.; Song, L. Thermal Degradation and Flame Retardance of Biobased Polylactide Composites Based on Aluminum Hypophosphite. *Ind Eng Chimestry Res* **2012**, *51*, 12009–12016.
72. Lyon, R.E.; Walters, R.N. Pyrolysis combustion flow calorimetry. *J Anal Appl Pyrolysis* **2004**, *71*, 27–46, doi:10.1016/S0165-2370(03)00096-2.
73. Murariu, M.; Laure, A.; Bonnaud, L.; Paint, Y.; Gallos, A.; Fontaine, G.; Bourbigot, S.; Dubois, P. The production and properties of polylactide composites filled with expanded graphite. *Polym Degrad Stab* **2010**, *95*, 889–900, doi:10.1016/j.polymdegradstab.2009.12.019.
74. Matusinovic, Z.; Wilkie, C.A. Fire retardancy and morphology of layered double hydroxide nanocomposites : a review. *J Mater Chem* **2012**, *22*, 18701–18704, doi:10.1039/c2jm33179a.
75. Cheng, X.W.; Guan, J.P.; Tang, R.C.; Liu, K.Q. Improvement of flame retardancy of poly(lactic acid) nonwoven fabric with a phosphorus- containing flame retardant. *J Ind Text* **2016**, *46*, 914–928, doi:10.1177/1528083715606105.
76. Murariu, M.; Dechief, A.L.; Paint, Y.; Peeterbroeck, S.; Bonnaud, L.; Dubois, P. Polylactide (PLA)-Halloysite Nanocomposites: Production, Morphology and Key-Properties. *J Polym Environ* **2012**, *20*, 932–943, doi:10.1007/s10924-012-0488-4.
77. Avinc, O.; Day, R.; Carr, C.; Wilding, M. Effect of combined flame retardant, liquid repellent and softener finishes on poly(lactic acid) (PLA) fabric performance. *Text Res J*

2012, *82*, 975–984, doi:10.1177/0040517511418557.

78. Lin, H.; Han, L.; Dong, L. Thermal degradation behavior and gas phase flame-retardant mechanism of polylactide/PCPP blends. *J Appl Polym Sci* **2014**, *131*, 1–11, doi:10.1002/app.40480.
79. Katsoulis, C.; Kandare, E.; Kandola, B.K. The combined effect of epoxy nanocomposites and phosphorus flame retardant additives on thermal and fire reaction properties of fiber-reinforced composites. *J Fire Sci* **2011**, *29*, 361–383, doi:10.1177/0734904111398785.
80. Laachachi, A.; Cochez, M.; Leroy, E.; Ferriol, M.; Lopez-cuesta, J.M.; Verlaine-metz, P.; Demange, V.; Cedex, S. Fire retardant systems in poly (methyl methacrylate): Interactions between metal oxide nanoparticles and phosphinates. *Polym Degrad Stab* **2007**, *92*, 61–69, doi:10.1016/j.polymdegradstab.2006.09.011.
81. Vassilev, S. V; Baxter, D.; Andersen, L.K.; Vassileva, C.G. An overview of the chemical composition of biomass. *Fuel* **2010**, *89*, 913–933, doi:10.1016/j.fuel.2009.10.022.
82. Petrovic, Z. Polyurethanes from Vegetable Oils. *Polym Rev* **2008**, *48*, 109–155, doi:10.1080/15583720701834224.
83. Alongi, J.; Carosio, F.; Malucelli, G. Layer by layer complex architectures based on ammonium polyphosphate, chitosan and silica on polyester-cotton blends: flammability and combustion behaviour. *Cellulose* **2012**, *19*, 1041–1050, doi:10.1007/s10570-012-9682-8.
84. Bozic, M.; Liu, P.; Mathew, A.; Kokol, V. Enzymatic phosphorylation of cellulose nanofibers to new highly-ions adsorbing, flame-retardant and hydroxyapatite-growth induced natural nanoparticles. *Cellulose* **2014**, doi:10.1007/s10570-014-0281-8.
85. Alongi, J.; Han, Z.; Bourbigot, S. Intumescence: Tradition versus novelty . A comprehensive review. *Prog Polym Sci* **2015**, *51*, 28–73, doi:10.1016/j.progpolymsci.2015.04.010.
86. Wang, B.; Qian, X.; Shi, Y.; Yu, B.; Hong, N.; Song, L.; Hu, Y. Cyclodextrin microencapsulated ammonium polyphosphate: Preparation and its performance on the thermal, flame retardancy and mechanical properties of ethylene vinyl acetate copolymer. *Compos Part B* **2015**, *69*, 22–30, doi:10.1016/j.compositesb.2014.09.015.
87. Pack, S.; Bobo, E.; Muir, N.; Yang, K.; Swaraj, S.; Ade, H.; Cao, C.; Korach, C.S.; Kashiwagi, T.; Rafailovich, M.H. Engineering biodegradable polymer blends containing flame retardant-coated starch/nanoparticles. *Polymer (Guildf)* **2012**, *53*, 4787–4799,

doi:10.1016/j.polymer.2012.08.007.

88. Zhang, T.; Yan, H.; Shen, L.; Fang, Z.; Zhang, X.; Wang, J.; Zhang, B. Chitosan/phytic acid polyelectrolyte complex: A green and renewable intumescent flame retardant system for ethylene-vinyl acetate copolymer. *Ind Eng Chem Res* **2014**, *53*, 19199–19207, doi:10.1021/ie503421f.
89. Logithkumar, R.; Keshavnarayan, A.; Dhivya, S.; Chawla, A.; Saravanan, S.; Selvamurugan, N. A Review of Chitosan and its Derivatives in Bone Tissue Engineering. *Carbohydr Polym* **2016**, doi:10.1016/j.carbpol.2016.05.049.
90. Liu, Y.; Zhao, X.; Peng, Y.; Wang, D.; Yang, L.; Peng, H.; Zhu, P.; Wang, D. Effect of reactive time on flame retardancy and thermal degradation behavior of bio-based zinc alginate film. *Polym Degrad Stab* **2016**, 1–12, doi:10.1016/j.polymdegradstab.2015.12.024.
91. Costes, L.; Laoutid, F.; Aguedo, M.; Richel, A.; Brohez, S.; Delvosalle, C.; Dubois, P. Phosphorus and nitrogen derivatization as efficient route for improvement of lignin flame retardant action in PLA. *Eur Polym J* **2016**, *84*, 652–667, doi:10.1016/j.eurpolymj.2016.10.003.
92. Ding, P.; Kang, B.; Zhang, J.; Yang, J.; Song, N.; Tang, S.; Shi, L. Phosphorus-containing flame retardant modified layered double hydroxides and their applications on polylactide film with good transparency. *J Colloid Interface Sci* **2015**, *440*, 46–52, doi:10.1016/j.jcis.2014.10.048.
93. Lin, H.J.; Liu, S.R.; Han, L.J.; Wang, X.M.; Bian, Y.J.; Dong, L.S. Effect of a phosphorus-containing oligomer on flame-retardant, rheological and mechanical properties of poly (lactic acid). *Polym Degrad Stab* **2013**, *98*, 1389–1396, doi:10.1016/j.polymdegradstab.2013.03.025.
94. Lligadas, G.; Callau, L.; Ronda, J.; Galia, M.; Cadiz, V. Novel Organic – Inorganic Hybrid Materials from Renewable Resources: Hydrosilylation of Fatty Acid Derivatives. *J Polym Sci Part A Polym Chem* **2005**, *43*, 6295–6307, doi:10.1002/pola.21039.
95. Kimura, K.; Horikoshi, Y. Bio-based polymers. *Fujitsu Sci Tech J* **2005**, *41*, 173–180, doi:10.2115/fiber.66.P_124.
96. Nishida, H.; Fan, Y.; Mori, T.; Oyagi, N.; Shirai, Y.; Endo, T. Feedstock Recycling of Flame-Resisting Poly (lactic acid)/ Aluminum Hydroxide Composite to L , L -lactide. *Ind Eng Chimestry Res* **2005**, *44*, 1433–1437, doi:10.1021/ie049208+.

97. Yanagisawa, T. Enhanced flame retardancy of polylactic acid with aluminum tri-hydroxide and phenolic resins. *Kobunshi Ronbunshu* **2009**, *66*, 49–54.

98. Kubokawa, H.; Hatakeyama, T. Thermal decomposition behavior of polylactide fabrics treated with flame retardants. *Sen'i Gakkaishi,* **1999**, *55*, 349–355.

99. Wang, D.Y.; Song, Y.P.; Lin, L.; Wang, X.L.; Wang, Y.Z. A novel phosphorus-containing poly(lactic acid) toward its flame retardation. *Polymer (Guildf)* **2011**, *52*, 233–238, doi:10.1016/j.polymer.2010.11.023.

100. Wei, L.L.; Wang, D.Y.; Chen, H.B.; Chen, L.; Wang, X.L.; Wang, Y.Z. Effect of a phosphorus-containing flame retardant on the thermal properties and ease of ignition of poly(lactic acid). *Polym Degrad Stab* **2011**, *96*, 1557–1561, doi:10.1016/j.polymdegradstab.2011.05.018.

101. Bourbigot, S.; Duquesne, S.; Fontaine, G.; Bellayer, S.; Turf, T.; Samyn, F. Characterization and Reaction to Fire of Polymer Nanocomposites with and without Conventional Flame Retardants. *Mol Cryst Liq Cryst* **2008**, *486*, 37–41, doi:10.1080/15421400801921983.

102. Solarski, S.; Mahjoubi, F.; Ferreira, M.; Devaux, E.; Bachelet, P.; Bourbigot, S.; Delobel, R.; Coszach, P.; Murariu, M.; Da Silva Ferreira, A.; et al. (Plasticized) Polylactide/clay nanocomposite textile: Thermal, mechanical, shrinkage and fire properties. *J Mater Sci* **2007**, *42*, 5105–5117, doi:10.1007/s10853-006-0911-0.

103. Wang, N.; Hu, L.; Vignesh, H. Effect of tea saponin-based intumescent flame retardant on thermal stability, mechanical property and flame retardancy of natural rubber composites. *J Therm Anal Calorim* **2016**, doi:10.1007/s10973-016-5931-7.

104. Mngomezulu, M.E.; Luyt, A.S.; John, M.J. Morphology, thermal and dynamic mechanical properties of poly(lactic acid)/expandable graphite (PLA/EG) flame retardant composites. *J Thermoplast Compos Mater* **2017**, 1–19, doi:10.1177/0892705717744830.

105. Mauldin, T.; Zammarano, M.; Gilman, J.; Shields, J.; Boday, J. Synthesis and characterization of isosorbide-based polyphosphonates as biobased flame-retardants. *Polym Chem* **2014**, *5*, 5139–5146, doi:10.1039/C4PY00591K.

106. Fox, D.M.; Lee, J.; Citro, C.J.; Novy, M. Flame retarded poly(lactic acid) using POSS-modified cellulose. 1. Thermal and combustion properties of intumescing composites. *Polym Degrad Stab* **2013**, *98*, 590–596, doi:10.1016/j.polymdegradstab.2012.11.016.

CHAPTER 2

Investigation of the flammability and thermal stability of halogen-free intumescent system in biopolymer composites containing biobased carbonization agent and mechanism of their char formation

Abstract

Starch, being a polyhydric compound with its natural charring ability, is an ideal candidate to serve as a carbonization agent in an intumescent system. This charring ability of starch, if accompanied by an acidic source, can generate an effective intumescent flame retardant (IFR) system, but the performance of starch-based composites in an IFR system has not been tested in detail. Here, we describe a PLA-based IFR system consisting of ammonium polyphosphate (APP) as acidic source and cornstarch as carbon source. We prepared different formulations by melt compounding followed by molding into sheets by hot pressing. The thermal behavior and surface morphology of the composites was investigated by thermogravimetric analysis and scanning electron microscopy respectively. We also conducted limiting oxygen index (LOI), UL-94, and cone calorimetry tests to characterize the flame-retardant properties. Cone calorimetry revealed a 66% reduction in the peak heat release rate of the IFR composites compared to pure PLA and indicated the development of an intumescent structure by leaving a residual mass of 43% relative to the initial mass of the sample. A mechanism of char formation has also been discussed in detail.

Keywords

Biopolymer composites; Carbonization agent; Thermal analysis; Flame retardancy; Char formation

2.1. Introduction

Biobased polymers are derived from renewable resources, and their importance has grown over the last decade because they address current challenges such as the depletion of petroleum reserves (the feedstock for conventional plastics) and the environmental harm caused by the irresponsible disposal of non-degradable polymers [1]. One of the most widely used biobased polymers is polylactic acid (PLA), a thermoplastic polymer obtained from renewable resources such as corn starch [2]. PLA is less flammable than synthetic thermoplastics and produces less visible smoke when burning, resulting in a lower peak heat release rate than polyethylene terephthalate (PET) [3]. Even so, PLA is still combustible, which limits its applications in the automobile, electrical, and electronics sectors and in the production of flame-retardant materials [4].

Intumescent flame retardant (IFR) systems offer a highly effective strategy to enhance the fire retardancy of PLA because a char structure is developed that acts as a shield between the polymer and heat source, hence protecting the polymer material from further burning and dripping [5,6]. Modern IFR systems are based on halogen-free flame retardants (HFFRs) which, unlike their halogen-containing counterparts, are most of the time environmentally safe [6]. Furthermore, HFFRs are not only environmentally safe but also extremely efficient [7]. IFR system typically comprise three constituents: an acidic source, a blowing agent, and carbonic source to produce a char layer [8].

In previous studies various attempts have been made in order to improve the flame retardancy of PLA by using different formulations and additive types such as nitrogen-based compounds [9], phosphorous-based compounds [10], silicon-based compounds [11], expanded graphite or carbon-based compounds [12], halogen-containing compounds [13,14], and halogen-free compounds as flame retardants [15,16]. However, intumescent flame retardants (IFRs) containing an acidic and carbonic source have proven to be the most effective [17,18]. Traditional IFR systems often contain ammonium polyphosphate (APP) as the acidic source, melamine (MEL) as the blowing agent, and pentaerythritol (PER) as the carbonic source [16]. The thermal degradation of phosphorous-comprising fire retardants such as APP results in the formation of pyrophosphate and the release water, which eventually dilutes the gas phase such that the dehydration reaction is catalysed by pyro-phosphoric acid [19, 20]. Various alternative formulations have also been tested

including PLA-based composites containing spirocyclic PER, bisphosphorate disphosphoryl melamine [17] and microcellular PLA composite foams with graphene as the carbonization agent [18].

The importance of IFRs containing biopolymers with biobased carbonic source and halogen free acidic source has grown interest throughout the last decade in order to promote the sustainable approach toward flame retardancy of polymers [4]. Therefore, in continuation to this approach various researchers tried different formulations in IFR systems with different halogen-free acidic sources such as phytic acid [19], fumaric acid [20], and biobased carbonic sources such as cyclodextrin [21], sorbitol [22] and chitosan [23]. Conventional carbonization agents are effective in some polyolefin-based IFR systems [24] but are not compatible with PLA [25]. For example, although PER combined with APP resulted in a substantial progress in flame retardancy, the composites achieved only a V-2 rating in the UL94 test despite of the addition of 30–40% w/w of the additive [26].

We therefore investigated the effect of cornstarch (ST) as a carbonization agent in IFR systems as a potential biobased substitute for PER together with non-toxic and halogen-free flame retardant and studied the mechanism of char formation. The mechanism of intumescence indicating catalytic phosphorylation to produce phosphate esters, which eventually dehydrated the starch and formed char structure containing residue up to 43% has also been discussed in detail. We prepared PLA-based IFR systems containing different amounts of APP or APP together with starch by melt compounding and then molding the composites into sheets by hot pressing. Thermogravimetric analysis (TGA) was done to test the thermal behavior whereas scanning electron microscopy was used to determine the surface morphology of the composites. The limiting oxygen index and UL-94 vertical burning tests were conducted to determine the flame-retardant properties of the composites, whereas char residues were characterized by cone calorimetry test.

2.2. Materials and methods

The materials and methods used in this chapter are discussed in the following sections.

2.2.1. Materials

PLA polymer in granule form was obtained from Total-Corbion NV (Gorinchem, The Netherlands). Non-halogenated flame retardant Exolit AP 422, a fine-particle ammonium polyphosphate (APP) containing 14% (w/w) nitrogen and 31% (w/w) phosphorous, was obtained

from Clariant AG (Muttenz, Switzerland). The decomposition temperature of Exolit AP 422 was higher than 275 °C. Corn-based starch (particle size 100 μm) was obtained from Royal Ingredients Group BV (Alkmaar, The Netherlands). PLA, APP, and starch were vacuum-dried at 80 °C for 6 h before use.

2.2.2. Preparation of PLA/IFR composites

PLA/APP and PLA/APP/ST composites were prepared using a KETSE 20/40 compounder (Brabender, Duisburg, Germany) at 190 °C. Initially, PLA/APP composites containing 10%, 15%, or 20% (w/w) APP (hereafter PLA/APP10, PLA/APP15, and PLA/APP20) were compounded at a screw rotation speed of 150 rpm. The temperatures of the three heating zones were kept at 180, 185, and 190 °C, respectively. The extrudate was cut in to pellets. We also modified the PLA/APP20 pellets to incorporate 3%, 5%, or 7% (w/w) corn starch (hereafter PLA/APP20/ST3, PLA/APP20/ST5, and PLA/APP20/ST7) at a screw rotation speed of 200 rpm. PLA/APP20 pellets were incorporated in the first feeding zone whereas starch was added in the second feeding zone. This procedure was used to ensure proper mixing of all the components. Sheets of the prepared composites (100 × 100 × 3 mm^3) were produced by compression molding at 190 °C. Sheets of pure PLA were also prepared with the same dimensions for comparison. Sheets were cut in to different specimens as per the requirement of each fire test. The formulations of the as-prepared composites are summarized in Table 2.1.

Table 2.1. FR properties of PLA/APP and PLA/APP/ST composites

No.	Formulations	PLA wt%	APP %	ST %	LOI %	UL-94	Dripping
1	PLA	100	0	0	19.5	Failed	Y/Y
2	PLA/APP10	90	10	0	24.4	V-2	Y/Y
3	PLA/APP15	85	15	0	28.5	V-1	N/Y
4	PLA/APP20	80	20	0	31.9	V-0	N/Y
5	PLA/APP20/ST3	77	20	3	34.5	V-0	N/N
6	PLA/APP20/ST5	75	20	5	36.2	V-0	N/N
7	PLA/APP20/ST7	73	20	7	37.3	V-0	N/N

FR = Flame retardant, PLA = Polylactic acid, APP = Ammonium polyphosphate, ST = Starch, LOI = Limiting oxygen index, N/Y corresponds to NO/YES for dripping during the first/second flame application.

2.2.3. Mechanism of char formation

Long chain APP (Form II) was used as flame retardant in PLA polymer. Upon decomposition of APP, phosphoric acid and ammonia was formed. Phosphoric acid acted as acid catalyst in the dehydration process of hydroxyl groups in starch. Upon reaction of acid catalyst (phosphoric acid) with hydroxyl groups in starch, phosphate esters were formed that were decomposed later to release carbon dioxide, and dehydration of starch took place. In the gas phase, the emission of carbon dioxide helped in dilution of the oxygen present in air together with the by-products that were ignited during decomposition of the materials, whereas the resultant char layer in the condensed phase protected the underlying polymeric material from further burning by restricting the free passage of radiant heat and oxygen. This mechanism of intumescence is shown in Figure 2.1.

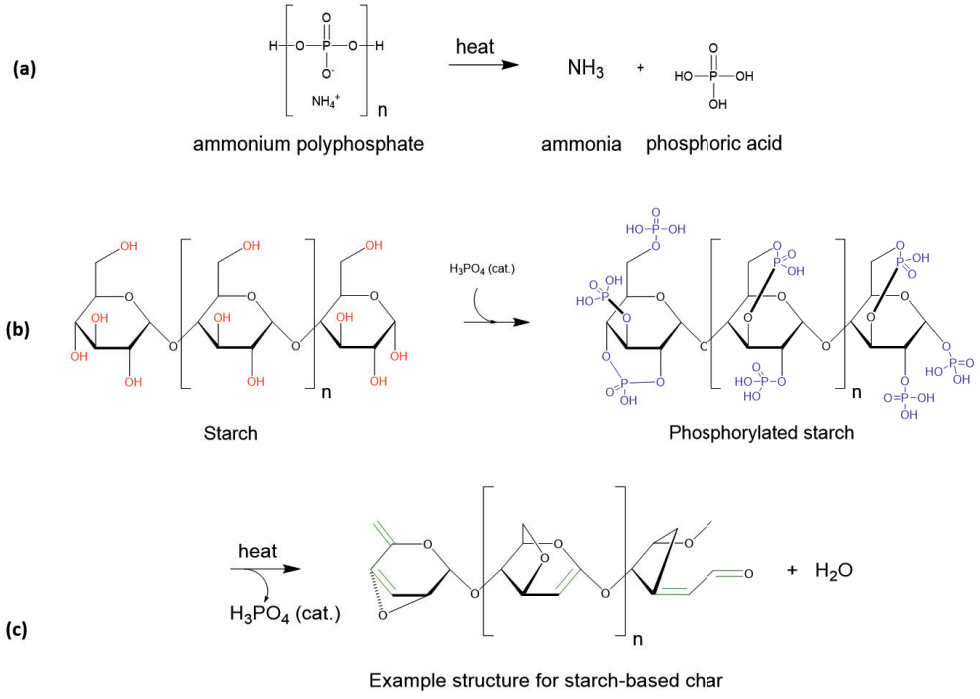

Figure 2.1. Thermal decomposition of ammonium polyphosphate into ammonia and ortho-phosphoric acid (**a**), Catalytic phosphorylation to produce phosphate esters (**b**), Dehydration of starch and formation of starch-based char structure (**c**).

2.2.4. Limiting oxygen index and UL-94 vertical burning test

The limiting oxygen index (LOI) is the fraction of oxygen that must be present to support burning, hence higher LOI values indicate lower flammability. The specimens (100 × 10 × 3 mm^3, as required by ISO 4589) were vertically placed in a glass column supplied with a mixture of oxygen and nitrogen gas and were then ignited from above using a downward-pointing flame. The LOI test was conducted using a Stanton Redcroft instrument (Illinois Toolworks, Glenview, IL, USA). The UL-94 test classifies materials based on their ability to either promote or inhibit the spread of fire once it has been ignited. UL-94 tests were conducted using specimens with dimensions of 100 × 10 × 3 mm^3 as required by ISO 9773. A flame was applied to the bottom of a vertically supported specimen, and the response was assessed after removing the flame. Specimens that self-extinguish and do not drip after burning are ranked highest in the classification (V-0).

2.2.5. Cone calorimetry test

Cone calorimetry works on the principle of oxygen consumption and states that the total heat of combustion of a specimen depends on the quantity of oxygen consumed. The cone calorimeter tests were conducted on specimens with dimensions of 100 × 100 × 3 mm^3 as required by ISO 5660 using a Stanton Redcroft instrument. The samples were exposed to a heat flux of 35 kW m^{-2}. We then recorded the heat release rate (HRR), total heat release (THR), time to ignition (TTI), and percentage mass residue after burning.

2.2.6. Thermogravimetric analysis

Thermogravimetric analysis (TGA) was conducted using a Q5000 device (TA Instruments, New Castle, DE, USA). The specimens (4–5 mg) were heated at a constant rate of 10 °C min^{-1} up to 700 °C under nitrogen at a flow rate of 50 mL min^{-1}. The thermal degradation temperature and the temperature at which maximum degradation took place were calculated along with the residual percentage mass of the sample and TGA curves were plotted for each specimen.

2.2.7. Scanning electron microscopy

The surface morphology, dispersion of FR additives in the PLA matrix and char residues of PLA/APP and PLA/APP/ST composites were investigated by scanning electron microscopy (SEM) using a TM-1000 table-top microscope (Hitachi, Chiyoda, Tokyo, Japan). The samples

were immersed in liquid nitrogen followed by freeze fracturing and gold sputtering to produce a conductive surface.

2.2.8. Mechanical testing

Mechanical properties such as tensile strength, elongation at break and Young's modulus of PLA, PLA/APP and PLA/APP/ST composites were tested by Zwick Roell Z020TH allround-line table-top machine (Zwick GmbH & Co.KG, Ulm, Germany) at a speed of 50 mm min^{-1}. The test specimens of dog bone shape were prepared as per standard EN ISO 527-2 method using a molding press. Six specimens were prepared from each formulation, and their average results with standard deviations were recorded. Specimens dimensions used were 170 × 20 × 3 mm^3.

2.3. Results and discussion

2.3.1. Determining the burning behavior of PLA/IFR samples

The LOI and UL-94 tests are widely accepted to assess the flame retardancy of FR composites and the corresponding results (including dripping behavior) for the PLA/APP and PLA/APP/ST composites are summarized in Table 2.1. Pure PLA did not pass UL-94 test because it was highly flammable with prolific dripping, and the LOI was 19.5%. The addition of 10 wt% APP (PLA/APP10) increased the LOI to 24.4% and the composite achieved a V-2 rating in UL-94 test. The presence of 15 and 20 wt% APP (PLA/APP15 and PLA/APP/20) increased the LOI to 28.5% and 31.9%, respectively, and both composites obtained a V-1 and V-0 rating in UL-94 test respectively. Even so, both of these composites showed some dripping behavior during second flame application.

With the addition of 3 wt% ST (PLA/APP20/ST3), the LOI increased from 31.9% to 34.5%, and the composite retained its V-0 rating in the UL-94 test. There was also no evidence of dripping during first and subsequent test. Higher concentrations of ST (PLA/APP20/ST5 and PLA/APP20/ST7) increased the LOI to 36.2% and 37.3%, respectively, and both composites obtained V-0 classification in the UL-94 test. In this case, however, there was no dripping during either the first or the second test.

The char structure sheltered the underlying material from the external heat source, pyrolysis gases as well as from thermal degradation therefore the ignition process was either delayed or prevented

hence enhancing the flame retardancy of starch-based composites. The formation of char is ascribed by the decarboxylation and dehydration reactions caused by the catalytic effect of starch in PLA/APP/ST composites. These results confirmed that the introduction of ST as a natural carbonization agent increased the LOI values of the FR composites significantly while simultaneously inhibiting the melt-dripping phenomenon. All composites containing ST managed to obtain a V-0 rating in the UL-94 test. Compared to a similar study done by Marosi et al. [25], where they achieved LOI value of 34% by adding up to 11 wt% of carbon source, we managed to achieve LOI value of 37.3% by adding only 7 wt% of starch.

The addition of APP in the concentration range of 10% (w/w) to 20% (w/w) enhanced the LOI from 24.4% (PLA/APP10) to 31.9% (PLA/APP20) (Table 2.1). By increasing the amount of APP, a higher concentration of oxygen is needed to achieve the ignition of the sample due to the dilution of the fuel in the gas phase by the discharge of water vapor as a result of the dehydration of APP. The addition of ST to the formulations not only increased the LOI of the samples but also increased the mass residue, providing enhanced shielding against heat and a barrier against the emission of pyrolysis gases that act as fuel. Therefore, the emission of fuel in the gas phase is minimized by the addition of ST.

The UL-94 test classifies materials based on their ability to either promote or inhibit the spread of fire once it has been ignited. Pure PLA ignited during the first flame application (10 s), and the sample continued to burn until it was fully consumed. Although PLA/APP10 and PLA/APP15 performed better as flame-retardants (flame extinguished less than 30 s after each flame application; V-2 and V-1 ratings, respectively), the dripping of the burning sample ignited the cotton placed beneath. Similarly, PLA/APP20 achieved a V-0 rating because the flame was extinguished in less than 10 s, but these samples still showed dripping behavior during second flame application. In contrast, none of the composites containing starch was dripping even after the second application of flame and all achieved a V-0 rating due to the generation of char layer on the surface, which isolated the remaining sample and prevented the propagation of the flame. In previous studies [9,27], even the addition of 30–40% (w/w) PER as a carbonization agent was sufficient to achieve only a V-2 rating, whereas here we found that as little as 3% starch in the presence of 20% APP accomplished the target rating of V-0. Hence, these results are in good

relation with the main hypothesis of this study. The photographs of the test samples after UL-94 test are shown in Figure 2.2, which confirms the formation of char layer after burning on samples surface containing starch as carbonization agent.

Figure 2.2. Photographs of pure PLA (**a**), PLA/APP10 (**b**), PLA/APP15 (**c**), PLA/APP20 (**d**), PLA/APP20/ST3 (**e**), PLA/APP20/ST5 (**f**), and PLA/APP20/ST7 (**g**) composites after UL-94 test.

2.3.2. Measuring the heat release rate, total heat release and residual mass%

Cone calorimetry provides broad information about the combustion behavior of polymers by measuring parameters such as time to ignition (TTI), peak heat release rate (PHRR), and total heat release (THR), which can predict their behavior in real-life fires. The heat release rate (HRR) curves of pure PLA, PLA/APP10, PLA/APP15, PLA/APP20, PLA/APP20/ST3, PLA/APP20/ST5, and PLA/APP20/ST7 are presented in Figure 2.3 (a & b). Following ignition,

pure PLA burnt much faster than the other samples and produced a very sharp HRR curve with a PHRR of 570 kW m^{-2}. For composite PLA/APP20, the PHRR declined to 337 kW m^{-2}, and with the further addition of 3 wt% ST (PLA/APP20/ST3), the PHRR was even lower, at 212 kW m^{-2}. At the maximum 7 wt% ST content we tested (PLA/APP20/ST7), the PHRR was only 192 kW m^{-2}, which is 66.30% of the pure PLA value. These findings indicated that the combined effect of APP and ST allowed the formation of a much thicker char layer on the surface of the composites after ignition, which prevented the degradation of the composite by restricting the fire passage into the polymer matrix.

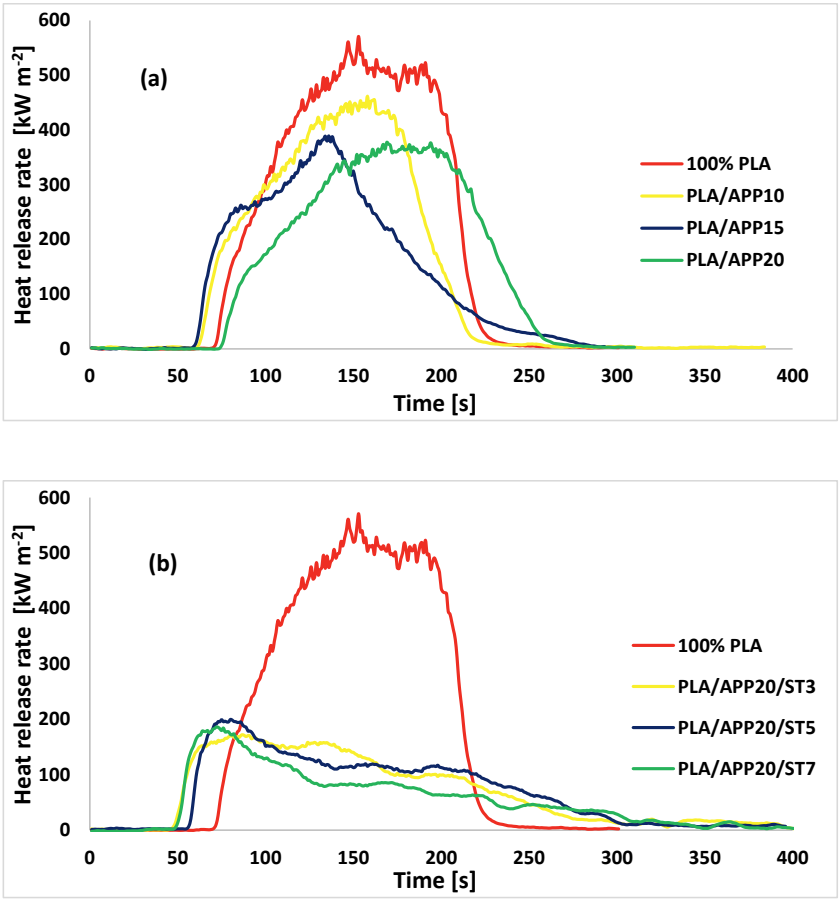

Figure 2.3. (**a**) Heat release rate curves of pure PLA and PLA/APP composites. (**b**) Heat release rate curves of pure PLA and PLA/APP/ST composites.

In IFR systems, flame retardancy is achieved by the swelling of the substrate in the condensed phase, which generates a sponge-like multicellular structure called char that shelters the principal material from heat transfer. The char structure also acts as a physical barrier against fuel and mass transfer from the condensed phase to the site of burning. Figure 3 (a,b) demonstrates that the heat release rate of the composites containing APP alone (PLA/APP10, PLA/APP15, and PLA/APP20) or together with starch (PLA/APP20/ST3, PLA/APP20/ST5, and PLA/APP20/ST7) changed dramatically in comparison to pure PLA (570 kW m^{-2}). In samples containing APP alone, the intumescent char layer was thinner and more porous than in samples containing APP and ST. This is because the absence of ST lowered the viscosity of the char layer, in turn allowing vapor and gas bubbles to escape and reducing the degree of swelling because little pressure was allowed to build up. The resulting porous structure allowed further fuel gases and water vapor to pass through the unclosed cells, increasing the PHRR. In contrast, the higher viscosity of the char layer containing ST made the char more compact and prevented the escape of gases and vapor, resulting in a pressure build up that increased the melt viscosity of the condensed phase and resulted in more swelling of the char. The combined effect of APP and ST therefore reduced the PHRR to 192 kW m^{-2}, which is 66.30% less than pure PLA. The HRR in this study is much lower than reported in other studies of PLA composites containing different carbonization agents [28–30].

Table 2.2 shows that the TTI of pure PLA was 41 s, increasing to 58 s when APP was incorporated into the PLA matrix (PLA/APP20) and to 77 s when the maximum content of starch was included (PLA/APP20/ST7). The ignition of a material is normally dependent on the concentration of pyrolysis gases, which are released when a material is degraded. The concentration of the gases increases during material degradation and ignition starts when they reach a certain threshold. Longer ignition times reflect the slower decomposition of the material mainly due to the presence of starch together with APP. A uniform and compact char structure can hinder the diffusion of pyrolysis gases from the melting substrate to the site of burning. The lower TTI of the samples containing APP alone is mainly due to the emission of more pyrolysis gases, reflecting the weaker swelling of the substrate and the generation of a porous structure as discussed above. The TTI is therefore, increased by the more compact char structure in the PLA/APP/ST composites.

Table 2.2. Cone calorimetry data for pure PLA, PLA/APP, and PLA/APP/ST composites.

No.	Formulation	TTI (s)	PHRR (kW m^{-2})	THR (MJ m^{-2})	Residual Mass (%)
1	PLA	41 ± 1.3	570 ± 4	58 ± 0.11	0 ± 0.00
2	PLA/APP10	48 ± 1.7	461 ± 6	46 ± 0.18	14 ± 0.03
3	PLA/APP15	53 ± 2.2	378 ± 7	44 ± 0.32	17 ± 0.06
4	PLA/APP20	58 ± 1.5	337 ± 4	38 ± 0.23	22 ± 0.08
5	PLA/APP20/ST3	63 ± 2.1	212 ± 6	28 ± 0.19	26 ± 0.05
6	PLA/APP20/ST5	67 ± 1.4	200 ± 5	26 ± 0.13	37 ± 0.04
7	PLA/APP20/ST7	77 ± 1.8	192 ± 3	24 ± 0.28	43 ± 0.06

TTI = time to ignition; PHHR = peak heat release rate; THR = total heat release

Figure 2.4 (a & b) shows the THR curves of pure PLA and the PLA composites. Figure 2.4 (a) indicates that the THR of pure PLA was 58 MJ m^{-2} whereas the PLA/APP20 and PLA/APP20/ST7 composites emitted only 37 and 24 MJ m^{-2}, respectively. The PLA/APP20 and PLA/APP20/ST7 composites therefore limited the total amount of fuel accessible for burning, which confirms the superior FR properties of these composites. The combination of starch and APP makes the composites more flame resistant. The formation of intumescent char on matrix surface improves the thermal insulation between the flame and material's surface. This extinguishes the flame by preventing access to combustible gases and oxygen at the site of the fire.

The combination of ST and APP makes the composites more flame resistant, and the formation of intumescent char on the matrix surface introduced a layer of thermal insulation between the flame and the surface of the material, which extinguished the flame by preventing contact with combustible gases as well as oxygen. The high concentrations of APP and ST diluted the polymer matrix, providing less material for continued burning. Thermal decomposition therefore led to the dehydration of APP, and the resulting water vapors cooled the gas phase and diluted the fuel, thus reducing the total heat release (THR) in proportion with the increasing APP content. Due to the endothermic decomposition of APP, the heating of the condensed phase was also limited. The presence of ST exacerbated this effect because the emission of pyrolysis gases was inhibited by the formation of the char layer, which provided a physical barrier and enhanced the heat shielding

effect. In previous studies involving PLA composites with other carbonization agents, the THR was much higher than the values reported here [11,31,32].

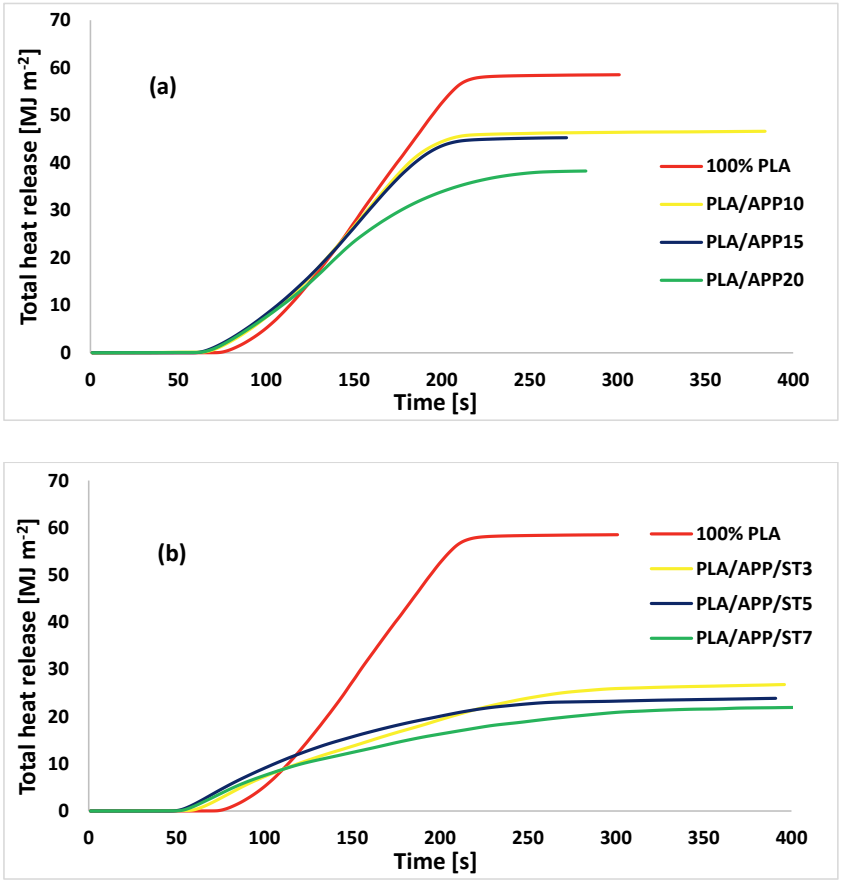

Figure 2.4. (**a**) Total heat release curves of pure PLA and PLA/APP composites. (**b**) Total heat release curves of pure PLA and PLA/APP/ST composites.

Figure 2.5 (a & b) shows the residual mass% after burning for pure PLA, PLA/APP, and PLA/APP/ST composites. No residual mass was left following the burning of pure PLA, but both PLA/APP20 and PLA/APP20/ST7 left mass residues corresponding to 22.74% and 43.00% of the starting mass, respectively, as shown in Table 2.2. The relatively large proportion of residual mass (char residue) for PLA/APP20/ST7 probably reflects the development of a structure that hindered

the passage of fuel and heat during combustion. The higher residual mass correlated with the production of more char, which in turn reflects the lower THR values. The greater residual mass also reflects an increase in char formation due to the combined effect of the acid and carbonization agent. The percentage residual mass achieved in this study is also higher than that reported in previous studies of PLA composites containing alternative carbonization agents [17,33].

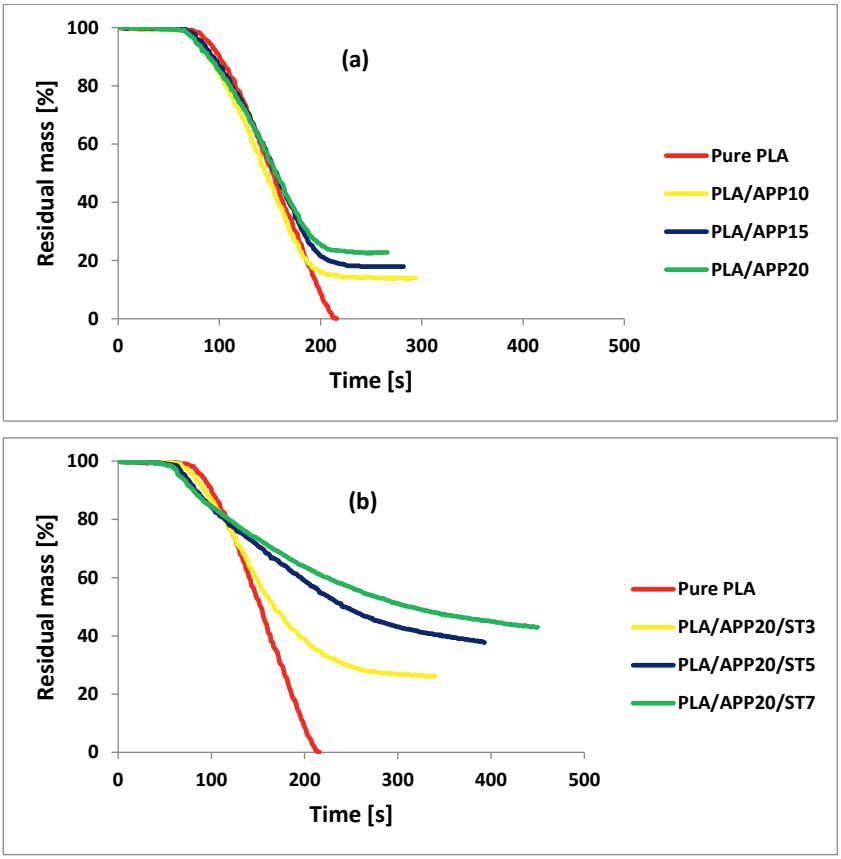

Figure 2.5. (**a**) Residual mass% of pure PLA and PLA/APP composites. (**b**) Residual mass% of pure PLA and PLA/APP/ST composites.

Figure 2.6 shows images of the residual samples after cone calorimetry test. As stated above, there was almost no residue of pure PLA, but the samples containing APP and starch presented intumescence with char on the surface, which was thicker and more stable in the case of

PLA/APP20/ST7. The char residues of PLA/APP10, PLA/APP15 and PLA/APP20 were loosely bound due to the non-cohesion of the agglomerates, and the structure in each case was porous and discontinuous due to insufficient char formation as indicated by the SEM analysis of char residues in Figure 2.7. Heat and mass transfer therefore could not be inhibited effectively in these composites. In contrast, the samples containing ST (particularly PLA/APP20/ST7) produced a more compact char (Figure 2.7) with a dense and uniform structure, reducing the heat and mass transfer to inhibit combustion and prevent further burning of the underlying polymeric substrate. These char structures were stable, more uniform, and compact due to the cohesion of the agglomerates. ST particles were supposed to fill the empty spaces between the APP particles, with a resulting increase in density. The thickness of the samples containing ST also increased dramatically due to char formation after burning, from an initial thickness of 3 mm to approximately 1.5–2.0 cm.

Figure 2.6. Photographs of the residues of PLA/APP10 (**a**), PLA/APP15 (**b**), PLA/APP20 (**c**), PLA/APP20/ST3 (**d**), PLA/APP20/ST5 (**e**), and PLA/APP20/ST7 (**f**) after cone calorimetry test.

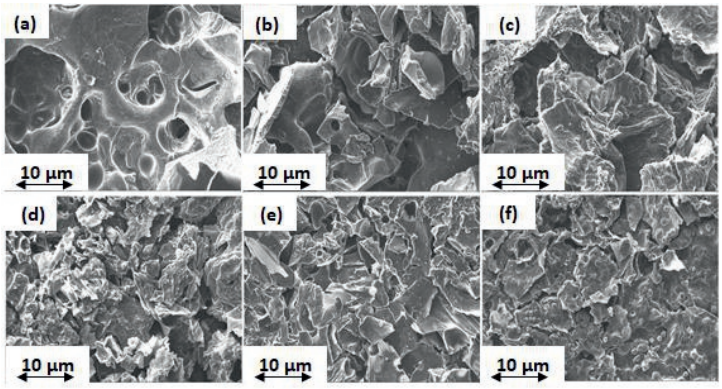

Figure 2.7. SEM analysis of the residues of PLA/APP10 (**a**), PLA/APP15 (**b**), PLA/APP20 (**c**), PLA/APP20/ST3 (**d**), PLA/APP20/ST5 (**e**), and PLA/APP20/ST7 (**f**) after cone calorimetry test. Scale bar in all panels = 10 µm, Magnification = 710×

2.3.3. Investigating the thermal stability of PLA/IFR samples

The thermal decomposition and thermal stability of polymers is assessed by thermogravimetric analysis (TGA). The thermal degradation and mass residue of the samples were compared to determine the influence of flame-retardants and starch on PLA-based composites. TGA curves and data for all the composites heated in a nitrogen atmosphere are presented in Figure 2.8 (a & b) and in Table 2.3, respectively.

Table 2.3. Thermogravimetric analysis of PLA/APP and PLA/APP/ST composites.

No	Formulations	T_5 (°C)	T_{50} (°C)	T_{max} (°C)	Residue at 700 °C (wt %)
1	PLA	325	372	377	0.00
2	PLA/APP10	320	374	379	5.90
3	PLA/APP15	346	376	378	8.16
4	PLA/APP20	358	376	378	9.21
5	PLA/APP20/ST3	365	380	379	13.34
6	PLA/APP20/ST5	371	381	380	15.32
7	PLA/APP20/ST7	373	383	380	19.30

T_5 = 5% weight loss, T_{50} = 50% weight loss, T_{max} = Maximum rate of weight loss

In Table 2.3, the temperatures corresponding to 5% and 50% weight loss for each composite are represented by the T5 and T50 values, respectively, whereas the temperature corresponding to the maximum rate of weight losses is represented by T max. The degradation of pure PLA started at 325 °C and 50% loss occurred at 372 °C, with no residue left at 700 °C. A similar trend was observed for PLA/APP10 for the T5 and T50 temperatures, but the residue left at 700 °C was 5.90% of the initial mass. For PLA/APP15 and PLA/APP20, the initial decomposition temperatures and thermal stabilities were greater than the corresponding values for PLA/APP10, with 8.16% and 9.21% residual mass left at 700 °C. The introduction of starch further improved the thermal stability of the composites. The initial decomposition temperatures and thermal stabilities of all composites containing starch are higher compared to composites without starch. For example, composite PLA/APP20/ST3 increased the residual mass at 700 °C from 9.21% to 13.34%, but this increased even further to 19.30% in the case of composite PLA/APP20/ST7.

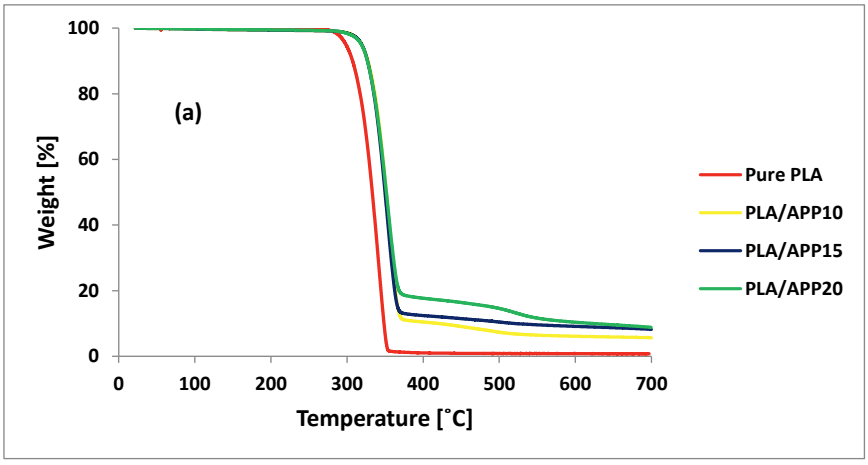

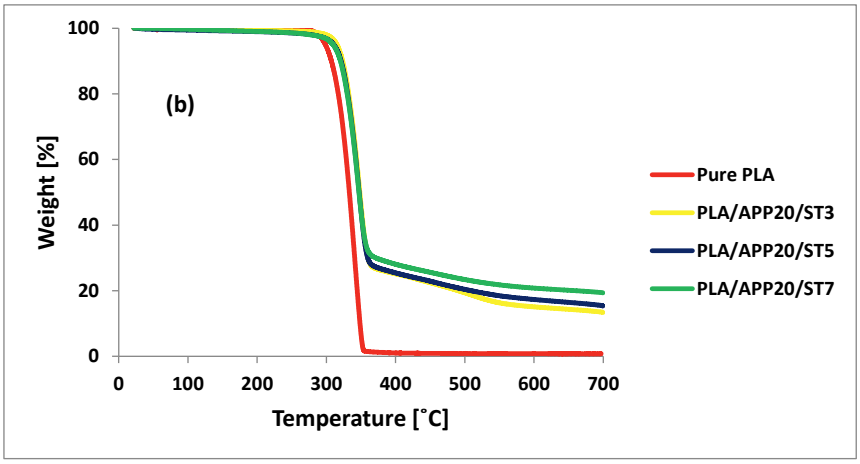

Figure 2.8. (**a**) Thermogravimetric analysis curves of pure PLA and PLA/APP composites. (**b**) Thermogravimetric analysis curves of pure PLA and PLA/APP/ST composites

Figure 2.8 (a) represents the TGA curves for PLA/APP composites in comparison to pure PLA whereas Figure 2.8 (b) shows TGA curves for PLA/APP/ST composites. These composites differ in terms of their initial decomposition temperatures and thermal stabilities. The initial decomposition temperature of PLA/APP20/ST7 was 373 °C, compared to 365 °C for PLA/APP20/ST3, and the residues left at 700 °C were 19.30% and 13.34% of the initial mass, respectively. PLA/APP20/ST7 is therefore more thermally stable, reflecting the denser and more compact char layer as discussed above. These TGA data are in strong agreement with the LOI, UL-94 and cone calorimetry experiments, indicating that composites containing starch are superior in performance to composites containing APP alone.

2.3.4. Dispersion of the additives in PLA matrix

Better FR properties are achieved by the uniform dispersion of additives in the PLA matrix. We therefore investigated the appearance of various percentages of FR additives (APP) and starch (ST) dispersed into the PLA matrix by scanning electron microscopy (SEM). Figure 2.9 shows the SEM images of the PLA/APP10 (a), PLA/APP15 (b), PLA/APP20 (c), PLA/APP20/ST3 (d), PLA/APP20/ST5 (e), and PLA/APP20/ST7 (f) composites. We observed APP and ST particles of

different sizes and shapes, and with different levels of interfacial adhesion with the PLA matrix. In all formulations of PLA/APP, the FR additive was uniformly distributed. The appearance of the dispersions was similar regardless of the FR content, indicating that the additives and substrate mixed uniformly during sample preparation. However, we observed very weak interfacial bonding between the FR additive and PLA substrate as shown by the appearance of small holes during fracturing. In the PLA/APP/ST composites, the dispersion of APP and ST was less uniform compared to the PLA/APP composites because the additives were less compatible with each other in PLA matrix, therefore forming isolated or aggregated particles on the composites surfaces. These clustered and agglomerated particles were clearly seen in the SEM images. However, all images indicated that APP and ST were successfully incorporated into the PLA matrix.

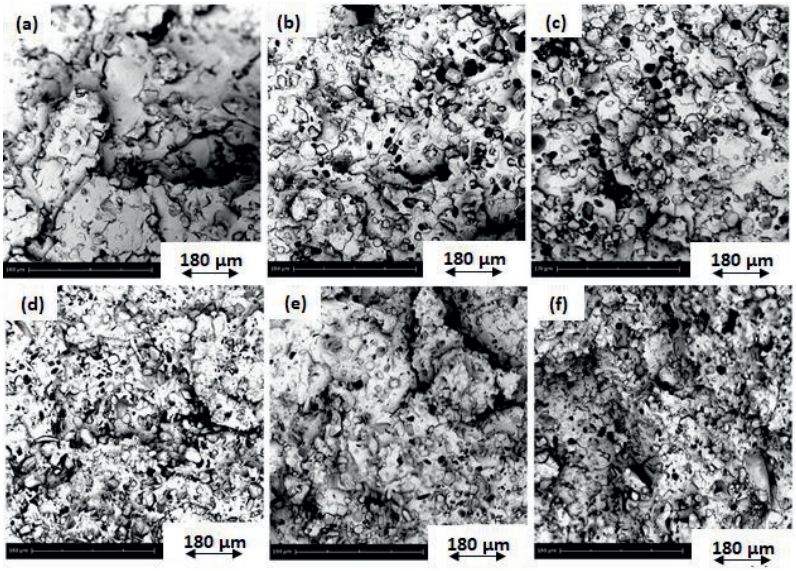

Figure 2.9. SEM analysis of PLA/APP10 (**a**), PLA/APP15 (**b**), PLA/APP20 (**c**), PLA/APP20/ST3 (**d**), PLA/APP20/ST5 (**e**), and PLA/APP20/ST7 (**f**) composites. Scale bar in all panels = 180 µm, Magnification = 710×

2.3.5. Determining the tensile strength, Young's modulus and elongation at break%

The mechanical properties of composites are dependent on the actual stress sharing between matrix and the additives incorporated. Therefore, in order to get better mechanical properties of a

composite a uniform interfacial bonding between additives and matrix is needed. Moreover, the size of particles, wt% (w/w) of additives incorporated as well as the adhesion between additives and matrix influence the mechanical properties of polymer composites. As indicated in SEM images in the previous section a weak interfacial bonding between additives and polymer matrix was observed, due to which clustered and agglomerated particles were formed which affected the mechanical strength of the composites.

It can be seen in Table 2.4 that the tensile strength and elongation at break of pure PLA was 69.19 (MPa) and 2.49% respectively. However, with the addition of APP alone the tensile strength and elongation at break started to decrease and reached to 45.62 (MPa) and 1.98%, respectively, when 20 wt% of APP (PLA/APP20) was incorporated in PLA matrix. When starch was incorporated together with APP in polymer matrix (PLA/APP/ST), tensile strength and elongation at break was further reduced. The reduction in mechanical properties of PLA/APP and PLA/APP/ST composites is mainly due to weak interfacial bonding initiated by the difference in polarity among PLA matrix, APP, and starch additives.

Table 2.4. Mechanical properties of PLA, PLA/APP, and PLA/APP/ST composites.

Formulations	Tensile Strength ± (MPa)	Elongation at Break ± (%)	Young's Modulus ± (MPa)
PLA	69.19 ± 3	2.49 ± 0.2	4695.43 ± 21
PLA/APP10	47.86 ± 1	2.35 ± 0.4	4146.65 ± 18
PLA/APP15	46.12 ± 2	2.03 ± 0.3	4087.90 ± 17
PLA/APP20	45.62 ± 2	1.98 ± 0.1	3822.11 ± 15
PLA/APP20/ST3	43.93 ± 2	1.94 ± 0.1	3750.73 ± 13
PLA/APP20/ST5	39.30 ± 1	1.87 ± 0.1	2870.04 ± 14
PLA/APP20/ST7	38.41 ± 1	1.66 ± 0.1	2522.32 ± 11

Another reason of weaker mechanical properties could be due to the degradation of PLA as well as of starch during preparation of PLA composites due to higher extrusion temperature, which might have reduced the adsorbed chains mobility on the surface of the particles. Therefore, in order to improve the mechanical properties of PLA composites a uniform dispersion of additives in polymer matrix may be required which sometimes can be obtained by the use of a compatibilizer.

Although the addition of starch in polymer matrix decreased the mechanical properties of the composites, however extraordinary improvements in the flame-retardant properties of these composites were seen.

2.4. Conclusions

We have produced intumescent flame-retardant composites by combining PLA and APP with starch as a carbonization agent. PLA/APP and PLA/APP/ST composites were prepared, and their flammability was assessed by LOI, UL-94 and cone calorimetry tests. The addition of 10–20 wt% APP improved the LOI of PLA from 19.5 to 24.4–31.9%, but the further inclusion of 7 wt% starch (PLA/APP20/ST7) improved the LOI from 31.9% to 37.3% and the composite achieved a V-0 rating in the UL-94 test with no dripping. The PHRR and THR of the composites containing starch were significantly lower than the corresponding values for pure PLA and composites containing APP alone. A remarkably low PHRR was observed for PLA/APP20/ST7 (192 kW m^{-2}) which is 66% less than the PHRR of pure PLA. The presence of 20 wt% APP in PLA matrix (PLA/APP20) increased the TTI to 58 s, but the addition of 7 wt% starch in addition to APP (PLA/APP20/ST7) extended this to 77 s. The THR of pure PLA was 58 MJ/m^2, falling to 38 MJ/m^2 for PLA/APP20 and 24 MJ/m^2 for PLA/APP20/ST7. The composites therefore limited the total quantity of fuel accessible for burning. The introduction of APP together with starch enhanced the thermal stability of the composites, with PLA/APP20/ST7 leaving 19.30% residual mass at 700 °C comparted to only 9.21% for PLA/APP20 and no residue for pure PLA. The fire-retardant mechanism was determined by cone calorimetry, revealing that char formation inhibited the initial decomposition of the composite and improved its thermal stability by creating a char layer, which prevented the transfer of sufficient fuel and oxygen to the site of burning. Our tests therefore, confirmed that intumescent system containing starch as a renewable carbonization agent can be used to produce superior PLA composites.

2.5. References

1. Cayla, A.; Rault, F.; Giraud, S.; Salaün, F.; Fierro, V.; Celzard, A. PLA with intumescent system containing lignin and ammonium polyphosphate for flame retardant textile. Polymers **2016**, 8, doi:10.3390/polym8090331.
2. Cheng, K.C. Flammability and tensile properties of polylactide nanocomposites with short carbon fibers. J. Mater. Sci. **2015**, 50, 1605–1612, doi:10.1007/s10853-014-8721-2.

3. Cheng, X.; Guan, J.; Tang, R.; Liu, K. Improvement of flame retardancy of poly (lactic acid) nonwoven fabric with a phosphorus- containing flame retardant. J. Ind. Text. **2015**, 1–12, doi:10.1177/1528083715606105.
4. Idumah, C.I.; Hassan, A. Emerging trends in flame retardancy of biofibers, biopolymers, biocomposites, and bionanocomposites. Rev. Chem. Eng. **2016**, 32, 115–148, doi:10.1515/revce-2015-0017.
5. Atabek Savas, L.; Mutlu, A.; Dike, A.S.; Tayfun, U.; Dogan, M. Effect of carbon fiber amount and length on flame retardant and mechanical properties of intumescent polypropylene composites. J. Compos. Mater. **2017**, 1–12, doi:10.1177/0021998317710319.
6. Depeng, L.; Chixiang, L.; Xiulei, J.; Tao, L.; Ling, Z. Synergistic effects of intumescent flame retardant and nano-$CaCO_3$ on foamability and flame-retardant property of polypropylene composites foams. J. Cell. Plast. **2017**, 1–17, doi:10.1177/0021955X17720157.
7. Duquesne, S.; Samyn, F.; Ouagne, P.; Bourbigot, S. Flame retardancy and mechanical properties of flax reinforced woven for composite applications. J. Ind. Text. **2015**, 44, 665–681, doi:10.1177/1528083713505633.
8. Wang, D.Y.; Leuteritz, A.; Wang, Y.Z.; Wagenknecht, U.; Heinrich, G. Preparation and burning behaviors of flame retarding biodegradable poly(lactic acid) nanocomposite based on zinc aluminum layered double hydroxide. Polym. Degrad. Stab. **2010**, 95, 2474–2480, doi:10.1016/j.polymdegradstab.2010.08.007.
9. Bourbigot, S.; Duquesne, S.; Fontaine, G.; Bellayer, S.; Turf, T.; Samyn, F. Characterization and Reaction to Fire of Polymer Nanocomposites with and without Conventional Flame Retardants. Mol. Cryst. Liq. Cryst. **2008**, 486, 37–41, doi:10.1080/15421400801921983.
10. Wang, D.Y.; Song, Y.P.; Lin, L.; Wang, X.L.; Wang, Y.Z. A novel phosphorus-containing poly(lactic acid) toward its flame retardation. Polymer **2011**, 52, 233–238, doi:10.1016/j.polymer.2010.11.023.
11. Qian, Y.; Wei, P.; Jiang, P.; Li, Z.; Yan, Y.; Ji, K. Aluminated mesoporous silica as novel high-effective flame retardant in polylactide. Compos. Sci. Technol. **2013**, 82, 1–7, doi:10.1016/j.compscitech.2013.03.019.
12. Solarski, S.; Mahjoubi, F.; Ferreira, M.; Devaux, E.; Bachelet, P.; Bourbigot, S.; Delobel, R.; Coszach, P.; Murariu, M.; Da Silva Ferreira, A.; et al. Designing Polylactide/Clay nanocomposites for textile applications: Effect of processing conditions, spinning, and

characterization. Polym. Polym. Compos. **2013**, 21, 449–456, doi:10.1002/app.

13. Thunga, M.; Chen, K.; Grewell, D.; Kessler, M.R. Bio-renewable precursor fibers from lignin/polylactide blends for conversion to carbon fibers. Carbon **2014**, 68, 159–166, doi:10.1016/j.carbon.2013.10.075.
14. Katsoulis, C.; Kandare, E.; Kandola, B.K. The combined effect of epoxy nanocomposites and phosphorus flame retardant additives on thermal and fire reaction properties of fiber-reinforced composites. J. Fire Sci. **2011**, 29, 361–383, doi:10.1177/0734904111398785.
15. Wang, J.; Manley, R.S.J.; Feldman, D. Synthetic polymer-lignin copolymers and blends. Prog. Polym. Sci. **1992**, 17, 611–646, doi:10.1016/0079-6700(92)90003-H.
16. Wang, K.; Wang, J.; Zhao, D.; Zhai, W. Preparation of microcellular poly(lactic acid) composites foams with improved flame retardancy. J. Cell. Plast. **2017**, 53, 45–63, doi:10.1177/0021955X16633644.
17. Zhan, J.; Song, L.; Nie, S.; Hu, Y. Combustion properties and thermal degradation behavior of polylactide with an effective intumescent flame retardant. Polym. Degrad. Stab. **2009**, 94, 291–296, doi:10.1016/j.polymdegradstab.2008.12.015.
18. Zhang, R.; Xiao, X.; Tai, Q.; Huang, H.; Yang, J.; Hu, Y. Preparation of lignin-silica hybrids and its application in intumescent flame-retardant poly(lactic acid) system. High Perform. Polym. **2012**, 24, 738–746, doi:10.1177/0954008312451476.
19. Cheng, X.W.; Guan, J.P.; Tang, R.C.; Liu, K.Q. Phytic acid as a bio-based phosphorus flame retardant for poly(lactic acid) nonwoven fabric. J. Clean. Prod. **2016**, 124, 114–119, doi:10.1016/j.jclepro.2016.02.113.
20. Zhang, T.; Yan, H.; Shen, L.; Fang, Z.; Zhang, X.; Wang, J.; Zhang, B. Chitosan/phytic acid polyelectrolyte complex: A green and renewable intumescent flame retardant system for ethylene-vinyl acetate copolymer. Ind. Eng. Chem. Res. **2014**, 53, 19199–19207, doi:10.1021/ie503421f.
21. Feng, J.X.; Su, S.P.; Zhu, J. An intumescent flame retardant system using β-cyclodextrin as a carbon source in polylactic acid (PLA). Polym. Adv. Technol. **2011**, 22, 1115–1122, doi:10.1002/pat.1954.
22. Laufer, G.; Kirkland, C.; Cain, A.A.; Grunlan, J.C. Clay-chitosan nanobrick walls: Completely renewable gas barrier and flame-retardant nanocoatings. ACS Appl. Mater. Interfaces **2012**, 4, 1643–1649, doi:10.1021/am2017915.

23. Wang, J.; Ren, Q.; Zheng, W.; Zhai, W. Improved flame-retardant properties of poly(lactic acid) foams using starch as a natural charring agent. Ind. Eng. Chem. Res. **2014**, 53, 1422–1430, doi:10.1021/ie403041h.
24. Reti, C.; Casetta, M.; Duquesne, S.; Bourbigot, S.; Delobel, R. Flammability properties of intumescent PLA including starch and lignin. Polym. Adv. Technol. **2006**, 17, 395–418, doi:10.1002/pat.
25. Bocz, K.; Szolnoki, B.; Marosi, A.; Tábi, T.; Wladyka-Przybylak, M.; Marosi, G. Flax fibre reinforced PLA/TPS biocomposites flame retarded with multifunctional additive system. Polym. Degrad. Stab. **2014**, 106, 63–73, doi:10.1016/j.polymdegradstab.2013.10.025.
26. Pack, S.; Bobo, E.; Muir, N.; Yang, K.; Swaraj, S.; Ade, H.; Cao, C.; Korach, C.S.; Kashiwagi, T.; Rafailovich, M.H. Engineering biodegradable polymer blends containing flame retardant-coated starch/nanoparticles. Polymer **2012**, 53, 4787–4799, doi:10.1016/j.polymer.2012.08.007.
27. Teoh, E.L.; Mariatti, M.; Chow, W.S. Thermal and Flame Resistant Properties of Poly (Lactic Acid)/Poly (Methyl Methacrylate) Blends Containing Halogen-free Flame Retardant. Procedia Chem. **2016**, 19, 795–802, doi:10.1016/j.proche.2016.03.087.
28. Fukushima, K.; Murariu, M.; Camino, G.; Dubois, P. Effect of expanded graphite/layered-silicate clay on thermal, mechanical and fire retardant properties of poly(lactic acid). Polym. Degrad. Stab. **2010**, 95, 1063–1076, doi:10.1016/j.polymdegradstab.2010.02.029.
29. Lin, H.J.; Liu, S.R.; Han, L.J.; Wang, X.M.; Bian, Y.J.; Dong, L.S. Effect of a phosphorus-containing oligomer on flame-retardant, rheological and mechanical properties of poly (lactic acid). Polym. Degrad. Stab. **2013**, 98, 1389–1396, doi:10.1016/j.polymdegradstab.2013.03.025.
30. Murariu, M.; Bonnaud, L.; Yoann, P.; Fontaine, G.; Bourbigot, S.; Dubois, P. New trends in polylactide (PLA)-based materials: "Green" PLA-Calcium sulfate (nano)composites tailored with flame retardant properties. Polym. Degrad. Stab. **2010**, 95, 374–381, doi:10.1016/j.polymdegradstab.2009.11.032.
31. Wei, L.L.; Wang, D.Y.; Chen, H.B.; Chen, L.; Wang, X.L.; Wang, Y.Z. Effect of a phosphorus-containing flame retardant on the thermal properties and ease of ignition of poly(lactic acid). Polym. Degrad. Stab. **2011**, 96, 1557–1561, doi:10.1016/j.polymdegradstab.2011.05.018.

32. Fox, D.M.; Lee, J.; Citro, C.J.; Novy, M. Flame retarded poly(lactic acid) using POSS-modified cellulose. 1. Thermal and combustion properties of intumescing composites. Polym. Degrad. Stab. **2013**, 98, 590–596, doi:10.1016/j.polymdegradstab.2012.11.016.
33. Shabanian, M.; Kang, N.J.; Wang, D.Y.; Wagenknecht, U.; Heinrich, G. Synthesis of aromatic-aliphatic polyamide acting as adjuvant in polylactic acid (PLA)/ammonium polyphosphate (APP) system. Polym. Degrad. Stab. **2013**, 98, 1036–1042, doi:10.1016/j.polymdegradstab.2013.02.007.

CHAPTER 3

The efficiency of biobased carbonization agent and intumescent flame retardant on flame retardancy of biopolymer composites and investigation of their melt-spinnability

Abstract

The objective of this study is to assess the efficiency of biobased carbonization agent in intumescent formulations (IFRs) to examine the flame retardant properties of polylactic acid (PLA) composites and to investigate their melt-spinnability. We used phosphorous-based halogen free flame retardant (FR) and kraft lignin (KL) as bio-based carbonization agent. After melt compounding and molding into sheets by hot pressing various fire related characteristics of IFR composites were inspected and were characterized by different characterization methods. It was fascinating to discover that the introduction of 5−20 wt% FR increased the limiting oxygen index (LOI) of PLA composites from 20.1% to 23.2−33.5%. The addition of KL with content of 3−5 wt% further increased the LOI up to 36.6−37.8% and also endowed PLA/FR/KL composites with improved anti-dripping properties. Cone calorimetry revealed a 50% reduction in the peak heat release rate of the IFR composites in comparison to 100% PLA and confirmed the development of an intumescent char structure, containing residue up to 40%. For comparative study, IFR composites containing pentaerythritol (PER) as a carbonization agent were also prepared and their FR properties were compared. IFR composites were melt spun and mechanical properties of multifilament yarns were tested. The analysis of char residues by energy dispersive X-ray spectrometry (EDS) and SEM images confirmed that PLA/FR/KL composites developed a thicker and more homogeneous char layer with better flame retardant properties confirming that the fire properties of PLA can be enhanced by using KL as a carbonization agent.

Keywords

Bio-resources; Intumescence; Melt-spinning; Cone calorimetry

3.1. Introduction

Biodegradable polymers from renewable resources have attracted interest due to environmental pollution caused by the disposal of non-degradable polymers derived from finite petroleum reserves [1–4]. Polylactic acid (PLA) is a biobased thermoplastic polymer obtained from bio-resources and it is progressively replacing oil-based polymers and can be used to develop fire resistant products [5,6]. PLA is less flammable than synthetic thermoplastics such as polyethylene terephthalate (PET), with less visible smoke on burning and a lower peak heat release rate [7,8]. However, PLA is nevertheless combustible which restricts its applications in industry sectors where flame-retardant materials are required [9,10].

The fire retardancy of PLA can be enhanced by mixing with inorganic additives containing silicon or phosphorous [11–14]. Intumescent flame retardant (IFR) systems offer a highly effective strategy to enhance the fire retardancy of PLA because a char structure is developed which acts as a shield between the polymer and heat source hence protecting the polymer material from further burning and dripping [15]. These systems use halogen-free flame retardants (HFFRs) which are not only better for the environment but also more effective [16,17]. IFR systems generally comprise a carbonization agent, an acid source and a blowing agent that produces the char structure. In most of the studies [18–21] pentaerythritol (PER) a petroleum-based carbonization agent has been used in PLA based IFR systems. Flame retardancy in phosphorous based flame retardants is achieved by the thermal degradation of phosphorous compounds into pyrophosphate and the release of water which eventually dilutes the gas phase, hence the dehydration reaction is catalysed by pyro phosphoric acid [22,23].

Conventional carbonization agents such as PER achieve very low flame retardancy in PLA-based IFR systems [15,19] and different formulations have been therefore developed to overcome this challenge [22–24]. For example, PLA-based IFR composites containing PER achieved only a V-2 value in UL-94 vertical burning tests despite the addition of about 30–40% by weight of the flame-retardant additives, although a combination of PER and APP reduced the dripping behavior of PLA during combustion [25]. To replace PER in PLA-based IFR systems, other researchers have used additives such as spirocyclic pentaerythritol bisphosphorate disphosphoryl melamine [22], and graphene [13]. Another potential carbon source is lignin, which is an important component of

plant cells and the second most abundant natural material after cellulose [26]. Therefore lignin can be a potential candidate for carbonization agent in IFR systems because it contains phenyl-propane repeat units together with aromatic and aliphatic hydroxyl groups [27-28]. Moreover, the melt spinning of PLA/IFR composites is also unknown [29-30]. In this study, we have tried to optimize the wt% of the additives to improve the FR properties of the composites and to spin multifilaments from FR compounds.

We therefore investigated the effect of kraft lignin (KL) from wood waste as a carbonization agent in IFR systems as a potential biodegradable substitute for PER together with non-toxic and halogen free flame retardant. The mechanism of intumescence indicating catalytic phosphorylation to produce phosphate esters, which eventually dehydrated the lignin and formed char structure containing residue up to 52% has also been discussed in detail. We also tested flammability of different formulations of PLA/APP/KL prepared by melt compounding and then molding into sheets by hot pressing. We characterized the materials by different characterization techniques and measured their fire-retardant properties by conducting UL-94 vertical burning tests, cone calorimetry analysis and by determining the limiting oxygen index. The melt-spinnability of as prepared composites was investigated by producing multifilament yarns on pilot scale melt spinning machine and their mechanical properties were tested.

3.2. Materials and methods

The materials and methods used in this chapter are discussed in the following sections.

3.2.1. Materials

Granular PLA resin (Luminy L130) was attained from Total-Corbion NV (Gorinchem, Netherlands). Non-halogenated flame retardant Exolit APP 422, a fine-particle APP containing 14% w/w nitrogen and 31% w/w phosphorous (decomposition temperature > 275 °C), was obtained from Clariant Plastics & Coatings SA (Louvain-la-Neuve, Belgium). Exolit APP 422 is insoluble in water and thermally stable at higher temperatures due to long chains (n > 1000) and has been used as acid donor in this study. The kraft lignin powder “UPM BioPiva 100” was purchased from UPM Biochemicals OYJ (Helsinki, Finland). Pentaerythritol (PER) was obtained

from Acros (Molinons, France). PLA, APP, PER and KL were vacuum dried at 100 °C for 6 h before compounding.

3.2.2. Preparation of PLA/IFR composites

Coperion twin-screw compounder was used to prepare PLA/APP, PLA/APP/PER and PLA/APP/KL composites at 190 °C. In the first phase, PLA/APP composites with an APP content of 5%, 10%, 15% and 20% (w/w) were compounded at screw rotation speed of 150 rpm and were entitled PLA/APP5, PLA/APP10, PLA/APP15 and PLA/APP20, respectively. The temperatures of the three heating zones were kept at 175 °C, 180 °C and 185 °C, respectively. The extrudate was cut into pellets. In the second phase, PLA/APP20 pellets (APP content = 20% w/w) with a KL content of 3%, and 5% (w/w) were compounded at screw rotation speed of 200 rpm and were named PLA/APP20/KL3 and PLA/APP20/KL5, respectively. PLA/APP20 pellets were dosed in the first feeding zone whereas KL was fed in the second feeding zone to ensure proper mixing. The same procedure was adopted for PLA/APP20/PER3 and PLA/APP20/PER5 composites. Sheets of the as prepared composites were produced by compression molding at 190˚C for the subsequent testing along with sheets of pure PLA for comparison.

3.2.3. Thermogravimetric analysis

Thermogravimetric behavior of the composites as well as of 100% PLA was assessed using a TGA Q5000 from TA Instruments. The specimens (10–15 mg) were heated at a constant rate of 10˚C min^{-1} up to 700 °C under nitrogen at a flow rate of 50 $mL.min^{-1}$. The thermal decomposition temperature and the temperature at which maximum degradation took place were calculated along with the residual percentage of the sample compared to the initial mass. The thermogravimetric curves of specimens were plotted after analysis.

3.2.4. Scanning electron microscopy

The surface morphology of IFR composites, inspection of additives dispersion in the PLA matrix and energy dispersive X-ray spectrometry (EDS) was done by scanning electron microscopy using a Hitachi TM-1000 device (Chiyoda, Tokyo, Japan). Strands of IFR composites were fractured after dipping in liquid nitrogen and later on gold sputtering was done to produce a conductive surface prior to analysis.

3.2.5. Limiting oxygen index and UL-94 vertical burning tests

The limiting oxygen index (LOI) is known as the fraction of oxygen necessary to facilitate the burning of a test sample, so high LOI values indicate low flammability. The LOI test was conducted using a Stanton Redcroft instrument (Thermal Sciences, Mansfield, MA, USA) by placing samples (100 mm × 10 mm × 3 mm) vertically in a glass column and supplying a combination of oxygen and nitrogen gas. The specimens were burned with the flame pointing downwards to the non-burnt part according to standard test method ISO 4589. The UL-94 test classifies materials according to their ability to promote or inhibit the spread of fire. UL-94 vertical burning tests were conducted by suspending specimens (100 mm × 10 mm × 3 mm) vertically and applying a flame to the lower surface according to ISO 9773. Samples that demonstrate self-extinguishing behavior and that do not drip after burning are ranked highest in the classification (V-0).

3.2.6. Cone calorimetry test

Cone calorimetry tests were conducted by placing samples (100 mm × 100 mm × 3 mm) in a Stanton Redcroft instrument (Thermal Sciences) and exposing them to a heat flux of 35 kW m^{-2} according to a standard test method ISO 5660. We recorded important flammability parameters and mass residue as a proportion of initial sample weight.

3.2.7. Mechanical testing of multifilament yarns

The tenacity and elongation at break of multifilaments were tested on Zwick Roell testing machine by using EN ISO 5079 standard method. The specimen lengths (50 mm) and rate of deformation (50 mm min^{-1}) were kept constant for all samples. Ten specimens were prepared from each sample and their average results with standard deviations were recorded.

3.2.8. Melt spinning of IFR composites

IFR composites were melt spun using Fourne Maschinenbau GmbH (Impekoven, Germany) pilot scale melt spinning machine. Pellets were first fed into a hopper and then transported to a single screw extruder where they were melted at a temperature range of 195 °C to 220 °C. The melted material was then injected in a spinneret die of 1.2 mm diameter each with the help of spinning pump rotating at constant revolutions per minute ensuring a homogeneous flow of the material.

These single filaments coming out of the spinneret were then cooled at 18 °C by maintaining the cool air velocity of 0.5 $m \cdot s^{-1}$ and then combined together to multifilaments by applying a spin finish. The multifilaments were collected by a take up roller rotating at 450 m/min speed. The filaments were then hot drawn between two set of rollers rotating at varying speeds. The speeds of the first and second set of heated rollers were maintained at 550 m/min and 650 m/min respectively ensuring a draw ratio of 1.4 (maximum possible draw ratio). The multi-filaments were then winded on the winder at 650 m/min. A schematic diagram of pilot scale melt spinning machine is shown in Figure 3.1.

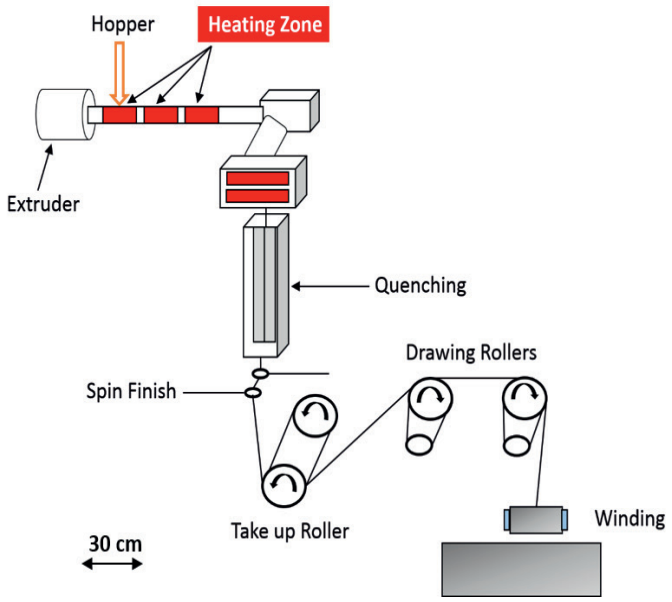

Figure 3.1. Schematic diagram of pilot scale melt spinning machine.

Composites were melt spun and it was observed that as the loading content of APP and KL was increased, the multifilament yarns were not able to withstand the same draw ratio, which was applied for pure PLA. For other compositions of composites, draw ratio was reduced gradually from 2 to 1.4 in order to spin the composites without breakage. This reduction in draw ratio resulted in lower mechanical properties of multifilament yarns produced from these composites predominantly due to amorphous nature with little or no crystallinity induced in the filament structure.

The tenacity and elongation at break of multifilament yarns are mainly influenced by the wt% (w/w) of the additives incorporated in the PLA matrix therefore the mechanical properties of the multifilament yarns containing higher amount of APP, PER and KL were on the lower side (Table 3.1) than that of multifilament yarns produced from pure PLA.

Table 3.1. Mechanical properties of pure PLA, PLA/APP and PLA/APP/KL multifilament yarns.

Formulations	Tenacity ± (cN/tex)	Elongation at Break ± (%)
PLA	17.88 ± 6	123.11 ± 23
PLA/APP5	14.44 ± 4	94.73 ± 21
PLA/APP10	13.19 ± 7	80.66 ± 14
PLA/APP15	10.37 ± 8	64.97 ± 13
PLA/APP20	9.81 ± 6	58.16 ± 24
PLA/APP20/PER3	9.33 ± 7	55.43 ± 12
PLA/APP20/PER5	8.10 ± 5	49.56 ± 17
PLA/APP20/KL3	8.76 ± 3	50.12 ± 11
PLA/APP20/KL5	7.43 ± 4	45.25 ± 19

3.3. Results

3.3.1. Mechanism of intumescence

The detailed description of intumescence mechanism was given in previous chapter however, in this study chemical reactions showing the mechanism has been discussed. Long chain APP (Form II) was used as flame retardant in PLA polymer. Upon decomposition of APP, phosphoric acid and ammonia was formed. Phosphoric acid acted as acid catalyst in the dehydration process of carbon-based poly-alcohols in lignin. Upon reaction of acid catalyst (phosphoric acid) with alcohol groups in lignin, phosphate esters were formed which were decomposed later to release carbon dioxide and dehydration of lignin was taken place. In the gas phase, the emission of non-flammable carbon dioxide assisted in diluting the oxygen of the air and flammable decomposed products of the material that were burning whereas the resultant char layer in the condensed phase protected the underlying polymeric material from further burning by restricting the free passage of radiant heat and oxygen. This mechanism of intumescence is shown in Figure 3.2.

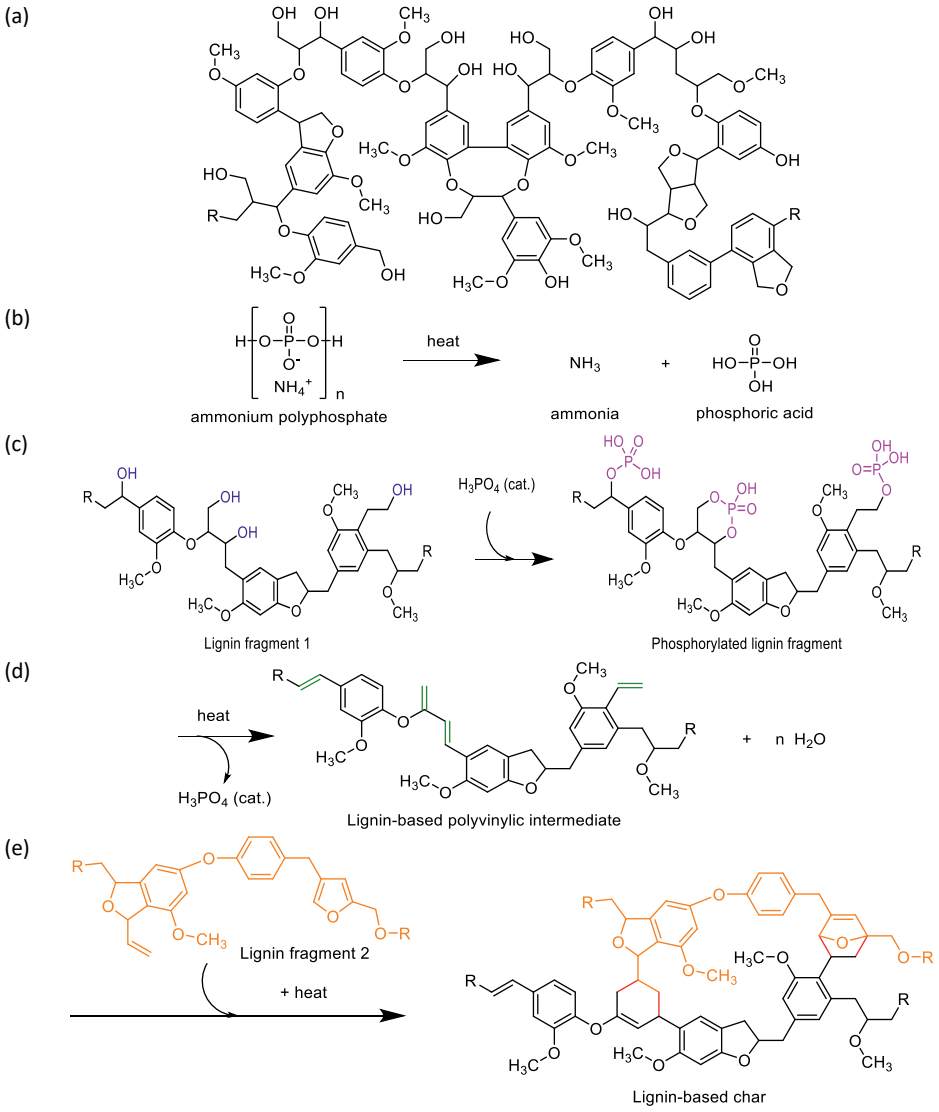

Figure 3.2. Lignin structure (**a**), Thermal decomposition of ammonium polyphosphate into ammonia and ortho-phosphoric acid (**b**), Catalytic phosphorylation to produce phosphorylated lignin (**c**), Dehydration of lignin and formation of lignin based polyvinylic intermediate (**d**), Diels alder reaction to produce lignin-based char (**e**).

3.3.2. Measuring the flammability and dripping behavior of composites

The LOI and UL-94 tests were conducted to assess the flammability of the composites. These flame retardant properties together with the dripping behavior of PLA/APP and PLA/APP/KL IFR composites are mentioned in Table 3.2.

Table 3.2. Fire retardant properties of 100% PLA, the PLA/APP and PLA/APP/KL, IFR composites

No	Formulations	PLA % (w/w)	APP % (w/w)	KL % (w/w)	LOI%	UL-94	Dripping
1	PLA	100	0	0	20.1	Failed	Y/Y
2	PLA/APP5	95	5	0	23.2	V-2	Y/Y
3	PLA/APP10	90	10	0	25.7	V-1	Y/Y
4	PLA/APP15	85	15	0	29.4	V-1	N/Y
5	PLA/APP20	80	20	0	33.5	V-1	N/Y
6	PLA/APP20/PER3	77	20	3	33.9	V-1	N/Y
7	PLA/APP20/PER5	75	20	5	34.4	V-1	N/Y
8	PLA/APP20/KL3	77	20	3	36.6	V-0	N/N
9	PLA/APP20/KL5	75	20	5	37.8	V-0	N/N

PLA = Polylactic acid, APP = Ammonium polyphosphate, KL = Kraft lignin, LOI = Limiting Oxygen Index, N/Y corresponds to NO/YES for dripping in first/second flame application.

100% PLA could not pass UL-94 vertical burning test because it was highly flammable with severe dripping. The LOI of pure PLA was 20.1%. The presence of 5% (w/w) APP enhanced the LOI of the composite (PLA/APP5) to 23.2% and could only manage to obtain a V-2 rating in UL-94V test. The presence of 10% (w/w) APP improved the LOI of the composite (PLA/APP10) to 25.7% and managed to obtain a V-1 rating in UL-94V test. When the proportion of APP increased to 15% and 20% (w/w), the LOI increased to 29.4% (PLA/APP15) and 33.5% (PLA/APP/20) however, both composites managed to achieve only V-1 rating. All of the PLA/APP composites showed evidence of the dripping phenomenon when burning. Although the samples containing PER as carbonization agent improved the LOI to 33.9% and 34.4% by the addition of 3 and 5% (w/w) of PER but not a significant difference was seen in their UL-94 tests. None of the sample containing PER managed to achieve V-0 rating.

The addition of 3% (w/w) KL to PLA/APP20 increased the LOI of the new composite (PLA/APP20/KL3) from 33.5% to 36.6% while maintaining the V-0 rating in the UL-94V test. PLA/APP20/KL3 also showed no evidence of dripping when burning. Similar results were observed with higher proportions of KL. The LOI of the composites PLA/APP20/KL5 was 37.8%, and managed to obtain V-0 ratings with no evidence of dripping. These results confirmed that the introduction of KL as a natural carbonization agent increased the LOI of the composites significantly and abolished the melt dripping phenomenon observed in composites lacking KL. All composites containing KL managed to obtain a V-0 rating.

The UL-94 vertical burning test determines material's ability to either support or extinguish the flame once it catches fire. The results presented in Table 3.2 shows no rating of pure PLA to V-1 rating of PLA/APP and V-0 rating of PLA/APP/KL composites. It was observed that the ignition of pure PLA started during the first flame application of 10 s and the burning was continued till the sample was completely burnt up to the sample holding clamp. Although the burning behavior of the sample containing 5% (w/w) of APP (PLA/APP5) was slightly better to that of pure PLA as the flame extinguished in less than 30 s in each flame application and it achieved V-2 rating but the sample was dripping and ignited the cotton sample placed underneath. Same was the case with 10% (w/w) of APP (PLA/APP10), although it achieved V-1 rating with slower burning rate compared to PLA/APP5 but it also ignited the cotton sample placed underneath due to dripping. However, with the addition of 15 and 20% (w/w) of APP (PLA/APP15 and PLA/APP20) the samples achieved better LOI values however, V-1 rating still showed dripping during second application of flame. Furthermore, the flammability of the composites was completely changed by the incorporation of KL in the formulations. The composites containing 3 and 5% (w/w) of KL were not ignited even after the second application of flame and achieved V-0 rating without dripping in both flame applications. This behavior is attributed to the generation of char layer on specimen's surface which did not allow the flame to pass through the layer hence the underlying material remained unburnt and restricted the propagation of flame. It can be seen in Table 3.2 that in comparison to samples containing PER, samples having KL as carbonization agent not only achieved higher LOI% values but also managed to obtain V-0 ratings without dripping phenomenon in UL-94 tests despite of having the same wt% of the additives.

3.3.3. Time to ignition, heat release rate, total heat release and residual mass%

The cone calorimeter is equipment used to assess the fire retardancy of a polymeric material and gives useful insight about the flammability of the material. This instrument gives broad information about the combustion behavior of the polymer by measuring parameters such as peak heat release rate (PHRR), time to ignition (TTI), total heat release (THR) and residual mass as a proportion of original mass. Cone calorimetry data for 100% PLA and IFR composites we prepared are summarized in Table 3.3.

Table 3.3. Cone calorimetry data for 100% PLA, and PLA/APP and PLA/APP/KL IFR composites.

Formulation	TTI (s)	PHRR (kWm^{-2})	THR ($MJ \cdot m^{-2}$)	Residual Mass (%)	TSP ($m^2 \cdot m^{-2}$)	EHC ($kJ \cdot g^{-1}$)
PLA	63 ± 1.1	428 ± 7	55.7 ± 0.27	0 ± 0.00	43 ± 2	17.33 ± 1.60
PLA/APP5	66 ± 1.4	382 ± 6	52.1 ± 0.16	9 ± 0.03	274 ± 13	16.10 ± 0.90
PLA/APP10	69 ± 2.3	361 ± 3	49.7 ± 0.22	14 ± 0.01	230 ± 17	16.05 ± 1.22
PLA/APP15	72 ± 1.8	336 ± 2	49.1 ± 0.17	17 ± 0.09	190 ± 19	15.93 ± 1.13
PLA/APP20	76 ± 2.8	316 ± 8	47.9 ± 0.31	22 ± 0.04	164 ± 9	15.46 ± 0.86
PLA/APP20/PER3	78 ± 3.4	310 ± 9	47.5 ± 0.41	23 ± 0.05	221 ± 23	15.13 ± 1.56
PLA/APP20/PER5	80 ± 2.9	300 ± 7	46.4 ± 0.29	25 ± 0.07	209 ± 17	14.62 ± 1.34
PLA/APP20/KL3	79 ± 1.1	250 ± 4	45.0 ± 0.29	25 ± 0.05	155 ± 21	12.68 ± 1.43
PLA/APP20/KL5	81 ± 1.4	210 ± 6	44.6 ± 0.12	40 ± 0.03	103 ± 14	11.72 ± 1.18

TTI = time to ignition; PHRR = peak heat release rate; THR = total heat release; TSP = Total smoke production; EHC = Effective heat of combustion.

Heat release curves for pure PLA, PLA/APP10, PLA/APP20 and PLA/APP20/KL5 are presented in Figure 3.3 (a) whereas that of PLA/APP20/PER5 is shown in Figure 3.3 (b) respectively. After ignition, pure PLA kept on burning for longer period of time than other samples and therefore, produced a steep curve with a high PHRR (428 kW m^{-2}). In contrast, the PHRR of PLA/APP10 and PLA/APP20 were 361 and 316 kW m^{-2} respectively. The addition of PER as carbonization agent in PLA/APP20 composites further reduced the PHRR, as samples containing 5% (w/w) of PER achieved 300 kW m^{-2}. A significant reduction in PHRR was observed when KL was added in PLA/APP20 composites as samples containing 3 and 5% (w/w) reduced PHRR to 250 and 210 kW m^{-2} respectively. These findings indicated that the combined effect of APP and KL yielded a

much thicker char structure after burning, preventing the degradation of the composite by restricting the fire passage to the polymer matrix. It can be seen in Table 3.3 and simultaneously in Figure 3.3 (a and b) that samples containing KL as carbonization agent have much lower PHRR than samples containing PER as carbonization agent despite of having same wt% in PLA/APP20 composites.

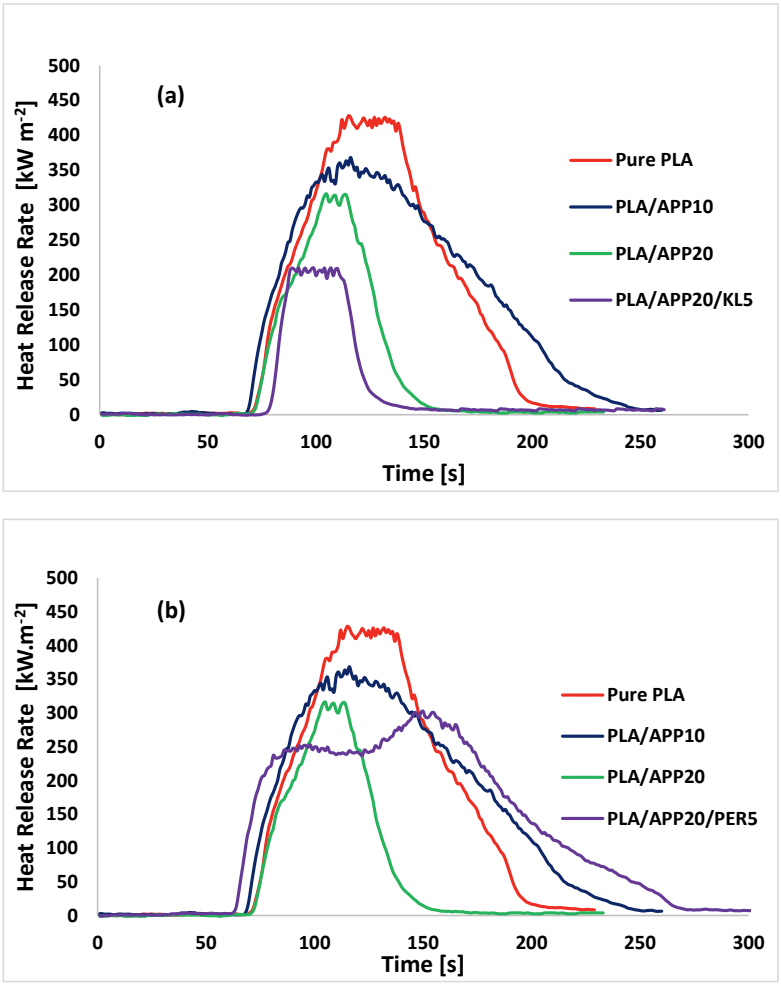

Figure 3.3. (a) Heat release curves for pure PLA, PLA/APP10, PLA/APP20 and PLA/APP20/KL5 composites; **(b)** Heat release rate curves for pure PLA, PLA/APP10, PLA/APP20 and PLA/APP20/PER5 composites.

Figure 3.3 (a) demonstrates that the heat release rate of the composites containing APP alone (PLA/APP10, PLA/APP20) and together with KL (PLA/APP20/KL5) changed quite dramatically in comparison to pure PLA (428 kW m^{-2}). The production of intumescent char in case of samples containing APP alone was delayed due to the emission of volatile compounds and the degree of swelling in the char was also reduced, hence a porous char structure was formed as shown in Figure 3.4 and Figure 3.5.

Figure 3.4 demonstrates images of the residual samples after conducting cone calorimetry test. The char residues of PLA/APP5, PLA/APP10, PLA/APP15 and PLA/APP20 were loosely bound, and the structure in each case was porous and discontinuous due to insufficient char formation as shown by the SEM images of char residues in Figure 3.5. Heat and mass transfer therefore, could not be inhibited effectively in these composites. In contrast, the samples containing KL (particularly PLA/APP20/KL5) produced a more compact char with a dense and uniform structure, reducing fuel and heat transfer to inhibit combustion and prevent further burning of the underlying polymeric substrate.

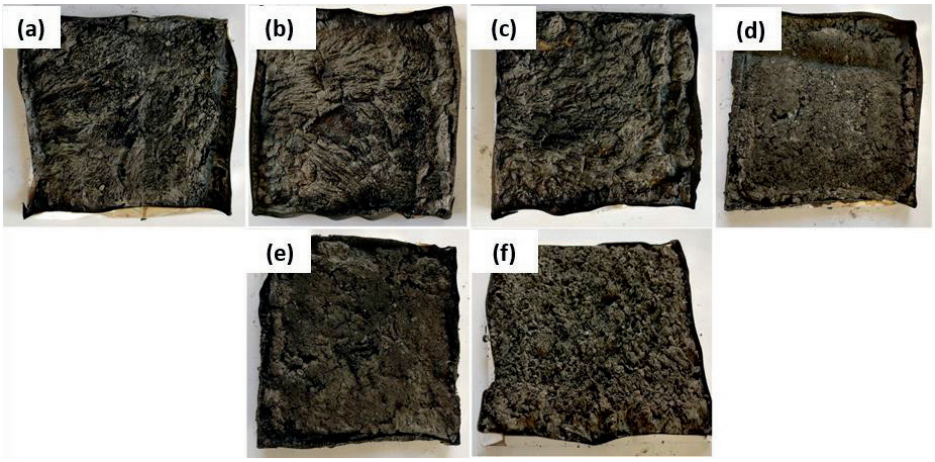

Figure 3.4. Char residues after cone calorimetry: PLA/APP5 (**a**), PLA/APP10 (**b**), PLA/APP15 (**c**), PLA/APP20 (**d**), PLA/APP20/KL3 (**e**), and PLA/APP20/KL5 (**g**).

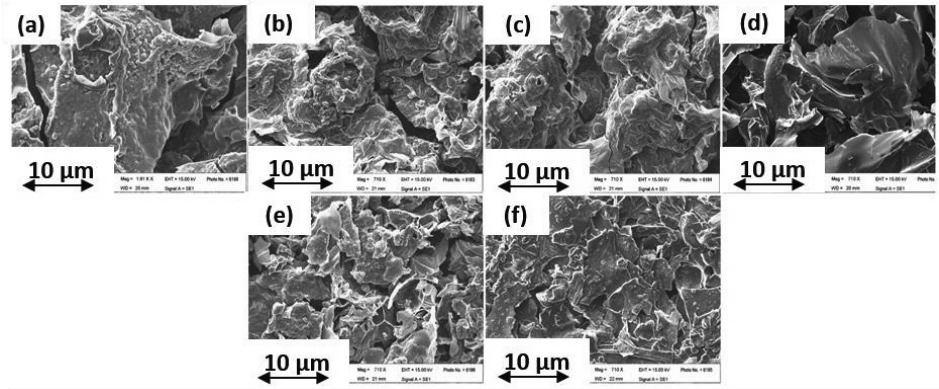

Figure 3.5. SEM images of the char residues of PLA/APP5 (**a**), PLA/APP10 (**b**), PLA/APP15 (**c**), PLA/APP20 (**d**), PLA/APP20/KL3 (**e**), and PLA/APP20/KL5 (**f**) after cone calorimetry test. Scale bar in all panels = 10 µm, Magnification = 710×

The barrier effectiveness and shielding efficiency of a residue is identified by the compactness of a char structure. The char structures of the residues improved with increasing APP content however, the char formed was loosely bound and porous due to non-cohesion of the agglomerates. Furthermore, the char structures of residues of the composites containing APP and KL were stable, more uniform and compact due to cohesion of the agglomerates. KL particles were supposed to fill the empty spaces between the APP particles, which densified the agglomerates of the residues hence more stable, uniform and compact char structures were produced for the samples containing KL. The thickness of the samples containing lignin also increased dramatically due to char formation after burning, from an initial thickness of 3 mm to approximately 1–1.5 cm.

Table 3.3 shows that the TTI of 100% PLA was 63 s, but when mixed with 20% (w/w) APP in the composite PLA/APP20, the TTI increased to 76 s. The samples containing PER as carbonization agent also had similar TTI values to what we get with samples containing KL as carbonization agent. The ignition of a material is typically dependent on the concentration of pyrolysis gases, which are released when a material is degraded until the concentration reaches a value that ignition is supported. A long TTI therefore, reflects slower decomposition mainly due to the presence of APP and KL.

Figure 3.6 (a) demonstrates the THR curves of 100% PLA and the PLA/APP and PLA/APP/KL composites. The THR of 100% PLA was 55.7 MJ m^{-2} whereas the values for PLA/APP20 and PLA/APP20/KL5 were 47.9 and 44.6 MJ m^{-2}, respectively. This indicates that both PLA/APP20 and PLA/APP20/KL5 reduced the total quantity of fuel accessible for burning, which confirms the superior fire retardant performance of these composites. Figure 3.6 (b) shows the THR curves of PLA/APP20/PER composites as a comparison to THR curves of PLA/APP20/KL composites in Figure 3.6 (a). THR value for PLA/APP20/PER5 composite was 46.4 MJ m^{-2} in comparison to 44.6 MJ m^{-2} for PLA/APP20/KL5 composite. The combination of KL and APP makes the composites more flame resistant, and the production of intumescent char on the matrix surface introduced a layer of thermal insulation between the flame and the surface of the material, which extinguished the flame by preventing contact with combustible gases as well as oxygen. The high concentrations of APP and KL diluted the polymer matrix very strongly and there was not much material available to continue the burning process. The thermal decomposition process led to the dehydration of APP and water vapors released in due course cooled down the gas phase and accessible fuel for combustion was diluted therefore, the total heat release (THR) was decreased with increasing APP content. Due to the endothermic decomposition reaction of APP the heating of the condensed phase was also reduced. THR was further reduced by the addition of KL as the emission of pyrolysis gases were decelerated by the formation of char layer, which not only provided the physical barrier to the emission of pyrolysis gases but also enhanced heat shielding effect. The hypothesis of this study is also in good relation with the THR as the previous studies [21,33,34] done with PLA in relation with other carbonization agents had much higher THR than what we achieved in this study.

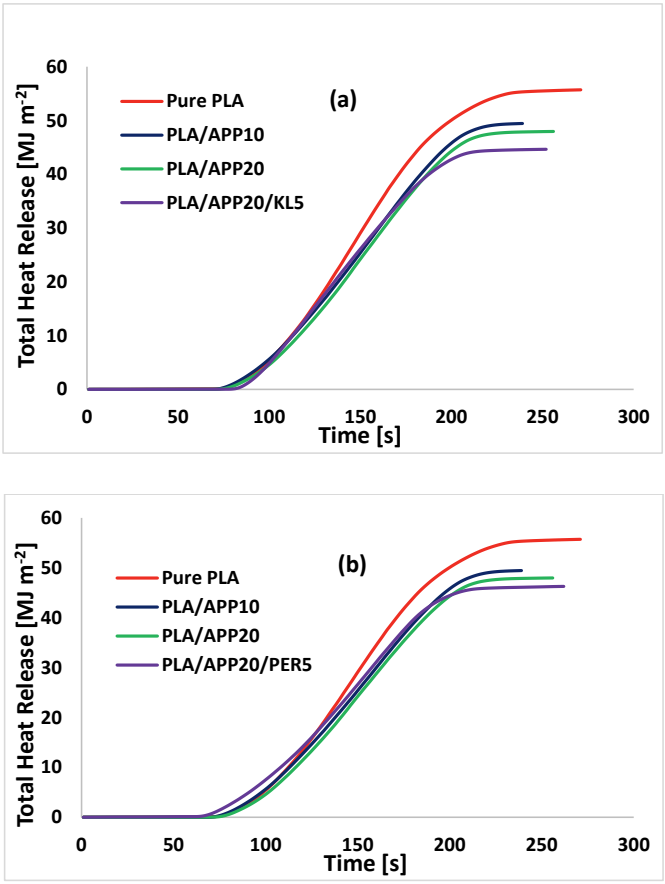

Figure 3.6. **(a)** Total heat release curves of 100% PLA, PLA/APP and PLA/APP/KL composites; **(b)** Total heat release curves of 100% PLA, PLA/APP and PLA/APP/PER composites.

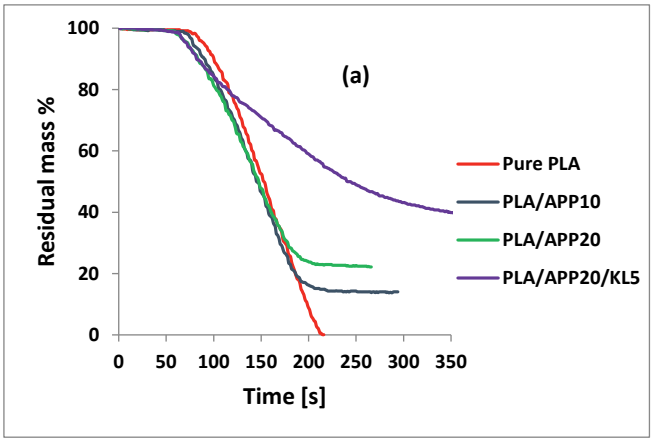

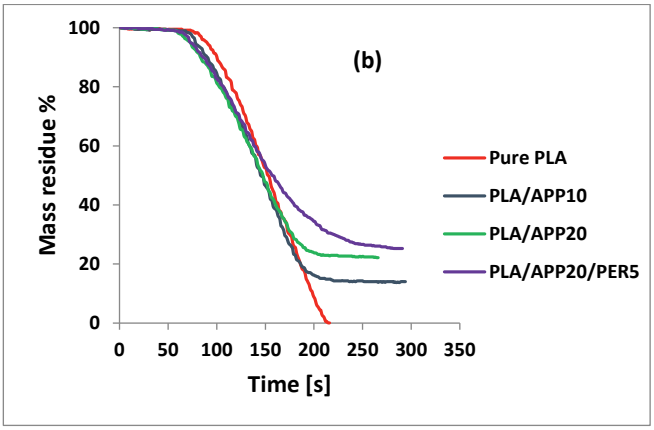

Figure 3.7. (a). Residual mass (percentage of original mass) of 100% PLA, PLA/APP and PLA/APP/KL composites; **(b).** Residual mass (percentage of original mass) of 100% PLA, PLA/APP and PLA/APP/PER composites

Figure 3.7 (a) shows the residual mass curves for 100% PLA and the PLA/APP and PLA/APP/KL composites as a percentage of the original mass. The residual mass of PLA/APP20/KL5 was 40%, much higher than that of PLA/APP20 (22%), and the residual mass of pure PLA was close to 0%. Figure 3.7 (b) shows the residual mass curves of PLA/APP20/PER composites as a comparison to residual mass curves of PLA/APP20/KL composites in Figure 3.7 (a). The residual mass% for PLA/APP20/PER5 was 25% in comparison to 40% for PLA/APP20/KL5 composites. The higher

residual mass correlated with the production of more char, which in turn reflects the lower THR values. The greater residual mass also reflects in greater char formation due to the combined effect of acid and carbonization agent. The residual mass% achieved in this study is also higher than the residual mass% of other studies done with PLA in relation to other carbonization agents [35,36,37].

3.3.4. Energy dispersive X-ray spectrometry

EDS spectrometry was used to inspect the composition of elements present in the char residues. The wt% of the elements present in char residues are compared in Table 3.4.

Table 3.4 Elemental analysis of char residues

No.	Samples	C (wt %)	O (wt %)	P (wt %)	Al (wt %)
1	PLA/APP20	21.2	40.9	34.6	3.3
2	PLA/APP20/KL3	34.9	38.0	26.6	0.5
3	PLA/APP20/KL5	37.7	34.2	26.4	1.7

It can be seen in Table 3.4 that PLA/APP20 contained highest wt% of Oxygen (40.9%) and least wt% of Carbon (21.2%) in char residues. KL favored charring as proved by the increase of C content and the decrease of O content. It is likely that the main part of P remains in the residue (high value of P content). Since the char content increases with increasing KL content, the P content in the char residue necessarily decreases. However, P content is over estimated and quantitative EDS must be performed on flat sample. Moreover, the phosphate compounds developed by the reaction of APP-KL enhanced the char production rate because they stayed in the condensed phase. The increment in the Carbon content (wt%) of PLA/APP/KL residues is due to an increased char formation by the addition of KL.

3.3.5. Investigating the dispersion of additives in PLA matrix

The dispersion of different proportions of APP and KL in the PLA matrix was investigated by scanning electron microscopy to characterize the distribution of the additives, given that a uniform distribution achieves better fire retardant properties. Figure 3.8 shows images of the composites PLA/APP5, PLA/APP10, PLA/APP15, PLA/APP20, PLA/APP20/KL3 and PLA/APP20/KL5. APP and KL particles of different sizes and shapes, and showing different levels of interfacial adhesion with the PLA matrix, were incorporated successfully. In the PLA/APP formulations

lacking KL, the additive was dispersed uniformly regardless of its proportion in the mixture (5–20% w/w), indicating the uniform mixing of APP with the substrate during sample preparation. However, weak interfacial bonding between PLA and APP was apparent based on the appearance of small holes during fracturing. Nevertheless, all images confirmed that APP and KL has been incorporated successfully into the PLA matrix.

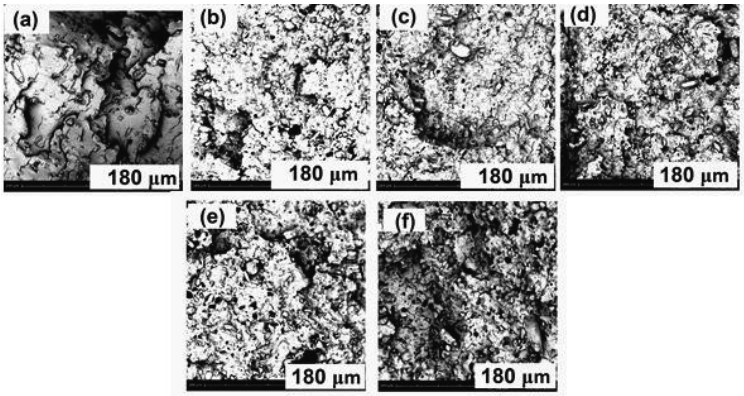

Figure 3.8. SEM images of composites PLA/APP5 (**a**), PLA/APP10 (**b**), PLA/APP15 (**c**), PLA/APP20 (**d**), PLA/APP20/KL3 (**e**), and PLA/APP20/KL5 (**f**). Scale bar in all panels = 180 µm, Magnification = 710×

3.3.6. Assessment of thermal stability of composites

The thermal decomposition and thermal stability of the polymers was assessed by thermogravimetric analysis and the residual mass of the samples was determined at 700 °C. The thermogravimetric behavior of pure PLA and of the IFR composites was expressed as the temperature corresponding to 5% and 50% weight loss in a nitrogen atmosphere (T5 and T50, respectively) as shown in Table 3.5, and the corresponding thermogravimetric curves (Figure 3.9 a, and 3.9 b). The decomposition of PLA/APP5 started at 310 °C and 50% loss was recorded at 343 °C. The residue at 700 °C represented 3.54% of the weight of the original sample. PLA/APP10 showed a similar performance but with slightly higher T5 and T50 values and a residual weight of 5.63%. The trend continued for PLA/APP15 and PLA/APP20, with marginal further increases in the T5 and T50 values and residual weights of 8.16% and 8.78%, respectively. The introduction of KL enhanced the thermal stability of the composites even further. The T5 and T50 values of

PLA/APP20/KL3 were higher than those of any composite without KL, and the residual weight increased to 13.34%. As more KL was incorporated, the T5 and T50 values increased further and the residual weight was 15.32% for PLA/APP20/KL5.

Table 3.5. Thermogravimetric analysis of pure PLA and the PLA/APP and PLA/APP/KL composites

No	Formulations	T_5 (°C)	T_{50} (°C)	Residue at 700 °C (%, w/w)
1	PLA	298	333	0
2	PLA/APP5	310	343	3.54
3	PLA/APP10	318	351	5.63
4	PLA/APP15	320	355	8.16
5	PLA/APP20	328	358	8.78
6	PLA/APP20/PER3	329	360	10.63
7	PLA/APP20/PER5	328	365	13.20
8	PLA/APP20/KL3	330	362	13.34
9	PLA/APP20/KL5	330	365	15.32

T_5 = 5% weight loss, T_{50} = 50% weight loss

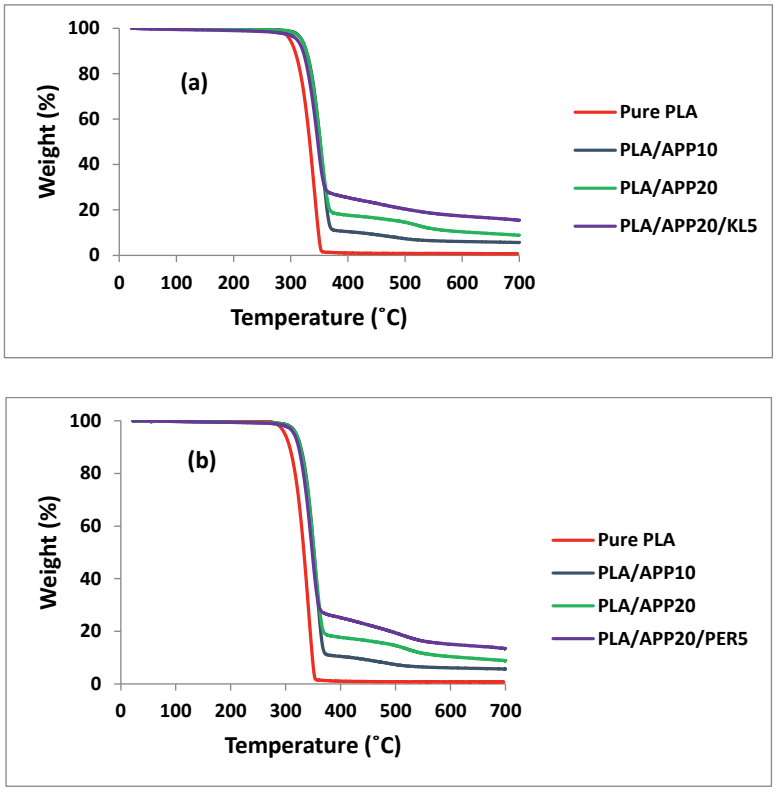

Figure 3.9. (a) Thermogravimetric curves of 100% PLA, PLA/APP and PLA/APP/KL composites; **(b)** Thermogravimetric curves of 100% PLA, PLA/APP and PLA/APP/KL composites

Thermogravimetric curves of 100% PLA, PLA/APP10, PLA/APP20 and PLA/APP20/KL5 show the residual weight as a function of temperature, up to 700 °C (Figure 3.9 a). Figure 3.9 (b) shows the residual weight% for TG curves of PLA/APP20/PER composites as a comparison to residual weight% for TG curves of PLA/APP20/KL composites in Figure 3.9 (a). The residual weight% for PLA/APP20/PER5 composite was 13.20 in comparison to 15.32 for PLA/APP20/KL5. The curves indicate that most of the thermal decomposition occurs between 300 °C and 400 °C and that pure PLA decomposes at a lower temperature than all the composites. Whereas the composites all degrade within a narrow temperature window, increasing the concentration of APP causes more residual weight to remain at temperatures between 375 °C and 700 °C, and adding KL at increasing

concentrations has a further, additive effect. The thermal stabilities of the composites containing KL are therefore better than those of composites containing APP alone or composites containing PER.

3.4. Discussion

The addition of APP in the concentration range of 5% (w/w) to 20% (w/w) enhanced the LOI from 20% (pure PLA) to 33.5% (PLA/APP20) (Table 3.2). With an increasing amount of APP, a higher percentage of oxygen is required in order to sustain ignition of the sample. This is due to the fuel dilution in the gas phase by the discharge of water vapor and NH_3, as a result of dehydration of APP. The addition of KL in the formulations (3%, and 5%) not only increased the LOI% of the samples but also increased the mass residue. Moreover, the increased amount of residue establishment is suggested to enhance the shielding of the samples against heat and to slow down the pyrolysis process by acting as a barrier against the emission of pyrolysis gases. Therefore, the emission of fuel in the gas phase is minimized by the addition of APP. Hence, these results are in good relation with the main hypothesis of this study. In previous studies [25,30] the use of PER as carbonization agent could only achieve V-2 rating despite the addition of 30 to 40% (w/w) in the polymer matrix, whereas in this study V-0 rating was achieved at much lower loading% (w/w) due to the combined effect of APP and KL.

In intumescent system flame-retardancy is achieved by the swelling of the substrate in the condensed phase (as explained in mechanism of intumescence) which generates a sponge like multicellular structure called char which shields the fundamental material from heat transfer to the sample. Moreover, the char structure also provides shielding against fuel and heat transfer from the condensed phase to the sight of burning. The weaker intumescence or a porous char structure in the samples containing APP alone is caused by decreased viscosity in the condensed phase. The production of a uniform and compact char structure is mainly dependent on the viscosity of the sample in condensed phase. The lower viscosity in the condensed phase released the water vapors via bubbling, which were produced by the dehydration of APP and hence no longer available for the swelling of the char structure. If the viscosity in the condensed phase is too low then APP alone cannot generate enough pressure for the swelling of the substrate. Due to this, porous char structure both fuel gases (volatile compounds) and water vapors could easily pass through the unclosed

cells, therefore the HRR of the samples containing APP alone is higher in comparison to HRR of the samples containing APP and KL. The reason is that the combined effect of acid (APP) and carbon source (KL) produced more compact char structure, which hindered the discharge of fuel gases and water vapors which ultimately increased the viscosity of the condensed phase and a result more swelling of the char was observed. Therefore, the combined effect of APP and KL further decreased the PHRR down to 210 kW m^{-2}, which is 50% less than pure PLA. The hypothesis of this study also had a positive influence on the heat emitted during combustion process as HRR in this study is much lower to that we witnessed in other studies done with PLA using other carbonization agents [9,11–14].

The higher TTI of the samples is predominantly attributed to the lower emission of pyrolysis gases which serve as a fuel material for the flame. Therefore, a uniform and compact char structure will be required which can hinder the diffusion of pyrolysis gases from the melt substrate to the sight of burning. But the lower TTI of the samples containing APP alone is mainly due to higher emission of pyrolysis gases which are caused by weaker swelling of the substrate which generates porous char structure with unclosed cells provides empty spaces for the pyrolysis gases to escape and serve as a fuel source to the flame. However, with the combined effect of APP and KL the melt viscosity of the substrate increased which improved the swelling of the substrate which generates more compact char structure thereby hindering the free escape of pyrolysis gases hence the ignition time is prolonged.

The lower mechanical properties of multifilament yarns containing KL and APP are mainly due to lower interfacial adhesion between the components and large parts of additives with relative low aspect ratio. It is more likely, that the large particles acted as starting point of failure during loading. The other reason could be due to higher lignin content, hydroxyl groups present in lignin formed hydrogen bonds with PLA substrate, as a result molecular chain gets more entangled. This created free void spaces in the multifilament yarns by restricting molecular chain mobility, hence their elongation at break reduced and they broke at much lower force compared to pure PLA as explained by Cayla et al. [32].

3.5. Conclusions

In this study, the efficiency of KL as a biobased carbonization agent in intumescent formulations was assessed and compared with conventional carbonization agent (PER) to examine the flame retardant properties of PLA/APP/KL composites. The mechanism of intumescence and melt-spinnability of IFR composites was also investigated. IFR composites comprising different formulations were produced with and without carbonization agents (KL and PER) by melt extrusion and their flammability was assessed by UL-94, LOI and cone calorimetry tests. The introduction of 5–20% (w/w) APP improved the LOI from 20.1 (pure PLA) to 23.2–33.5% for the composites, but the further addition of 5% (w/w) KL (PLA/APP20/KL5) increased the LOI to 37.8% and the composite achieved a V-0 value in UL-94 test with no dripping. In comparison, sample containing 5wt% of PER achieved LOI only up to 34.4% with V-1 rating moreover dripping phenomenon was observed in second flame application. The PHRR and THR of the composites containing KL were significantly lower than the equivalent values for composites containing PER. A remarkably low PHRR was observed for PLA/APP20/KL5 (210 kW m^{-2}) which is 50% less than the PHRR of 100% PLA. The occurrence of 20% APP increased the TTI to 76 s and the further addition of 5% KL increased the TTI to 81 s however, the TTI for PER composites were almost in the same range to that of KL composites. The presence of APP and KL also made IFR composites more thermally stable. Thermogravimetric curves showed that whereas PLA left almost no residual weight after heating to 700 °C, the PLA/APP20 composite produced 8.78% residual mass and this increased to 15.32% for composite PLA/APP20/KL5. In comparison a composite containing 5wt% of PER (PLA/APP20/PER5) could only achieve a residual mass up to 13.20%, confirming that PLA/APP/KL composites are more thermally stable. The analysis of char residues by energy dispersive X-ray spectrometry (EDS) and SEM images confirmed that PLA/FR/KL composites developed a thicker and more homogeneous char layer with better flame retardant properties confirming that the fire properties of PLA can be enhanced by using KL as a carbonization agent.

3.6. References

1. Al-itry, R.; Lamnawar, K.; Maazouz, A. Improvement of thermal stability, rheological and mechanical properties of PLA , PBAT and their blends by reactive extrusion with functionalized epoxy. *Polym. Degrad. Stab.* **2012**, 97, 1898–1914, doi:10.1016/j.polymdegradstab.2012.06.028.

2. Hussain, T.; Tausif, M.; Ashraf, M. A review of progress in the dyeing of eco-friendly aliphatic polyester- based polylactic acid fabrics. *J. Clean. Prod.* **2015,** 108, 476–483, doi:10.1016/j.jclepro.2015.05.126.
3. Armentano, I.; Bitinis, N.; Fortunati, E.; Mattioli, S.; Rescignano, N.; Verdejo, R.; Lopez-manchado, M.A.; Kenny, J.M. Multifunctional nanostructured PLA materials for packaging and tissue engineering. *Prog. Polym. Sci.* **2013**, 38, 1720–1747, doi:10.1016/j.progpolymsci.2013.05.010.
4. Martin, J.A. An effect of lactic acid oligomers on the barrier properties of polylactide. *J. Mater. Sci.* **2014**, 49, 2975–2986, doi:10.1007/s10853-013-7929-x.
5. Cheng, K.C. Flammability and tensile properties of polylactide nanocomposites with short carbon fibers. *J. Mater. Sci.* **2015**, 50, 1605–1612, doi:10.1007/s10853-014-8721-2.
6. Nofar, M.; Park, C.B. Poly (lactic acid) foaming. *Prog. Polym. Sci.* **2014,** 39, 1721–1741, doi:10.1016/j.progpolymsci.2014.04.001.
7. Cheng, X.; Guan, J.; Tang, R.; Liu, K. Improvement of flame retardancy of poly (lactic acid) nonwoven fabric with a phosphorus- containing flame retardant. *J. Ind. Text.* **2015,** 1–12, doi:10.1177/1528083715606105.
8. Rhim, J.; Park, H.; Ha, C. Bio-nanocomposites for food packaging applications. *Prog. Polym. Sci.* **2013,** 38, 1629–1652, doi:10.1016/j.progpolymsci.2013.05.008.
9. Fukushima, K.; Murariu, M.; Camino, G.; Dubois, P. Effect of expanded graphite/layered-silicate clay on thermal, mechanical and fire retardant properties of poly(lactic acid). *Polym. Degrad. Stab.* **2010**, 95, 1063–1076, doi:10.1016/j.polymdegradstab.2010.02.029.
10. Uddin, F. Flame-retardant fibrous materials in an aircraft. *J. Ind. Text.* **2016**, 45, 1128–1169, doi:10.1177/1528083714540700.
11. Lin, H.J.; Liu, S.R.; Han, L.J.; Wang, X.M.; Bian, Y.J.; Dong, L.S. Effect of a phosphorus-containing oligomer on flame-retardant, rheological and mechanical properties of poly (lactic acid). *Polym. Degrad. Stab*. **2013,** 98, 1389–1396, doi:10.1016/j.polymdegradstab.2013.03.025.
12. Lin, H.; Han, L.; Dong, L. Thermal degradation behavior and gas phase flame-retardant mechanism of polylactide/PCPP blends. *J. Appl. Polym. Sci.* **2014,** 131, 1–11, doi:10.1002/app.40480.

13. Mngomezulu, M.E.; Luyt, A.S.; John, M.J. Morphology, thermal and dynamic mechanical properties of poly(lactic acid)/expandable graphite (PLA/EG) flame retardant composites. *J. Thermoplast. Compos. Mater.* **2017**, 1–19, doi:10.1177/0892705717744830.
14. Murariu, M.; Bonnaud, L.; Yoann, P.; Fontaine, G.; Bourbigot, S.; Dubois, P. New trends in polylactide (PLA)-based materials: "Green" PLA-Calcium sulfate (nano)composites tailored with flame retardant properties. *Polym. Degrad. Stab.* **2010,** 95, 374–381, doi:10.1016/j.polymdegradstab.2009.11.032.
15. Atabek Savas, L.; Mutlu, A.; Dike, A.S.; Tayfun, U.; Dogan, M. Effect of carbon fiber amount and length on flame retardant and mechanical properties of intumescent polypropylene composites. *J. Compos. Mater*. **2017,** 1–12, doi:10.1177/0021998317710319.
16. Depeng, L.; Chixiang, L.; Xiulei, J.; Tao, L.; Ling, Z. Synergistic effects of intumescent flame retardant and nano-CaCO 3 on foamability and flame-retardant property of polypropylene composites foams. *J. Cell. Plast.* **2017,** 1–17, doi:10.1177/0021955X17720157.
17. Duquesne, S.; Samyn, F.; Ouagne, P.; Bourbigot, S. Flame retardancy and mechanical properties of flax reinforced woven for composite applications. *J. Ind. Text.* **2015,** 44, 665–681, doi:10.1177/1528083713505633.
18. Wang, D.Y.; Leuteritz, A.; Wang, Y.Z.; Wagenknecht, U.; Heinrich, G. Preparation and burning behaviors of flame retarding biodegradable poly(lactic acid) nanocomposite based on zinc aluminum layered double hydroxide. *Polym. Degrad. Stab.* **2010,** 95, 2474–2480, doi:10.1016/j.polymdegradstab.2010.08.007.
19. Wang, J.; Ren, Q.; Zheng, W.; Zhai, W. Improved flame-retardant properties of poly(lactic acid) foams using starch as a natural charring agent. *Ind. Eng. Chem. Res.* **2014,** 53, 1422–1430, doi:10.1021/ie403041h.
20. Wang, K.; Wang, J.; Zhao, D.; Zhai, W. Preparation of microcellular poly(lactic acid) composites foams with improved flame retardancy. *J. Cell. Plast.* **2017,** 53, 45–63, doi:10.1177/0021955X16633644.
21. Qian, Y.; Wei, P.; Jiang, P.; Li, Z.; Yan, Y.; Ji, K. Aluminated mesoporous silica as novel high-effective flame retardant in polylactide. *Compos. Sci. Technol.* **2013,** 82, 1–7, doi:10.1016/j.compscitech.2013.03.019.

22. Zhan, J.; Song, L.; Nie, S.; Hu, Y. Combustion properties and thermal degradation behavior of polylactide with an effective intumescent flame retardant. *Polym. Degrad. Stab.* **2009,** 94, 291–296, doi:10.1016/j.polymdegradstab.2008.12.015.
23. Wang, D.Y.; Song, Y.P.; Lin, L.; Wang, X.L.; Wang, Y.Z. A novel phosphorus-containing poly(lactic acid) toward its flame retardation. *Polymer* (Guildf). **2011,** 52, 233–238, doi:10.1016/j.polymer.2010.11.023.
24. Zhang, R.; Xiao, X.; Tai, Q.; Huang, H.; Yang, J.; Hu, Y. Preparation of lignin–silica hybrids and its application in intumescent flame-retardant poly(lactic acid) system. *High Perform. Polym.* **2012,** 24, 738–746, doi:10.1177/0954008312451476.
25. Bourbigot, S.; Duquesne, S.; Fontaine, G.; Bellayer, S.; Turf, T.; Samyn, F. Characterization and Reaction to Fire of Polymer Nanocomposites with and without Conventional Flame Retardants. *Mol. Cryst. Liq. Cryst.* **2008,** 486, 37–41, doi:10.1080/15421400801921983.
26. Reti, C.; Casetta, M.; Duquesne, S.; Bourbigot, S.; Delobel, R. Flammability properties of intumescent PLA including starch and lignin. *Polym. Adv. Technol.* **2006,** 17, 395–418, doi:10.1002/pat.
27. Zhang, R.; Xiao, X.; Tai, Q.; Huang, H.; Hu, Y. Modification of lignin and its applications as a char agent in intumescent flame retardant polylactic acid. *Polym. Eng. Sci.* **2012,** 2620–2626, doi:10.1002/pen.
28. Zhang, R.; Xiao, X.; Tai, Q.; Huang, H.; Yang, J.; Hu, Y. Preparation of lignin-silica hybrids and its application in intumescent flame-retardant poly(lactic acid) system. *High Perform. Polym.* **2012,** 24, 738–746, doi:10.1177/0954008312451476.
29. Costes, L.; Laoutid, F.; Aguedo, M.; Richel, A.; Brohez, S.; Delvosalle, C.; Dubois, P. Phosphorus and nitrogen derivatization as efficient route for improvement of lignin flame retardant action in PLA. *Eur. Polym. J.* **2016,** 84, 652–667, doi:10.1016/j.eurpolymj.2016.10.003.
30. Costes, L.; Laoutid, F.; Brohez, S.; Delvosalle, C.; Dubois, P. Phytic acid – lignin combination : A simple and e ffi cient route for enhancing thermal and fl ame retardant properties of polylactide. *Eur. Polym. J.* **2017,** 94, 270–285, doi:10.1016/j.eurpolymj.2017.07.018.
31. Gordobil, O.; Delucis, R.; Egüés, I.; Labidi, J. Kraft lignin as filler in PLA to improve ductility and thermal properties. *Ind. Crop. Prod.* **2015,** 72, 46–54, doi:10.1016/j.indcrop.2015.01.055.

32. Cayla, A.; Rault, F.; Giraud, S.; Salaün, F.; Fierro, V.; Celzard, A. PLA with intumescent system containing lignin and ammonium polyphosphate for flame retardant textile. *Polymers (Basel)*. **2016,** 8, doi:10.3390/polym8090331.
33. Maqsood, M.; Seide, G. Investigation of the Flammability and Thermal Stability of Halogen-Free Intumescent System in Biopolymer Composites Containing Biobased Carbonization Agent and Mechanism of Their Char Formation. *Polymers (Basel)*. **2018,** 11, 1–16, doi:10.3390/polym11010048.
34. Teoh, E.L.; Mariatti, M.; Chow, W.S. Thermal and Flame Resistant Properties of Poly (Lactic Acid)/Poly (Methyl Methacrylate) Blends Containing Halogen-free Flame Retardant. *Procedia Chem.* **2016,** 19, 795–802, doi:10.1016/j.proche.2016.03.087.
35. Wei, L.L.; Wang, D.Y.; Chen, H.B.; Chen, L.; Wang, X.L.; Wang, Y.Z. Effect of a phosphorus-containing flame retardant on the thermal properties and ease of ignition of poly(lactic acid). *Polym. Degrad. Stab.* **2011,** 96, 1557–1561, doi:10.1016/j.polymdegradstab.2011.05.018.
36. Fox, D.M.; Lee, J.; Citro, C.J.; Novy, M. Flame retarded poly(lactic acid) using POSS-modified cellulose. 1. Thermal and combustion properties of intumescing composites. *Polym. Degrad. Stab*. **2013,** 98, 590–596, doi:10.1016/j.polymdegradstab.2012.11.016.
37. Shabanian, M.; Kang, N.J.; Wang, D.Y.; Wagenknecht, U.; Heinrich, G. Synthesis of aromatic-aliphatic polyamide acting as adjuvant in polylactic acid (PLA)/ammonium polyphosphate (APP) system. *Polym. Degrad. Stab.* **2013,** 98, 1036–1042, doi:10.1016/j.polymdegradstab.2013.02.007.

CHAPTER 4

Investigation of melt-spinnability of plasticized polylactic acid biocomposites containing intumescent flame retardant

Abstract

Biodegradable polymers from renewable resources have attracted interest due to environmental pollution caused by the disposal of non-degradable polymers and engineering them to produce fibres of textile grade can improve the environmental sustainability of textile sector. Flame retardancy of Polylactic acid (PLA) can be improved if used in intumescent system containing acidic and carbonic source, however spinning them to produce fibres of textile grade is a big challenge. We therefore have prepared PLA composites containing phosphorous-nitrogen based flame retardant as acidic source together with kraft lignin as carbonic source. Different quantities of flame retardant and kraft lignin were added into PLA-matrix by melt blending and then hot pressed to form moulding sheets. A modified polyester based plasticizer was also incorporated to facilitate the spinnability of the composites. Limiting oxygen index (LOI) values and UL-94 ratings of the composites were reported. The melt-spinnability of composites was then assessed and flame retardancy of knitted structures produced from multifilament yarns were tested by cone calorimetry. Composites containing up to 7% (m/m) of lignin were spinnable together with 10% (m/m) of plasticizer. A substantial decrease of 59% in heat release rate was observed compared to pure PLA. The mechanism of intumescence was also reported.

Keywords

Melt spinning; Biopolymers; Plasticizer; Cone calorimetry; Flame retardancy

4.1. Introduction

Polylactide (PLA) is a thermoplastic synthetic biopolymer which is obtained from renewable resources such as corn, potato and cane biomass [1]. Due to its biodegradability and compostability, PLA can replace oil based synthetic polymers in many applications in general and textile sector in particular where disposal of non-degradable products is a big threat to environmental sustainability [2, 3]. The importance of PLA has grown over the last decade because it addresses current challenges, i.e. the depletion of petroleum reserves (the feedstock for conventional plastics) and the environmental harm caused by the irresponsible disposal of non-degradable polymers [4, 5]. Nowadays PLA is more progressively used in fibers and fabrics applications [6, 7] because it can be spun by using techniques such as solution spinning, electrospinning and melt spinning [8, 9].

Initially the applications of PLA were limited to fiber-reinforced composites mainly in medical sector in the form of biodegradable sutures, vascular grafts and implants due to its biocompatibility [10, 11]. Later, PLA was more commonly used in the textile sector (clothing, home textiles and carpets) to replace the petroleum based polyethylene terephthalate (PET) polymer because some of the physical and mechanical properties of PLA are comparable to that of PET [12, 13]. However, flame retardancy of PLA is considered better to that of PET since the limiting oxygen index (LOI) of neat PLA is 24-26% and that of neat PET is 18-20% [14, 15]. Moreover, the smoke generation after ignition and self-extinguishing character of PLA is better to that of PET which makes this polymer even an interesting choice to be used in textile sector [16, 17]. Even so, PLA is still combustible and in order to be used in some technical-textile applications the flame retardant properties of PLA needs to be improved further [18]. In previous studies various attempts have been made in order to improve the flame retardancy of PLA by using different formulations and additive types such as nitrogen based compounds [19], phosphorous based compounds [14], silicon based compounds [20], expanded graphite or carbon based compounds [21], halogen containing compounds [22] and halogen free compounds as flame retardants [23, 24]. However intumescent flame retardant's (IFR's) containing an acidic and carbonic source have proven to be the most effective one [25]. The importance of IFR's containing biopolymers with biobased carbonic source and halogen free acidic source has grown interest throughout the last decade in order to promote the sustainable approach towards flame retardancy of polymers [26]. Therefore in continuation to

this approach various researchers tried different formulations in IFR systems with different halogen free acidic sources such as phytic acid [27], fumaric acid [28] and biobased carbonic sources such as cyclodextrin [29], sorbitol [30], chitosan [31, 32].

Majority of the studies reported in literature related to spinnability of flame retardant composites [33, 34] have used predominantly petroleum based carbonization agents or in case of biobased carbonization agents either the trials were unsuccessful [28, 29] or the loading content of the carbonic sources were not sufficient enough to achieve the desirable flame retardancy [35]. Therefore, the aim of the present study is to investigate the melt-spinnability of PLA based IFR composites comprising biobased (lignin) carbonic source and to engineer the polymer composition to spin multifilaments that can achieve acceptable range of flame retardancy in fabric form. A modified polyester based plasticizer was also incorporated into composites to facilitate the spinnability of composites. Composites were melt spun to multifilament yarns on pilot scale melt spinning machine and later used to form knitted structures.

4.2. Materials and methods

The materials and methods used in this chapter are discussed in the following sections.

4.2.1. Materials

Granular PLA Luminy® L130 (≥99% L-isomer) was attained from Total-Corbion NV (Gorinchem, Netherlands). A phosphorous-nitrogen based non-halogenated flame retardant with commercial name (EXP PP/37) which is a fine-particle off-white powder containing ammonium polyphosphate with 19% (m/m) nitrogen and 20% (m/m) phosphorous (thermally stable upto 250˚C), was obtained from Italmatch Chemicals S.p.A (Genova, Italy). The kraft lignin (KL) powder “UPM BioPiva 100” was purchased from UPM Biochemicals OYJ (Helsinki, Finland). A modified polyester based plasticizing agent (PES) in white granular form (thermally stable up to 280˚C) was obtained from Preluna GmbH (Ludwigshafen, Germany), to improve spinnability of composites. PLA, EXP, PES and KL were vacuum dried at 100˚C for 4 h before compounding.

4.2.2. Preparation of composites

PLA/PES, PLA/EXP/PES and PLA/EXP/PES/KL composites were prepared using Coperion ZSK Mc^{18} twin screw extruder (Coperion GmbH, Stuttgart, Germany) at 190˚C. In the first phase,

PLA/EXP/PES composites with EXP content of 5%, 10%, 15% (m/m) and PES content of 10% (m/m) were compounded at screw rotation speed of 150 rpm. The temperatures of the three heating zones were kept at 180˚C, 185˚C and 190˚C, respectively. In the second phase, PLA/EXP/PES/KL composites with a KL content of 3%, 5%, 7% and 10% (m/m) were compounded at screw rotation speed of 200 rpm. PLA/EXP/PES pellets were dosed in the first feeding zone whereas KL was fed in the second feeding zone to ensure proper mixing. Sheets of the as prepared composites were produced by compression moulding at 190˚C for the subsequent testing along with sheets of pure PLA for comparison. The formulations with additives composition are presented in Table 4.1.

Table 4.1. Additives composition in composites

No.	Formulations	PLA mass (%)	EXP mass (%)	PES mass (%)	KL mass (%)
1	PLA	100	0	0	0
2	PLA/PES10	90	0	10	0
3	PLA/EXP5/PES10	85	5	10	0
4	PLA/EXP10/PES10	80	10	10	0
5	PLA/EXP15/PES10	75	15	10	0
6	PLA/EXP15/PES10/KL3	72	15	10	3
7	PLA/EXP15/PES10/KL5	70	15	10	5
8	PLA/EXP15/PES10/KL7	68	15	10	7
9	PLA/EXP15/PES10/KL10	65	15	10	10

4.2.3. Yarn manufacturing

Pure PLA, PLA/PES, PLA/EXP/PES and PLA/EXP/PES/KL composites were melt spun using Fourne Maschinenbau GmbH (Impekoven, Germany) pilot scale melt spinning machine. Pellets were first fed into a hopper and then transported to a single screw extruder where they were melted at a temperature range of 195˚C to 220˚C. The melted material was then injected in a spinneret die of 1.2 mm diameter each, with the help of spinning pump rotating at constant revolutions per minute ensuring a homogeneous flow of the material. These single filaments coming out of the spinneret were cooled at 18˚C by maintaining the cool air velocity of 0.5 $m.s^{-1}$. The monofilaments were combined together to multifilaments by applying a spin finish. The multifilaments were

collected by a take up roller rotating at 250 m min^{-1}. The multifilaments were hot drawn between two set of rollers rotating at varying speeds. The speeds of the first and second set of heated rollers were maintained at 300 m min^{-1} and 350 m min^{-1} respectively ensuring a draw ratio of 1.4 (maximum possible draw ratio). The multi-filaments were then winded on the winder at 350 m min^{-1}. A schematic diagram of pilot scale melt spinning machine is shown in Figure 4.1.

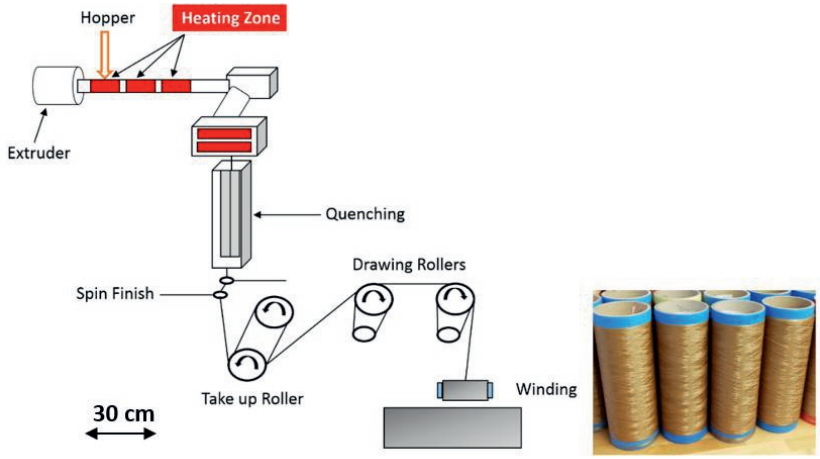

Figure 4.1. Schematic diagram of pilot scale melt spinning machine and multifilament yarn produced

To further investigate the spinnability of as prepared composites containing KL, a design of experiment was prepared using half factorial design in MINITAB 18 statistical software. Four factors/variables with two levels each, were considered in this study and are shown in Table 4.2. The design of experiment to investigate the spinnability of the composites is shown in Table 4.3.

Table 4.2. Factors and their levels

No	Factors	Levels	
1	No. of filaments	24	48
2	Draw ratio	1.2	1.4
3	Temperature of draw rollers (°C)	60	80
4	Yarn linear denisty (dtex)	350	500

Table 4.3. Design of experiment for spinning the composites containing KL

Sample	No. of filaments	Draw ratio	Temperature of draw rollers (°C)	Yarn linear denisty (dtex)
PLA/EXP15/PES10/KL3	24	1.2	60	350
	48	1.2	60	500
	24	1.4	60	500
	48	1.4	60	350
	24	1.2	80	500
	48	1.2	80	350
	24	1.4	80	350
	48	1.4	80	500
PLA/EXP15/PES10/KL5	24	1.2	60	350
	48	1.2	60	500
	24	1.4	60	500
	48	1.4	60	350
	24	1.2	80	500
	48	1.2	80	350
	24	1.4	80	350
	48	1.4	80	500
PLA/EXP15/PES10/KL7	24	1.2	60	350
	48	1.2	60	500
	24	1.4	60	500
	48	1.4	60	350
	24	1.2	80	500
	48	1.2	80	350
	24	1.4	80	350
	48	1.4	80	500

Two different spinneret types containing 24 and 48 number of filaments, two maximum possible draw ratios of 1.2 and 1.4, two different drawing roller temperatures (60°C and 80°C) and two different yarn linear densities (350 and 500 dtex) of composites containing KL were investigated.

It was observed that all 24 possible combinations were spinnable however, their mechanical properties were almost in the same range since there was not much difference in the draw ratio of the filaments considering it as the main factor responsible for variation in the yarn mechanical properties. An average of their tenacity (cN tex^{-1}) and elongation at break (%) were recorded and discussed in the results and discussion section.

4.2.4. Fabric manufacturing

Multifilament yarns of linear denisty 500 dtex were knitted to form a fabric structure. Knitted fabrics were preferred over woven or nonwovens because of their easier processibility and drapeability. Single jersey structure was selected for fabric manufacturing in order to characterize their flammability by cone calorimetry. The areal densities of all the knitted fabrics were approximately 800 g m^{-2} with a fabric thickness of around about 3 mm.

4.2.5. Thermogravimetric analysis

Thermogravimetric behavior of composites was assessed using a TGA Q5000 device (TA Instruments, New Castle, Delaware, USA). The specimens (10–15 mg) were heated at a constant rate of 10˚C min^{-1} up to 700˚C under nitrogen at a flow rate of 50 mL min^{-1}. The thermal decomposition temperature and the temperature at which maximum degradation took place were calculated along with the residual percentage of the sample compared to the initial mass. The thermogravimetric curves of specimens were plotted after analysis.

4.2.6. Scanning electron microscopy

The surface morphology and dispersion of additives in the PLA matrix were investigated by scanning electron microscopy (SEM) using a TM-1000 table-top microscope (Hitachi, Chiyoda, Tokyo, Japan). The samples were immersed in liquid nitrogen followed by freeze fracturing and gold sputtering to produce a conductive surface. In case of multifilament yarns, morphology and additives deposition on yarns surface were also studied by SEM.

4.2.7. Mechanical testing

Mechanical properties such as tensile strength, elongation at break and Young's modulus of PLA composites were tested by Zwick Roell Z020TH allround-line table-top machine (Zwick GmbH & Co.KG, Ulm, Germany) at a speed of 50 mm min^{-1}. The test specimens of dog bone shape were

prepared as per standard EN ISO 527-2 method using moulding press. Specimens dimensions used were 170×20×3 mm^3. The tenacity and elongation at break of multifilaments were also tested on Zwick Roell testing machine by using EN ISO 5079 standard method. The specimen lengths (50 mm) and rate of deformation (50 mm min^{-1}) were kept constant for all samples. Ten specimens were prepared from each sample and their average results with standard deviations were recorded.

4.2.8. Limiting oxygen index and UL-94 vertical burning test

The limiting oxygen index (LOI) is the fraction of oxygen that must be present to support burning, hence higher LOI values indicate lower flammability. The specimens (100×10×3 mm^3, as required by ISO 4589) were vertically placed in a glass column supplied with a mixture of oxygen and nitrogen gas, and were then ignited from above using a downward-pointing flame. The LOI tests for pure PLA and PLA composites were conducted using a Stanton Redcroft instrument (Illinois Toolworks, Glenview, Illinois, USA).

The UL-94 test classifies materials based on their ability to either promote or inhibit the spread of fire once it has been ignited. UL-94 tests for pure PLA and PLA composites were conducted using specimens with dimensions of 100×10×3 mm^3 as required by ISO 9773. A flame was applied to the bottom of a vertically supported specimen, and the response was assessed after removing the flame. Specimens that self-extinguish and do not drip after burning are ranked highest in the classification (V-0).

4.2.9. Cone calorimetry

Cone calorimetry works on the principle of oxygen consumption and states that the total heat of combustion of a specimen depends on the quantity of oxygen consumed [36, 37]. The cone calorimetery tests of knitted fabrics were conducted on specimens with dimensions of 100×100×3 mm^3 as required by ISO 5660 using a Stanton Redcroft instrument. The samples were exposed to a heat flux of 35 kW m^{-2}. We then recorded the heat release rate (HRR), total heat release (THR), time to ignition (TTI) and percentage mass residue after burning of specimens. Three specimens from each sample were tested and their average results were recorded.

4.3. Results and discussion

4.3.1. Mechanism of intumescence

EXP containing long chain ammonium polyphosphate (Form II) was used as flame retardant in PLA polymer. Upon decomposition of ammonium polyphosphate, phosphoric acid and ammonia was formed. Phosphoric acid acted as acid catalyst in the dehydration process of carbon-based poly-alcohols in lignin. Upon reaction of acid catalyst (phosphoric acid) with hydroxyl groups in lignin, phosphate esters were formed which were decomposed later to release carbon dioxide and dehydration of lignin was taken place. In the gas phase, the emission of carbon dioxide helped in dilution of the oxygen present in air together with the by-products that were ignited during decomposition of the materials whereas the resultant char layer in the condensed phase protected the underlying polymeric material from further burning by restricting the free passage of radiant heat and oxygen. This mechanism of intumescence is shown in Scheme 4.1.

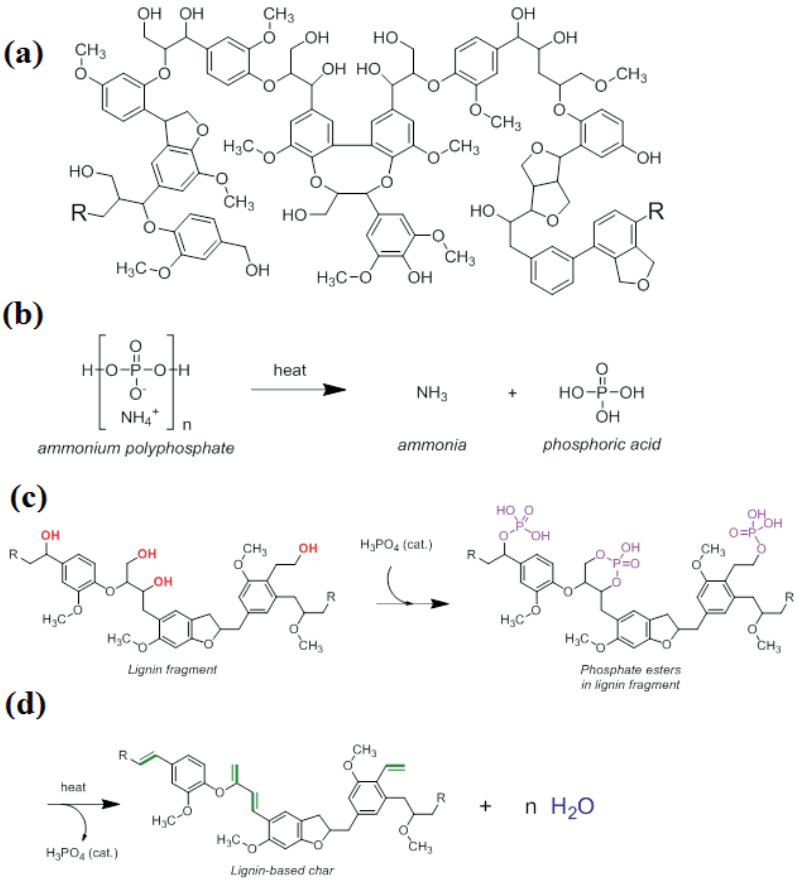

Scheme 4.1. Lignin structure (a), Thermal decomposition of ammonium polyphosphate into ammonia and ortho-phosphoric acid (b), Catalytic phosphorylation to produce phosphate esters (c), Dehydration of lignin and formation of lignin based char structure (d)

4.3.2. Dispersion of additives in composites and multifilament yarns

The dispersion of different proportions of EXP/PES and EXP/PES/KL in the PLA matrix was investigated by scanning electron microscopy to characterise the distribution of the additives, given that a uniform distribution achieves better fire retardant properties. Figure 4.2 (a) shows SEM-images of the composites and Figure 4.2 (b) represents SEM-images of multifilament yarns containing different % (m/m) of additives. We observed EXP, PES and KL particles of different

sizes and shapes, and with different levels of interfacial adhesion with the PLA matrix. In all formulations of PLA/EXP/PES and PLA/EXP/PES/KL, the additives were randomly distributed and non-uniform dispersion of the additives in PLA matrix was observed. However, we observed very weak interfacial bonding between the additives and PLA substrate as shown by the appearance of small holes during fracturing. In case of multifilament yarns, the physical and mechanical properties are highly dependent on the loading content of the additives incorporated in the polymer matrix. As depicted by the SEM images of multifilament yarns in Figure 4.2 (b), a non-uniform dispersion of additives was noticed and the addition of KL led to the development of irregularities in the yarn mainly due to higher loading content of viscous blends coupled with lower draw ratio (1.4) used during spinning process.

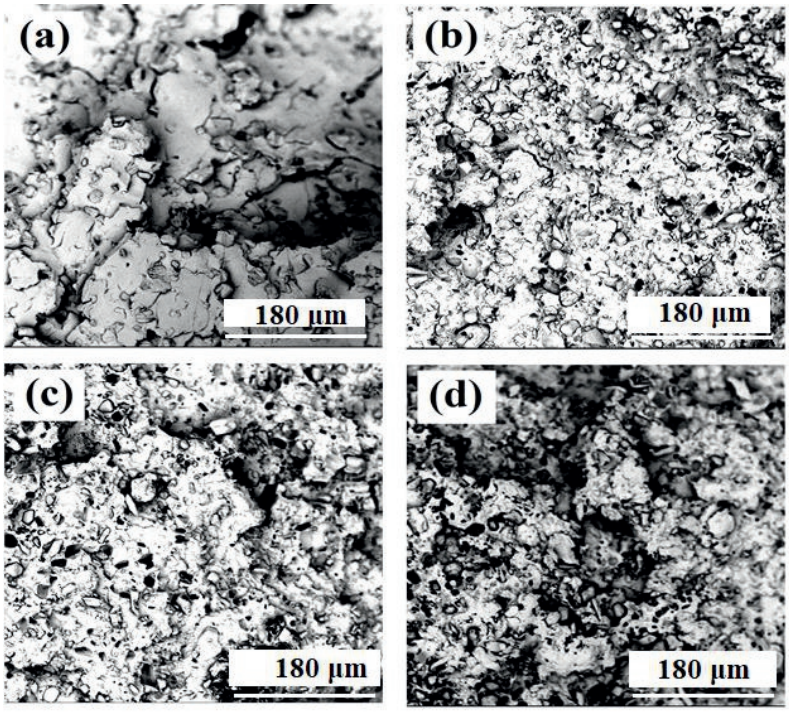

Figure 4.2 (a). SEM images of composites containing PLA/EXP15/PES10 (a), PLA/EXP15/PES10/KL3 (b), PLA/EXP15/PES10/KL5 (c), and PLA/EXP15/PES10/KL7 (d) Scale bar in all panels = 180 µm, Magnification = 710×

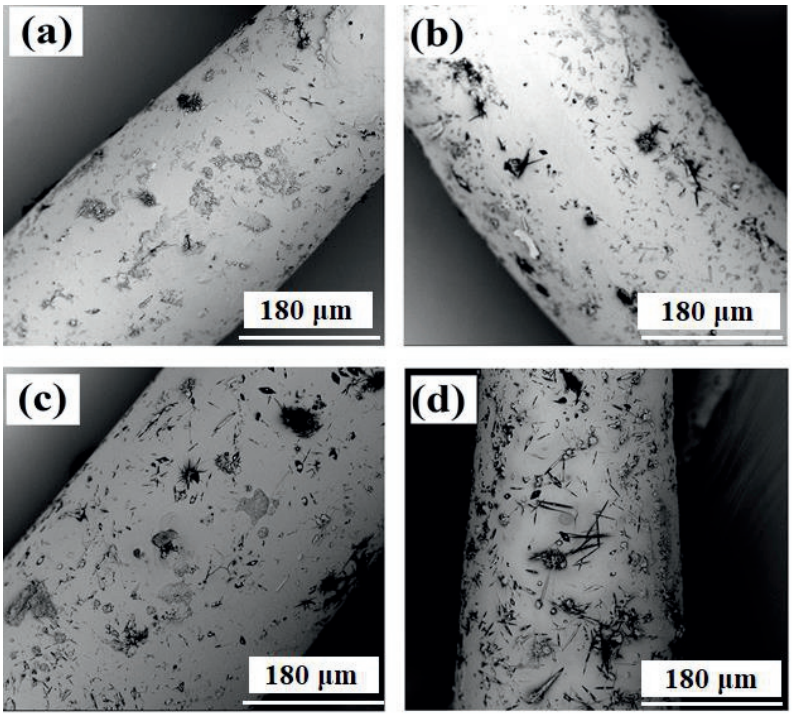

Figure 4.2 (b). SEM images of multifilament yarns containing PLA/EXP15/PES10 (a), PLA/EXP15/PES10/KL3 (b), PLA/EXP15/PES10/KL5 (c), and PLA/EXP15/PES10/KL7 (d) Scale bar in all panels = 180 µm, Magnification = 710×

4.3.3. Measuring the fire retardancy and dripping behavior of composites

LOI and UL-94 tests were carried out to determine the flame-retardant properties of the composites, and we also monitored their dripping behaviour when burning (Table 4.4).

Table 4.4. Flame retardant properties of pure PLA and PLA composites

No	Formulations	LOI /%	UL-94	Dripping
1	PLA	21.5	Failed	Y/Y
2	PLA/PES10	20.3	Failed	Y/Y
3	PLA/EXP5/PES10	24.6	V-2	Y/Y
4	PLA/EXP10/PES10	26.4	V-1	Y/Y
5	PLA/EXP15/PES10	30.4	V-1	N/Y
6	PLA/EXP15/PES10/KL3	32.8	V-0	N/N
7	PLA/EXP15/PES10/KL5	34.1	V-0	N/N
8	PLA/EXP15/PES10/KL7	36.7	V-0	N/N
9	PLA/EXP15/PES10/KL10	38.1	V-0	N/N

PLA = Polylactic acid, EXP = Flame retardant, KL = Kraft lignin, PES = Plasticizer, LOI = Limiting oxygen index, N/Y corresponds to NO/YES for dripping during the first/second flame application

Pure PLA did not pass the UL-94 vertical burning test because it was highly flammable with severe dripping. The LOI of pure PLA was 21.5% and that of PLA/PES10 was 20.3%. The presence of 5% (m/m) EXP increased the LOI of the composite (PLA/EXP5/PES10) to 24.6% and achieved a V-2 rating in the UL-94 test. The presence of 10% (m/m) EXP increased the LOI of the composite (PLA/EXP10/PES10) to 26.4% and achieved a V-1 rating in the UL-94 test. When the proportion of EXP increased to 15% (m/m), the LOI of the composite increased to 30.4% (PLA/EXP15/PES10) and composite achieved a V-1 rating in the UL-94 test, despite the composite did not show dripping behaviour during first flame application. However all of the PLA/EXP/PES composites showed evidence of the dripping phenomenon when burning.

The addition of 3% (m/m) KL increased the LOI of the new composite (PLA/EXP15/PES10/KL3) from 30.4% to 32.8% and achieved V-0 rating in the UL-94 test and also showed no evidence of dripping when burning. Similar results were observed with higher proportions of KL. The LOI of the composites PLA/EXP15/PES10/KL5 and PLA/EXP15/PES10/KL7 were 34.1% and 36.7%, respectively, and both achieved V-0 ratings in the UL-94 test with no evidence of dripping. The

highest LOI value of 38.1% was achieved with the composite containing 10% (m/m) of lignin (PLA/EXP15/PES10/KL10) however, this composite was not spinnable due to higher % (m/m) of KL. These results confirmed that the introduction of KL as a natural carbonization agent increased the LOI of the composites significantly and abolished the dripping phenomenon observed in composites lacking KL. All composites containing KL achieved a V-0 rating in the UL-94 vertical burning test. By increasing the amount of EXP and KL, a higher concentration of oxygen is needed to achieve the ignition of the sample due to the dilution of the fuel in the gas phase by the discharge of water vapour as a result of the dehydration of EXP and KL. The addition of KL to the formulations not only increased the LOI of the samples but also increased the mass residue, providing enhanced shielding against heat transfer, and a barrier against the emission of pyrolysis gases which act as fuel.

The UL-94 vertical burning test determines a material's tendency to either extinguish or spread the flame once the specimen has been ignited. Pure PLA ignited during the first flame application (10 s) and the sample continued to burn until it was fully consumed as was the case with sample containing PLA/PES10. Although PLA/EXP5/PES10 and PLA/EXP10/PES10 composites performed better as flame-retardants (flame extinguished less than 30s after each flame application; V-2 and V-1 ratings, respectively), the dripping of the burning sample ignited the cotton placed beneath. Similarly, PLA/EXP15/PES10 achieved a V-1 rating, although the flame was extinguished in less than 10 s, but this sample still showed dripping behavior during second flame application. In contrast, none of the composites containing KL were ignited even after the second application of flame and all achieved a V-0 rating without dripping due to the generation of char layer on the surface which isolated the remaining sample and prevented the propagation of the flame. In previous studies [12, 19], the addition of 30–40% (m/m) PER as a carbonization agent was sufficient to achieve only a V-2 rating, whereas here we found that as little as 3% KL in the presence of 15% EXP and 10% PES accomplished the target rating of V-0.

4.3.4. Thermal stability measurement by thermogravimetric analysis

The thermal decomposition and thermal stability of the composites was assessed by thermogravimetric analysis and the residual mass of the samples was determined at 700˚C. The thermal degradation and mass residue of the samples were compared to determine the influence of flame retardant (EXP) and carbonization agent (KL) on PLA-based composites. TG curves and

data for the samples heated in a nitrogen atmosphere are presented in Figure 4.3 and in Table 4.5 respectively.

Table 4.5. Data of thermogravimetric analysis

No	Formulations	T_5 (˚C)	T_{50} (˚C)	T_{max} (˚C)	Residual mass (%)
1	PLA	318	369	371	0.0
2	PLA/PES10	317	362	370	0.0
3	PLA/EXP5/PES10	320	370	375	3.8
4	PLA/EXP10/PES10	323	371	377	5.9
5	PLA/EXP15/PES10	342	372	376	8.4
6	PLA/EXP15/PES10/KL3	359	374	382	13.8
7	PLA/EXP15/PES10/KL5	362	376	383	15.5
8	PLA/EXP15/PES10/KL7	369	378	385	17.3
9	PLA/EXP15/PES10/KL10	376	381	390	20.1

In Table 4.5, the temperatures corresponding to 5% and 50% mass loss for pure PLA and for each composite are represented by the T_5 and T_{50} values, respectively, whereas the temperature corresponding to the maximum rate of mass losses is represented by T_{max}. The degradation of pure PLA started at 318˚C and 50% loss occurred at 369˚C, with no residue left at 700˚C as almost the same case was observed with PLA/PES10 composite. A similar trend was observed for PLA/EXP5/PES10 composite for the T_5 and T_{50} temperatures but the residue left at 700˚C was 3.85% of the initial mass. For PLA/EXP10/PES10 and PLA/EXP15/PES10, the initial decomposition temperatures and thermal stabilities were greater than the corresponding values for PLA/EXP5/PES10, with 5.93% and 8.42% residual mass left at 700˚C. The introduction of lignin further improved the thermal stability of the composites. The initial decomposition temperatures and thermal stabilities of all composites containing lignin are higher compared to composites without lignin. For example, composite PLA/EXP15/PES10/KL3 increased the residual mass at 700˚C from 8.42% to 13.83% with higher initial decomposition temperature (359 ˚C). The addition of 5 and 7% (m/m) of lignin (PLA/EXP15/PES10/KL5 and PLA/EXP15/PES10/KL7) further improved the initial decomposition temperatures (362˚C and 369˚C respectively) with 15.54% and 17.31% residual mass left at 700˚C. The highest thermal stability with maximum residual mass%

(20.12%) at 700˚C was observed in case of composite containing 10% (m/m) of lignin (PLA/EXP15/PES10/KL10).

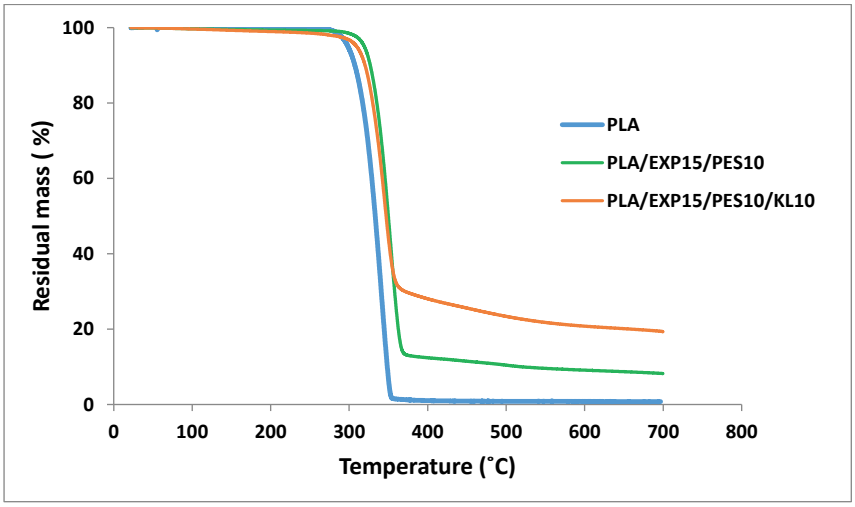

Figure 4.3. TG curves of pure PLA, PLA/EXP/PES and PLA/EXP/PES/KL composites

Figure 4.3 represents the TG curves for PLA/EXP/PES and PLA/EXP/PES/KL composites in comparison to pure PLA. These composites differ in terms of their initial decomposition temperatures and thermal stabilities. PLA/EXP15/PES10/KL10 containing 10% (m/m) of lignin was found to be more thermally stable and presented denser and more compact char layer with higher residual mass% (20.12%). All the composites containing lignin presented higher residual mass% at 700˚C due to charring ability of KL as a result of polycyclic aromatic hydrocarbons formation as indicated by Sharma et al. [38], hence composites containing lignin are superior in performance to composites without lignin. Thermogravimetric curves presented in Figure 4.3 of pure PLA, PLA/EXP15/PES10 and PLA/EXP15/PES10/KL10 composites show the residual mass as a function of temperature, up to 700˚C. The curves indicate that most of the thermal decomposition occurs between 300˚C and 400˚C and that pure PLA decomposes at a lower temperature than all the composites. Whereas all the composites degrade within a narrow temperature window, increasing the concentration of EXP causes more residual mass to remain at temperatures between 375˚C and 700˚C, and adding KL at increasing concentrations has a further, additive effect. The thermal stabilities of the composites containing KL are therefore, better than

those of composites containing EXP alone. This behaviour is due to the combined effect of char forming ability of the polyhydric component (KL) and dehydration mechanism established by acid source (EXP) due to the formation of phosphate compounds, which further enhances the dehydration of lignin resulting in higher char formation with compact structures.

4.3.5. Measuring the tensile strength, elongation at break and Young's modulus

The mechanical properties of multi-component based composites are dependent on the effective stress sharing between matrix and the additives incorporated. Therefore, in order to get acceptable mechanical strength of composites a uniform interfacial bonding between additives and matrix is needed. Moreover, the size of particles, % (m/m) of additives incorporated as well as the adhesion between additives and matrix influence the mechanical properties of polymer composites. As indicated in SEM images in the previous section a weak interfacial bonding between additives and polymer matrix was observed due to which clustered and agglomerated particles were formed which affected the mechanical strength.

Table 4.6. Mechanical properties of pure PLA, PLA/PES, PLA/EXP/PES and PLA/EXP/PES/KL composites

Formulations	Tensile strength (MPa)	Elongation at break (%)	Young's modulus (MPa)
PLA	76.2 ± 5	15.3 ± 0.4	4742.4 ± 14
PLA/PES10	65.3 ± 7	19.5 ± 0.3	4666.2 ± 19
PLA/EXP5/PES10	52.9 ± 6	13.4 ± 0.6	4376.4 ± 18
PLA/EXP10/PES10	49.8 ± 7	13.0 ± 0.5	4237.7 ± 21
PLA/EXP15/PES10	46.4 ± 8	10.3 ± 0.7	3978.2 ± 17
PLA/EXP15/PES10/KL3	41.3 ± 9	9.6 ± 0.4	3854.2 ± 14
PLA/EXP15/PES10/KL5	40.4 ± 6	8.8 ± 0.6	3664.1 ± 16
PLA/EXP15/PES10/KL7	38.9 ± 7	7.6 ± 0.5	3343.1 ± 13
PLA/EXP15/PES10/KL10	37.2 ± 5	6.6 ± 0.4	3237.5 ± 16

It can be seen in Table 4.6 that the tensile strength and elongation at break of pure PLA was 76.21 (MPa) and 15.33% respectively. The addition of PES in PLA polymer (PLA/PES10) not only improved the ductility of the composite but elongation at break (19.54%) also increased. However, with the addition of EXP 15% (m/m) in PLA matrix, the tensile strength and elongation at break

started to decrease and reached to 46.49 (MPa) and 10.33% respectively. When 3% (m/m) of KL was incorporated together with 15% (m/m) of EXP in polymer matrix, tensile strength (41.31 MPa) and elongation at break (9.66%) was further reduced. The reduction in mechanical properties of PLA/EXP/PES and PLA/EXP/PES/KL composites is mainly due to weak interfacial bonding initiated by the difference in secondary valence forces among PLA matrix and additives incorporated [35, 39]. Another reason of weaker mechanical properties could be due to the degradation of PLA as well as of KL during preparation of PLA composites due to higher extrusion temperature, which might have reduced the adsorbed chains mobility on the surface of the particles. Therefore, in order to improve the mechanical properties of PLA composites a uniform dispersion of additives in polymer matrix may be required, which sometimes can be obtained by the use of a compatibilizer. The Young's modulus of pure PLA was 4742.43 MPa and it reduced gradually by the addition of EXP and at 15% (m/m) loading of EXP it decreased to 3978.21 MPa. However, addition of KL in the composites led to further reduction in Young's Modulus of the composites as it was 3237.54 MPa at 10% (m/m) loading of KL.

4.3.6. Mechanical properties of multifilament yarns

To increase the loading content of flame retardant (EXP) and carbonization agent (KL) in PLA-matrix, a plasticizer (PES) was incorporated as the third additive. The role of the plasticizer was to improve the spinnability of composites by reducing the rigidity of materials and to increase the elongation at break of multifilament yarns, although tenacity of multifilaments is mainly affected by its addition.

Composites containing PLA/EXP/PES and PLA/EXP/PES/KL were melt spun and it was observed that as the loading content of EXP and KL was increased, the multifilament yarns were not able to withstand the same draw ratio, which was applied for pure PLA and only PLA/EXP5/PES10 could be spun at the same processing conditions. For other compositions of composites, draw ratio was reduced gradually from 2 to 1.4 in order to spin the composites without breakage. This reduction in draw ratio resulted in lower mechanical properties of multifilament yarns produced from these composites predominantly due to amorphous nature with little or no crystallinity induced in the filament structure. The tenacity and elongation at break of multifilament yarns are mainly influenced by the % (m/m) of the additives incorporated in the PLA matrix therefore, the

mechanical properties of the multifilament yarns containing higher amount of EXP and KL were on the lower side (Table 4.7) than that of multifilament yarns produced from pure PLA.

Table 4.7. Mechanical properties of pure PLA, PLA/PES, PLA/EXP/PES and PLA/EXP/PES/KL multifilament yarns

Formulations	Tenacity (cN tex^{-1})	Elongation at break (%)
PLA	19.8 ± 3	110.1 ± 23
PLA/PES10	17.9 ± 4	123.4 ± 22
PLA/EXP5/PES10	12.4 ± 1	74.3 ± 33
PLA/EXP10/PES10	10.9 ± 2	61.7 ± 19
PLA/EXP15/PES10	9.5 ± 2	54.2 ± 24
PLA/EXP15/PES10/KL3	7.3 ± 2	45.6 ± 37
PLA/EXP15/PES10/KL5	7.1 ± 1	43.3 ± 28
PLA/EXP15/PES10/KL7	6.7 ± 1	39.9 ± 17
PLA/EXP15/PES10/KL10	Not spun	Not spun

The lower mechanical properties of multifilament yarns containing KL and EXP are mainly due to non-uniform dispersion of the additives in PLA matrix due to which clustered and agglomerated particles were formed which produced cracks on the yarn's surface. At the SEM investigations, it turned out that the interfacial adhesion between the components was on a low level and large parts of additives with relative low aspect ratio were present. It is more likely, that the large particles acted as starting point of failure during loading. The other reason could be higher lignin content due to which, hydroxyl groups present in lignin formed hydrogen bonds with PLA substrate, as a result molecular chain gets more entangled that created free void spaces in the multifilament yarns by restricting molecular chain mobility. Hence, their elongation at break reduced and they broke at much lower force compared to pure PLA as explained by Cayla et al. and Wang et al. [25, 35]. Due to this reason, it was not possible to spin composite containing 10% (m/m) of KL (PLA/EXP15/PES10/KL10). Although mechanical properties of multifilament yarns seem to be on the lower side but they were sufficient enough to produce knitted structures.

4.3.7. Heat release rate, total heat release, time to ignition and residual mass%

Cone calorimetry data for pure PLA and PLA composite fabrics are presented in Table 4.8.

Table 4.8. Cone calorimetry data for pure PLA and PLA composites

No.	Formulation	TTI (s)	PHRR (kW m^{-2})	THR (MJ m^{-2})	Residual mass (%)
1	PLA	79	461	58.5	0
2	PLA/PES10	77	477	60.2	0
3	PLA/EXP5/PES10	66	415	55.7	9
4	PLA/EXP10/PES10	61	388	46.4	14
5	PLA/EXP15/PES10	55	352	44.6	17
6	PLA/EXP15/PES10/KL3	53	230	38.4	22
7	PLA/EXP15/PES10/KL5	48	205	26.1	25
8	PLA/EXP15/PES10/KL7	43	191	22.9	32

TTI = time to ignition; PHHR = peak heat release rate; THR = total heat release

Five types of samples (pure PLA, PLA/EXP10/PES10, PLA/EXP15/PES10, PLA/EXP15/PES10/KL5 and PLA/EXP15/PES10/KL7) were knitted in order to assess the influence of flame retardant's and lignin's content on their reaction to fire. The time to ignition (TTI) of fabrics produced from pure PLA and from PLA composites are presented in Table 4.8. TTI of a fabric knitted from pure PLA was 79 s. However, with the addition of 15% (m/m) of EXP (PLA/EXP15/PES10), TTI of the fabric reduced to 55 s, which was further decreased to 43 s when 15% (m/m) of EXP together with 7% (m/m) of lignin was incorporated in PLA. The decrease in ignition time of samples containing lignin can be attributed to the degradation of lignin during compounding and melt spinning since the degradation temperature of lignin is lower (230˚C) to that of EXP (270 ˚C) and PLA (280 ˚C). The decrease in ignition time for knitted fabrics containing lignin can also be attributed to the short fibres present on the surface of multifilament yarns due to partial degradation of filaments during spinning, which were easier to ignite, hence reducing the ignition time.

Heat release curves for pure PLA, PLA/EXP10/PES10, PLA/EXP15/PES10, PLA/EXP15/PES10/KL5 and PLA/EXP15/PES10/KL7 knitted fabrics are presented in Figure 4.4. Pure PLA fabric burnt much faster than the other samples and produced a steep curve with a high PHRR (461 kW m^{-2}). In contrast, PHRR of PLA/EXP10/PES10 fabric was lower (388 kWm^{-2}) and the further addition of 15% (m/m) EXP in PLA/EXP15/PES10 fabric reduced the PHRR to 352 kWm^{-2}. The introduction of 5% (m/m) of KL in PLA/EXP15/PES10/KL5 fabric led to

significant reduction of PHRR to 205 kW m^{-2}. Remarkably, increasing the KL content to 7% (m/m) in PLA/EXP15/PES10/KL7 fabric resulted in substantial additional fall in PHRR (191 kW m^{-2}), which is 58.50% lower than the PHRR of pure PLA. These findings indicated that the combined effect of EXP and KL yielded a much thicker char layer on the surface of the knitted fabric after ignition, preventing further degradation of fabric and presenting higher residual mass% than the fabrics containing EXP alone.

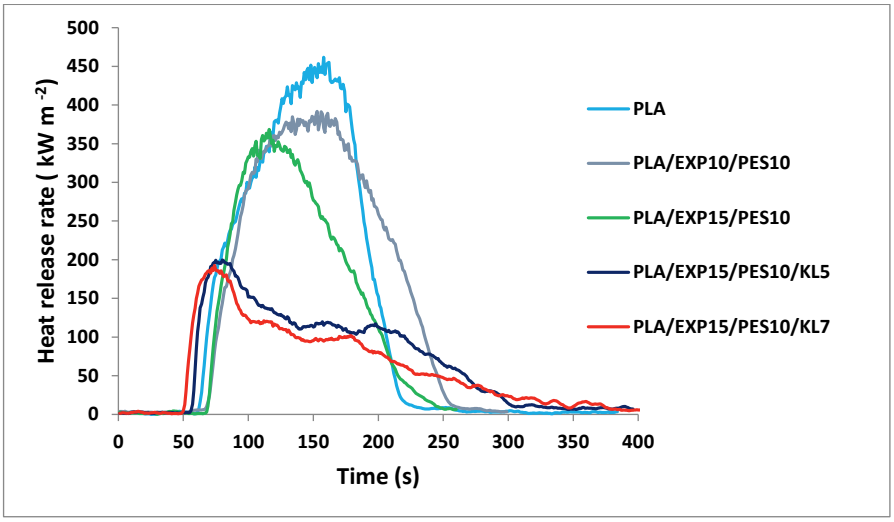

Figure 4.4. Heat release rate of pure PLA, PLA/EXP/PES and PLA/EXP/PES/KL fabrics

Figure 4.5 shows the THR curves of pure PLA and the PLA/EXP/PES and PLA/EXP/PES/KL composites fabrics. The THR of pure PLA was 58.52 MJ m^{-2} whereas the values for PLA/EXP15/PES10 and PLA/EXP15/PES10/KL7 knitted fabrics were 44.67 and 22.91 MJ m^{-2}, respectively.

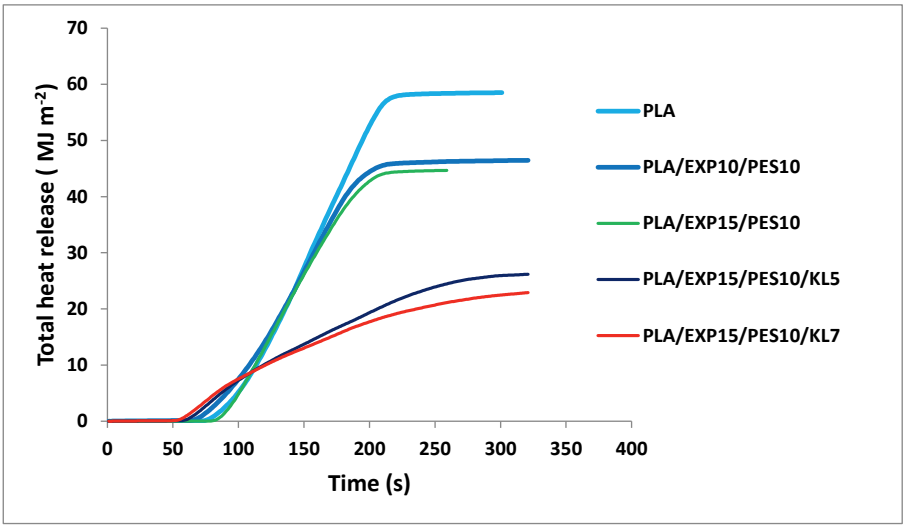

Figure 4.5. Total heat release curves of pure PLA, PLA/EXP/PES and PLA/EXP/PES/KL fabrics

Figure 4.6 demonstrates SEM images of char residues after conducting cone calorimetry test. The char residues of PLA/EXP10/PES10 and PLA/EXP15/PES10 were loosely bound, and the structure in each case was porous and discontinuous due to insufficient char formation as shown by the SEM images of char residues. Heat and mass transfer therefore, could not be inhibited effectively in these composites. In contrast, the samples containing KL, i.e. PLA/EXP15/PES10/KL5 and PLA/EXP15/PES10/KL7 produced a more compact char with a dense and uniform structure, reducing fuel and heat transfer to inhibit combustion and prevent further burning of the underlying polymeric substrate.

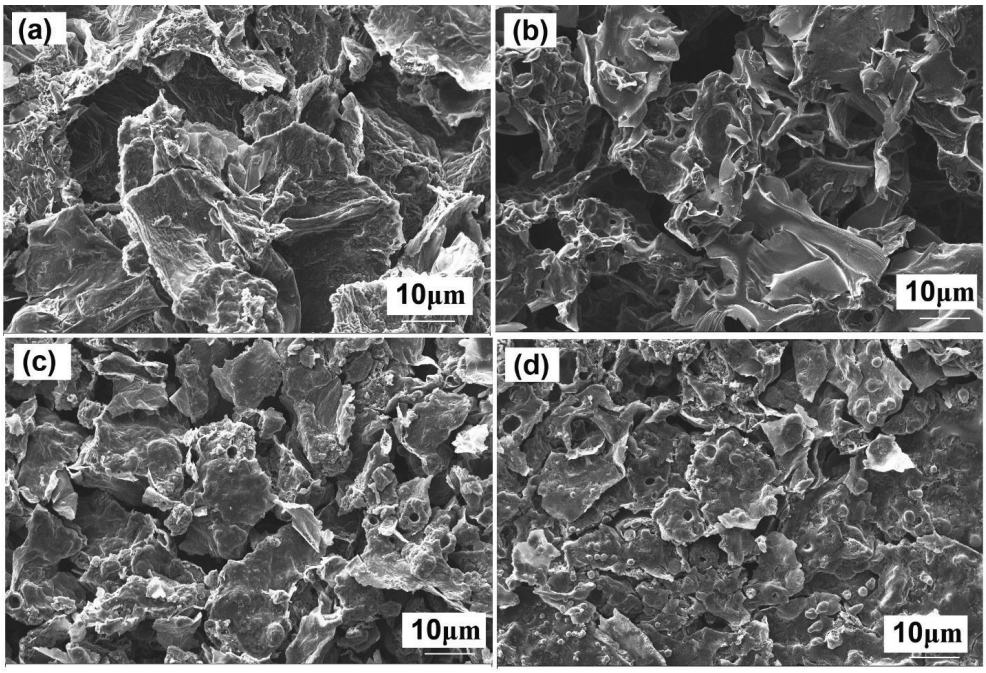

Figure 4.6. SEM analysis of char residues; PLA/EXP10/PES10 (a), PLA/EXP15/PES10 (b), PLA/EXP15/PES10/KL5 (c) and PLA/EXP15/PES10/KL7 (d)

The weaker intumescence or a porous char structure in the samples containing EXP alone is caused by decreased viscosity in the condensed phase. The production of a uniform and compact char structure is mainly dependent on the viscosity of the sample in condensed phase. The lower viscosity in the condensed phase released the water vapors via bubbling, which were produced by the dehydration of EXP and hence no longer available for the swelling of the char structure. If the viscosity in the condensed phase is too low then EXP alone cannot generate enough pressure for the swelling of the substrate. Due to the porous char structure both fuel gases (volatile compounds) and water vapors could easily pass through the unclosed cells therefore, the HRR of the samples containing EXP alone is higher in comparison to HRR of the samples containing EXP and KL. The reason is that the combined effect of acid source (EXP) and carbon source (KL) produced more compact char structure, which hindered the discharge of fuel gases and water vapors, which

ultimately increased the viscosity of the condensed phase and a result more swelling of the char was observed.

In samples containing EXP alone, residual mass% was lower (Table 4.8) compared to samples containing KL. This is because the absence of KL lowered the viscosity of the char layer, in turn allowing vapour and gas bubbles to escape and reducing the degree of swelling because little pressure was allowed to build up as confirmed by SEM images of char residues in Figure 4.6. The resulting porous structure allowed further fuel gases and water vapour to pass through the unclosed cells, increasing the PHRR. In contrast, the higher viscosity of the char layer containing KL made the char on fabric surface more compact and prevented the escape of gases and vapour, resulting in a pressure build up that increased the melt viscosity of the condensed phase and resulted in more swelling of char. The combined effect of EXP and KL therefore, reduced PHRR to 191 kW m^{-2}, which is 58.50% less than pure PLA.

This indicates that the combined effect of KL and EXP reduced the total quantity of fuel accessible for burning, which confirms the superior flame-retardant performance of these fabrics. The high concentrations of EXP and KL diluted the substrate, providing less material for continued burning. Thermal decomposition therefore led to the dehydration of EXP, and the resulting water vapours cooled the gas phase and diluted the fuel, thus reducing the total heat release (THR) in proportion with the increasing EXP and KL content. The presence of KL exacerbated this effect because the emission of pyrolysis gases was inhibited by the formation of the char layer, which not only provided a physical barrier but also enhanced the heat shielding effect.

4.4. Conclusions

In this study, melt spinnability, thermal stability, mechanical properties and fire related properties of PLA composites prepared by melt blending on twin screw extruder comprising phosphorous-nitrogen based flame retardant (EXP), kraft lignin (KL) and plasticizer (PES) were investigated. Composites containing up to 3% (m/m) of KL were comparatively easier to spin than composites containing 5% or 7% (m/m) of KL due to lesser molecular chain mobility with higher loading content of KL. However, composites containing up to 7% (m/m) of KL together with 15% (m/m) of EXP and 10% (m/m) of PES (plasticizer) were spinnable but breakage of individual filaments were seen during melt spinning. With higher loading content of KL and EXP elongation at break

of multifilaments were decreased and multifilaments with lower mechanical properties were obtained. Thermal stabilities of PLA composites containing KL were improved with higher residual mass% (20.12%) at 700˚C due to greater charring ability of the compound. Flame retardant properties of knitted fabrics produced from these composites were investigated by cone calorimetry. The HRR and THR of the knitted fabrics containing KL were significantly lower than the corresponding values for pure PLA and composites containing EXP alone. A remarkably low HRR was observed for PLA/EXP15/PES10/KL7 knitted fabric (191 kW m^{-2}) which is 58.50% less than the HRR of pure PLA. Higher loading content of KL could not delay the ignition time, as TTI of knitted fabrics containing KL were lower than without KL but a substantial decline in HRR and THR were observed.

4.5. References

1. Fox, D.M.; Lee, J.; Citro, C.J.; Novy, M. Flame retarded poly(lactic acid) using POSS-modified cellulose. 1. Thermal and combustion properties of intumescing composites. *Polym Degrad Stab* **2013**, *98*, 590–596, doi:10.1016/j.polymdegradstab.2012.11.016.
2. Fukushima, K.; Murariu, M.; Camino, G.; Dubois, P. Effect of expanded graphite/layered-silicate clay on thermal, mechanical and fire retardant properties of poly(lactic acid). *Polym Degrad Stab* **2010**, *95*, 1063–1076, doi:10.1016/j.polymdegradstab.2010.02.029.
3. Gui, H.; Xu, P.; Hu, Y.; Wang, J.; Yang, X.; Bahader, A.; Ding, Y. Synergistic effect of graphene and an ionic liquid containing phosphonium on the thermal stability and flame retardancy of polylactide. *RSC Adv* **2015**, *5*, 27814–27822, doi:10.1039/C4RA16393A.
4. Karim, M.N.; Rigout, M.; Yeates, S.G.; Carr, C. Surface chemical analysis of the effect of curing conditions on the properties of thermally-cured pigment printed poly (lactic acid) fabrics. *Dye Pigment* **2014**, *103*, 168–174, doi:10.1016/j.dyepig.2013.12.010.
5. Lin, H.J.; Liu, S.R.; Han, L.J.; Wang, X.M.; Bian, Y.J.; Dong, L.S. Effect of a phosphorus-containing oligomer on flame-retardant, rheological and mechanical properties of poly (lactic acid). *Polym Degrad Stab* **2013**, *98*, 1389–1396, doi:10.1016/j.polymdegradstab.2013.03.025.
6. Lin, H.; Han, L.; Dong, L. Thermal degradation behavior and gas phase flame-retardant mechanism of polylactide/PCPP blends. *J Appl Polym Sci* **2014**, *131*, 1–11, doi:10.1002/app.40480.

7. Murariu, M.; Bonnaud, L.; Yoann, P.; Fontaine, G.; Bourbigot, S.; Dubois, P. New trends in polylactide (PLA)-based materials: "Green" PLA-Calcium sulfate (nano)composites tailored with flame retardant properties. *Polym Degrad Stab* **2010**, *95*, 374–381, doi:10.1016/j.polymdegradstab.2009.11.032.
8. Murariu, M.; Dechief, A.L.; Paint, Y.; Peeterbroeck, S.; Bonnaud, L.; Dubois, P. Polylactide (PLA)-Halloysite Nanocomposites: Production, Morphology and Key-Properties. *J Polym Environ* **2012**, *20*, 932–943, doi:10.1007/s10924-012-0488-4.
9. Reti, C.; Casetta, M.; Duquesne, S.; Bourbigot, S.; Delobel, R. Flammability properties of intumescent PLA including starch and lignin. *Polym Adv Technol* **2006**, *17*, 395–418, doi:10.1002/pat.
10. Solarski, S.; Mahjoubi, F.; Ferreira, M.; Devaux, E.; Bachelet, P.; Bourbigot, S.; Delobel, R.; Coszach, P.; Murariu, M.; Da Silva Ferreira, A.; et al. (Plasticized) Polylactide/clay nanocomposite textile: Thermal, mechanical, shrinkage and fire properties. *J Mater Sci* **2007**, *42*, 5105–5117, doi:10.1007/s10853-006-0911-0.
11. Suardana, N.; Kyoo, M. Effects of diammonium phosphate on the flammability and mechanical properties of bio-composites. *Mater Des* **2011**, *32*, 1990–1999, doi:10.1016/j.matdes.2010.11.069.
12. Teoh, E.L.; Mariatti, M.; Chow, W.S. Thermal and Flame Resistant Properties of Poly (Lactic Acid)/Poly (Methyl Methacrylate) Blends Containing Halogen-free Flame Retardant. *Procedia Chem* **2016**, *19*, 795–802, doi:10.1016/j.proche.2016.03.087.
13. Wang, D.Y.; Leuteritz, A.; Wang, Y.Z.; Wagenknecht, U.; Heinrich, G. Preparation and burning behaviors of flame retarding biodegradable poly(lactic acid) nanocomposite based on zinc aluminum layered double hydroxide. *Polym Degrad Stab* **2010**, *95*, 2474–2480, doi:10.1016/j.polymdegradstab.2010.08.007.
14. Wang, D.Y.; Song, Y.P.; Lin, L.; Wang, X.L.; Wang, Y.Z. A novel phosphorus-containing poly(lactic acid) toward its flame retardation. *Polymer (Guildf)* **2011**, *52*, 233–238, doi:10.1016/j.polymer.2010.11.023.
15. Wang, K.; Wang, J.; Zhao, D.; Zhai, W. Preparation of microcellular poly(lactic acid) composites foams with improved flame retardancy. *J Cell Plast* **2017**, *53*, 45–63, doi:10.1177/0021955X16633644.
16. Wei, L.L.; Wang, D.Y.; Chen, H.B.; Chen, L.; Wang, X.L.; Wang, Y.Z. Effect of a

phosphorus-containing flame retardant on the thermal properties and ease of ignition of poly(lactic acid). *Polym Degrad Stab* **2011**, *96*, 1557–1561, doi:10.1016/j.polymdegradstab.2011.05.018.

17. Zhan, J.; Song, L.; Nie, S.; Hu, Y. Combustion properties and thermal degradation behavior of polylactide with an effective intumescent flame retardant. *Polym Degrad Stab* **2009**, *94*, 291–296, doi:10.1016/j.polymdegradstab.2008.12.015.
18. Bourbigot, S.; Fontaine, G. Flame retardancy of polylactide: An overview. *Polym Chem* **2010**, *1*, 1413–1422, doi:10.1039/c0py00106f.
19. Bourbigot, S.; Duquesne, S.; Fontaine, G.; Bellayer, S.; Turf, T.; Samyn, F. Characterization and Reaction to Fire of Polymer Nanocomposites with and without Conventional Flame Retardants. *Mol Cryst Liq Cryst* **2008**, *486*, 37–41, doi:10.1080/15421400801921983.
20. Qian, Y.; Wei, P.; Jiang, P.; Li, Z.; Yan, Y.; Ji, K. Aluminated mesoporous silica as novel high-effective flame retardant in polylactide. *Compos Sci Technol* **2013**, *82*, 1–7, doi:10.1016/j.compscitech.2013.03.019.
21. Solarski, S.; Mahjoubi, F.; Ferreira, M.; Devaux, E.; Bachelet, P.; Bourbigot, S.; Delobel, R.; Coszach, P.; Murariu, M.; Da Silva Ferreira, A.; et al. Designing Polylactide/Clay nanocomposites for textile applications: Effect of processing conditions, spinning, and characterization. *Polym Polym Compos* **2013**, *21*, 449–456, doi:10.1002/app.
22. Thunga, M.; Chen, K.; Grewell, D.; Kessler, M.R. Bio-renewable precursor fibers from lignin/polylactide blends for conversion to carbon fibers. *Carbon N Y* **2014**, *68*, 159–166, doi:10.1016/j.carbon.2013.10.075.
23. Di Blasi, C.; Branca, C.; Galgano, A. Effects of diammonium phosphate on the yields and composition of products from wood pyrolysis. *Ind Eng Chem Res* **2007**, *46*, 430–438, doi:10.1021/ie0612616.
24. Katsoulis, C.; Kandare, E.; Kandola, B.K. The combined effect of epoxy nanocomposites and phosphorus flame retardant additives on thermal and fire reaction properties of fiber-reinforced composites. *J Fire Sci* **2011**, *29*, 361–383, doi:10.1177/0734904111398785.
25. Wang, J.; Manley, R.S.J.; Feldman, D. Synthetic polymer-lignin copolymers and blends. *Prog Polym Sci* **1992**, *17*, 611–646, doi:10.1016/0079-6700(92)90003-H.
26. Idumah, C.I.; Hassan, A. Emerging trends in flame retardancy of biofibers, biopolymers, biocomposites, and bionanocomposites. *Rev Chem Eng* **2016**, *32*, 115–148,

doi:10.1515/revce-2015-0017.

27. Cheng, X.W.; Guan, J.P.; Tang, R.C.; Liu, K.Q. Phytic acid as a bio-based phosphorus flame retardant for poly(lactic acid) nonwoven fabric. *J Clean Prod* **2016**, *124*, 114–119, doi:10.1016/j.jclepro.2016.02.113.
28. Zhang, T.; Yan, H.; Shen, L.; Fang, Z.; Zhang, X.; Wang, J.; Zhang, B. Chitosan/phytic acid polyelectrolyte complex: A green and renewable intumescent flame retardant system for ethylene-vinyl acetate copolymer. *Ind Eng Chem Res* **2014**, *53*, 19199–19207, doi:10.1021/ie503421f.
29. Feng, J.X.; Su, S.P.; Zhu, J. An intumescent flame retardant system using β-cyclodextrin as a carbon source in polylactic acid (PLA). *Polym Adv Technol* **2011**, *22*, 1115–1122, doi:10.1002/pat.1954.
30. Zhang, R.; Xiao, X.; Tai, Q.; Huang, H.; Hu, Y. Modification of lignin and its applications as a char agent in intumescent flame retardant polylactic acid. *Polym Eng Sci* **2012**, 2620–2626, doi:10.1002/pen.
31. Zhang, R.; Xiao, X.; Tai, Q.; Huang, H.; Yang, J.; Hu, Y. Preparation of lignin–silica hybrids and its application in intumescent flame-retardant poly(lactic acid) system. *High Perform Polym* **2012**, *24*, 738–746, doi:10.1177/0954008312451476.
32. Laufer, G.; Kirkland, C.; Cain, A.A.; Grunlan, J.C. Clay-chitosan nanobrick walls: Completely renewable gas barrier and flame-retardant nanocoatings. *ACS Appl Mater Interfaces* **2012**, *4*, 1643–1649, doi:10.1021/am2017915.
33. Wang, J.; Ren, Q.; Zheng, W.; Zhai, W. Improved flame-retardant properties of poly(lactic acid) foams using starch as a natural charring agent. *Ind Eng Chem Res* **2014**, *53*, 1422–1430, doi:10.1021/ie403041h.
34. Maqsood, M.; Seide, G. Investigation of the Flammability and Thermal Stability of Halogen-Free Intumescent System in Biopolymer Composites Containing Biobased Carbonization Agent and Mechanism of Their Char Formation. *Polymers (Basel)* **2018**, *11*, 1–16, doi:10.3390/polym11010048.
35. Cayla, A.; Rault, F.; Giraud, S.; Salaün, F.; Fierro, V.; Celzard, A. PLA with intumescent system containing lignin and ammonium polyphosphate for flame retardant textile. *Polymers (Basel)* **2016**, *8*, doi:10.3390/polym8090331.
36. Afriyie, R.; Qiang, M.; Solomon, X.; Jin, A.C. Correlation analysis of cone calorimetry and

microscale combustion calorimetry experiments. *J Therm Anal Calorim* **2019**, *136*, 589–599, doi:10.1007/s10973-018-7661-5.

37. An, W.; Jiang, L.; Sun, J.; Liew, K.M. Correlation analysis of sample thickness , heat flux , and cone calorimetry test data of polystyrene foam. *J Therm Anal Calorim* **2015**, *119*, 229–238, doi:10.1007/s10973-014-4165-9.
38. Sharma, R.K.; Wooten, J.B.; Baliga, V.L.; Lin, X.; Chan, W.G.; Hajaligol, M.R. Characterization of chars from pyrolysis of lignin. *Fuel* **2004**, *83*, 1469–1482, doi:10.1016/j.fuel.2003.11.015.
39. Arrieta, M.P.; López, J.; López, D.; Kenny, J.M.; Peponi, L. plasticized PLA – PHB blends reinforced with cellulose nanocrystals. *Ind Crop Prod* **2015**, 1–12, doi:10.1016/j.indcrop.2015.12.058.

CHAPTER 5

Novel bicomponent functional fibers with sheath/core configuration containing intumescent flame-retardants for textile applications

Abstract

The objective of this study is to examine the effect of intumescent flame-retardants (IFR's) on the spinnability of sheath/core bicomponent melt-spun fibers produced from Polylactic acid (PLA) single polymer composites, as IFR's have not been tested in bicomponent fibers so far. Highly crystalline PLA containing IFR's was used in the core component while amorphous PLA was tested in the sheath component of melt-spun bicomponent fibers. Ammonium polyphosphate and lignin powder were used as acid and carbon source respectively together with PES as a plasticizing agent in the core component of bicomponent fibers. Multifilament fibers with sheath/core configurations were produced on pilot-scale melt spinning machine and the changes in fibers mechanical properties and crystallinity were recorded in response to varying process parameters. The crystallinity of bicomponent fibers was studied by differential scanning calorimetry and thermal stabilities were analyzed by thermogravimetric analysis. Thermally bonded nonwoven fabric samples from as prepared bicomponent fibers were produced and their fire properties such as limiting oxygen index and cone calorimetry values were measured, while the ignitability of fabric samples was tested by single-flame source test. Cone calorimetry showed a 46% decline in the heat release rate of nonwovens produced from FR PLA bicomponent fibers compared to pure PLA nonwovens and indicated the development of an intumescent char by leaving a residual mass of 34% relative to the initial mass of the sample. It was found that IFR's can be melt spun into bicomponent fibers by sheath/core configuration and enhanced functionality in the fibers can be achieved with suitable mechanical properties.

Keywords

Bicomponent fibers; Intumescent flame-retardants; Nonwoven; Cone calorimetry

5.1. Introduction

The development in process technologies for the value addition of commercially available polymers has been steered in synthetic fiber industry in the recent past [1, 2]. Among these technologies, bicomponent melt spinning has established substantial interest in synthetic fiber industry due to its prospective applications in the development of numerous innovative fibers such as ultra-fine fibers, crimped fibers, conductive fibers and fibers with various cross-sectional shapes [3, 4]. Bicomponent fibers with sheath/core (or shell/core) structures are widely used in the industry for the thermal bonding of nonwoven fabrics [5, 6]. Such applications of bicomponent fibers are based on the difference in melting temperatures of the polymers used in the sheath/core structure, e.g. the polymers with lower melting temperatures are employed in the sheath whereas high melting temperature polymers are used in the core [7, 8]. The objective of bicomponent fibers is to enhance the material's performance for specific end application however, the performance of melt-spun bicomponent fibers are dependent on various factors but mainly on the type of interfaces between both components and behavior of each component in the composition [9, 10]. For superior performance of bicomponent fibers, a stable and uniform interface with better adhesion of the components is required [11, 12]. Due to mutual interaction of both the components involved in bicomponent spinning, the thermal behavior and stress witnessed by each component in spin-line during extrusion is considerably different to what they experience in single component melt spinning [13, 14]. This difference in their behavior may affect in the development of the intended fiber structure. Therefore, the selection of appropriate polymer for each component is necessary for a stable and uniform interface for better adhesion of the components [15, 16]. Nowadays, single polymer composites containing reinforcement and matrix from the same polymer are being used in bicomponent melt spinning to have uniform interface and better interfacial bonding between the components [17, 18]. Polylactic acid (PLA) is a synthetic biopolymer, which can be processed into different forms of crystallinity. The amorphous PLA can be used as a matrix whereas highly-crystalline form can be used as reinforcement in bicomponent melt spinning process [19, 20].

Bicomponent spinning is used to impart diverse functionalities in the fibers such as electrical conductivity, chemical resistance, tactile comfort and fire resistance [21-23]. Hu et al. developed bicomponent fibers with sheath-core and segment-pie configurations for antistatic fabric applications in textiles [24]. Yeom et al. produced spun bonded nonwoven webs from PA6/PE

islands-in-the-sea bicomponent fibers for aerosol filtration applications [8]. Yu et al. discussed radar wave absorbing characterizations of bicomponent fibers with infrared camouflage [22]. The application of bicomponent fibers in fire resistant textiles is a fascinating approach to enhance the performance properties [25]. Fire resistant textiles have diverse applications, such as firefighter or military apparel, professional racer equipment, beddings and carpets [26, 27]. Therefore, it is critical to develop fire resistant or flame retardant textiles. Currently halogen-containing flame-retardants (HCFR) are forbidden in the industry however, exclusions are there for some special applications [28]. The main downside of HCFR is their release of toxic by-products during combustion and their harmfulness to the environment and human health. One such solution could be provided by halogen free flame-retardants (HFFR) which are non-toxic alternatives to HCFR as they do not release toxic by-products during combustion [29]. Intumescent flame retardant (IFR) systems are HFFRs that rely on char formation mechanisms and are safe to environment [30, 31]. IFR's usually contain an acid source, a carbon source and a blowing agent. The degradation of the acid source will be catalyzed by heat, resulting in a release of acid which in turn dilutes the gas phase and catalyze the dehydration of the carbon source [32]. The resulting char layer creates a barrier between the gas phase and the polymer, reducing heat and mass transfer, thus protecting the material from combustion [33]. Some studies investigated the melt-spinnability of IFR compounds only in single component fibers but their mechanical properties were too low to be considered for industrial applications [34, 35]. In one of our previous research paper [36], we investigated the spinnability of PLA/IFR's composites in mono-component configuration and found that although the multifilament fibers achieved excellent flame retardancy but we only managed to get fibers with tenacity of up to 7.3 $cN.tex^{-1}$. We therefore, in this study, developed bicomponent multifilament fibers with sheath/core configuration to investigate their effect not only on fiber's mechanical properties but also to test the fire behavior of these novel multifilament fibers.

Although various aspects of bicomponent spinning process has been studied in different applications [37-42] however, to the best of our knowledge no published study exists addressing the effect of IFR's in bicomponent fibers for textile applications. We therefore, developed melt spun bicomponent multifilament functional fibers from single polymer with sheath/core configuration by using highly crystalline PLA with IFR's in the core component while amorphous

PLA in the sheath component. IFR bicomponent fibers were produced on pilot scale melt spinning machine and the changes in fiber mechanical properties and crystallinity were recorded in response to varying process parameters. Thermally bonded nonwoven fabric samples from as prepared bicomponent fibers were produced and their fire properties such as limiting oxygen index and cone calorimetry data such as, heat release rate, time to ignition and residual mass% were measured, while the ignitability of fabric samples were tested by single-flame source test.

5.2. Materials and methods

The materials and methods used in this chapter are discussed in the following sections.

5.2.1. Materials

Two different types of PLA pellets, i.e. highly crystalline PLA (Luminy L130) and amorphous PLA (Luminy LX930) were purchased from Total-Corbion NV (Gorinchem, Netherlands). The physical properties of both types of PLA are presented in Table 5.1. Halogen free flame retardant (Exolit AP 422) having decomposition temperature higher than 275°C was attained from Clariant AG (Muttenz, Switzerland). Exolit AP 422 is a fine-particle ammonium polyphosphate (APP) containing 31% (w/w) phosphorous and 14% (w/w) nitrogen, having density of 1.9 $g.cm^{-3}$ and average particle size of 17 µm, used as acid donor in intumescent formulations. The kraft lignin (KL) powder "UPM BioPiva 100" was purchased from UPM Biochemicals OYJ (Helsinki, Finland). A modified polyester based plasticizing agent (PES) in white granular form (thermally stable up to 280˚C) was obtained from Preluna (Ludwigshafen, Germany), to improve spinnability of IFR composites. PLA (Luminy L130), APP, PES and KL were vacuum dried at 100˚C for 4 h before compounding.

Table 5.1. Physical properties of PLA pellets

Physical properties	Unit	PLA Luminy L130	PLA Luminy LX930
Density	g/cm^3	1.24	1.24
Melt flow index	g/10 min	24	17
Stereochemical purity	%	≥ 99 (L-isomer)	90 (L-isomer)
Appearance	Visual	Crystalline white pellets	Amorphous white pellets
Melting temperature	°C	175-180	125-135
Glass transition temperature	°C	55-60	55-60

5.2.2. Preparation of IFR composites

Coperion ZSK Mc[18] twin-screw extruder (Coperion GmbH, Stuttgart, Germany) was used to prepare PLA/APP/PES/KL composites for the core component of bicomponent fibers. In the first feeding zone, highly crystalline PLA pellets (Luminy L130) were mixed together with plasticizing agent (PES) whereas in the second feeding zone, flame retardant (APP) was mixed with kraft lignin powder (KL). PLA/APP/PES/KL composites were prepared at screw rotation speed of 500 rpm to use as core component for bicomponent fibers. The melt flow index (MFI) of the blends were in the range of 26-30 g/10 min. The formulations with content of each component (w/w) of as prepared composites are presented in Table 5.2. The temperatures of the three heating zones were kept at 170˚C, 175˚C and 180˚C, respectively.

Table 5.2. Additives composition in PLA composites

No.	Formulations	PLA (wt%)	APP (wt%)	PES (wt%)	KL (wt%)
1	PLA/APP5/PES10/KL1	84	5	10	1
2	PLA/APP5/PES10/KL3	82	5	10	3
3	PLA/APP5/PES10/KL5	80	5	10	5

5.2.3. Bicomponent spinning

PLA/APP/PES/KL pellets to be used as the core component were vacuum dried at 100˚C for 4h whereas PLA Luminy LX930 pellets to be used as sheath component were vacuum dried at 40˚C for 24h before spinning as per the instructions of the suppliers. Vacuum drying of the polymers is necessary to avoid possible filament breakage during melt spinning due to lowered viscosity of the melt because of the hydrolysis caused by excessive moisture in the polymers. The moisture contents of the pellets were lower than 75 ppm as determined by Karl Fischer Titrations method according to ASTM D6869. Bicomponent fibers were melt spun using Fourne Maschinenbau GmbH (Impekoven, Germany) pilot scale melt spinning machine, which have the capacity to produce bicomponent fibers consisting of two different polymers with a throughput of up to few kilograms per hour. A schematic diagram of the bicomponent plant is shown in Figure 5.1. PLA/APP/PES/KL pellets (core component) were fed into one hopper and PLA Luminy LX930 pellets (sheath component) were dosed in the second hopper of bicomponent melt spinning

machine. Pellets were melted at a temperature range of 195˚C to 220˚C by using separate extruder for each type of pellets. The coaxially combined melted material was then injected in a spinneret plate with each hole for bicomponent monofilaments of sheath/core configuration. Spin pumps rotating at constant revolutions per minute (rpm) ensured a homogeneous supply of the material to the spinneret plate. The spin pump for each component delivered a fixed quantity of the melt to the specially designed spinneret for the bicomponent fibers. Through the different rpm of the spin pumps for sheath and core, the fixed quantity of the melt for each component was delivered, and hence in this way, the thickness of each component was adjusted.

The monofilaments were passed through quenching section (quenching length = 1.4 m) where they were cooled down by maintaining the cool air velocity of 0.5 $m.s^{-1}$ and then combined together to multifilaments by applying a spin finish before they were collected by the suction gun. The multifilaments were passed through a take up roller followed by hot drawing at two set of heated rollers rotating at varying speeds. The multifilaments with sheath/core configuration were then wound on bobbins rotating on a winder for further analysis. The extruding sheath/core ratio for all bicomponent fibers was set to 1:2 (thin sheath and thick core) under constant melt flow.

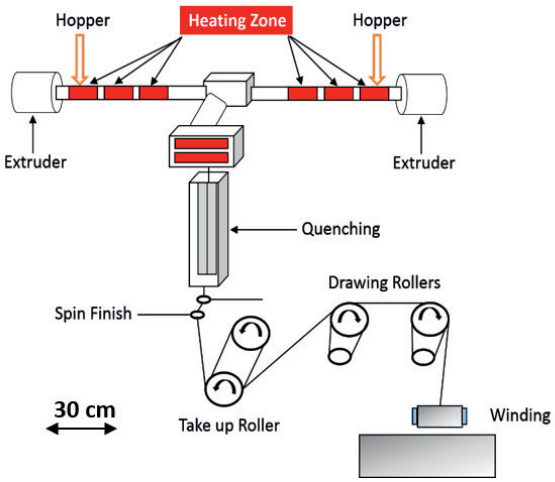

Figure 5.1. Schematic diagram of pilot scale bicomponent melt spinning machine

To further investigate the spinnability of bicomponent functional fibers in response to varying process parameters, a design of experiment was prepared using half factorial design in MINITAB 18 statistical software. Four factors/variables with two levels each were considered in this study and are shown in Table 5.3. Spinning parameters such as solid state draw ratio (SSDR), temperature (°C) of the heating rollers, linear density (dtex) of multifilaments and spinneret type with different no. of filaments were varied to analyze the effect of these parameters on the mechanical, structural and thermal properties of the bicomponent fibers. It is important to mention here that SSDR is a term used for solid-state draw ratio that means fibers are drawn when they are solidified. It is different from the term, melt draw ratio (MDR). In MDR, filaments are drawn from the spinneret plate until the take up roller by varying its speed, whereas in SSDR, filaments are drawn from the take up roller until the last pair of drawing rollers on melt spinning machine. The design of experiment showing different spinning parameters used to produce bicomponent fibers is presented in Table 5.4. Two spinneret types consisting of 24 and 34 number of filaments, two SSDR of 1.2 and 1.4, two temperature conditions 50°C and 70°C of the heating rollers and two different linear densities 400 dtex and 600 dtex of multifilaments were selected to investigate the effect of these parameters on fibers properties.

Table 5.3. Factors and their levels

No.	Factors	Levels	
1	No of filaments	24	34
2	Solid state draw ratio (SSDR)	1.2	1.4
3	Temperature of draw rollers (°C)	50	70
4	Linear density (dtex)	400	600

Table 5.4. Design of experiment

Sample	No. of filaments	Solid state draw ratio (SSDR)	Temperature of draw rollers (°C)	Yarn linear density (dtex)
PLA/APP5/PES10/KL1	24	1.2	50	400
	34	1.2	50	600
	24	1.4	50	600
	34	1.4	50	400
	24	1.2	70	600
	34	1.2	70	400
	24	1.4	70	400
	34	1.4	70	600
PLA/APP5/PES10/KL3	24	1.2	50	400
	34	1.2	50	600
	24	1.4	50	600
	34	1.4	50	400
	24	1.2	70	600
	34	1.2	70	400
	24	1.4	70	400
	34	1.4	70	600
PLA/APP5/PES10/KL5	24	1.2	50	400
	34	1.2	50	600
	24	1.4	50	600
	34	1.4	50	400
	24	1.2	70	600
	34	1.2	70	400
	24	1.4	70	400
	34	1.4	70	600

5.2.4. Mechanical testing

Mechanical properties of bicomponent fibers such as tenacity ($cN.tex^{-1}$) and elongation at break (%) were tested on Zwick Roell testing machine by using EN ISO 5079 standard method. The specimen lengths (50 mm) and rate of deformation (50 mm min^{-1}) were kept constant for all samples. Ten specimens were prepared from each sample and their average results with standard deviations were recorded.

5.2.5. Thermogravimetric analysis

Thermogravimetric analysis of bicomponent fibers was done using a TGA Q5000 device (TA Instruments, New Castle, Delaware, USA). The specimens (15–20 mg) were heated at a constant

rate of 10˚C min^{-1} up to 700˚C under nitrogen at a flow rate of 50 mL min^{-1}. The thermal decomposition temperature and the temperature at which maximum degradation took place were calculated along with the residual mass percentage of the sample compared to the initial mass. The thermogravimetric curves of specimens were plotted after analysis.

5.2.6. Scanning electron microscopy

The surface morphology, cross sectional images and additives dispersion in bicomponent fibers were evaluated by using a Hitachi S-3200 scanning electron microscope (Chiyoda, Tokyo, Japan). For better cross-sectional images, bicomponent fibers were first immersed in liquid nitrogen to be freezed and then were cut with razor blade. Standard specimen stubs with silver coating were used to attach the samples, which were, then sputter coated with gold. Selective samples were inspected at a magnification of 1000 × and at an accelerating voltage of 20 kV.

5.2.7. Differential scanning calorimetry

Differential scanning calorimetry (DSC) analysis of bicomponent fibers was done using a DSC Q2000 (TA instruments). Nitrogen gas was used at a stream rate of 50 mL min^{-1}. The samples were heated at a constant rate of 10˚C min^{-1} starting from 0˚C to 230˚C and were then cooled at the same rate. The degree of crystallinity (Xc) of bicomponent fibers was calculated by equation (1),

$$Xc\,\% = \frac{\Delta Hm - \Delta Hcc}{\Delta Hf \times Wfr} \times 100 \qquad (1)$$

Where, Xc corresponds to degree of crystallinity of the sample; ΔHm implies to heat of fusion of the sample; ΔHcc corresponds to cold crystallization enthalpy; ΔHf relates to the heat of fusion of 100% crystalline material, and Wfr is the net weight fraction of the polymer. The heat of fusion of 100% crystalline PLA (ΔHf) is approximately 93.6 $J.g^{-1}$.

5.2.8. Thermally bonded nonwoven as carpet backing

Thermally bonded nonwoven fabrics were produced from flame retardant bicomponent fibers to be used as carpet backing. The process comprised the steps of laying down the continuous bicomponent filaments and entangling them together at filament crossover points by air pressure, which then were laid on the conveyer belt to form a nonwoven web. The as such produced

nonwoven web was thermally bonded by calendaring at a temperature of 135 ˚C, which actually is the melting temperature of the sheath material (low melting PLA) in the bicomponent yarn. After bonding the web thermally by passing over a rotating roller heated by a hot air; the web was passed through a cooling section to consolidate the fixation and then wound up on fabric rolls. The resultant nonwoven flame retardant fabric was dimensionally stable and had a width of around 50 cm as shown in Figure 5.2. The nonwoven fabric produced had an areal density of 120 g m^{-2}.

Figure 5.2. Bicomponent filaments and thermal bonded nonwoven fabric

5.2.9. Fire testing

The limiting oxygen index (LOI) of samples was tested. LOI is the fraction of oxygen that must be present to support burning, hence higher LOI values indicate lower flammability. The nonwoven samples (100×10×3 mm^3, as required by ISO 4589) were vertically placed in a glass column supplied with a mixture of oxygen and nitrogen gas, and were then ignited from above using a downward-pointing flame. The LOI tests for nonwoven samples were conducted using the Fire Testing Technology (FTT) Oxygen Index Apparatus (Stanton Redcroft, Sussex, UK).

Thermally bonded nonwoven fabric samples with dimensions of 100 × 100 × 3 mm^3 were prepared to perform cone calorimetry test according to ISO 5660 with heat flux of 35 kW m^{-2} by using Stanton Redcroft instrument. Cone calorimeter equipment operates on oxygen consumption principle and measures total heat of combustion based on the amount of oxygen consumed. Peak heat release rate (PHRR), time to ignition (TTI) and residual mass (%) of thermally bonded nonwoven fabric samples produced from FR bicomponent fibers were recorded after the test. Cone calorimetry test was also performed on pure PLA nonwoven fabric sample for the comparison purpose.

The single-flame source test (ignitability test) as required by EN ISO 11925-2 was conducted by using FTT Ignitability Apparatus (FTT Sussex, UK). In this fire test, nonwoven fabric samples of size 250 mm × 90 mm were exposed to a direct gas flame of a height of 20 mm after placing them vertically on a U-shaped sample holder. The flame application point was 40 mm above the bottom surface of the fabric sample. To observe the falling flame droplets, a filter paper was also positioned underneath the sample holder. The flame application time was set for 15 seconds for each test and after 20 seconds of removal of flame the test was terminated. After terminating the test, flame spread distance (mm) and burning time was measured. The fabric classification was based on whether the flame spread reached 150 mm distance in a given time period or not or whether the filter paper positioned below the sample holder was ignited by the flame droplets or not.

5.3. Results and discussion

5.3.1. Melt spinning and mechanical properties of bicomponent fibers

The spinning of bicomponent multifilament fibers was not only challenging but also it took a while to find the right parameters to make the spinning process stable for continuous collection of fibers. The melt spinning process was stable without filament breakage for as spun fibers or for the fibers drawn at lower solid-state draw ratio (SSDR) however, an occasional filament breakage were observed when drawn at higher SSDR. This suggests that bicomponent fibers containing IFR's in the core component can be melt spun in to multifilaments if not drawn at too high SSDR. In our case, SSDR up to 1.4 was sufficient to produce bicomponent fibers without filament breakage however; beyond this SSDR, filaments kept on breaking and continuous collection of the fibers was not possible. IFR's were used in the core component and not in the sheath component of the bicomponent fibers because previous studies [38, 43] suggests that the components with higher viscosities should be placed in the core and not in the sheath. The reason is that, in coaxial flow, the sheath component is driven through higher stress areas than core component and therefore, if additives are used in the sheath component its melt viscosity will be increased further therefore, will not be able to withstand the tensions and stresses during processing hence, stable process will not be built up. The summary of the test results are presented in Table 5.5 while mechanical properties of the melt-spun bicomponent fibers are shown in Figure 5.3. The tenacity of the as spun fibers containing 1 wt% of KL were on the lower side (6.9 $cN.tex^{-1}$) as expected, since no

crystallinity was induced in the fibers however, it was significantly improved by increasing SSDR as a maximum tenacity of 12.6 cN.tex^{-1} containing 1 wt% KL was achieved at SSDR of 1.4. The tenacity was gradually reduced by increasing the wt% of KL in the core component at the same SSDR of 1.4. It can be seen in Table 5.5 that the addition of 3 and 5 wt% of KL in the core of bicomponent fibers could only achieve a tenacity of 11.4 and 10.7 cN.tex^{-1} respectively at the same SSDR of 1.4. Compared to as spun fibers, the fibers drawn at SSDR of 1.2, showed lower elongation at break (%) however, with increasing SSDR of 1.4, the elongation at break further reduced as shown in Table 5.5 and Figure 5.3. These results indicated that the mechanical properties of melt spun bicomponent fibers were not only dependent of SSDR but, loading concentration (%) of KL also played a significant role in defining the mechanical properties of bicomponent fibers. It is noteworthy to mention here that amongst all factors only SSDR was found to be the most significant factor that affected the mechanical properties of fibers. Other factors such as, number of filaments, drawing roller temperatures and yarn linear density hardly affected mechanical or thermal properties of fibers therefore, their effect on fiber properties has not been mentioned here.

Table 5.5. Summary of mechanical properties of bicomponent melt-spun fibers

Formulation	SSDR	Tenacity (cN.tex^{-1})	Elongation at break (%)
PLA/APP5/PES10/KL1	As spun	6.9 ± 1.3	95.3 ± 6.4
	SSDR 1.2	8.1 ± 1.6	86.1 ± 9.7
	SSDR 1.4	12.6 ± 1.1	69.5 ± 11.3
PLA/APP5/PES10/KL3	As spun	6.1 ± 1.5	88.1 ± 10.5
	SSDR 1.2	7.4 ± 1.9	81.2 ± 11.1
	SSDR 1.4	11.4 ± 1.6	64.6 ± 13.5
PLA/APP5/PES10/KL5	As spun	5.9 ± 1.2	85.8 ± 10.9
	SSDR 1.2	6.5 ± 1.7	76.3 ± 16.6
	SSDR 1.4	10.7 ± 1.9	59.9 ± 12.8

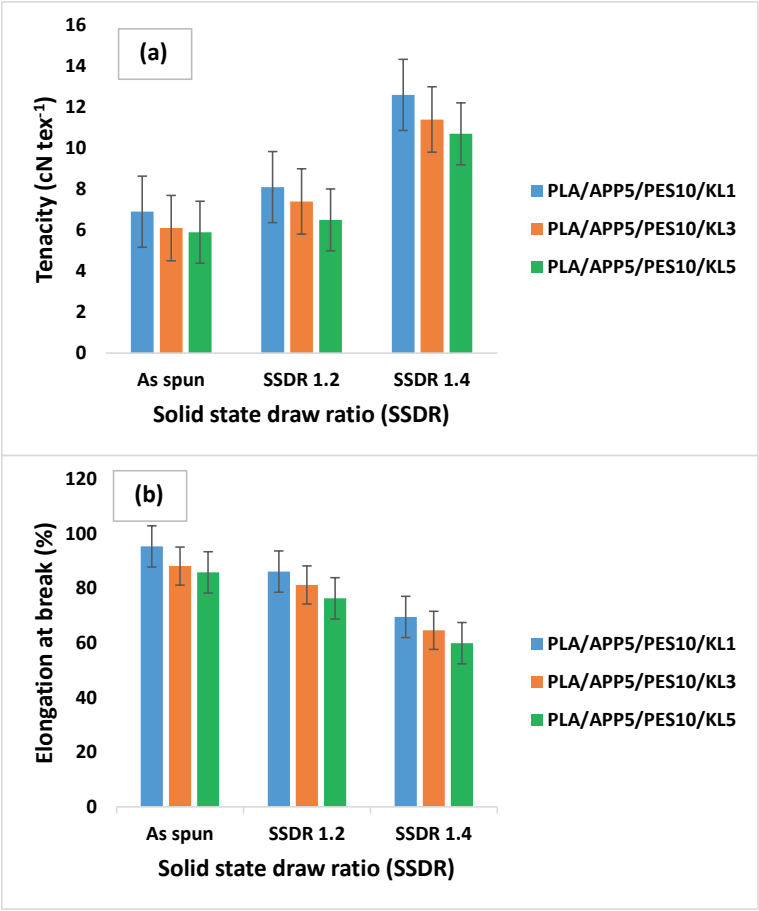

Figure 5.3. Tenacity (a) and elongation at break (b) of PLA/APP/PES/KL bicomponent fibers

Similar findings were reported by Hu et al. [24] and observed that a dramatic down fall in mechanical properties of core/sheath bicomponent fibers containing antistatic agents occurred by increasing filler content and suggested that a strong interaction between matrix and filler content is required in order to improve mechanical properties of composite fibers. Lund et al. [44] used carbon black as conductive core in poly (vinylidene fluoride) (PVDF) matrix and found that mechanical properties of fibers decreased quite significantly at any loading concentration of

carbon black compared to neat PVDF fibers, even though the fillers were uniformly distributed within the matrix.

5.3.2. Thermal stability of bicomponent fibers

The effect of IFR additives on thermal stability and thermal decomposition of bicomponent fibers was investigated by thermogravimetric analysis and the residual mass% of samples was determined at 700˚C. The thermal decomposition temperatures and mass residue% of the samples after TG analysis were compared to determine the influence of carbonization agent (KL) on thermal stabilities of bicomponent composite fibers. TG curves of bicomponent fibers and their respective data for the samples heated in a nitrogen atmosphere are presented in Figure 5.4 and Table 5.6 respectively.

Table 5.6. Data of thermogravimetric analysis

No.	Formulations	T5 (˚C)	T50 (˚C)	T max (˚C)	Residual mass (%)
1	Pure PLA	300.3 ± 1.7	334.6 ± 1.3	340.1 ± 1.8	0.0 ± 0.0
2	PLA/APP5/PES10/KL1	315.2 ± 2.3	343.3 ± 1.9	356.4 ± 2.9	5.3 ± 1.6
3	PLA/APP5/PES10/KL3	317.8 ± 3.1	347.9 ± 2.6	359.2 ± 2.1	9.0 ± 1.8
4	PLA/APP5/PES10/KL5	321.4 ± 2.9	351.6 ± 3.6	363.7 ± 1.9	11.3 ± 1.1

The temperatures corresponding to 5% and 50% mass loss for the bicomponent fibers are represented by T5 and T50 values in Table 5.6, whereas the temperature corresponding to the maximum rate of mass losses is represented by T max. The degradation of the bicomponent fiber containing 1 wt% of KL (PLA/APP5/PES10/KL1) started at 315.2˚C and 50% loss occurred at 343.3˚C, with residual mass left at 700˚C of 5.3%. The thermal stabilities of the bicomponent fiber containing 3 wt% of KL (PLA/APP5/PES10/KL3) were slightly higher to that of composite fiber containing 1 wt% of KL however, the residue left at 700˚C was 9.0% of the initial mass of the sample. For the bicomponent fiber containing 5 wt% of KL (PLA/APP5/PES10/KL5), the initial decomposition temperatures and thermal stabilities were greater than the corresponding values for the bicomponent fibers containing 1 and 3 wt% of KL, with 11.3% residual mass left at 700˚C. No residual mass was left for pure PLA fibers and their T5 and T50 values were also lower compared to fibers containing KL. The addition of higher wt% of lignin (3 and 5%) not only improved the

thermal stability of the composite fibers but also increased the residual mass% at 700˚C. For example, the bicomponent fiber containing 3 wt% of KL (PLA/APP5/PES10/KL3) increased the residual mass to 9.0% compared to 5.3% of composite fiber containing 1 wt% of KL. The addition of 5 wt% of KL (PLA/APP5/PES10/KL5) further increased the residual mass to 11.3% at 700˚C. The thermogravimetric curves of bicomponent fibers containing 1, 3 and 5 wt% of KL are presented in Figure 5.4. The bicomponent fiber containing 5 wt% of KL was found to be more thermally stable and presented denser and more compact char structure with higher residual mass (11.3%) due to charring ability of KL as a result of polycyclic aromatic hydrocarbons formation as indicated by Sharma et al. [45]. Thermogravimetric curves presented in Figure 5.4 of bicomponent fibers show the residual mass% as a function of temperature, up to 700˚C. The reason for the selection of only as spun fibers for TGA analysis is that, SSDR did not had any effect on the thermal stability or on residual mass (%) of fibers. The parameter that affects most the thermal stability of fibers was the loading concentration of the additives incorporated in the polymer blends. Therefore, we only selected the as spun fibers with different loading concentration of KL for TGA analysis.

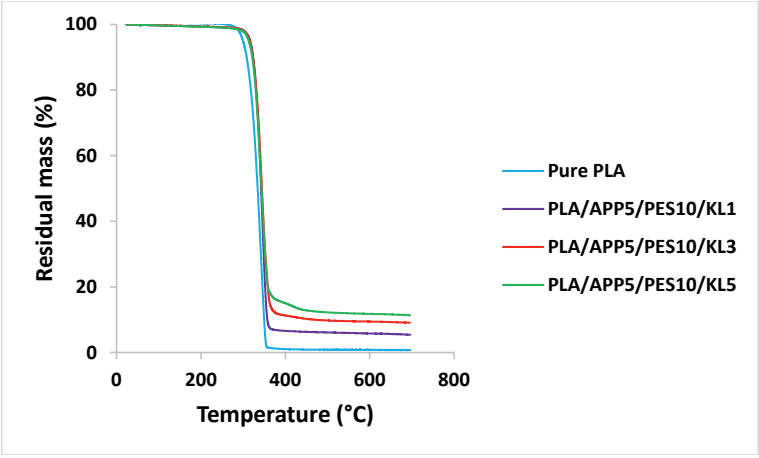

Figure 5.4. Thermogravimetric curves of bicomponent fibers

The curves indicate that most of the thermal decomposition occurs between 300˚C and 400˚C. Whereas all the bicomponent fibers decompose within a narrow temperature window and increasing the concentration of KL causes more residual mass to remain at temperatures between 375˚C and 700˚C. The thermal stabilities of bicomponent fibers containing 5 wt% of KL are

therefore better than those bicomponent fibers containing 1 and 3 wt% of KL. This behavior is mainly due to higher decomposition temperatures of these fibers for 5 and 50% mass loss (T5 and T50 values) than other fibers. The other reason could also be due to greater char forming ability of the polyhydric component (KL) and dehydration mechanism established by acid source (APP) due to the formation of phosphate compounds that further enhances the dehydration of KL resulting in higher char formation with compact structures.

5.3.3. Surface morphology and cross sectional images of bicomponent fibers

The dispersion characteristics of IFR additives and microstructures of bicomponent fibers were examined by scanning electron microscopy. The cross-sectional images and surface morphology of bicomponent fibers are shown in Figure 5.5 and 5.6 respectively. It can be seen by SEM images that the dispersion state of IFR additives is uniform in the bicomponent fibers. SEM images showed some exfoliated and tactoid regions which were developed due to the large aggregates of the additives accumulated at the fiber surface however, due to a strong shear rate and consistent elongational stress applied at higher draw ratios during melt spinning, a significant intercalation was seen, hence a more uniform dispersion of IFR additives were observed. In the longitudinal direction of bicomponent fibers, a stripe was observed as shown in Figure 5.6 (b and c) which was developed due to thermal shrinkage of the core component of the fibers. It happened due to the crystallization (solidification) of the sheath component at much lower temperature to that of the core component, as similar effect was observed by Houis et al [46] and Kazemi et al [47]. As a result the crystallized sheath component had a much lower coefficient of thermal expansion than the polymer melt in the core component. Therefore, a significant volume reduction happened with cooling of the polymer melt in the core component of the fibers which led to the stripe development in the longitudinal direction of the fibers, as similar behavior of the core/sheath components was reported by Ayad et al [10]. Since the core-sheath configuration we used had a higher volume flow rate for the core therefore, a faster cooling rate had to be applied in the quenching section to maintain the balance. Due to faster cooling rate in the quenching section, the filaments from the outside (sheath) solidified much earlier than from the inner side (core) therefore, as a consequence shrinkage of the core material took place during congealing.

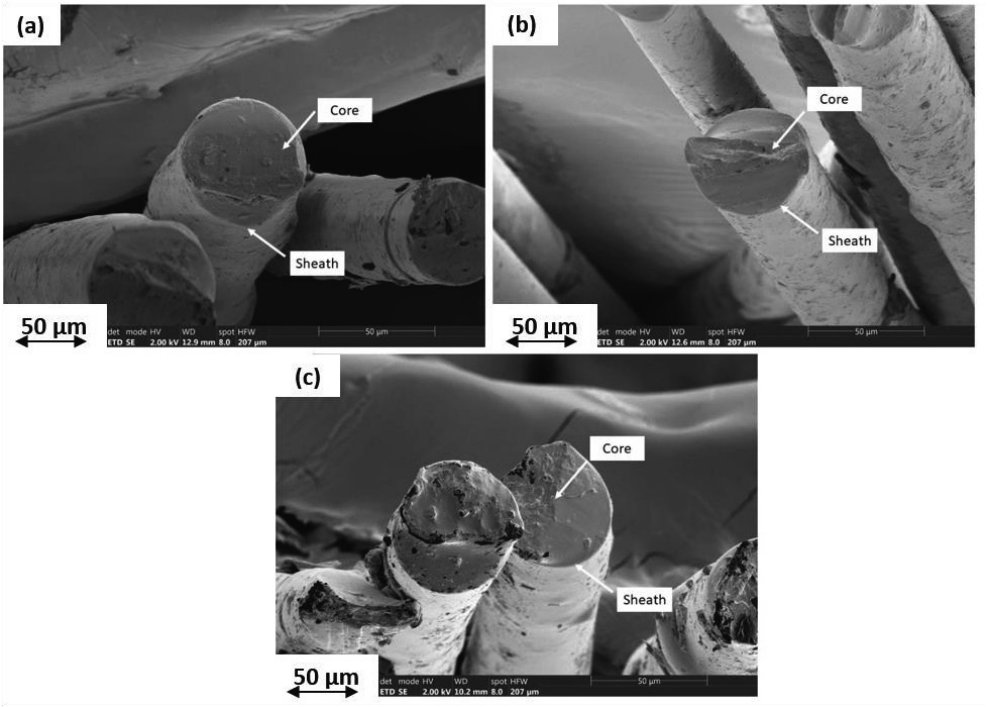

Figure 5.5. Cross-sectional SEM images of PLA/APP5/PES10/KL1 (a), PLA/APP5/PES10/KL3 (b), PLA/APP5/PES10/KL5 (c), bicomponent composite fibers [1000 × and 50 µm].

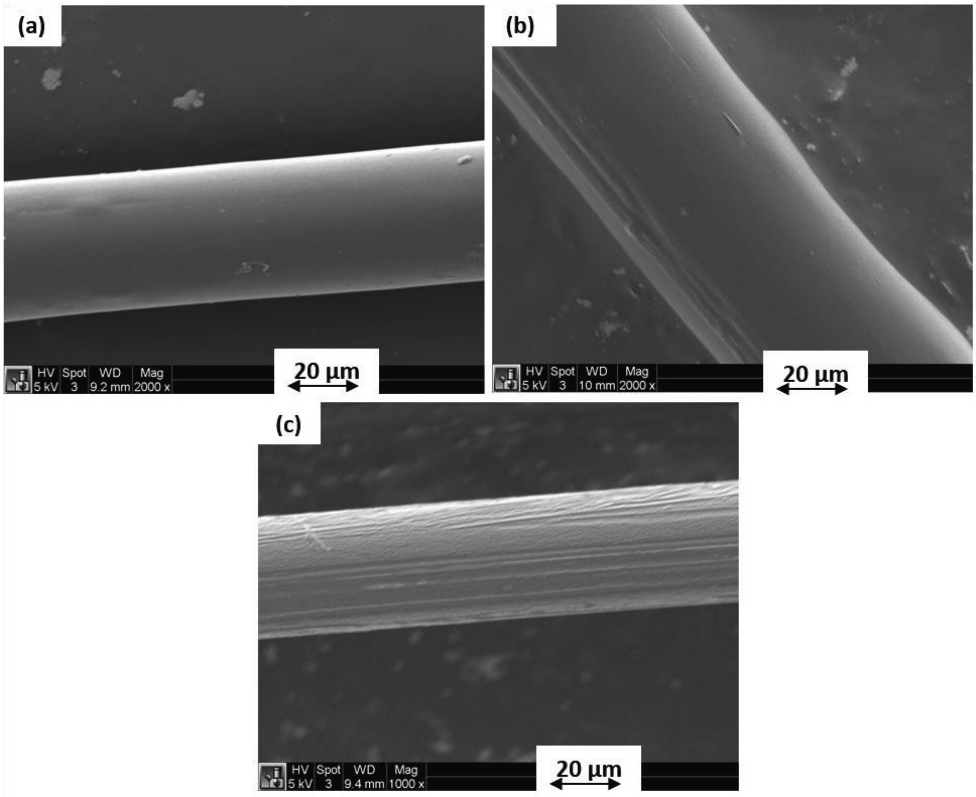

Figure 5.6. Surface SEM images of PLA/APP5/PES10/KL1 (a), PLA/APP5/PES10/KL3 (b), PLA/APP5/PES10/KL5 (c), bicomponent composite fibers [1000 × and 20 µm].

5.3.4. Differential scanning calorimetry

Differential scanning calorimetry was used to investigate the crystallinity of the bicomponent fibers. DSC curves of the bicomponent fibers are presented in Figure 5.7.

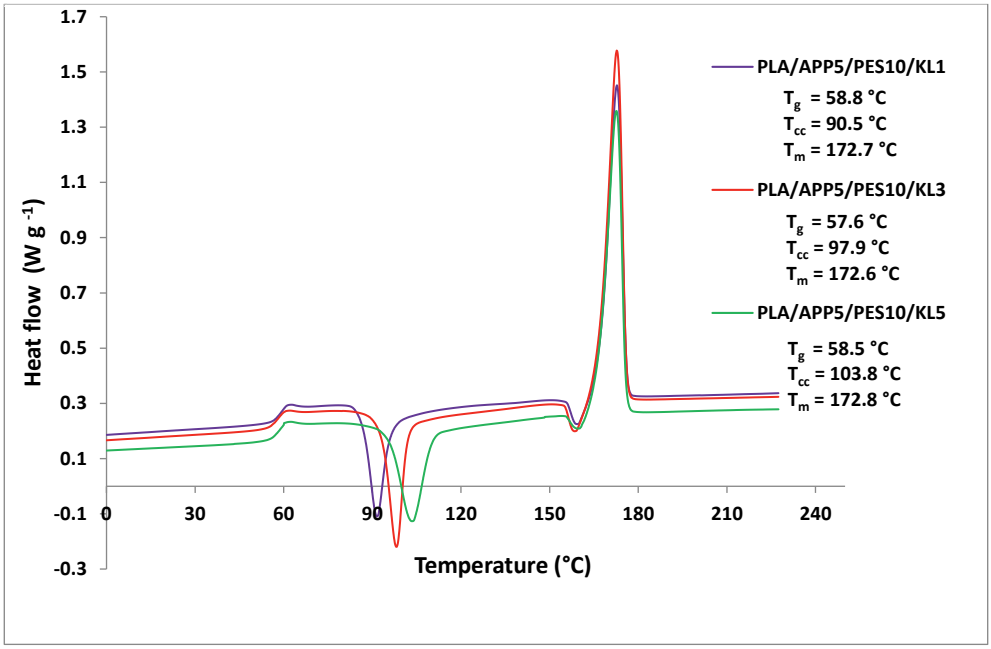

Figure 5.7. DSC thermograms of bicomponent fibers

The peaks for the glass transition temperatures, cold crystallization temperatures and melting temperatures can be clearly seen of all the three-bicomponent fibers in the DSC thermograms. However, all the three bicomponent fibers have different cold crystallization exotherms which is attributed to the differently oriented and semi-crystallized core and sheath components. The thermal properties and crystallinity (%) of the bicomponent fibers calculated by equation (1) are presented in Table 5.7 whereas the crystallinity (%) of the bicomponent fibers as a function of draw ratio is shown in Figure 5.8. It was observed that crystallinity of the bicomponent fibers increased by increasing the SSDR, which is due to the better alignment of the molecular chain within the polymers.

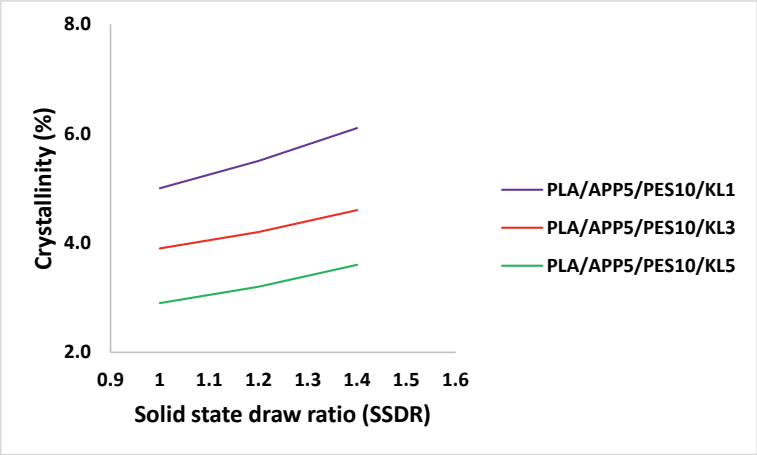

Figure 5.8. Crystallinity of bicomponent fibers as a function of draw ratio

In melt spinning, the crystallinity of fibers changes by hot drawing the fibers (stretching between two heated rollers) which attenuates and align the molecular chain within the fibers and therefore, by doing so their crystallinity is increased. The bicomponent fibers containing 1, 3 and 5 wt% of KL in the core component (PLA/APP5/PES10/KL1, PLA/APP5/PES10/KL3 and PLA/APP5/PES10/KL5) showed glass transition temperatures at 58.8˚C, 57.6 ˚C and 58.5 ˚C respectively whereas, melting peaks at 172.7 ˚C, 172.6 ˚C and 172.8 ˚C respectively. However, a major difference in their cold crystallization peaks was seen.

Table 5.7. Thermal properties of bicomponent fibers by DSC analysis

Samples	Tg (°C)	Tcc (°C)	Tm (°C)	Xc (%)
PLA/APP5/PES10/KL1	58.8 ± 0.6	90.5 ± 0.8	172.7 ± 0.9	6.1 ± 0.7
PLA/APP5/PES10/KL3	57.6 ± 0.4	97.9 ± 0.6	172.6 ± 1.1	4.6 ± 0.3
PLA/APP5/PES10/KL5	58.5 ± 0.5	103.8 ± 0.7	172.8 ± 1.3	3.6 ± 0.8

Tg = glass transition temperature, Tcc = cold crystallization temperature, Tm = melting temperature, Xc = crystallinity of fibers.

It can be seen in Table 5.7 that the bicomponent fibers containing 5 wt% of KL (PLA/APP5/PES10/KL5) presented cold crystallization peak at higher temperature (103.8˚C) whereas the bicomponent fibers containing 1 wt% of KL (PLA/APP5/PES10/KL1) showed cold crystallization peak at much lower temperature (90.5˚C). This is because the higher concentration

of KL (5 wt%) increased the viscosity of the melt hence more agglomerates were formed and less uniform dispersion of additives was taken place and therefore, cold crystallization temperature increased due to the restriction in polymer chain mobility. In DSC thermograms of all three bicomponent fibers, another exothermic peak before the melting peak was observed at around 158˚C.

It can be seen in Table 5.7 that the bicomponent fiber containing 1 wt% of KL have the highest crystallinity (6.1%) than rest of the bicomponent fibers. The reason for that is bicomponent fiber having least wt% of the additives got enough time in the processing apparatus for cooling which enables it to form all possible crystallites. Contrary to that, the bicomponent fibers with higher wt% of additives in the core took longer to crystallize because fast cooling in the processing apparatus did not enable them to form all possible crystallites, hence their crystallinity was reduced. Therefore, it presented less time for the orientation of the macromolecules in the cooling section, which led to partial crystallinity of the core component hence, overall crystallinity of the fiber was reduced. Another factor which influence the crystallization behavior of the polymers is the heat transfer from core to the sheath component and then to the air. Greater the heat transfer from the core to the sheath component, higher will be the crystallinity of the fibers [48].

5.3.5. Cone calorimetry measurements and ignitability by single flame source test

Cone calorimetry gives useful insights about the burning behavior of materials by calculating parameters such as peak heat release rate (PHRR), time to ignition (TTI) and residual mass (%) after burning of the material. Cone calorimetry data of pure PLA nonwoven fabric sample and nonwoven fabric samples produced from FR PLA bicomponent fibers are presented in Table 5.8. The influence of three different wt% of KL (i.e. 1, 3 and 5 wt%) in nonwoven fabric samples were assessed against their reactions to fire. TTI of pure PLA nonwoven fabric sample was 73.2 s. TTI of the fabric sample containing 1 wt% of KL (PLA/APP5/PES10/KL1) was 62.4 s, which was decreased to 59.3 s in case of 3 wt% of KL (PLA/APP5/PES10/KL3) and to 57.1 s when 5 wt% of KL was incorporated in the fabric sample.

Table 5.8. Cone calorimetry data for pure PLA and FR PLA nonwoven fabric samples

Formulation	TTI (s)	PHRR (kW m^{-2})	THR (MJ m^{-2})	Residual Mass (%)	LOI (%)
Pure PLA	73.2 ± 1.4	573.6 ± 12.1	58.1± 0.4	0.0 ± 0.0	19.3 ± 1.9
PLA/APP5/PES10/KL1	62.4 ± 1.3	368.2 ± 7.4	38.4 ± 0.2	21.3 ± 0.4	25.2 ± 1.2
PLA/APP5/PES10/KL3	59.3 ± 1.7	337.1 ± 4.8	35.8 ± 0.9	26.7 ± 0.6	27.1 ± 0.9
PLA/APP5/PES10/KL5	57.1 ± 1.3	309.3 ± 6.9	33.1 ± 0.4	34.5 ± 0.5	30.4 ± 1.6

TTI = time to ignition; HHR = heat release rate; THR = total heat release; LOI = limiting oxygen index

When a material is decomposed, pyrolysis gases are released and if the concentration of such gases is reached at certain threshold, ignition of the material is started. Prolonged ignition time of a material is mainly due to slower decomposition of the material. The samples containing KL showed lower TTI than pure PLA because it fits with common intumescent systems as degradation of the intumescent samples has to begin prior charred layer is developed.

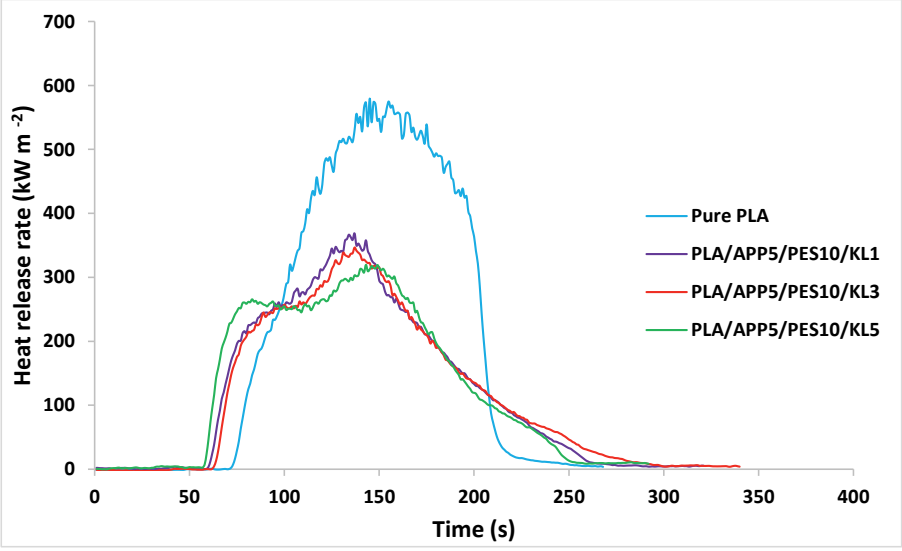

Figure 5.9. Heat release curves of pure PLA and FR PLA nonwoven fabric samples.

The curves showing peak heat release rate (PHRR) of the fabric samples after cone calorimetry are presented in Figure 5.9. Pure PLA nonwoven sample burnt considerably quicker than the other

nonwoven samples and produced a very steep PHRR curve with a PHRR of 573.6 kWm^{-2}. The fabric sample containing 1 wt% of KL after ignition presented PHRR of 368.2 kW m^{-2}. For the fabric sample containing 3 wt% of KL, PHRR declined to 337.1 kW m^{-2}, which was further reduced to 309.3 kW m^{-2} by the addition of 5 wt% of KL. These findings suggested that higher loading (%) of KL formed thicker and compact char layer on fabric surface which restricted further burning of the sample and helped in extinguishing the fire. The residual mass (%) of nonwoven fabric samples after cone calorimetry are also presented in Table 5.8. There was no residual mass left for pure PLA nonwoven sample after cone calorimetry test. The residual mass left for fabric sample containing 1 wt% of KL was 21.3% which was increased to 26.7% and 34.5% by the addition of 3 and 5 wt% of KL respectively. The higher residual mass (%) in case of fabric sample containing 5 wt% of KL reflected an increased char production due to lower PHRR values.

The intumescent system operates in the condensed phase where burning of the material generates sponge-like multicellular structure (char) which protects the underlying material from further heat and mass transfer by acting as a physical barrier between the material and source of fire. Figure 5.10 showed the char residues of the fabric samples after cone calorimetry test.

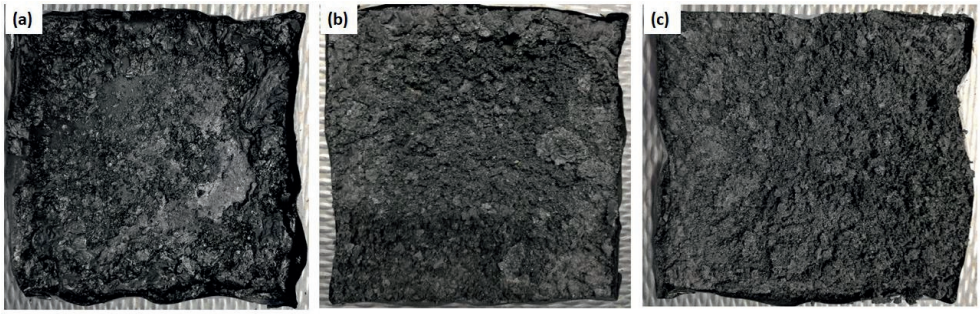

Figure 5.10. Char residues of fabric samples (a) 1% KL (b) 3% KL (c) 5 % KL after cone calorimetry

The fabric samples containing 1 wt% of KL presented a thinner and porous char layer because due to decreased viscosity of the substrate a very little pressure was built up which allowed gas bubbles and vapors to escape from the unclosed cells resulting in reduced swelling of the char layer and increased heat release rate. On the other hand, more compact and uniform char presented by the sample containing 5 wt% of KL prevented the free escape of gas bubbles and vapor particles which

resulted in more pressure build up due to closed cells which further increased the melt viscosity of the condensed substrate hence, greater swelling of char can be seen.

The limiting oxygen index (LOI) test is widely accepted to assess the flame retardancy of materials. We also tested the LOI values of nonwoven fabric samples, which are presented in Table 5.8. The LOI value of fabric sample containing 1 wt% of KL was 25.2%. The addition of 3 wt% of KL increased the LOI value to 27.1% and the presence of 5 wt% of KL further enhanced the LOI value to 30.4%. Higher LOI values for the samples containing greater content% of KL is mainly due to the formation of char layer which not only protected the fabric sample from external heat source but also protected it from further degradation.

The ignitability test under EN ISO 11925-2 method was used to determine the ignitability of nonwoven fabric samples in the vertical direction by direct flame impingement. Six specimens from each fabric sample were subjected to surface exposure to flame and their results are presented in Table 5.9. Six specimens from each fabric sample were exposed to flame for 15 (s) and their flame spread time (s) and flame spread distance (mm) were measured. It can be seen in Table 5.9 that none of the fabric sample containing KL was ignited after 15 (s) of flame exposure and therefore, flame spread distance (mm) and time (s) could not be recorded. Neither the burning droplets from the specimen could be seen nor was the ignition of the filter paper placed underneath of the specimen.

Table 5.9. Ignitability test results of nonwoven fabric samples.

Formulation	Ignition (Yes/No)	Time for flame tip to reach 150 mm (s)	Extent of flame spread (mm)	Burning droplets	Ignition of filter paper
PLA/APP5/PES10/KL1	No	Did not reach	None	No	No
PLA/APP5/PES10/KL3	No	Did not reach	None	No	No
PLA/APP5/PES10/KL5	No	Did not reach	None	No	No

The reason for no ignition of the specimen was an increase in the gap between flame and the specimen due to the fleeing of heat flux therefore, the temperature at the specimen surface

decreased and heat flow was reduced hence, fuel availability was no more to continue ignition. Based on this test our fabric samples got the classification of E and Efl. To get E and Efl (for floorings) classification the flame should not reach the top marking (150 mm) within 20 s after 15 s of flame exposure and there should be no burning droplets and no ignition of the filter paper placed underneath. It can be seen in Figure 5.11 that flame could not reach the distance of 150 mm after 15 s of flame exposure.

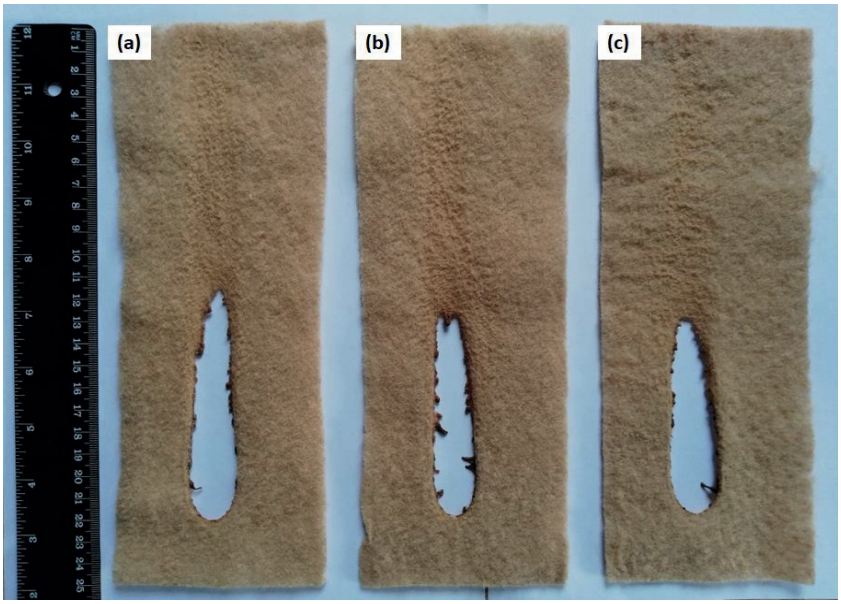

Figure 5.11. Images of PLA/APP5/PES10/KL1 (a), PLA/APP5/PES10/KL3 (b), PLA/APP5/PES10/KL5 (c) FR nonwoven fabric samples after ignitability test

5.4. Conclusions

In this study, novel bicomponent functional fibers based on single polymer consisting of highly-crystalline PLA with intumescent flame retardants in the core and low melting PLA in the sheath were produced. Thermogravimetric analysis confirmed that the thermal stabilities of bicomponent fibers increased quite significantly and fibers containing 5 wt% of KL presented the highest residual mass%. Thermally bonded nonwoven fabric samples produced from bicomponent fibers showed remarkable flame retardancy. A significantly low PHRR (309.3 kW m^{-2}) of sample

containing 5 wt% of KL was observed which is 46% less than the PHRR of nonwoven sample made from pure PLA. TTI of KL samples decreased quite significantly since fabric sample containing 5 wt% of KL presented TTI of 57.1 (s) compared to 73.2 (s) for pure PLA which fits best with common intumescent systems as degradation of the intumescent samples has to begin prior charred layer is developed.. The nonwoven fabric sample containing 5 wt% of KL showed residual mass up to 34.5% relative to the initial mass of the sample indicating the development of an intumescent char which protected fabric sample from further burning. Limiting oxygen index of the fabric samples was also tested and the highest LOI (30.4%) was observed for the sample containing 5 wt% of KL. The ignitability test showed none of the fabric sample produced from bicomponent fibers was ignited after 15 (s) of flame exposure and therefore, achieved classification of E and Efl as per the standards set for EN ISO 11925-2 method which certifies that this product can be used commercially for floor coverings. Compared to our previously published PLA/IFR mono-component multifilament fibers with tenacity of up to 7.3 $cN.tex^{-1}$, in this study, the tenacity of the bicomponent fibers was improved up to 12.6 $cN.tex^{-1}$. Hence, it was confirmed that IFR's can be melt spun into bicomponent fibers by sheath/core configuration and flame retardant nonwoven fabrics can be produced for FR applications.

5.5. References

1. Prahsarn, C.; Klinsukhon, W.; Padee, S.; Suwannamek, N. Hollow segmented-pie PLA / PBS and PLA / PP bicomponent fibers : an investigation on fiber properties and splittability. *J Mater Sci* **2016**, *51*, 10910–10916.
2. Oh, T.H. Effects of Spinning and Drawing Conditions on the Crimp Contraction of Side-by-Side Poly (trimethylene terephthalate) Bicomponent Fibers. *J Appl Polym Sci* **2006**, *102*, 1322–1327.
3. Kikutani, T.; Radhakrishnan, J.; Arikawa, S.; Takaku, A.; OKUI, N.; Jin, X.; Niwa, F.; Kudo, Y. High-speed Melt Spinning of Bicomponent Fibers : Mechanism of Fiber Structure Development in Poly (ethylene terephthalate)/ Polypropylene System. *J Appl Polym Sci* **1996**, *62*, 1913–1924.
4. Zhang, D.; Sun, C.; Beard, J.; Brown, H.; Carson, I.A.N.; Hwo, C. Development and Characterization of Poly (trimethylene terephthalate) -Based Bicomponent Meltblown Nonwovens. *J Appl Polym Sci* **2002**, *83*, 1280–1287.

5. Godshall, D.; White, C.; Wilkes, G.L. Effect of Compatibilizer Molecular Weight and Maleic Anhydride Content on Interfacial Adhesion of Polypropylene–PA6 Bicomponent Fibers. *J Appl Polym Sci* **2001**, *80*, 130–141.
6. Yeom, B.; Pourdeyhimi, B. Web fabrication and characterization of unique winged shaped, area-enhanced fibers via a bicomponent spunbond process. *J Mater Sci* **2011**, *46*, 3252–3257.
7. Durany, A.; Anantharamaiah, N.; Pourdeyhimi, B. High surface area nonwovens via fibrillating spunbonded nonwovens comprising Islands-in-the-Sea bicomponent filaments: structure– process–property relationships. *J Mater Sci* **2009**, *44*, 5926–5934.
8. Yeom, B.; Pourdeyhimi, B. Aerosol filtration properties of PA6/ PE islands-in-the-sea bicomponent spunbond web fibrillated by high-pressure water jets. *J Mater Sci* **2011**, *46*, 5761–5767.
9. Dasdemir, M.; Maze, B.; Anantharamaiah, N.; Pourdeyhimi, B. Influence of polymer type, composition, and interface on the structural and mechanical properties of core/sheath type bicomponent nonwoven fibers. *J Mater Sci* **2012**, *47*, 5955–5969.
10. Ayad, E.; Rault, A.; Gonthier, A.; Campagne, C.; Devaux, E. Effect of Viscosity Ratio of Two Immiscible Polymers on Morphology in Bicomponent Melt Spinning Fibers. *Adv Polym Technol* **2018**, *37*, 1–8.
11. Dasdemir, M.; Maze, B.; Anantharamaiah, N.; Pourdeyhimi, B. Formation of novel thermoplastic composites using bicomponent nonwovens as a precursor. *J Mater Sci* **2011**, *46*, 3269–3281.
12. Oh, T.H. Melt Spinning and Drawing Process of PET Side-by-Side Bicomponent Fibers. *J Appl Polym Sci* **2006**, *101*, 1362–1367.
13. Choi, Y.B.; Kim, S.Y. Effects of Interface on the Dynamic Mechanical Properties of PET/Nylon 6 Bicomponent Fibers. *J Appl Polym Sci* **1999**, *74*, 2083–2093.
14. Sun, C.Q.; Zhang, D.; Liu, Y.; Xiao, R. Preliminary Study on Fiber Splitting of Bicomponent Meltblown Fibers. *J Appl Polym Sci* **2004**, *93*, 2090–2094.
15. Cho, H.H.; Kim, K.H.; Kang, Y.A.; Ito, H.; Kikutani, T. Fine Structure and Physical Properties of Polyethylene/Poly (ethylene terephthalate) Bicomponent Fibers in High-Speed Spinning. I. Polyethylene Sheath/ Poly (ethylene terephthalate) Core Fibers. *J Appl Polym Sci* **1999**, *77*, 2254–2266.

16. Zhao, R.R.; Wadsworth, L.C. Study of Polypropylene/Poly (ethylene terephthalate) Bicomponent Melt-Blowing Process: The Fiber Temperature and Elongational Viscosity Profiles of the Spinline. *J Appl Polym Sci* **2003**, *89*, 1145–1150.
17. Naeimirad, M.; Zadhoush, A.; Kotek, R.; Khorasani, S.N.; Ramakrishna, S. Recent advances in core / shell bicomponent fibers and nanofibers : A review. *J Appl Polym Sci* **2018**, *46265*, 1–23.
18. Zhao, R.O.N.R.; Wadsworth, L.C.; Zhang, D.; Sun, C. Polymer Distribution During Bicomponent Melt Blowing of Poly (propylene)/Poly (ethylene terephthalate). *J Appl Polym Sci* **2002**, *85*, 2885–2889.
19. Maqsood, M.; Seide, G. Statistical modeling of thermal properties of biobased compostable gloves developed from sustainable polymer. *Fibers Polym* **2018**, *19*, 1094–1101.
20. Maqsood, M.; Seide, G. Development of biobased socks from sustainable polymer and statistical modeling of their thermo-physiological properties. *J Clean Prod* **2018**, *197*, 170–177.
21. Cho, H.H.; Kim, K.H.; Kang, Y.A.; Ito, H.; Kikutani, T. Fine Structure and Physical Properties of Poly (ethylene terephthalate)/Polyethylene Bicomponent Fibers in High-Speed Spinning . II . Poly (ethylene terephthalate) Sheath/ Polyethylene Core Fibers. *J Appl Polym Sci* **1999**, *77*, 2267–2277.
22. Yu, B.; Qi, L.; Ye, J.; Sun, H. Preparation and Radar Wave Absorbing Characterization of Bicomponent Fibers with Infrared Camouflage. *J Appl Polym Sci* **2006**, *104*, 2180–2186.
23. Wang, X.Y.; Gong, R.H. Thermally Bonded Nonwoven Filters Composed of Bicomponent Polypropylene/Polyester Fiber. I. Statistical Approach for Minimizing the Pore Size. *J Appl Polym Sci* **2005**, *101*, 2689–2699.
24. Hu, C.; Chang, S.; Liang, N. Fabrication of antistatic fibers with core/sheath and segmented-pie configurations. *J Ind Text* **2018**, *47*, 569–586.
25. Houis, S.; Schmid, M.; Lubben, J. New Functional Bicomponent Fibers with Core/Sheath-Configuration Using Poly (phenylene sulfide) and Poly (ethylene terephthalate). *J Appl Polym Sci* **2007**, *106*, 1757–1767.
26. Avinc, O.; Day, R.; Carr, C.; Wilding, M. Effect of combined flame retardant, liquid repellent and softener finishes on poly(lactic acid) (PLA) fabric performance. *Text Res J* **2012**, *82*, 975–984.

27. Cheng, X.W.; Guan, J.P.; Tang, R.C.; Liu, K.Q. Improvement of flame retardancy of poly(lactic acid) nonwoven fabric with a phosphorus- containing flame retardant. *J Ind Text* **2016**, *46*, 914–928.
28. Karim, M.N.; Rigout, M.; Yeates, S.G.; Carr, C. Surface chemical analysis of the effect of curing conditions on the properties of thermally-cured pigment printed poly (lactic acid) fabrics. *Dye Pigment* **2014**, *103*, 168–174.
29. Bourbigot, S.; Duquesne, S.; Fontaine, G.; Bellayer, S.; Turf, T.; Samyn, F. Characterization and Reaction to Fire of Polymer Nanocomposites with and without Conventional Flame Retardants. *Mol Cryst Liq Cryst* **2008**, *486*, 37–41.
30. Maqsood, M.; Seide, G. Investigation of the Flammability and Thermal Stability of Halogen-Free Intumescent System in Biopolymer Composites Containing Biobased Carbonization Agent and Mechanism of Their Char Formation. *Polymers (Basel)* **2018**, *11*, 1–16.
31. Gordobil, O.; Delucis, R.; Egüés, I.; Labidi, J. Kraft lignin as filler in PLA to improve ductility and thermal properties. *Ind Crop Prod* **2015**, *72*, 46–54.
32. Maqsood, M.; Langensiepen, F.; Seide, G. The Efficiency of Biobased Carbonization Agent and Intumescent Flame Retardant on Flame Retardancy of Biopolymer Composites and Investigation of their melt spinnability. *Molecules* **2019**, *24*, 1–18.
33. Costes, L.; Laoutid, F.; Aguedo, M.; Richel, A.; Brohez, S.; Delvosalle, C.; Dubois, P. Phosphorus and nitrogen derivatization as efficient route for improvement of lignin flame retardant action in PLA. *Eur Polym J* **2016**, *84*, 652–667.
34. Cayla, A.; Rault, F.; Giraud, S.; Salaün, F.; Fierro, V.; Celzard, A. PLA with intumescent system containing lignin and ammonium polyphosphate for flame retardant textile. *Polymers (Basel)* **2016**, *8*, 1-16.
35. Solarski, S.; Mahjoubi, F.; Ferreira, M.; Devaux, E. et al (Plasticized) Polylactide/clay nanocomposite textile : thermal , mechanical , shrinkage and fire properties. *J Mater Sci* **2007**, *42*, 5105–5117.
36. Maqsood, M.; Langensiepen, F.; Seide, G. Investigation of melt spinnability of plasticized polylactic acid biocomposites-containing intumescent flame retardant. *J Therm Anal Calorim* **2019**, 1-14.

37. Kazemi, S.; Mojtahedi, M.; Takarada, W.; Kikutani, T. Morphology and Crystallization Behavior of Nylon 6-Clay/Neat Nylon 6 Bicomponent Nanocomposite Fibers. *J Appl Polym Sci* **2014**, *128*, 1–8.
38. Lund, A.; Jonasson, C.; Johansson, C.; Haagensen, D.; Hagstr, B. Piezoelectric Polymeric Bicomponent Fibers Produced by Melt Spinning. *J Appl Polym Sci* **2012**, *126*, 490–500.
39. Liu, Y.; Cheng, B.; Wang, N.; Kang, W.; Zhang, W.; Xing, K.; Yang, W. Development and Performance Study of Polypropylene/Polyester Bicomponent Melt-Blowns for Filtration. *J Appl Polym Sci* **2012**, *124*, 296–301.
40. Straat, M.; Rigdahl, M.; Hagstrom, B. Conducting Bicomponent Fibers Obtained by Melt Spinning of PA6 and Polyolefins Containing High Amounts of Carbonaceous Fillers. *J Appl Polym Sci* **2011**, *123*, 936–943.
41. Ding, Z.; Qi, L. Preparation of Sheath–Core Bicomponent Composite Ion-Exchange Fibers and Their Properties. *J Appl Polym Sci* **2008**, *109*, 492–500.
42. Wang, X.Y.; Gong, R.H. Thermal Oxidative Degradation of Bicomponent PP/PET Fiber During Thermal Bonding Process. *J Appl Polym Sci* **2006**, *104*, 391–397.
43. Naeimirad, M.; Zadhoush, A.; Kotek, R.; Khorasani, S.N.; Ramakrishna, S. Recent advances in core/shell bicomponent fibers and nanofibers : A review. *J Appl Polym Sci* **2018**, *46265*, 1–23.
44. Lund, A.; Hagstro, B. Melt Spinning of b -Phase Poly (vinylidene fluoride) Yarns With and Without a Conductive Core. *J Appl Polym Sci* **2011**, *120*, 1080–1089.
45. Sharma, R.K.; Wooten, J.B.; Baliga, V.L.; Lin, X.; Chan, W.G.; Hajaligol, M.R. Characterization of chars from pyrolysis of lignin. *Fuel* **2004**, *83*, 1469–1482.
46. Houis, S.; Schmid, M.; Lubben, J. New Functional Bicomponent Fibers with Core / Sheath-Configuration Using Poly (phenylene sulfide) and Poly (ethylene terephthalate). *J Appl Polym Sci* **2007**, *106*, 1757–1767.
47. Kazemi, S.; Reza, M.; Mojtahedi, M.; Takarada, W.; Kikutani, T. Morphology and Crystallization Behavior of Nylon 6-Clay/Neat Nylon 6 Bicomponent Nanocomposite Fibers. *J Appl Polym Sci* **2014**, *39996*, 1–8.
48. Rwei, S.; Jue, Z.; Chen, F.L.; Laboratories, U.C. PBT/PET Conjugated Fibers: Melt Spinning, Fiber Properties and Thermal Bonding. Polym Eng Sci 2004, 44, 331–344.

CHAPTER 6

Improved thermal processing of polylactic acid/oxidized starch composites and flame-retardant behavior of intumescent nonwovens

Abstract

Thermoplastic processing and spinning of native starch is very challenging due to (a) the linear and branched polymers (amylose and amylopectin) present in its structure and (b) the presence of inter-and-intramolecular hydrogen bond linkages in its macromolecules that restrict the molecular chain mobility. Therefore, in this study, oxidized starch (OS) (obtained after oxidation of native starch with sodium perborate) was melt-blended with Polylactic acid (PLA) polymer to prepare PLA/OS blends which were then mixed together with ammonium polyphosphate (APP), a halogen free flame retardant used as acid donor in intumescent formulations on twin-screw extruder to prepare PLA/OS/APP composites. OS with different concentrations also served as biobased carbonic source in intumescent formulations. PLA/OS/APP composites were melt spun to multifilament fibers on pilot scale melt-spinning machine and their crystallinity and mechanical properties were optimized by varying spinning parameters. The crystallinity of the fibers was studied by differential scanning calorimetry and thermal stabilities were analyzed by thermogravimetric analysis. Scanning electron microscopy was used to investigate the surface morphology and dispersion of the additives in the fibers. Needle-punched nonwoven fabrics from as prepared melt-spun PLA/OS/APP fibers were developed and their fire properties such as heat release rate, total heat release, time to ignition, residual mass % etc. by cone calorimetry test were measured. It was found that PLA/OS/APP composites can be melt spun to multifilament fibers and nonwoven flame-retardant fabrics produced thereof can be used in industrial FR applications.

Keywords

Oxidized starch; Melt-spinning; Cone calorimetry; Needle-punching; Fire testing

6.1. Introduction

Bioplastics issued from renewable resources represent an interesting alternative to reduce carbon footprint instead of using polymers made of fossil carbon [1]. Therefore, a significant progress in the development of biobased polymers with renewable feedstock has generated great interest in polymer industry [2]. Starch is one of the abundant biopolymer with diverse applications in many fields such as food processing, sizing material in textiles as binding agent to reduce friction and in vat dyes for the printing of 100% cotton fabrics by virtue of its cost effectiveness, biodegradability and renewability [3]. It consists of amylose and amylopectin. Amylose being a linear polymer consisting of α-(1–4) glucose units, while amylopectin is a branched polymer consisting of α-(1–4) glucose units with intermittent divisions of α-(1–6) connections [4]. Therefore, thermoplastic processing of starch is difficult due to the presence of intermolecular and intramolecular hydrogen bond linkages in its macromolecules that restrict the molecular chain movement due to the presence of resilient interactive forces [5]. Such interactive forces are repelled by the use of plasticizers such as glycol, glycerol, sorbitol or urea that weaken the hydrogen bonds present within the macromolecules and thermoplastic processing of starch is improved [6]. These plasticizers disrupt the crystalline structure of starch macromolecules and allows free molecular chain movement by nullifying the resilient interactive forces by a process called gelatinization [7]. However, the foremost disadvantage of using plasticizers in starch is the emergence of hydrophilic characteristic that induces poor water resistance in the polymer hence negatively impacts the mechanical properties of polymer [8]. The other drawbacks associated with native starch are lack of fluidity and higher viscosity that limits its uses in many technical applications [9].

Such shortcomings can be remedied by the oxidation of starch by using oxidizing agents [10]. Starch oxidation results in de-polymerization by the hydrolysis of glucose units hence oxidized starches present low viscosities at higher concentrations: a property desired for thermoplastic processing of starch [11]. Many oxidizing agents for starch oxidation has been used in the past such as, sodium hypochlorite, hydrogen peroxide and ammonium persulfate. However, sodium hypochlorite has been found to be the most efficient one and widely used in industrial production, but in the recent past, this oxidizing agent has been abandoned due to the formation of hazardous chlorinated byproducts that are harmful for the environment [12]. We therefore, used maize starch that was oxidized by sodium perborate (SPB) which is an efficient and environment friendly

oxidizing agent for the oxidation of native starch. In practice, SPB is not only cost effective but also presents distinctive benefits such as being available as a solid form of hydrogen peroxide [13]. However, SPB has proven to be a better alternative to hydrogen peroxide since the former has not only provided superior stability at higher temperatures but also proven to be an efficient source of per hydroxyl anions, superoxide and active oxygen [14].

Blending two different polymers not only can offer valuable properties but also a new composite material can be developed that can present desired functionality for a certain application [15]. Polylactic acid (PLA) is a linear aliphatic polyester that is derived from renewable resources and one of the most important biobased polymer with attractive physical and performance properties can serve as an alternative to petroleum based polymers in many applications [16]. The blending of starch and PLA will not only make the composite material cost effective but also certain functional properties can be enhanced such as flame retardancy [17]. Although PLA is less flammable than other synthetic thermoplastics in its pure form by virtue of having higher limiting oxygen index (24-26) than other polyesters (20-22) and lower peak heat release rate, even so, PLA is still combustible, which limits its uses in many flame-retardant applications [18]. To improve the flame retardancy of PLA, intumescent flame-retardants (IFR's) present an extremely efficient approach through which a char layer is formed on the polymer surface that not only can protect it from further burning but also restricts the passage of heat, oxygen and volatile compounds to the sight of burning [19]. Although, IFR's generally contain a petroleum based carbonic source together with a halogen free acidic source, but in the recent past, a more sustainable approach towards flame retardancy has been promoted by using biopolymers that contains a biobased carbonic source [20]. Starch could be a suitable contender as a biobased carbonic source in intumescent formulations by virtue of its natural charring capability and presence of excessive polyhydric compounds however, the spinning of starch containing intumescent formulations is still unknown.

Therefore, in this study we have investigated the melt spinnability of PLA/OS composites containing halogen free intumescent flame-retardants with OS being a biobased carbonic source presenting sustainable approach towards flame retardancy. We used maize starch that was oxidized by sodium perborate (SPB) which is an efficient and environment friendly oxidizing agent for the

oxidation of native starch to improve its thermoplastic processing and spinnability. Composites were melt-spun to multifilament fibers on pilot-scale melt spinning machine and fibers were then needle-punched to form nonwoven structures. The changes in fiber crystallinity and mechanical properties were measured in response to the variations in spinning process parameters. We also tested the thermal stability of fibers by thermogravimetric analysis while, surface morphology and dispersion of the additives was recorded by scanning electron microscopy. The fire characteristics such as time to ignition, heat release rate, and total heat release were tested by cone calorimetry as per standard testing methods.

6.2.Materials and methods

The materials and methods used in this chapter are discussed in the following sections.

6.2.1. Materials

Oxidized starch (OS) 400L-NF, a white fine powder, containing 20 $mg.kg^{-1}$ of SPB as an oxidizing agent was kindly provided by Roquette Freres SA (Lestrem, France). PLA Luminy L130 which is a highly-crystalline polymer (L-isomer ≥ 99) with a density of 1.24 $g.cm^{-3}$ and melting temperature of 175-180°C was purchased from Total-Corbion NV (Gorinchem, Netherlands). Halogen free flame retardant (Exolit AP 422) having decomposition temperature higher than 275°C was attained from Clariant AG (Muttenz, Switzerland). Exolit AP 422 is a fine-particle ammonium polyphosphate (APP) containing 31% (w/w) phosphorous and 14% (w/w) nitrogen, having density of 1.9 $g.cm^{-3}$ and average particle size of 17 µm, used as acid donor in intumescent formulations. PLA, APP and OS were vacuum dried at 100˚C for 4 h before compounding.

6.2.2. Preparation of composites

PLA/OS/APP composites were prepared on twin-screw extruder (ZSK Mc^{18}) from Coperion GmbH (Stuttgart, Germany). OS was mixed together with PLA pellets in four different concentrations, i.e. 1, 3, 5 and 7 wt% in the first feeding zone which were then compounded together with APP present in the second feeding zone. PLA/OS1/APP10, PLA/OS3/APP10, PLA/OS5/APP10 and PLA/OS7/APP10 composites were prepared at screw rotation speed of 500 rpm. The formulations with content of each component (w/w) of as prepared composites are

presented in Table 6.1. The temperatures of the three heating zones were kept at 160˚C, 170˚C and 180˚C, respectively.

Table 6.1. Additives composition in PLA/OS/APP composites

No.	Formulations	PLA (wt%)	OS (wt%)	APP (wt%)
1	PLA/OS1/APP10	89	1	10
2	PLA/OS3/APP10	87	3	10
3	PLA/OS5/APP10	85	5	10
4	PLA/OS7/APP10	83	7	10

PLA=polylactic Acid; OS=oxidized starch; APP=ammonium polyphosphate

6.2.3. Melt spinning of composites

PLA/OS/APP composite pellets were vacuum dried at 100˚C for 4h prior to melt spinning. Drying the pellets before melt spinning is necessary to control moisture (%) in the polymer to avoid hydrolysis that can lower the viscosity of the melt and ultimately fiber breakage during spinning can occur. Karl Fischer Titrations analysed by ASTM D6869 method confirmed that the moisture content in the pellets were lower than 80 ppm. Pilot scale melt spinning machine (Figure 6.1) with a throughput of few kilograms an hour was used to spin PLA/OS/APP composite pellets to multifilament fibers. The composite pellets were dosed into the hopper of the melt-spinning machine and were then transferred to the extruder where they were melted at a temperature range of 190˚C to 215˚C. Constant rpm of spin pump ensured a homogeneous supply of the melt to the spinneret die containing 24 monofilament holes. After ejecting from spinneret die, monofilaments were delivered through the quenching section where chilled air running at a velocity of 0.5 $m.s^{-1}$ helped in lowering the temperature of the monofilaments. They were joined together to multifilaments by passing through spin finish before collected by take up roller. The bobbins carrying multifilaments were placed in standard atmospheric conditions before further analysis.

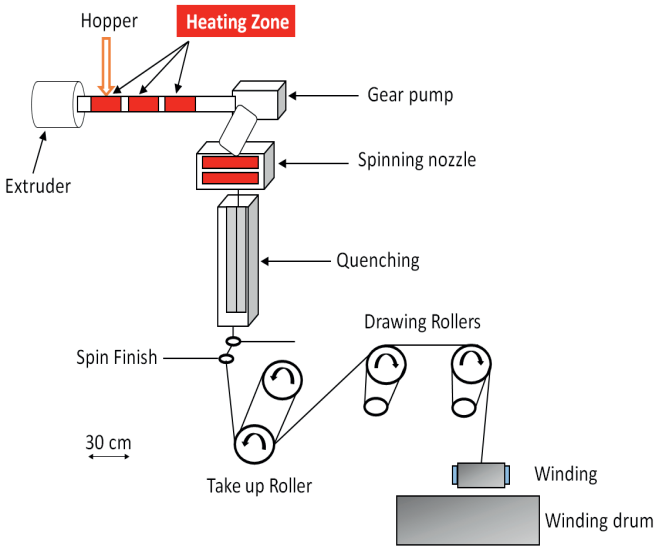

Figure 6.1. Schematic diagram of pilot scale melt spinning machine

6.2.4. Scanning electron microscopy

Hitachi S-3200 scanning electron microscope (Chiyoda, Tokyo, Japan) was used to determine surface morphology and dispersion of the additives in melt spun fibers. Multifilament fibers were first freezed in liquid nitrogen and then were delicately cut with razor blade to get clear SEM images. The cut samples were attached to the silver coated standard specimen stubs which were then sputter coated with gold. The thickness of the gold sputter coating was 150 A°. Fiber samples were examined at a magnification of 1000 × and at an accelerating voltage of 20 kV.

6.2.5. Apparent viscosity measurement

A Brookfield digital rheometer (Model, DV-III, Middleboro, USA) was used to measure the apparent viscosity of the composite samples. The samples were first dried and then around 5-10 grams from each sample were dispersed in 100 mL of distilled water to prepare the solutions. The as prepared solutions were stirred continuously for an hour and kept for 15 min at a temperature of 80°C. The volume to be used from each sample was adjusted to 100 mL and the pH used was 9.0. The solutions were then left for cooling at 25°C and then apparent viscosity of each sample was measured at a shear rate of up to 150 s^{-1}.

6.2.6. Mechanical testing

Mechanical properties of multifilament fibers such as tenacity (cN/tex) and elongation at break (%) were tested on Zwick Roell testing machine by using EN ISO 5079 standard method. The specimen lengths (50 mm) and rate of deformation (50 mm min^{-1}) were kept constant for all samples. Ten specimens were prepared from each sample and their average results with standard deviations were recorded.

6.2.7. Thermogravimetric analysis

Thermal stabilities and residual mass (%) of the fiber samples up to 500°C were analysed by thermogravimetric analysis using TGA Q5000 equipment (TA Instruments, New Castle, Delaware, USA). Fiber samples of 10-15 mg were heated at a constant rate of 10˚C min^{-1} up to 500˚C under nitrogen atmosphere at a flow rate of 50 mL min^{-1}. The temperatures at which maximum decomposition of fibers occurred were noted and the residual mass (%) of the samples were compared with the initial mass of the samples. TG curves of the samples were plotted and were analysed in detail.

6.2.8. Differential scanning calorimetry

Thermal properties (Tg, Tcc, Tm) and crystallinity (%) of the multifilament fibers were investigated by Differential scanning calorimetry (DSC) under nitrogen atmosphere at a stream rate of 50 mL min^{-1}. The samples were heated at a constant rate of 10˚C min^{-1} starting from 0˚C to 230˚C and were then cooled at the same rate followed by heating again as above. The degree of crystallinity (*Xc*) of multifilament fibers was calculated by equation (1),

$$Xc\ \% = \frac{\Delta Hm - \Delta Hcc}{\Delta Hf \times Wfr} \times 100 \quad (1)$$

Where *Xc* corresponds to degree of crystallinity of the sample; *ΔHm* implies to heat of fusion of the sample; *ΔHcc* corresponds to cold crystallization enthalpy*; ΔHf* relates to the heat of fusion of 100% crystalline material, and *Wfr* is the net weight fraction of the polymer. The heat of fusion of 100% crystalline PLA *(ΔHf)* is approximately 93.6 J g^{-1}.

6.2.9. Needlepunched nonwovens

Needlepunching is a process by which fibers are mechanically bonded by entangling them together with the barbed needles penetrating through the fibrous web to form nonwoven fabrics. Multifilament fibers produced by melt spinning were cut to short fibers and passed through carding machine: a process by which fibers were opened and homogeneously blended to form fibrous web of uniform areal density. The unbonded and voluminous fibrous web was fed to the needlepunching machine by a pair of feed rollers, and then passed between a pair of perforated plates as shown in Figure 6.2. The barbed needles responsible for entangling the fibrous web were arranged on the needle board that was placed on a reciprocating beam operated through an eccentric crank mechanism. In the downward motion, barbed needles ran down through the perforations of the top and bottom bed plates and during the upward motion were withdrawn upwards therefore, by doing so fibrous webs were mechanically bonded and mechanical strength of the nonwoven fabric was improved. The delivery rollers delivered the mechanically bonded nonwoven fabric, which was then thermally molded to impart uniform thickness and areal density.

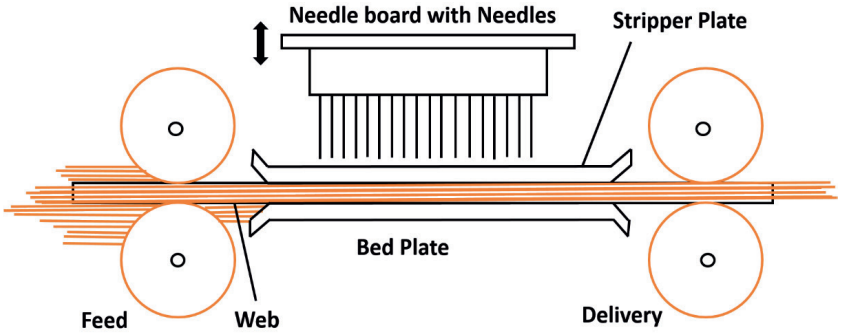

Figure 6.2. Needlepunching process to form nonwoven fabric from fibrous web

6.2.10. Fire testing

The cone calorimeter is one of the most important fire testing equipment that is used to measure the heat release rate (HRR) of the sample. The basic principle of this equipment is based on the consumption of oxygen and is considered equivalent to the amount of heat released during combustion. This equipment can also measure the amount of smoke produced during combustion. This test was conducted as per the standard operating procedure mentioned in ISO 5660 method

with heat flux of 35 kW m^{-2} by using Stanton Redcroft instrument. The other important fire testing results that can be obtained through this equipment are time to ignition (TTI), total heat release (THR), total smoke production (TSP) and residual mass % of the sample.

6.3. Results and discussion

6.3.1. Measuring the apparent viscosity of composites as a function of shear rate

The apparent viscosity as a function of shear rate of the PLA composite pellets containing OS and APP is depicted in Figure 6.3. The curves indicated that a significant decrease in apparent viscosity was observed by increasing the shear rate. As the shear rate increased up to 50 s^{-1} a very intense decrement in apparent viscosity was visible however, after 50 s^{-1} and up to 150 s^{-1} shear rate a minimal decrement in the apparent viscosity was observed. At the same time increasing OS concentration from 1 to 7 wt% initially showed a higher apparent viscosity but as the shear rate increased a significant reduction in the apparent viscosity can be seen. Especially the composite pellets containing only 1 wt% of OS had a very low apparent viscosity after shear rate of 50 s^{-1} which even levelled off at shear rate of 100 s^{-1}.

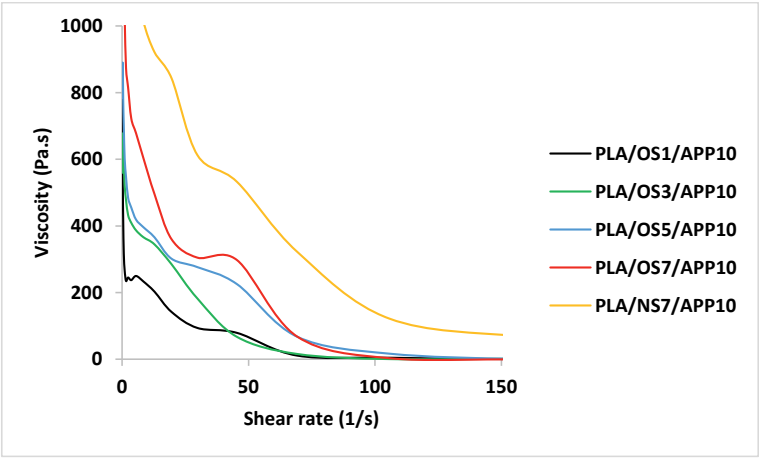

Figure 6.3. Apparent viscosity of the composite pellets

As a comparison, the viscosity of the composite pellets containing native starch with similar compositions (PLA/NS7/APP10) was also measured by the same method. It can be seen in Figure 6.3 that the apparent viscosity of the composite pellets containing oxidized starch was significantly

lower than the apparent viscosity of native starch (both containing equivalent wt% of additives) measured at the same parameters. This is attributed to the scission of the glucosidic linkages due to the oxidation caused by the presence of oxidizing agent in the formulations of composite pellets [21]. Scission in the glucosidic linkages also attributed to the reduction in the molecular weight of the oxidized starch hence its apparent viscosity decreased significantly. The oxidation of starch and an ease in the cleavage of glucosidic linkages shortened the starch chain molecules, which caused breakage in the structure and hence the apparent viscosity was decreased significantly [22]. Hence, it was found that the starch's fluidity and higher viscosity could be controlled by using oxidizing agent.

6.3.2. Multifilament fibers and their mechanical properties

The spinning of multifilament fibers from as prepared composites was not only challenging but also it took a while to find the right parameters to make the spinning process stable for continuous winding. The summary of the test results are presented in Table 6.2 while mechanical properties of the melt-spun fibers are shown in Figure 6.4. The tenacity and elongation at break (%) of the as spun fibers were on the lower side as expected since low crystallinity was induced in the fibers however, the tenacity was gradually improved by increasing the solid state draw ratio (SSDR) of fibers. Similarly, the initial modulus of the as spun fibers decreased with increasing OS content though, the difference was not significant. The tensile strength of melt-spun fibers was significantly improved by increasing the SSDR as a maximum tenacity of 13.4 cN/tex for fibers containing 3 wt% OS was achieved at SSDR of 1.6. In comparison to other fibers, the tenacity was gradually reduced by increasing the wt% of OS at the same SSDR, as 5 and 7 wt% of OS in PLA fibers could only achieve a tenacity of 11.7 and 10.1 cN/tex respectively at the same SSDR of 1.6. The same trend was observed in case of initial modulus of fibers as increasing loading content% of OS gradually reduced the initial modulus of the fibers. Compared to as spun fibers, the fibers drawn at SSDR=1.2, showed higher elongation at break (%) however, with increasing SSDR (1.4 and 1.6), the elongation at break gradually reduced. These results indicated that the mechanical properties of melt spun fibers were not only dependent of SSDR but, loading concentration (%) of OS also played a significant role in defining the mechanical properties of fibers. Similar findings were reported by Mittal et al. [23] and observed that a significant decrease in mechanical properties of fibers occurred by increasing filler content and suggested that a strong interaction between

matrix and filler content is required in order to improve mechanical properties of composite fibers. Chapple et al. [24] used hydroxyapatite as nano-filler reinforcement in PLA matrix and found that mechanical properties of fibers decreased quite significantly at any loading concentration of hydroxyapatite compared to neat PLA fibers, even though the nano-fillers were uniformly distributed within the matrix.

Table 6.2. Summary of mechanical properties of melt-spun fibers

Formulation	Draw ratio	Tenacity (cN/tex)	Elongation at break (%)
Neat PLA	As spun	8.4 ± 1.5	25.9 ± 5.7
	SSDR 1.2	12.7 ± 1.2	120.1 ± 11.8
	SSDR 1.4	14.8 ± 1.9	95.8 ± 16.3
	SSDR 1.6	17.3 ± 1.6	87.4 ± 15.6
PLA/OS1/APP10	As spun	5.7 ± 1.7	23.4 ± 8.2
	SSDR 1.2	8.7 ± 1.8	88.4 ± 10.9
	SSDR 1.4	9.4 ± 1.3	83.7 ± 17.9
	SSDR 1.6	12.9 ± 1.5	78.5 ± 12.6
PLA/OS3/APP10	As spun	5.1 ± 0.9	20.6 ± 10.5
	SSDR 1.2	7.4 ± 1.6	79.2 ± 18.1
	SSDR 1.4	10.9 ± 1.5	72.8 ± 19.5
	SSDR 1.6	13.4 ± 1.7	68.4 ± 17.2
PLA/OS5/APP10	As spun	4.7 ± 1.4	21.9 ± 12.9
	SSDR 1.2	6.9 ± 1.3	65.7 ± 19.6
	SSDR 1.4	8.2 ± 1.5	60.3 ± 13.8
	SSDR 1.6	10.6 ± 1.1	58.8 ± 16.4
PLA/OS7/APP10	As spun	3.8 ± 1.7	18.5 ± 10.1
	SSDR 1.2	6.1 ± 1.2	59.2 ± 11.3
	SSDR 1.4	6.4 ± 1.4	55.9 ± 10.5
	SSDR 1.6	7.8 ± 1.8	51.7 ± 19.2

PLA=polylactic acid; OS= oxidized starch; APP= ammonium polyphosphate

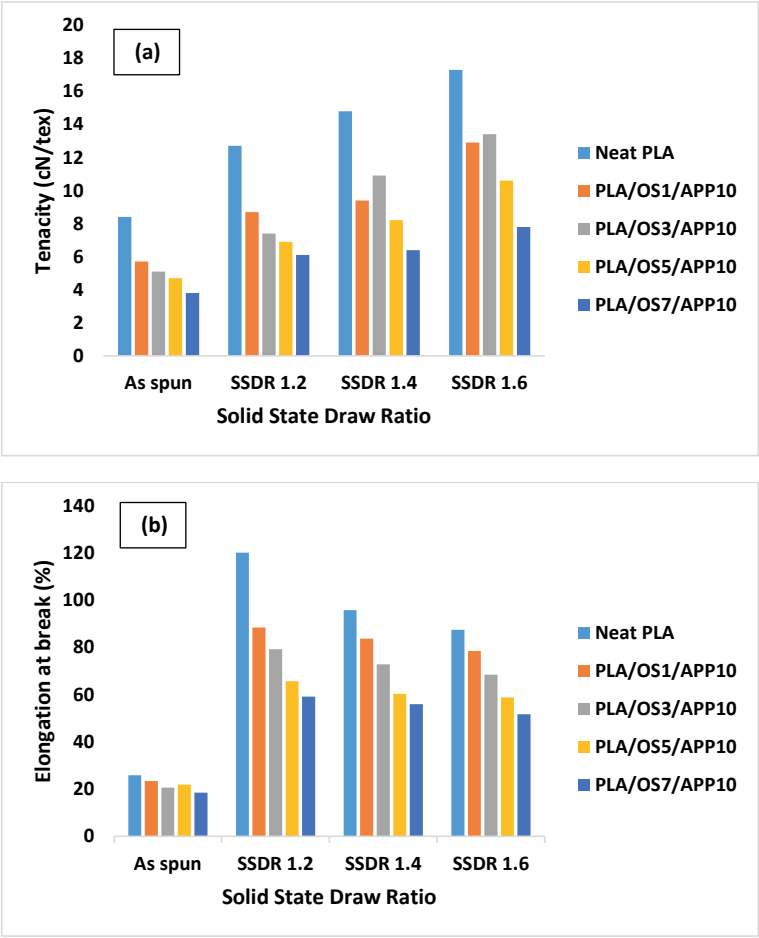

Figure 6.4. Tenacity (a) and elongation at break (b) of PLA/OS/APP composite fibers

6.3.3. Thermal stability of multifilament fibers

Figure 6.5 shows the residual mass (%) of fibers as a function of temperature (°C) of neat PLA and composite fibers. It can be seen in TG plots that the thermal decomposition of fibers started at around 310°C and completed around 390°C. Two distinct zones in TG curves can be seen such as (a) decomposition of PLA/OS/APP samples due to weight loss in the region of 315°C to 390°C and (b) residual mass remained as a solid left over in the region of 400°C to 500°C. Table 6.3 discloses the relationship between the types of samples and the temperature at which 5% and 50%

mass loss occurred are denoted with T_5 and T_{50} respectively, whereas the temperature corresponding to the maximum rate of mass loss is represented by T_{max}.

Table 6.3. Thermogravimetric analysis data

Formulations	T5 (˚C)	T50 (˚C)	T max (˚C)	Residual mass (%)
Neat PLA	312.4 ± 1.9	335.3 ± 1.2	350.4 ± 1.5	0.0 ± 0.0
PLA/OS1/APP10	330.1 ± 2.4	345.2 ± 1.9	352.8 ± 2.1	6.5 ± 0.9
PLA/OS3/APP10	341.7 ± 2.1	356.8 ± 3.5	362.1 ± 1.3	8.6 ± 1.4
PLA/OS5/APP10	347.9 ± 2.7	363.9 ± 2.1	369.5 ± 3.3	12.7 ± 1.8
PLA/OS7/APP10	349.2 ± 1.3	373.5 ± 1.7	379.9 ± 1.9	14.1 ± 1.2

PLA=polylactic acid; OS= oxidized starch; APP= ammonium polyphosphate; T5=temperature at 5% mass loss; T50=temperature at 50% mass loss; Tmax=temperature at maximum mass loss

The decomposition of neat PLA fiber started at 312˚C and 50% loss occurred at 335˚C, with no residual mass left at 500˚C. A slightly higher thermal stability was observed for PLA fibers containing 1 wt% of OS, as thermal decomposition started at around 330.1 °C and 50% mass loss occurred at 345.2°C with 6.5% residual mass left at 500°C.

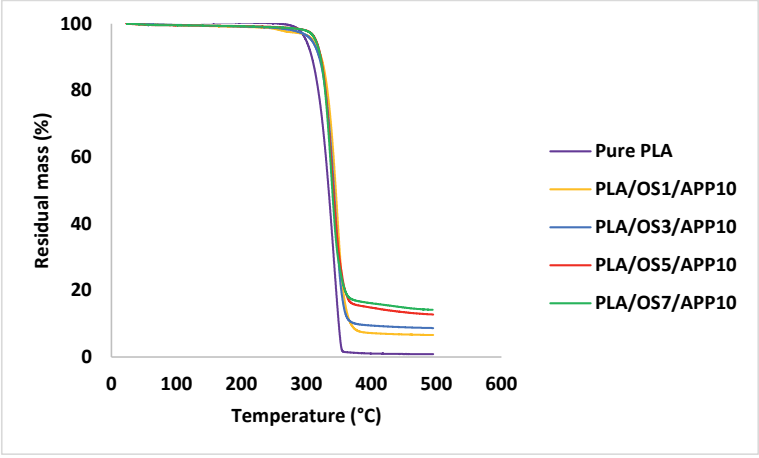

Figure 6.5. Thermogravimetric curves of fibers

For PLA fibers containing 3 and 5 wt% of OS, the initial decomposition temperatures and the temperatures at which 5 and 50% weight loss occurred were significantly higher than their corresponding values for PLA fibers containing 1 wt% of OS as shown in Table 6.3, and their residual masses were 8.6 and 12.7% respectively. A remarkable increase in thermal stability compared to neat PLA fibers was observed in case of PLA fibers containing 7 wt% of OS since the residual mass remained at 500°C was 14.1%. Higher thermal stabilities and greater residual mass % of composite fibers are due to the oxidation of starch by oxidizing agent (SPB) which led to substantial modifications in its molecular structure due to the development and abundance of carbonyl and carboxyl groups which enhanced the thermal stabilities of fibers even at elevated temperatures [7].

6.3.4. Thermal properties and crystallinity of multifilament fibers

DSC curves of SSD fibers drawn at maximum draw ratio (SSDR=1.6) are presented in Figure 6.6 and their respective data is shown in Table 6.4. The cold crystallization temperature (Tcc) of SSD fibers was in the range of 90.3 – 107.2 °C. It was observed that with increasing wt% of OS from 1 to 7 wt%, Tcc also increased. This changing behaviour of Tcc has been well explained by Solarski et al. [25] and concluded that Tcc is vastly dependent on the surface area of the loading particles and the number of particles present in a given area. Moreover, higher concentration of loading particles upsurge the interfacial area of the fibers, which decreases the polymer chain mobility.

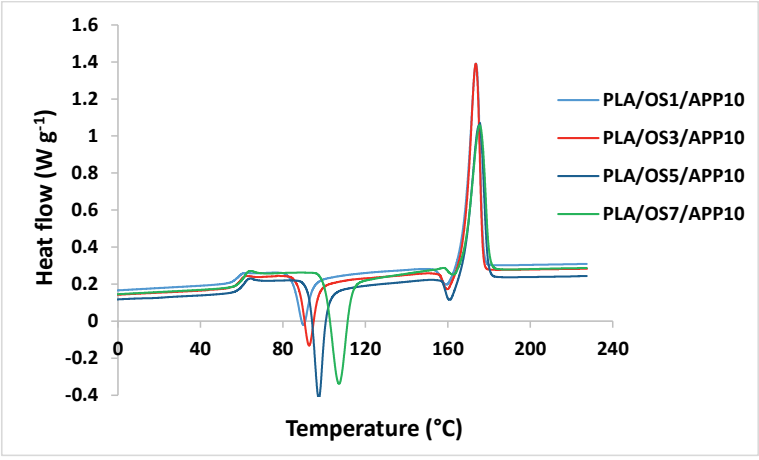

Figure 6.6. Differential scanning calorimetry thermograms of fibers

The as such increase in the Tcc of fibers due to higher loading concentration of OS can be attributed to comparatively high agglomeration of the additives which decreases the molecular chain mobility therefore, as a result higher energy is required to activate the polymer chains. At 3 wt% loading concentration of OS the cold crystallization peak was observed at 95.6 °C which further increased to 107.2 °C at 7 wt% concentration of OS. As explained in previous studies [26, 27] the reason for an increase in the cold crystallization temperature with higher loading percentage of particles is due to crystallization of PLA at higher heating temperatures.

Table 6.4. Thermal properties of fibers by DSC analysis

Formulations	Tg (˚C)	Tcc (˚C)	Tm (˚C)	Xc (%)
PLA/OS1/APP10	58.1 ± 0.4	90.3 ± 0.9	173.8 ± 1.1	3.4 ± 0.4
PLA/OS3/APP10	58.9 ± 0.7	95.6 ± 0.5	174.1 ± 0.9	7.4 ± 0.2
PLA/OS5/APP10	59.6 ± 0.3	98.1 ± 0.8	175.5 ± 1.5	8.6 ± 0.5
PLA/OS7/APP10	61.2 ± 0.6	107.2 ± 0.7	176.3 ± 1.2	10.8 ± 0.4

PLA=polylactic acid; OS= oxidized starch; APP= ammonium polyphosphate; Tg=glass transition temperature; Tcc=cold crystallization temperature; Tm=melting temperature; Xc=crystallinity%

At higher loading concentration of OS, an increase in degree of crystallinity was observed. As SSD fibers (SSDR=1.6) with 1 wt% loading concentration of OS achieved crystallinity of 3.4%; however, the degree of crystallinity was increased to 10.8% of SSD fibers containing 7 wt% of OS. These findings indicated that higher loading concentration of OS improved the crystallinity of SSD fibers and acted as nucleation sites that enhanced the crystallization rate of the fibers [28]. These findings indicated that drawing process enables the macromolecules to be straightened along the axis of the fibers that helps in faster crystallization of the filaments [29]. A slight increase in the melting temperatures (Tm) of the fibers was observed with increasing loading concentration of OS, which indicates that there is a direct correlation between the crystallinity and Tm of the fibers.

6.3.5. Surface morphology and diameter of multifilament fibers

The diameters of as spun fibers and SSD fibers are shown in Table 6.5 that were calculated by equation 2.

$$Diameter\ of\ fiber\ (\mu m) = 20\sqrt{\frac{Linear\ density\ of\ fiber\ (dtex)}{Density\ of\ polymer(g.cm^{-3}) \times \pi}} \quad (2)$$

The as spun fibers with average diameter of 175 µm were obtained as the additives incorporation had no effect on the average diameter of as spun fibers. Similarly, the average diameters of SSD fibers calculated by equation 2 were in the range of 139 -156 µm and their diameters were also not affected by the incorporation of additives. As estimated, the diameter of the SSD fibers decreased quite significantly with increasing SSDR as shown in Table 6.5.

Table 6.5. Calculated average diameters of multifilament fibers

Samples	As-spun	SSDR 1.2	SSDR 1.4	SSDR 1.6
PLA/OS1/APP10	175.3 ± 2.4	156.6 ± 2.2	147.4 ± 2.3	139.7 ± 2.9
PLA/OS3/APP10	177.1 ± 3.6	157.2 ± 2.9	148.1 ± 1.9	139.6 ± 3.4
PLA/OS5/APP10	174.6 ± 2.8	155.9 ± 3.1	149.7 ± 3.6	139.1 ± 2.2
PLA/OS7/APP10	176.7 ± 2.1	156.3 ± 2.6	147.8 ± 2.2	140.3 ± 3.2

PLA=polylactic acid; OS= oxidized starch; APP= ammonium polyphosphate; SSDR=solid state draw ratio

Compared to as spun fibers, the diameter of SSD fibers decreased 16-20% for SSDR 1.4 and 1.6 respectively. The surface morphology of SSD fibers (SSDR =1.6) was studied by SEM analysis (Figure 6.7). SEM images also confirmed the presence of additives on the surface of fibers drawn at highest SSDR. Even at the maximum loading concentration of the additives (7wt% of OS), no agglomerates on the surface of SSD fibers can be seen as shown in Figure 6.7 (d). No agglomerates were developed because there was better chemical affinity between the polymer and the additives incorporated. The drawback of the agglomerate formation is that fiber's surface tends to become rough and fibers mechanical properties are affected [30]. A well-dispersed additives in PLA matrix is generally required for smooth process otherwise, aggregation in the polymer matrix can cause fiber defects which can lower the draw-ability of the fibers hence overall mechanical strength and toughness of the fibers can be affected [31].

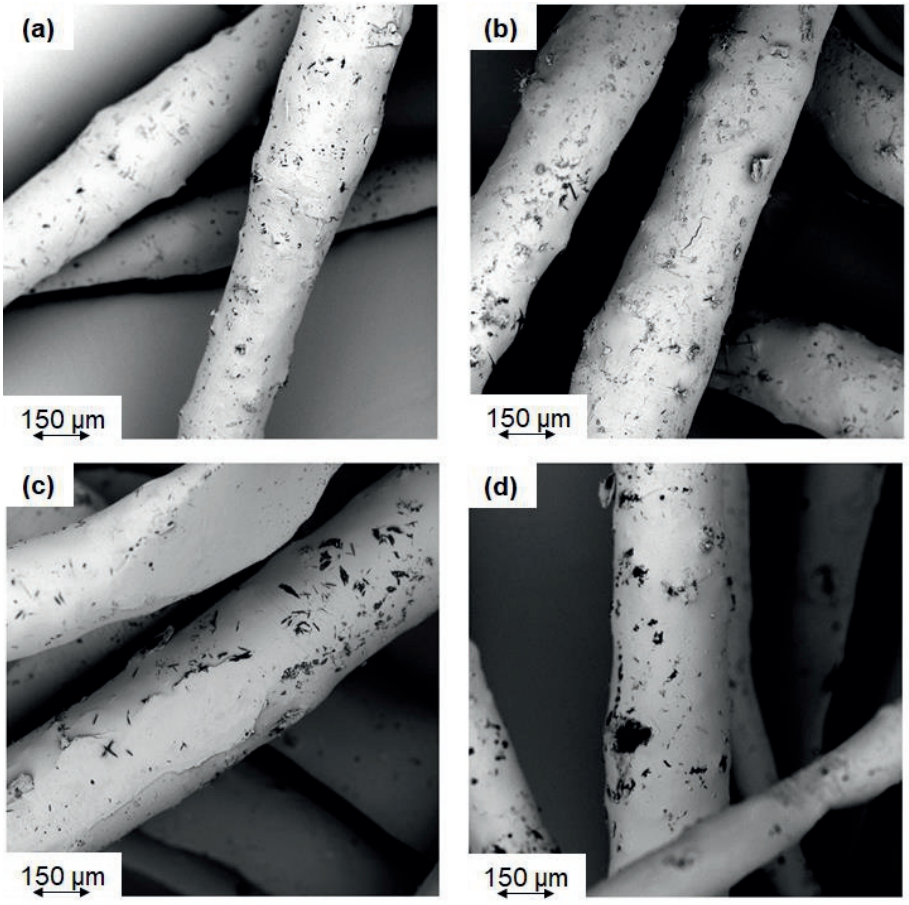

Figure 6.7. SEM images of (a) PLA/OS1/APP10, (b) PLA/OS3/APP10, (c) PLA/OS5/APP10 and (d) PLA/OS7/APP10 multifilaments fibers

6.3.6. Burning behavior of nonwovens by cone calorimetry

Cone calorimetry gives useful insights about the burning behavior of materials in similar situations to real fire scenario and simulate the possible fire hazards [32]. This test was conducted at a heat flux of 35 kWm^{-2} and to evaluate the combustion behavior of samples exposed to this heat flux, peak heat release rate, total heat release and residual mass% of the samples were determined. HRR and THR curves are presented in Figure 6.8 and 6.9 respectively and related data is shown in Table 6.6. The samples containing PLA/OS/APP presented lower TTI in comparison to unfilled PLA

samples. TTI value decreased with increasing loading content of OS from 1 to 7 wt% which is ascribed by the increased mass loss rate of OS compared to slower degradation of unfilled PLA. TTI of the samples investigated are presented in Table 6.6. Sample containing 1 wt% of OS presented TTI of 65.5 s while, sample containing 7 wt% of OS showed the lowest TTI (50.4 s).

Table 6.6. Cone calorimetry data

Formulation	TTI (s)	PHRR (kWm^{-2})	THR ($MJ \cdot m^{-2}$)	Residual mass (%)	TSP ($m^2 \cdot m^{-2}$)	EHC ($kJ \cdot g^{-1}$)
PLA	80.2 ± 0.9	449.3 ± 6.2	51.1 ± 0.5	0.0 ± 0.0	343.2 ± 2.5	21.3 ± 1.60
PLA/OS1/APP10	65.5 ± 2.6	273.9 ± 7.5	45.1 ± 0.9	15.1 ± 0.5	283.4 ± 20.4	17.1 ± 1.56
PLA/OS3/APP10	59.6 ± 3.8	261.2 ± 8.8	43.4 ± 0.4	22.5 ± 0.7	256.9 ± 11.5	12.6 ± 1.34
PLA/OS5/APP10	55.9 ± 2.5	235.4 ± 6.3	40.2 ± 0.8	29.1 ± 0.4	231.4 ± 24.1	10.6 ± 1.43
PLA/OS7/APP10	50.4 ± 3.4	216.1 ± 9.5	36.0 ± 0.4	33.5 ± 0.9	209.7 ± 19.9	8.7 ± 1.18

PLA=polylactic acid; OS= oxidized starch; APP= ammonium polyphosphate; TTI=time to ignition; PHRR=peak heat release rate; THR=total heat release; TSP=total smoke production; EHC=effective heat of combustion

Figure 6.8 shows the effect of increasing OS content on HRR of the samples investigated. A significant drop in the HRR of the samples containing PLA/OS/APP was observed; as sample containing 1 wt% of OS achieved HRR of 273.9 $kW.m^{-2}$ compared to 449.3 $kW.m^{-2}$ for sample containing unfilled PLA. For the sample containing 3 wt% of OS, HRR declined to 261.2 kW m^{-2}, which was further reduced to 216.1 kW m^{-2} by the addition of 7 wt% of OS. The HRR was significantly reduced due to char layer produced in the condensed phase on the surface of the samples that protected the samples underneath and effectively reduced the HRR during combustion [29]. The superior fire performance is due to the formation of proficient phosphate layer in the condensed phase that enhanced the stability of the char residues [33].

Figure 6.9 shows the THR curves of pure PLA and the PLA/OS/APP nonwoven fabrics. It indicates that the THR of pure PLA was 51.1 $MJ.m^{-2}$ whereas the PLA/OS5/APP10 and PLA/OS7/APP10 samples emitted only 40.2 and 36.0 $MJ.m^{-2}$, respectively. These samples therefore limited the total amount of fuel accessible for burning, which confirms the superior FR properties of these samples. The combination of OS and APP makes the samples more flame resistant. The formation of intumescent char on matrix surface improves the thermal insulation

between the flame and material's surface. This extinguishes the flame by preventing access to combustible gases and oxygen at the site of the fire [19].

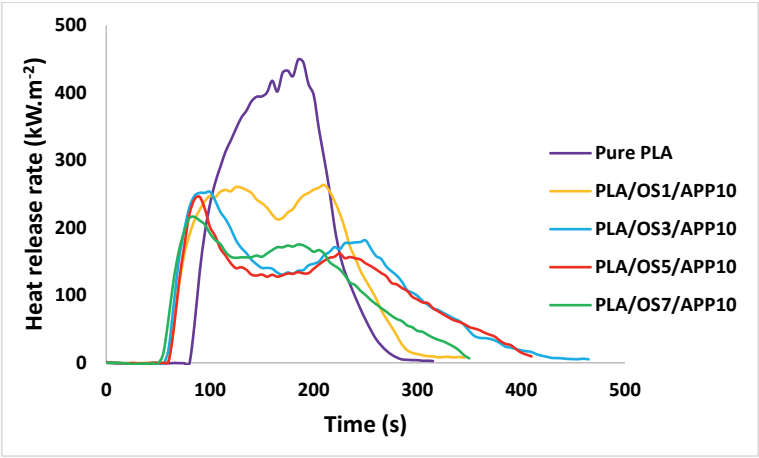

Figure 6.8. Heat release rate of samples

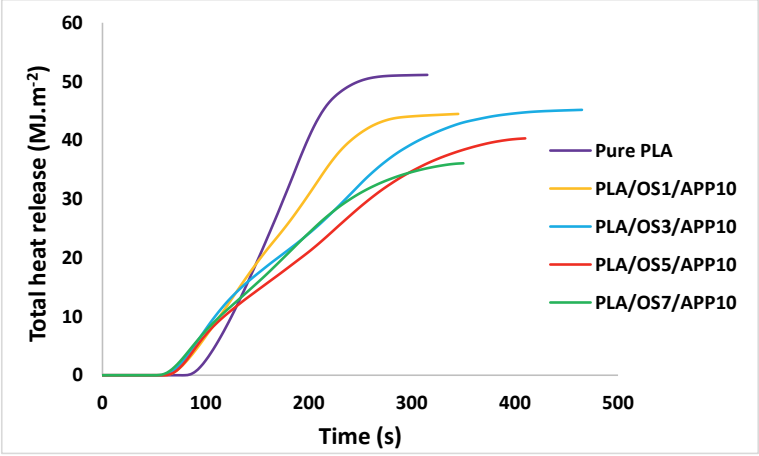

Figure 6.9. Total heat release of samples

Table 6.6 shows the residual mass% after burning for pure PLA and PLA/OS/APP samples. No residual mass was left following the burning of pure PLA, but PLA/OS5/APP10 and PLA/OS7/APP10 left mass residues corresponding to 29.1% and 33.5% of the starting mass, respectively, as shown in Table 6.6. The relatively large proportion of residual mass (char residue)

for PLA/OS7/APP10 probably reflects the development of char layer that hindered the passage of fuel and heat during combustion.

Compared to pure PLA sample, a significant decrease in effective heat of combustion (EHC) can be observed in case of gas phase flame retardant action (Table 6.6). EHC data of unfilled PLA and specimens containing OS/APP are presented in Table 6.6. The samples containing 1, 3, 5 and 7 wt% of OS showed lower EHC values compared to pure PLA because in case of these samples inhibition of flame occurred with partial combustion therefore, lower mass loss of the samples were observed [34]. The combustion of a material not only gives information about the release of volatile compounds and smoke but also provides an indication about the burning mechanism [35]. For example, a higher smoke production is initiated, by an unfinished oxidation of gaseous products, that means a flame is inhibited by radical ensnaring reactions in the gaseous phase [36]. On the other hand, a reduction in the smoke discharge shows a well-ventilated burning process, in which flame inhibition is achieved by either thermal barrier or dilution of the fuel [37]. For this reason, total smoke production were evaluated and the resultant values are reported in Table 6.6. It can be seen in Table 6.6 that samples containing 1 and 3 wt% of OS showed a comparatively higher total smoke production (TSP) than samples containing 5 and 7 wt% of OS. The release of higher TSP in case of samples containing 1 and 3 wt% of OS is mainly due to partial oxidation of the gaseous products. On the other hand higher wt% of OS (5 and 7 wt%) showed a significant reduction in TSP due to well ventilated combustion process by a complete oxidation of the developed gaseous products. Remarkably, the blends containing 7 wt% of OS showed the lowest TSP without conceding the other FR properties. This can be attributed to the reactions taken place between the APP and higher concentration of OS that enhanced the oxidation of the produced gaseous products and also by the formation of char layer in the condensed phase [38].

The images of the sample residues after cone calorimetry test are shown in Figure 6.10. There was no residue left from pure PLA sample as it was completely burnt. The residues of the sample containing 1 wt% of OS was relatively thin and virtually negligible, although this sample showed some charring characteristic. However, the sample with 3 wt% of OS slightly increased the char residues, even though the existence of open spaces in char residues (porous and loose surface) led to the development of a weak protective layer. Moreover, fabric samples with 5 and 7 wt% of OS

displayed relatively higher char residues: particularly, in PLA/OS7/APP10 sample, a very compact and coherent char layer was formed that protected the sample from further burning and against external heat flux therefore, reduced the discharge of flammable gases from the sample [39]. Importantly, the blend of higher wt% of OS with APP not only enhanced the char residues but also led to the development of established char layer having barrier properties against the discharge of flammable gases and external heat flux [40].

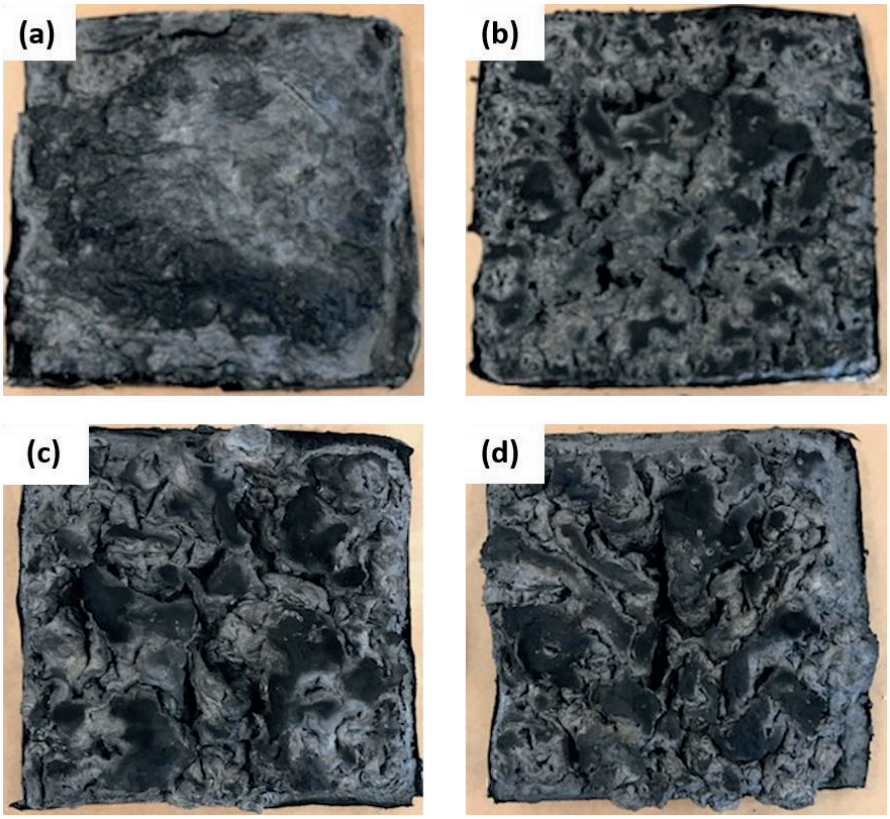

Figure 6.10. Char residues of **(a)** PLA/OS1/APP10, **(b)** PLA/OS3/APP10, **(c)** PLA/OS5/APP10 and **(d)** PLA/OS7/APP10 samples after cone calorimetry

The surface morphology of char residues was further investigated by SEM analysis to study the structure of charred layer as shown in Figure 6.11. It was noticed that the surface morphology of

charred layer produced by PLA/OS7/APP10 fabric sample was more compact and denser due to enhanced char production by the interaction of OS and APP that resulted in a firm and steady protective char layer, which added to enhanced fire protection [41].

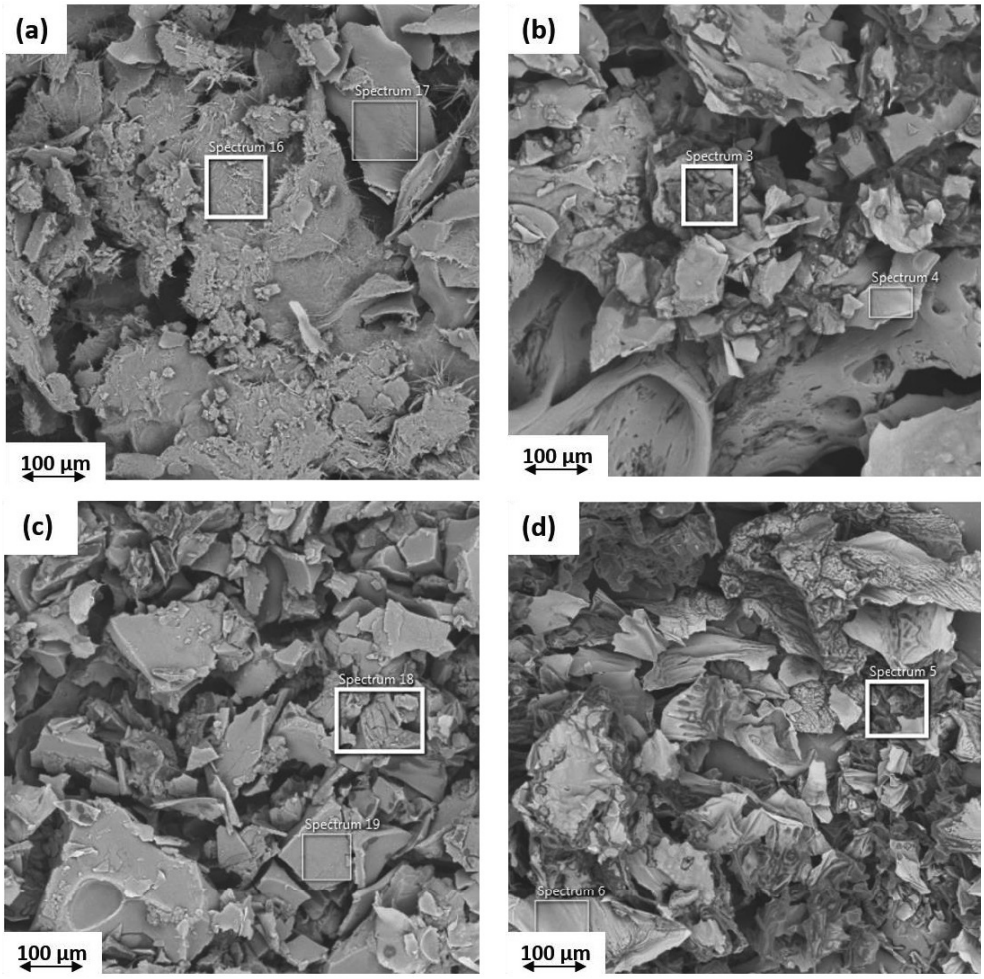

Figure 6.11. Surface morphology of char residues **(a)** PLA/OS1/APP10, **(b)** PLA/OS3/APP10, **(c)** PLA/OS5/APP10 and **(d)** PLA/OS7/APP10

The char residues of fabric samples containing 1 and 3 wt% of OS were relatively less compact and dense as some holes on the surface can be seen in Figure 6.11, compared to samples containing 5 and 7 wt% of OS. Conversely, the samples containing 1 wt% of OS did not produce an intact charred layer after combustion due to which a porous and loose char structure was produced.

6.4. Conclusions

In this study, modified starch oxidized by SPB was used as carbonization agent in intumescent flame retardant blends. PLA/OS/APP blends containing different wt% of OS were melt-blended using twin screw extruder and then melt spun on pilot scale melt spinning machine to develop flame retardant multifilament fibers. The impact of oxidized starch together with ammonium polyphosphate was thoroughly investigated by optimizing melt-spinnability, mechanical and thermal behavior of PLA multifilament fibers. These multifilament fibers were cut into short fibers, carded to form fibrous web and later needle-punched together to form nonwoven fabrics. The fire related properties of these nonwoven fabrics were tested by cone calorimetry test. SEM analysis of multifilament fibers revealed reasonably uniform dispersion of the additives incorporated in the blends however, some small agglomerates were also observed. The multifilament fibers containing 7 wt% of OS showed the highest thermal stability as confirmed by TG analysis alongside the residual mass% up to 14.1 %. Cone calorimetry revealed that the interaction between OS and APP stimulated a remarkable decrease in PHRR and THR of the nonwoven fabric samples. For instance, the lowest PHRR (216.1 $kW.m^{-2}$) was observed in case of fabric sample containing 7 wt% of OS which, is 51.8% lower than the PHRR of pure PLA sample. Similarly, THR of the same sample (7 wt% OS) was 36.0 $MJ.m^{-2}$ which, is 29.5% lower than the THR of pure PLA sample. On the other hand, effective heat of combustion and total smoke production was significantly reduced in case of samples containing higher wt% of OS. The morphology of char left overs confirmed that compact char structure is mainly responsible for enhanced flame retardant properties of the samples. To conclude this concisely, oxidized starch (OS) not only improved the spinnability of PLA/OS/APP blends compared to native starch (NS) but also the flame retardant properties of nonwovens were very promising to be used for industrial applications.

6.5. References

1. Murariu, M.; Dechief, A.; Ramy-ratiarison, R.; Paint, Y.; Raquez, J.; Dubois, P.; Murariu,

M.; Dechief, A.; Ramy-ratiarison, R.; Paint, Y. Recent advances in production of poly(lactic acid) (PLA) nanocomposites: a versatile method to tune crystallization properties of PLA. *Nanocomposites* **2014**, *1*, 71–82, doi:10.1179/2055033214Y.0000000008.

2. Rissanen, M.; Puolakka, A.; Hukka, T.; Ella, V.; Nousiainen, P.; Kellomaki, M. Effect of process parameters on properties of wet-spun poly (L,D-lactide) copolymer multifilament fibers. *J Appl Polym Sci* **2009**, *113*, 2683–2692, doi:10.1002/app.
3. Yingfeng, Z.U.O.; Jiyou, G.; Jun, C.; Al, E. Effect of Starch/Polylactic Acid Ratio on the Interdependence of Two-Phase and the Properties of Composites. *J Appl Polym Sci* **2013**, *30*, 1108–1114, doi:10.1007/s11595-015-1280-9.
4. Mujica-Garcia, A.; Hooshmand, S.; Skrifvars, M.; Al, E. Poly(lactic acid) melt-spun fibers reinforced with functionalized cellulose nanocrystals. *RSC Adv* **2016**, *6*, 9221–9231, doi:10.1039/c5ra22818b.
5. Thakore, I.M.; Iyer, S.; Desai, A.; Lele, A.; Devi, S. Morphology, Thermomechanical Properties and Biodegradability of Low Density Polyethylene/Starch Blends. *J Appl Polym Sci* **1999**, *74*, 2791–2802.
6. Kanerva, M.; Puolakka, A.; Takala, T.M.; Elert, A.M.; Mylläri, V.; Jönkkäri, I.; Sarlin, E.; Seitsonen, J.; Ruokolainen, J.; Saris, P.; et al. Antibacterial polymer fibres by rosin compounding and melt-spinning. *Mater Today Commun* **2019**, 1–9, doi:10.1016/j.mtcomm.2019.05.003.
7. Rosa, D.; Lopes, D.; Calil, M. The influence of the structure of starch on the mechanical, morphological and thermal properties of poly (e-caprolactone) in starch blends. *J Mater Sci* **2007**, *42*, 2323–2328, doi:10.1007/s10853-006-1105-5.
8. Ramkumar, D.; Bhattacharya, M. Effect of crystallinity on the mechanical properties of starch/synthetic polymer blends. *J Mater Sci* **1997**, *32*, 2565–2572.
9. Liu, Y.; Mo, X.; Pang, J.; Yang, F. Effects of silica on the morphology, structure, and properties of thermoplastic cassava starch/poly(vinyl alcohol) blends. *J Appl Polym Sci* **2016**, *44020*, 1–9, doi:10.1002/app.44020.
10. Jompang, L.; Thumsorn, S.; Wong, J.; Surin, P. Poly (lactic acid) and Poly (butylene succinate) Blend Fibers Prepared by Melt Spinning Technique. *Energy Procedia* **2013**, *34*, 493–499, doi:10.1016/j.egypro.2013.06.777.
11. Pivsa-Art, W.; Pivsa-Art, S.; Fujii, K.; Nomura, K.; Al, E. Compression molding and melt-

spinning of the blends of poly (lactic acid) and poly (butylene succinate- co -adipate). *J Appl Polym Sci* **2015**, *41856*, 1–9, doi:10.1002/app.41856.

12. Vignon, A.; Ayoub, A.; Massardier, V. The Effect of c -Irradiation and Reactive Extrusion on the Structure and Properties of Polycarbonate and Starch Blends : A Work Oriented to the Recycling of Thermoplastic Wastes. *J Appl Polym Sci* **2013**, 4169–4176, doi:10.1002/app.38024.
13. Dicastillo, C.; Rao, K.; Garrido, L.; Pereira, A.; Galotto, M. Novel Polyvinyl Alcohol/Starch Electrospun Fibers as a Strategy to Disperse Cellulose Nanocrystals into Poly (lactic acid). *Polymers (Basel)* **2017**, *9*, 117–133, doi:10.3390/polym9040117.
14. Hebeish, A.; Rabie, A.M.; El-naggar, M.E. Ultra-Microstructural Features of Perborate Oxidized Starch. *J Appl Polym Sci* **2014**, 40170–40179, doi:10.1002/app.40170.
15. Albano, M.; Garrido, L.; Plucknett, K.; Genova, L. Influence of starch content and sintering temperature on the microstructure of porous yttria-stabilized zirconia tapes. *J Mater Sci* **2009**, *44*, 2581–2589, doi:10.1007/s10853-009-3337-7.
16. Ayoub, A.; Rizvi, S.S.H. Properties of Supercritical Fluid Extrusion-Based Crosslinked Starch Extrudates. *J Appl Polym Sci* **2008**, *107*, 3663–3671, doi:10.1002/app.
17. Park, H.; Lee, W.; Park, C. Environmentally friendly polymer hybrids. *J Mater Sci* **2003**, *38*, 909–915.
18. Mostafa, K.; El-Sanabary, A. Graft Polymerization of Different Monomers onto Carbamated Starches Derived from Native and Hydrolyzed Starches. *J Appl Polym Sci* **2003**, *88*, 959–965.
19. Maqsood, M.; Seide, G. Investigation of the Flammability and Thermal Stability of Halogen-Free Intumescent System in Biopolymer Composites Containing Biobased Carbonization Agent and Mechanism of Their Char Formation. *Polymers (Basel)* **2018**, *11*, 1–16, doi:10.3390/polym11010048.
20. Maqsood, M.; Langensiepen, F.; Seide, G. The Efficiency of Biobased Carbonization Agent and Intumescent Flame Retardant on Flame Retardancy of Biopolymer Composites and Investigation of their melt spinnability. *Molecules* **2019**, *24*, 1–18.
21. Salimi, K.; Topuzogullari, M.; Dincer, S.; Aydin, H.M. Microwave-assisted green approach for graft copolymerization of L -lactic acid onto starch. *J Appl Polym Sci* **2016**, 42937–42944, doi:10.1002/app.42937.

22. Zhiqiang, L.; Yi, F.; Su, Y. Thermoplastic Starch/PVAl Compounds: Preparation, Processing and Properties. *J Appl Polym Sci* **1999**, *74*, 2667–2673.
23. Mittal, V.; Akhtar, T.; Luckachan, G. PLA, TPS and PCL binary and ternary blends: structural characterization and time-dependent morphological changes. *Colloid Polym Sci* **2015**, *293*, 573–585, doi:10.1007/s00396-014-3458-7.
24. Chapple, S.; Anandjiwala, R.; Ray, S. Mechanical, thermal, and fire properties of polylactide/starch blend/clay composites. *J Therm Anal Calorim* **2013**, *113*, 703–712, doi:10.1007/s10973-012-2776-6.
25. Solarski, S.; Mahjoubi, F.; Ferreira, M.; Devaux, E.; Bachelet, P.; Bourbigot, S.; Delobel, R.; Coszach, P.; Murariu, M.; Da Silva Ferreira, A.; et al. (Plasticized) Polylactide/clay nanocomposite textile: Thermal, mechanical, shrinkage and fire properties. *J Mater Sci* **2007**, *42*, 5105–5117, doi:10.1007/s10853-006-0911-0.
26. Fox, D.M.; Lee, J.; Citro, C.J.; Novy, M. Flame retarded poly(lactic acid) using POSS-modified cellulose. 1. Thermal and combustion properties of intumescing composites. *Polym Degrad Stab* **2013**, *98*, 590–596, doi:10.1016/j.polymdegradstab.2012.11.016.
27. Suardana, N.; Kyoo, M. Effects of diammonium phosphate on the flammability and mechanical properties of bio-composites. *Mater Des* **2011**, *32*, 1990–1999, doi:10.1016/j.matdes.2010.11.069.
28. Mngomezulu, M.E.; Luyt, A.S.; John, M.J. Morphology, thermal and dynamic mechanical properties of poly(lactic acid)/expandable graphite (PLA/EG) flame retardant composites. *J Thermoplast Compos Mater* **2017**, 1–19, doi:10.1177/0892705717744830.
29. Depeng, L.; Chixiang, L.; Xiulei, J.; Tao, L.; Ling, Z. Synergistic effects of intumescent flame retardant and nano-CaCO 3 on foamability and flame-retardant property of polypropylene composites foams. *J Cell Plast* **2017**, 1–17, doi:10.1177/0021955X17720157.
30. Fukushima, K.; Murariu, M.; Camino, G.; Dubois, P. Effect of expanded graphite/layered-silicate clay on thermal, mechanical and fire retardant properties of poly(lactic acid). *Polym Degrad Stab* **2010**, *95*, 1063–1076, doi:10.1016/j.polymdegradstab.2010.02.029.
31. Lin, H.J.; Liu, S.R.; Han, L.J.; Wang, X.M.; Bian, Y.J.; Dong, L.S. Effect of a phosphorus-containing oligomer on flame-retardant, rheological and mechanical properties of poly (lactic acid). *Polym Degrad Stab* **2013**, *98*, 1389–1396,

doi:10.1016/j.polymdegradstab.2013.03.025.

32. Maqsood, M.; Langensiepen, F.; Seide, G. Investigation of melt spinnability of plasticized polylactic acid biocomposites-containing intumescent flame retardant. *J Therm Anal Calorim* **2019**, 1–14, doi:10.1007/s10973-019-08405-3.
33. Katsoulis, C.; Kandare, E.; Kandola, B.K. The combined effect of epoxy nanocomposites and phosphorus flame retardant additives on thermal and fire reaction properties of fiber-reinforced composites. *J Fire Sci* **2011**, *29*, 361–383, doi:10.1177/0734904111398785.
34. Wang, K.; Wang, J.; Zhao, D.; Zhai, W. Preparation of microcellular poly(lactic acid) composites foams with improved flame retardancy. *J Cell Plast* **2017**, *53*, 45–63, doi:10.1177/0021955X16633644.
35. Teoh, E.L.; Mariatti, M.; Chow, W.S. Thermal and Flame Resistant Properties of Poly (Lactic Acid)/Poly (Methyl Methacrylate) Blends Containing Halogen-free Flame Retardant. *Procedia Chem* **2016**, *19*, 795–802, doi:10.1016/j.proche.2016.03.087.
36. Uddin, F. Flame-retardant fibrous materials in an aircraft. *J Ind Text* **2016**, *45*, 1128–1169, doi:10.1177/1528083714540700.
37. Zhan, J.; Song, L.; Nie, S.; Hu, Y. Combustion properties and thermal degradation behavior of polylactide with an effective intumescent flame retardant. *Polym Degrad Stab* **2009**, *94*, 291–296, doi:10.1016/j.polymdegradstab.2008.12.015.
38. Atabek Savas, L.; Mutlu, A.; Dike, A.S.; Tayfun, U.; Dogan, M. Effect of carbon fiber amount and length on flame retardant and mechanical properties of intumescent polypropylene composites. *J Compos Mater* **2017**, 1–12, doi:10.1177/0021998317710319.
39. Chapple, S.; Anandjiwala, R.; Ray, S.S. Mechanical, thermal, and fire properties of polylactide/starch blend/clay composites. *J Therm Anal Calorim* **2013**, *113*, 703–712, doi:10.1007/s10973-012-2776-6.
40. Bourbigot, S.; Duquesne, S.; Fontaine, G.; Bellayer, S.; Turf, T.; Samyn, F. Characterization and Reaction to Fire of Polymer Nanocomposites with and without Conventional Flame Retardants. *Mol Cryst Liq Cryst* **2008**, *486*, 37–41, doi:10.1080/15421400801921983.
41. Cheng, X.-W.; Guan, J.-P.; Tang, R.-C.; Liu, K.-Q. Improvement of flame retardancy of poly(lactic acid) nonwoven fabric with a phosphorus- containing flame retardant. *J Ind Text* **2016**, *46*, 914–928, doi:10.1177/1528083715606105.

CHAPTER 7

Development of biobased socks from sustainable polymer and statistical modeling of their thermo-physiological properties

Abstract

Polylactic acid (PLA) is a biodegradable and compostable polymer obtained from renewable and sustainable resources with substantial commercial prospective as a textile fiber however, this polymer has not been investigated much in apparel applications. Therefore, in this study it was aimed to develop compostable socks from PLA draw textured melt spun yarns and to examine the effect of yarn linear density, fabric structure and stitch density on thermo-physiological characteristics of these socks. Multifilament yarns from PLA of two different linear densities were melt spun and later draw textured on false twist texturing machine to be used for socks knitting. Single jersey and rib structures were produced with two different stitch densities to investigate their effect on thermal resistance, relative water vapour permeability, thermal conductivity, vertical wicking and air permeability of the socks. Minitab statistical software was used to analyze the results of test samples. The coefficients of determinations (R^2 values) presented good estimation capability of the established regression models. The outcomes of this research may be useful in determining suitable manufacturing requirements of PLA based socks to accomplish precise thermo-physiological properties.

Keywords

Poly (lactic acid); Biodegradable, Sustainable, Socks, Statistical modeling

7.1. Introduction

The physical properties and structure of Polylactic acid (PLA) has been the subject of multiple studies, indicating this polymer is equipped with substantial commercial prospective as a textile fiber. Contrary to oil based polymers, PLA is eco-friendly and sustainable, because it is derived from annually renewable resources such as corn; therefore, it is considered to be an environment friendly polymer as compared to conventional polyesters such as polyethylene terephthalate (PET) [1]. The monomer of PLA is sustainable therefore, eliminates the use of a finite supply of oil as a raw material [2]. Since the quantity of corn consumed in the manufacturing of PLA is not more than 0.02% of the entire corn production in the world therefore, PLA production from corn will not result in a food disaster [3]. PLA needs 25-55% less fossil resources in its production as compared to the production of oil-based polymers [4]. Moisture management and wicking properties of PLA fibers are considered better to that of PET therefore, PLA could be an interesting choice to be used in apparel applications [5, 6]. PLA fibers have the ability to wick moisture faster without holding huge quantity of water due to its lower contact angle compared to PET which aids in sports applications [7]. Despite of all these advantages of PLA over petroleum based polymers it has not been used much in apparel applications.

Gun et al. investigated the physical and dimensional characteristics of socks developed from reclaimed fibers and observed that reclaimed fibre socks exhibit higher pilling propensity than virgin fibers [8]. Amber et al studied the relative effects of wool and acrylic fibers, yarn type (high and low twist) and fabric type on moisture transfer properties of socks and found that the packing density within the fabrics affect the most on comfort characteristics of fabrics [9]. Cimilli et al. examined comfort characteristics of knitted fabrics produced from various kinds of fibers and concluded that fabric's comfort characteristics are mainly dependent on type of fiber along with properties of fabrics such as thickness, areal density and packing density [10]. Oglakcioglu and Marmarali examined thermo-physiological characteristics of different knitted structures and observed that rib and interlock knit structures presented greater thermal resistance than single jersey structures whereas single-jersey knit structures showed higher water vapor permeability [11]. Demeryurik studied the effect different fiber types and their structure on thermo-physiological characteristics of different fabrics and found that distinctive fibers enhanced the thermo-physiological characteristics of fabrics [12].

Majority of the studies [13-16] reported in literature has concentrated on the examination of thermal and comfort properties of socks knitted from petroleum based polymers, such as poly(ethylene terephthalate) (PET), PET/elastane and PET/polyamide. However, there isn't any literature available on the examination of thermo-physiological comfort properties of socks knitted from biobased polymers such as polylactides. The thermo-physiological characteristics of knitted socks containing PLA are yet to be investigated thoroughly therefore, the objective of the current research is to investigate the effect of yarn linear density, fabric structure and stitch density on thermal resistance, relative water vapour permeability, thermal conductivity, vertical wicking and air permeability of socks produced from PLA draw textured melt spun yarns. Minitab statistical software was used to analyze the results of test samples. The coefficients of determinations (R^2 values) presented good estimation capability of the established regression models. The outcomes of this research may be useful in determining suitable manufacturing requirements of PLA based socks to accomplish precise thermo-physiological properties.

7.2. Materials and methods

Polylactic acid with ≥99% L-isomer stereo-chemical purity was purchased from Total-Corbion NV (Gorinchem, Netherlands). DSC analysis revealed that the melting point of the polymer was 175 ˚C and the crystallinity content was about 75%. Before extrusion the polymer was dried at 100˚C in a vacuum oven for 6 hours. Melt spinning experiments were performed on Fournè high temperature single component melt spinning machine. The machine consists of single screw extruder to feed the material. Polymer is fed into extruder through a hopper and then melted at 230˚C in the extruder. The melt from the single screw extruder is transported to spinning head in a metered quantity with the help of spinning pumps. Spinnerets are constructed in such a way that uniform output of the material is maintained. Quenching zone was present below the spinneret area, where filaments were cooled at 18˚C by maintaining the cool air velocity of 0.5 m/s. The winding zone consists of take up roller, drawing rollers (godets) and the winder. Multifilament partially oriented yarns (POY) of PLA were produced on melt spinning machine of two different linear densities (dtex) and their properties are shown in Table 7.1.

Table 7.1. Yarn characteristics before and after texturing

Properties	Unit	Yarn type 1	Yarn type 2
Linear density before texturing	dtex	300	270
Tenacity before texturing	cN/tex	20.22	18.04
Elongation before texturing	%	63.29	78.88
Draw ratio at texturing	N/A	1.80	1.80
Linear density after texturing	dtex	167	150
Tenacity after texturing	cN/tex	17.14	15.39
Elongation after texturing	%	57.60	67.08

Yarn linear density (dtex) was measured by DIN EN ISO 1973 standard testing method whereas yarn tenacity (cN/tex) and elongation (%) were tested by standard testing method DIN EN ISO 2062. A view of different sections of melt spinning machine is shown in Figure 7.1.

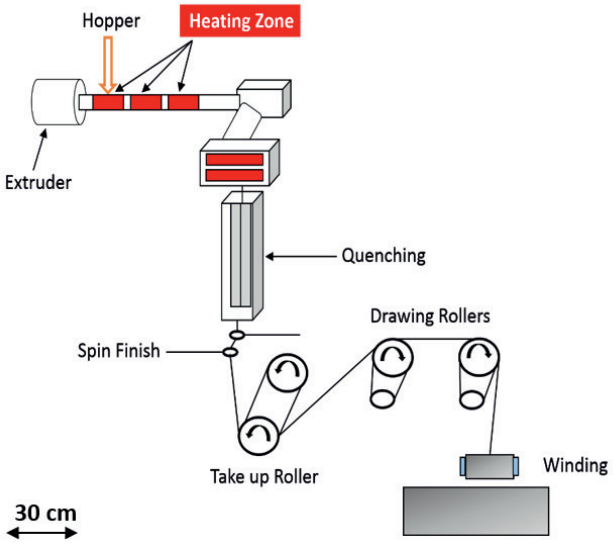

Figure 7.1. Different zones of melt spinning machine

After spinning, PLA-POY multifilament yarns were draw textured on Barmag AFK2 false twist texturing machine as shown in Figure 7.2.

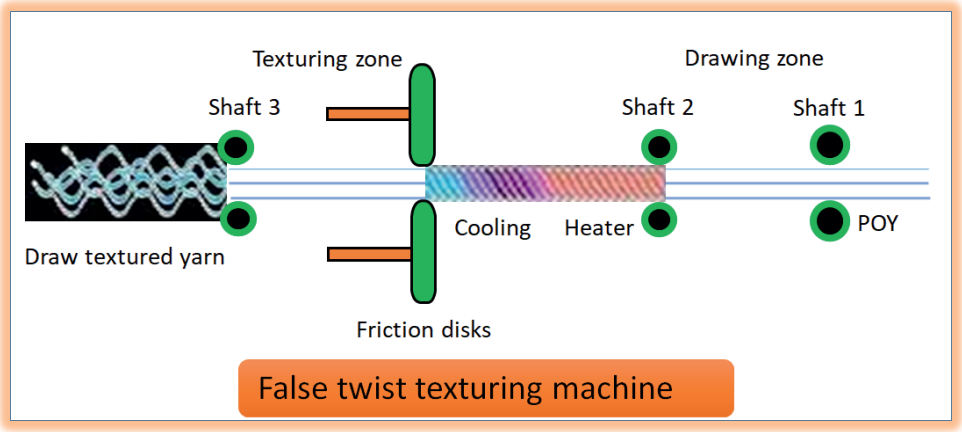

Figure 7.2. Schematic diagram of false twist texturing machine

Texturing of multifilament yarns is done in order to obtain similar properties to that of staple fiber yarn for apparel applications. False twist texturing machine consisted of a yarn holding stand, where the yarn bobbins were placed. The yarns were initially drawn with a vacuum pistol and passed through the first heating zone. First heating zone consisted of long heater and a short heater. The temperatures of long and short heaters were 190˚C and 75˚C respectively. The heated yarn was passed through the twisting zone, which consisted of a number of ceramic discs. The twisted yarn was passed through the tangling zone and then through the second heating zone. The temperature of second heating zone was kept at 50˚C. The draw textured yarn (DTY) was then wound at a winding speed of 400 m/min on a yarn bobbin at the winding zone. The process parameters used on false twist texturing machine is shown in Table 7.2.

Table7.2. Process parameters for false twist texturing machine

Linear density before texturing (dtex)	First heating temperature (°C)		No. of ceramic discs in twisting zone	Draw ratio	Second heating temperature (°C)	Speed (m/min)	Linear density after texturing (dtex)
	Long heater	Short heater					
300	190	75	9	1.8	50	400	167
270	190	75	9	1.8	50	400	150

The details regarding the knitting parameters of the socks are given in Table 7.3. Two different yarn linear densities (i.e. 150 dtex and 167 dtex), stitch densities (i.e. 56 and 64) and knit structures (i.e. single jersey and rib) were used to produce eight different socks structures as shown in Table 7.3.

Table 7.3. Socks knitting parameters

Yarn fineness (dtex)	Fabric structure	Stitch density (stitch/cm^2)	Loop length (cm)	Courses per cm	Wales per cm	Thickness (mm)
150	Single jersey	56	0.4	8	7	1.29
150	Single jersey	64	0.4	8	8	1.31
150	Rib	56	0.4	8	7	1.41
150	Rib	64	0.4	8	8	1.44
167	Single jersey	56	0.4	8	7	1.30
167	Single jersey	64	0.4	8	8	1.32
167	Rib	56	0.4	8	7	1.47
167	Rib	64	0.4	8	8	1.49

Socks from PLA draw textured yarns were knitted on E9 gauge, FDS Model Future 5C single cylinder socks knitting machine having 120 needles with 4 inches diameter of the cylinder. Sock developed from PLA draw textured yarns are shown in Figure 7.3. The socks were knitted at the

same knitting parameters (i.e. the loop length, number of needles and cylinder diameter). Sock samples were conditioned under standard atmospheric conditions.

Figure 7.3. Sock developed from PLA draw textured yarn

The factors and their levels used in this research are shown in Table 7.4. Yarn linear density (X_1), fabric structure (X_2) and stitch densities (X_3) has been nominated as factors. The levels of factor X_2 i.e. fabric structure is presented as 1 and 2 for single jersey and rib structure respectively. Factors and responses with L_8 orthogonal array are given in Table 7.5.

Table 7.4. Factors and levels investigated

Factor	Code	Unit	Levels	
Yarn linear density	X_1	dtex	150	167
Fabric structure	X_2	N/A	1	2
Stitch densities	X_3	stitches/cm^2	56	64

Table 7.5. Factors and test results of responses

X_1	X_2	X_3	Thermal conductivity (W/mK)	Thermal resistance (m^2K/W)	Relative water vapour permeability (%)	Air permeability (mm/s)	Vertical wicking (cm)
150	1	56	0.0479	0.0229	63	188	17
150	1	64	0.0472	0.0235	60	184	16
150	2	56	0.0399	0.0308	57	180	14
150	2	64	0.0391	0.0320	56	176	13
167	1	56	0.0458	0.0279	62	185	17
167	1	64	0.0446	0.0288	61	182	17
167	2	56	0.0388	0.0327	56	179	15
167	2	64	0.0381	0.0336	55	177	13

Thermal conductivity of the socks was tested by using Alambeta instrument whereas SDL sweating guard hotplate was utilized to investigate the thermal resistance of the knitted structures as per the standard testing method BS EN ISO 11092:2014. Water vapor permeability of the knitted structures were tested by using Permetest instrument according to ISO 11092 standard method. SDL Atlas air permeability tester was utilized to determine the air permeability of the samples as per the standard testing method EN ISO 9237:1997. ASTM D-1777:2002 standard test method was used to measure the fabric thickness. Vertical wicking of socks was measured by AATCC 197:2011 standard method. Five repetitions were conducted for the tests applied and the averages of the values were calculated.

7.3. Cost analysis

Biobased economy is considered to be a growing sector with viable economic opportunities presenting lucrative alternative to existing firms in comparison to conventional petroleum based economy because it can enhance the productivity through the development of state of the art technological innovations. The cost of manufacturing biobased socks is mainly dependent on the price of raw material (resin) which approximately accounts for 30-35% of the cost of the end product. Therefore, instabilities in the price of resins predominantly disturb the market price of the

end product produced out of it. However the cost involved in the process (melt spinning, yarn texturing) and product development (knitting) of PLA based socks is the same as compared to socks produced from conventional synthetic polymers. Since the cost per meter of standard 150 dtex PLA yarn is 7.5 cents/meter and that of PET yarn with same fineness is 6.5 cents/meter, therefore the cost of socks produced from PLA yarn will be slightly on the higher side. Calculating the exact cost of the socks in apparel form will be difficult due to several factors involved such as areal density (weight of the sock per square meter), loop length (yarn consumption in each loop) and number of wales and courses per cm of the fabric. Since PLA is a biodegradable material but sometimes it is misunderstood that under domestic conditions it will degrade automatically, but the fact of the matter is that in order to degrade PLA specific temperature and humidity conditions are required. The degradation of PLA is a two-step process; in the first step, the molecular weight of PLA is reduced in the presence of required temperature and humidity and then in second step microorganisms attack on smaller fragments to make them biodegradable. Therefore, PLA based socks will not degrade under domestic conditions unless they are treated under specific temperature and humidity at industrial scale.

7.4. Methodology

The methodological approach used for the product development is shown in Figure 7.4. The strategies involved; starting from the polymer analysis till the development of the final product has been described in detail in this section.

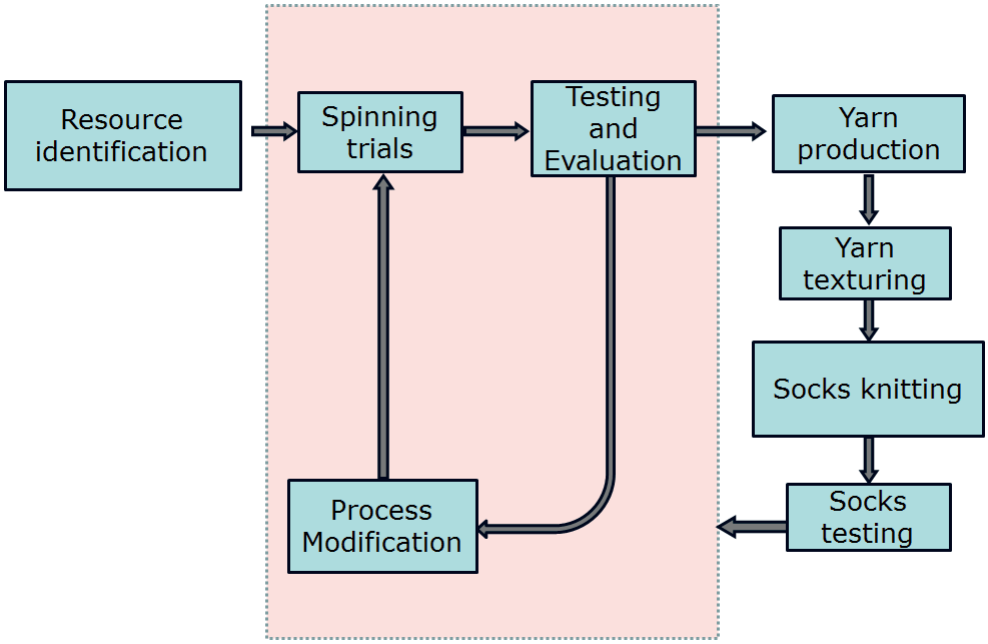

Figure 7.4. Methodological approach for the product development

In first step, yarn benchmark properties for the socks were identified and the polymer analysis was done for further experimental purpose. The melt spinning trails were done and target properties were set by keeping in mind the yarn benchmark properties. Yarn spinning parameters such as temperature, draw ratio and winding speeds were varied accordingly to achieve the target properties. The yarns produced were tested immediately to test the required mechanical properties such as tenacity (cN/tex), elongation (%) and fineness (dtex). In case of deviation from the required mechanical properties, spinning process parameters were modified to achieve the target properties. The trials that confirmed the required yarn mechanical properties were followed by the yarn production stage where yarn was produced in bulk for the subsequent processes. Yarn production stage was followed by the yarn texturing stage where yarn produced on melt spinning machine were textured to produce draw textured yarns and to obtain similar properties to that staple fiber yarn for apparel applications. Yarn texturing process has been explained in detail in the previous section. The draw textured yarn was then used in socks knitting to produce PLA based socks. The socks produced were tested as per the standard testing methods described in the previous section.

7.5. Results and discussion

The test results of the fabrics investigated are presented in Tables 7.5. Minitab®18 statistical software was used to statistically analyze the test results. Table 7.6 represents the regression coefficients of the terms with their p-values.

Table 7.6. Regression coefficients for response variables

Terms	Thermal conductivity (W/mK)		Thermal resistance (m^2K/W)		Relative water vapour permeability (%)	
	Coeff.	**p-value**	**Coeff.**	**p-value**	**Coeff.**	**p-value**
Constant	0.042675	0.000*	0.029025	0.000*	58750	0.000*
X_1	-0.000850	0.001*	0.001725	0.000*	N/A	N/A
X_2	-0.003700	0.000*	0.003250	0.000*	-2750	0.000*
X_3	-0.000425	0.006*	0.000450	0.005*	-0.750	0.030*
X_1X_2	0.000325	0.012*	-0.000850	0.001*	N/A	N/A

Terms	Air permeability (mm/s)		Vertical wicking (cm)	
	Coeff.	**p-value**	**Coeff.**	**p-value**
Constant	181375	0.000*	15250	0.000*
X_1	N/A	N/A	N/A	N/A
X_2	-3375	0.001*	-1500	0.001*
X_3	-1625	0.014*	-0.500	0.049*
X_1X_2	N/A	N/A	N/A	N/A

(*) statistically significant terms with 95% confidence level
(N/A) Terms were not estimated by Minitab

The terms are considered significant with 95% confidence if their p-values are less than 0.05. The regression coefficient with higher number demonstrates greater effect of representative term and vice versa. A negative (-) number demonstrates inverse relation of the response/output variable with the factor/input variable. It is clear from Table 7.6 that the factor, fabric structure (X_2) have significant effect on all the response variables, whereas the effect of factor, yarn linear density (X_1) is not significant on water vapor permeability, air permeability and vertical wicking of the fabric samples investigated. Similarly, the effect of factor, fabric stitch density (X_3) is significant on all response variables. The interaction of factors X_1 and X_2 (X_1X_2) is also significant on thermal conductivity and thermal resistance of the fabrics as demonstrated in Table 7.6. The regression models containing the significant factors are presented in Table 7.7 for every output variable. The effect of factors on each response variable is separately discussed in the following sections.

Table 7.7. Regression models for different fabric characteristics

Fabric Characteristics	Regression Models	R^2 (%)
Thermal conductivity (W/mK)	$0.09418 - 0.000215\ X_1 - 0.01952\ X_2 - 0.000106\ X_3 + 0.000076\ X_1 \times X_2$	99.93
Thermal resistance (m^2K/W)	$-0.06719 + 0.000503\ X_1 + 0.03820\ X_2 + 0.000112\ X_3 - 0.000200\ X_1 \times X_2$	99.92
Relative water vapour permeability (%)	$78.25 - 5.500\ X_2 - 0.1875\ X_3$	96.30
Air permeability (mm/s)	$215.87 - 6.750\ X_2 - 0.406\ X_3$	93.64
Vertical wicking (cm)	$27.25 - 3.000\ X_2 - 0.1250\ X_3$	93.02

7.5.1. Thermal conductivity

Thermal conductivity is the transmittance of heat across a given area at a defined temperature rise per unit length. The effect of all three factors (X_1, X_2 and X_3) on thermal conductivity is found to be significant, because their p-value is lower than 0.05 as presented in Table 7.6.

Thermal conductivity results in Table 7.5 showed all the socks knitted with single jersey structure have substantially greater thermal conductivity values than the socks knitted with rib structure, which may be attributed to the fact that the air percentage in the structure rises with higher thickness of the fabric. As rib structure is thicker than single jersey structure, therefore allowing more air to be trapped inside the structure, hence presenting less thermal conductivity values than single jersey structure. It is distinguished fact that the thermal conductivity of structure is mainly dependent on fibre type and air entrapped in the structure, as air is the least thermal conductive medium in comparison to all fibers (λ_{air} = 0.025 W/mK).

The other two factors, i.e. yarn linear density (X_1) and stitch density (X_3) have inverse relation with thermal conductivity of the fabric. Lower yarn linear density (i.e. 150 dtex) and lower stitch density (i.e. 56 stitch/cm^2) resulted in higher thermal conductivity of the knitted fabrics. This could also be explained in a way that lower yarn linear density and lower stitch density resulted in less thickness of the fabric, therefore allowing less air to be trapped inside the fabric structure hence resulting in higher thermal conductivity of the fabrics.

Surface plot of thermal conductivity versus yarn linear density and fabric structure has been presented in Figure 7.5 (a). In the surface plots, single jersey and rib structures has been replaced with numeric numbers 1 and 2 respectively. It can be noticed in Figure 7.5 (a) that fabric thermal conductivity is maximum when yarn linear density is minimum and single jersey structure showed higher thermal conductivity than rib structure due to the reasons mentioned earlier. Similarly surface plot of thermal conductivity versus yarn linear density and stitch density is presented in Figure 7.5 (b) which demonstrates that lower stitch density of the fabrics resulted in higher thermal conductivity due to less air trapped inside the fabric structure and vice versa. Regression model for thermal conductivity is presented in Table 7.7. The coefficient of determination of the regression model for thermal conductivity is 99.93%.

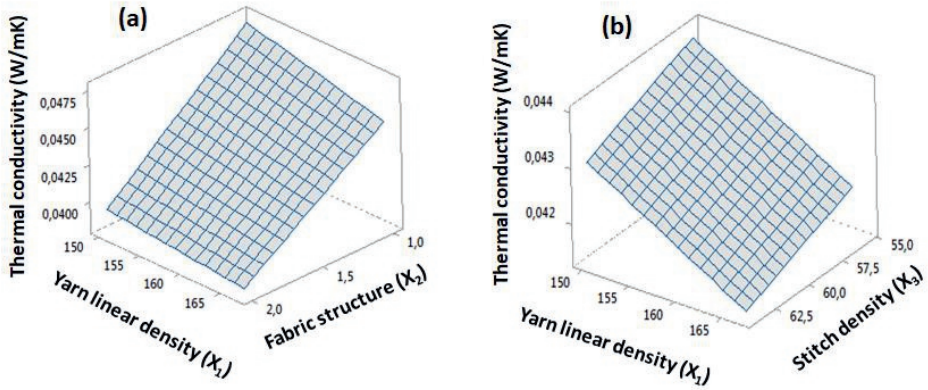

Figure 7.5. (a) Surface plot of thermal conductivity versus yarn linear density and fabric structure (b) Surface plot of thermal conductivity versus yarn linear density and stitch density

7.5.2. Thermal resistance

Thermal resistance determines the ability of a fabric to resist the heat flow and is measured by the ratio of fabric thickness to fabric thermal conductivity. The effect of all three factors (X_1, X_2 and X_3) on thermal resistance is found to be significant because their p-value is lower than 0.05 as shown in Table 7.6. Socks knitted by rib structure were found to be more thermal resistant than single jersey structure as indicated by results presented in Table 7.5. This may be due to more compact and dense structure of rib fabrics in comparison to single jersey fabrics whose structure is less compact and more open.

The single jersey structure is less thermal resistant than rib structure, which may be due to the reason that the density of the constituent yarns in single jersey structure is less hence, the structure is more open, and perhaps trapping lesser percentage of air than rib structure. Whereas rib structure appeared to be more thermal resistant maybe due to greater packing arrangement of yarns as packing density is recognized to have significant impact on thermal resistance. Therefore, for getting higher thermal resistance of socks, a densely knitted structure will be preferred. These results are in good relation with existing findings from other researchers [8, 9, 17] in which most of them have related thermal resistance to fabric compactness. The other two factors, i.e. yarn linear density (X_1) and stitch density (X_3) also have direct relation with thermal resistance of the

fabric. Higher yarn linear density (i.e. 167 dtex) and higher stitch density (i.e. 64 stitch/cm^2) resulted in higher packing density of the fabric hence increasing the thermal resistance of the structures.

Surface plot of thermal resistance versus yarn linear density and fabric structure has been presented in Figure 7.6 (a) and it was noticed that fabric thermal resistance became higher once yarn linear density increased. The rib structure showed higher thermal resistance than single jersey structure due to higher packing density of fibers, which ultimately increased the thickness of the rib structure, hence presenting higher thermal resistance than single jersey structure. Similarly, surface plot of yarn linear density and stitch density versus thermal resistance is shown in Figure 7.6 (b) which demonstrates that higher stitch density resulted in higher compactness of the fabric, which ultimately increased thermal resistance due to more air trapped inside the fabric structure. Regression model for thermal resistance is shown in Table 7.7. The coefficient of determination of the regression model for thermal resistance is 99.92%.

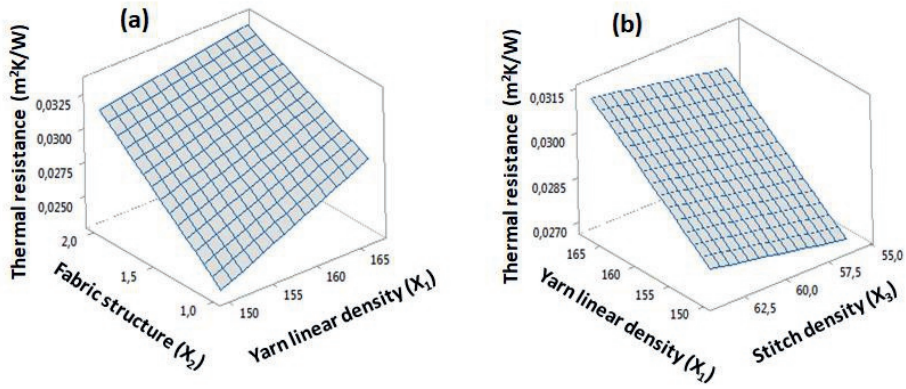

Figure 7.6. (a) Surface plot of thermal resistance versus yarn linear density and fabric structure (b) Surface plot of thermal resistance versus yarn linear density and stitch density

7.5.3. Relative water vapour permeability

The capability of a fabric to transfer water vapour through the fabric is known as water vapour permeability [13]. Socks offering high water vapour permeability are considered to be more

comfortable. From Table 7.5, it can be seen that socks knitted with single jersey structure presented higher water vapour permeability values than socks knitted with rib structure. The considerably dense and thick construction of the socks with rib structure might have inhibited the vapour diffusion through the structure. As far as fabric structure in relation to vapour diffusion through the fabrics is concerned, it is seen that socks knitted with rib structure presented lower water vapour permeability values than socks knitted with single jersey structure. This is due to the fact that considerably thick and dense constructions of the socks knitted with rib structure seemed to prevent the water vapour transfer more than single jersey structure. Similar trends were seen by other researchers [12, 14]. This trend perceived may be described by the socks thickness and the density of constituent fibres in the sock structure.

Table 7.6 signifies that, the effect of fabric structure (X_2) and stitch density (X_3) on vapour permeability is statistically significant because their p-value is less than 0.05 however, the effect of yarn linear density on vapour permeability is not significant. Stitch density also had inverse relation with water vapour permeability. Higher stitch density of the fabrics resulted in lower water vapour permeability as shown by the surface plot of water vapour permeability versus stitch density and fabric structure in Figure 7.7. This may be attributed to the reason that due to higher stitch density, fabric structures became bulky and it is known fact that vapor diffusion is considered lower in bulky structures, and higher for fabrics with open structures [15]. Regression model for relative water vapour permeability is presented in Table 7.7. The coefficient of determination of the regression model for relative water vapour permeability is 96.30%.

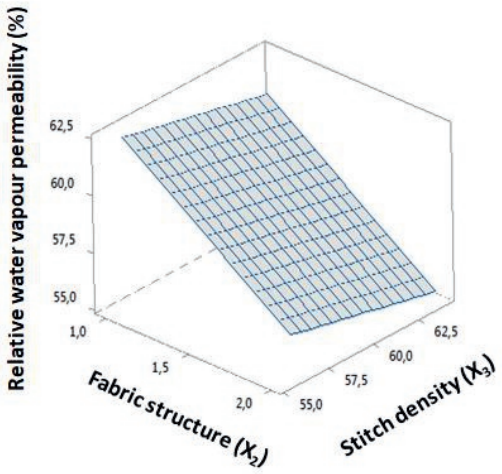

Figure 7.7. Surface plot of relative water vapour permeability versus stitch density and fabric structure

7.5.4. Air permeability

Air permeability is the air flow passing through a fabric under a given air pressure. As shown in Table 7.6, the effect of factors X_2 and X_3 on air permeability of the knitted structures is significant however, the effect of factor X_1 is not significant. The air permeability of rib structures was considerably lower to that of single-jersey structures. It might be due to higher packing density and greater fabric thickness of rib structures in comparison to single-jersey structures. It was also noticed that with an escalation in areal density (weight) of knitted structures, air permeability of structures reduced quite significantly; therefore, an inverse relation was observed between areal density and air permeability of knitted structures. However, fabric structure was found to be more significant than yarn linear density in terms of air permeability of the knits investigated. Similar trends were also observed by other researchers [11-13]. Stitch density was found to have inverse relation with the air permeability of the structures investigated. Higher the stitch density, lower will be the air permeability of the structures. Surface plot of air permeability versus stitch density and fabric structure in Figure 7.8 demonstrates that single jersey structure and lower stitch density resulted in higher air permeability of the structures irrespective of the yarn linear density.

Regression model for air permeability is shown in Table 7.7. The coefficient of determination of the regression model for air permeability is 93.64%.

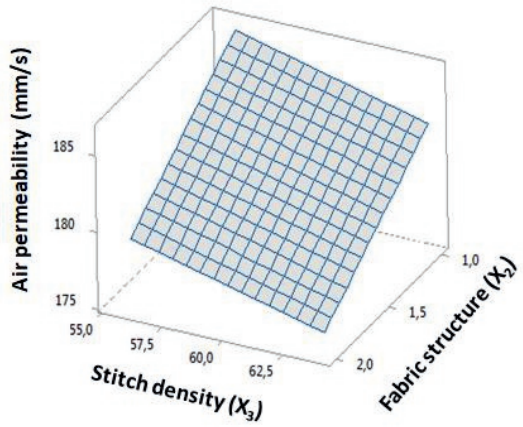

Figure 7.8. Surface plot of air permeability versus stitch density and fabric structure

7.5.5. Vertical wicking

Wicking is the ability of fibrous structures to transport liquid moisture. AATCC 197:2011 standard method was used to test the vertical wicking behavior of socks. It can be observed from results in Table 7.5 that the vertical wicking length of fabrics is highest for single jersey structures and lowest for fabrics with rib structures. This may be due to the reason that fabrics knitted with rib structure were less permeable to liquid moisture in comparison to fabrics knitted with single jersey structure due to smaller pore sizes found in rib structure. Similar trend was also seen in the research carried out by Kumar and Das on vertical wicking behavior of knitted fabrics [18]. For vertical wicking of fabrics, fabric structure (X_2) and stitch density (X_3) were found to be significant as shown in Table 7.6, however yarn linear density (X_1) was not statistically significant. Surface plot of vertical wicking versus fabric stitch density and fabric structure has been plotted in Figure 7.9 where it can be seen that higher stitch density resulted in lower vertical wicking of fabrics. This may be due to the reason that bulkier fabrics with higher packing density and areal density are produced with higher stitch density due to which fabric became less porous and hence offer smaller capillaries to rise the liquid in vertical wicking test. Regression model for vertical wicking of fabrics is presented

in Table 7.7. The coefficient of determination of the regression model for vertical wicking is 93.02%.

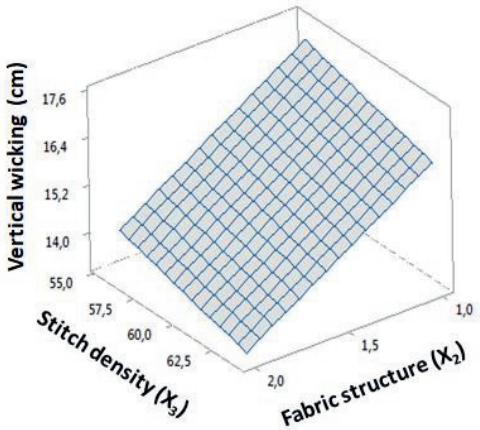

Figure 7.9. Surface plot of vertical wicking versus stitch density and fabric structure

7.6. Conclusion

In this study socks from biobased polymer were produced with different yarn linear densities, fabric structures and stitch densities. Yarn linear density (X_1), fabric structure (X_2) and stitch density (X_3) were taken as factors/input variables and their effect on different response variables such as thermal resistance, relative water vapour permeability, thermal conductivity, vertical wicking and air permeability of fabrics were investigated by using Minitab 18® statistical software. From the findings of this research, the following conclusions can be made.

- Socks knitted with single jersey structure have substantially greater thermal conductivity values than the socks knitted with rib structure.
- Single jersey structure found to be less thermal resistant than rib structure which may be due to the reason that the density of the constituent yarns in single jersey structure is less hence the structure is more open, and perhaps trapping lesser percentage of air than rib structure.

- Rib structure appeared to be more thermal resistant maybe due to greater packing arrangement of yarns as packing density is known to have significant impact on thermal resistance.
- As far as fabric structure in relation to vapour diffusion through the fabrics is concerned, it is seen that socks knitted with rib structure presented lower water vapour permeability values than socks knitted with single jersey structure.
- The air permeability of rib structures was considerably lesser to that of single-jersey structures. Higher stitch density resulted in lower air permeability of the fabrics.
- It was observed that the vertical wicking length of fabrics is highest for single jersey structures and lowest for rib structures due to smaller pore sizes found in rib structure.
- Statistical models were developed for thermal conductivity, thermal resistance, relative water vapour permeability, air permeability and vertical wicking of socks knitted from PLA draw textured yarns.
- The coefficients of determinations (R^2 values) presented good estimation capability of the established regression models. The outcomes of this research may be useful in determining suitable manufacturing requirements of PLA based socks to accomplish precise thermo-physiological properties.

7.7. References

1. Guruprasad, R.; Arputharaj, A.; Saxena, S. Development of cotton- rich / polylactic acid fiber blend knitted fabrics for sports textiles. *J Ind Text* **2015**, *45*, 405–415, doi:10.1177/1528083714555779.
2. Drumright, R.E.; Gruber, P.R.; Henton, D.E. Polylactic acid technology. *Adv Mater* **2000**, *12*, 1841–1846, doi:10.1002/1521-4095(200012).
3. Avinc, O.; Khoddami, A. Overview of poly (lactic acid) (PLA) fiber Part I : production , properties , performance , environmental impact and end-use applications of poly (lactic acid) fibres. *Fibre Chem* **2009**, *41*, 16–25.
4. Hussain, T.; Tausif, M.; Ashraf, M. A review of progress in the dyeing of eco-friendly aliphatic polyester- based polylactic acid fabrics. *J Clean Prod* **2015**, *108*, 476–483, doi:10.1016/j.jclepro.2015.05.126.
5. Abdrabbo, A.; Fotheringham, A.F. Treatment of polylactic acid fibre using low temperature

plasma and its effects on vertical wicking and surface characteristics. *J Text Inst* **2013**, *104*, 28–34, doi:10.1080/00405000.2012.693699.

6. Baig, G.A.; Carr, C.M. Kawabata evaluation of PLA-knitted fabric washed with various laundering formulations. *J Text Inst* **2015**, *106*, 111–118, doi:10.1080/00405000.2014.960249.
7. Bax, B. Impact and tensile properties of PLA / Cordenka and PLA / flax composites. *Compos Sci Technol* **2008**, *68*, 1601–1607, doi:10.1016/j.compscitech.2008.01.004.
8. Gun, A.D.; Akturk, H.N.; Macit, A.S.; Alan, G. Dimensional and physical properties of socks made from reclaimed fibre. *J Text Inst* **2014**, *105*, 1108–1117, doi:10.1080/00405000.2013.876152.
9. Van Amber, R.R.; Wilson, C.A.; Laing, R.M.; Lowe, B.J.; Niven, B.E. Thermal and moisture transfer properties of sock fabrics differing in fiber type, yarn, and fabric structure. *Text Res J* **2014**, *85*, 1269–1280, doi:10.1177/0040517514561926.
10. Cimilli, S.; Nergis, B.U.; Candan, C.; Ozdemir, M. A comparative study of some comfort-related properties of socks of different fiber types. *Text Res J* **2010**, *80*, 948–957, doi:10.1177/0040517509349782.
11. Oglakcioglu and Marmarali Thermal comfort properties of some knitted structures. *Fibers Text East Eur* **2007**, *15*, 94–99.
12. Demiryürek, O.; Uysaltürk, D. Thermal comfort properties of Viloft/cotton and Viloft/polyester blended knitted fabrics. *Text Res J* **2013**, *83*, 1740–1753, doi:10.1177/0040517513478458.
13. Prahsarn, C.; Barker, R.L.; Gupta, B.S. Moisture Vapor Transport Behavior of Polyester Knit Fabrics. *Text Res J* **2005**, *75*, 346–351, doi:10.1177/0040517505053811.
14. Abramavi, J. Investigation of the air permeability of socks knitted from yarns with peculiar properties. *Fibres Text East Eur* **2010**, *18*, 84–88.
15. Psikuta, A.; Rechsteiner, I.; Rossi, R.M.; Sta, R.; Bru, P.A. Transplanar and in-plane wicking effects in sock materials under pressure. *Text Res J* **2011**, *81*, 1549–1558, doi:10.1177/0040517511413317.
16. Purvis, A.J.; Tunstall, H. Effects of sock type on foot skin temperature and thermal demand during exercise. *Ergonomics* **2004**, *47*, 1657–1668, doi:10.1080/00140130412331290880.
17. Cimilli, S. ; Nergis, B. ; Candan, C. A comparative study of some comfort-related properties

of socks of different fiber types. *Text Res J* **2010**, *80*, 948–957, doi:10.1177/0040517509349782.

18. Kumar, B.; Das, A. Vertical wicking behavior of knitted fabrics. *Fibers Polym* **2014**, *15*, 625–631, doi:10.1007/s12221-014-0625-x

CHAPTER 8

General discussion and opportunities for industrial scale up

Halogen containing flame-retardants extinguish fire by flame poisoning mechanism, which definitely has some environmental consequences [1]. Halogen free flame-retardants on the other hand interrupt the burning cycle either by dilution mechanism or by removing the fuel supply to the flame and gradual reduction of the heat flow, which is required to keep the flame burning [2]. The commercially available flame-retardants are mostly non-biodegradable compounds; such as halogenated and organo-nitrogen based compounds therefore, their environmental impact and issues related to global warming is a major concern [3]. Traditionally halogenated, mainly brominated flame-retardants and their synergistic systems were in practice before the introduction of intumescent flame-retardants (IFR's) [4]. Although halogenated FR's were highly effective and cost competitive but proven not to be human and environment friendly [5]. In conventional IFR's, PER and melamine were traditionally used, together with an acid source however, these additives had some shortcomings towards the flame-retardancy of thermoplastics, such as higher water absorbency, lower thermal stability and difficult thermal processing compared to brominated flame-retardants [6]. For instance, thermal stability of IFR's is a major issue in thermoplastic polymers due to a number of additives involved in its thermal processing [7]. Therefore, in this dissertation not only those biobased carbonization agents in IFR's were tested, which are not sensitive to hydrolysis but also their thermal processing was optimized to get better flame-retardancy of thermoplastic polymer PLA in composites, fiber and fabric form.

8.1. Prospects of biobased flame-retardants for the industrial scale-up

The previous chapters have highlighted the importance of biodegradable and biobased flame-retardants and the approaches used to optimize the formulations to get appropriate FR-properties in the composites, fibers and nonwoven fabrics. There is a growing interest in the scientific community to develop new biobased flame-retardants due to a variety of biomolecules and green processes available so that new fire-retardant solutions can be proposed [8]. However, not all the solution strategies proposed at the lab scale, by different researchers might be scaled up to

industrial level. It is hard to forecast the success percentage of different solution strategies due to various factors however, to monitor the industrial scale up the three most important factors could be considered: health and environmental impact, fire performance and economic efficiency, which are discussed below.

8.1.1. Health and environmental impact

In last couple of decades, the most widely used flame-retardants such as brominated FR's have been ruled out due to environmental and health concerns. Most of them were halogenated flame-retardants, which have proven to be carcinogenic, neurotoxic and endocrine disruptors [9]. Therefore, for the development of new flame-retardants these issues should be addressed and those approaches should be adopted which do not create health and environmental issues. This is the prime responsibility of European Chemical Agency (ECHA) and REACH regulation to make sure no hazardous chemicals are used in industrial applications and consequently human health and environmental regulations are protected [10].

8.1.2. Fire performance

Fire performance is another criterion to look for industrial scale up of biobased flame-retardants. The conditions of fire regulations must be fulfilled by new biobased flame-retardants for the applications they are developed for. Generally, three different types of flammability tests are carried out to characterize the fire performance of flame-retardants, such as limiting oxygen index (LOI), UL-94 vertical burning test and cone calorimetry [11]. The parameters like, burning rate, time to ignition, heat release rate, char yield, residual mass%, self-extinguishing, smoke emission and effective heat of combustion are extracted from these tests.

8.1.3. Economic efficiency

The progress in the field of biobased flame-retardants is dependent on the economic efficiency of the developed biobased compounds. The cost of the raw material and the cost of the processes involved would be crucial as higher cost of the final product could hamper the growth of this

sector. The most favorable raw materials could be the one, which are obtained from well-established sectors such as the biomolecules obtained from the wood industry in the form of lignin, cellulose, ligno-sulfonate, vanillin and carbohydrates that are obtained from renewable resources such as starch and cellulose, as these biomolecules has great potential towards flame retardancy [12]. Lignin can also be obtained as by-product of other plants. The worldwide production capacity of lignin is approximately 50 million tons [13]. Lignin as biobased carbonization agent is not only effective but also cheaper than other petroleum based carbonization agents such as PER. Starch is another biomolecule, which is not very expensive. However, chitosan, which is a promising biobased molecule, equally effective in flame-retardant applications, has much higher production cost.

8.2. Future work and opportunities for industrial scale up

Few years ago, probably no one could have imagined that bio-macromolecules such as carbohydrates (cellulose, starch, chitosan, alginates etc.), phenolic compounds (lignin, tannins) and others can be used in flame-retardant applications. The results accomplished in this research work and the related studies has shown that it is possible, at least at the lab and pilot scale, to consider the chemical features of these biomass compounds for the development of biodegradable, non-toxic, environment friendly and at the same time effective flame-retardants for different technical applications. Some of these bio-macromolecules can be obtained as a waste material or a by-product from wood industry or from agro or food industry therefore, can present another added value to these industries. Hence, their repossessions and succeeding applications as flame-retardants may fulfill the current requirements of valorization of wood, food and agro-industries thus, avoiding their landfill detention. Due to the flame-retardant properties of such bio-macromolecules, their potentiality as an alternative to petroleum-based flame-retardants in technical applications is very high, although the approaches discussed in this research work still needs to be optimized for industrial scale-up. The industrial scale-up of such bio-macromolecules is still under evaluation due to certain limitations, for example, the development of biobased FR additives at such a large scale is still not practically feasible, and their thermal processing at industrial set-up has not been tested yet. Although their feasibility and thermal processing at pilot scale is well structured and documented in this thesis, which gave excellent results as discussed in previous chapters. The other factor that limits their industrial scale-up is the cost of these materials.

Undeniably, some of these bio-macromolecules are very expensive, for example, the cost of chitosan (deacetylation degree > 95%) is 190 € per kg, although their cost reduction might be foreseen in next few years due to higher production capacity at industrial level [14]. In addition to that, the possibility of exploiting the industrial apparatus for different technical applications used for conventional flame-retardants still needs to be tested and validated for such bio-macromolecules as flame-retardants.

Moreover, in textiles, the washing fastness or the laundering durability of bio-macromolecules based flame-retardants needs significant attention since; they are not very resistant until now [13]. The reason is such kind of additives or coatings come off after washing and cannot meet specific washing standards even when treated at very low temperature, i.e. 40°C [14]. Therefore, durability of biobased FR treated fabrics is certainly a big limitation towards their industrial scale up since washing durability of flame-retardants is obligatory for most of the textile applications. Hence, it is necessary to find promising solutions to this limitation without compromising the green features of biobased flame-retardants. One potential solution could be to apply the conventional textile finishing treatments to impart washing durability but that might affect the green features of biobased flame-retardants. To avoid this issue, biologically derived chemical treatments could be one option but to exploit their potential as a substitute to conventional finishing treatment needs an extensive and comprehensive research.

8.3. References

1. Menard, R.; Negrell, C.; Fache, M.; Ferry, L.; Sonnier, R.; David, G. From a bio-based phosphorus-containing epoxy monomer to fully bio-based flame-retardant thermosets. *RSC Adv* **2015**, *5*, 70856–70867, doi:10.1039/C5RA12859E.
2. Menard, R.; Negrell, C.; Ferry, L.; Sonnier, R.; David, G. Synthesis of biobased phosphorus-containing flame retardants for epoxy thermosets comparison of additive and reactive approaches. *Polym Degrad Stab* **2015**, *120*, 300–312, doi:10.1016/j.polymdegradstab.2015.07.015.
3. Zhang, J.; Ji, Q.; Shen, X.; Xia, Y.; Tan, L.; Kong, Q. Pyrolysis products and thermal degradation mechanism of intrinsically flame-retardant calcium alginate fibre. *Polym Degrad Stab* **2011**, *96*, 936–942, doi:10.1016/j.polymdegradstab.2011.01.029.
4. Wan, J.; Gan, B.; Li, C. A novel biobased epoxy resin with high mechanical stiffness and

low flammability: synthesis, characterization and properties. *J Mater Chem A* **2015**, doi:10.1039/C5TA02939B.

5. Moussout, H.; Ahla, H.; Aazza, M.; Bourakhouadar, M. Kinetics and mechanism of the thermal degradation of biopolymers chitin and chitosan using thermogravimetric analysis. *Polym Degrad Stab* **2016**, *130*, 1–9, doi:10.1016/j.polymdegradstab.2016.05.016.
6. González, A.; Dasari, A.; Herrero, B.; Plancher, E.; Santarén, J.; Esteban, A.; Lim, S. Fire retardancy behavior of PLA based nanocomposites. *Polym Degrad Stab* **2012**, *97*, 248–256, doi:10.1016/j.polymdegradstab.2011.12.021.
7. Lyon, R.E.; Walters, R.N. Pyrolysis combustion flow calorimetry. *J Anal Appl Pyrolysis* **2004**, *71*, 27–46, doi:10.1016/S0165-2370(03)00096-2.
8. Liao, F.; Ju, Y.; Dai, X.; Cao, Y.; Li, J.; Wang, X. A novel efficient polymeric flame retardant for poly (lactic acid) (PLA): synthesis and its effects on flame retardancy and crystallization of PLA. *Polym Degrad Stab* **2015**, doi:10.1016/j.polymdegradstab.2015.07.012.
9. Fontaine, G.; Bourbigot, S. Intumescent Polylactide: A Nonflammable Material. *J Appl Polym Sci* **2009**, *113*, 3860–3865, doi:10.1002/app.
10. Didane, N.; Giraud, S.; Devaux, E.; Lemort, G. A comparative study of POSS as synergists with zinc phosphinates for PET fire retardancy. *Polym Degrad Stab* **2012**, *97*, 383–391, doi:10.1016/j.polymdegradstab.2011.12.004.
11. Pan, Y.; Zhan, J.; Pan, H.; Wang, W.; Tang, G.; Song, L.; Hu, Y. Effect of Fully Biobased Coatings Constructed via Layer-by-Layer Assembly of Chitosan and Lignosulfonate on the Thermal, Flame Retardant, and Mechanical Properties of Flexible Polyurethane Foam. *Sustain Chem Eng* **2015**, 4–11, doi:10.1021/acssuschemeng.5b01423.
12. Moussout, H.; Ahla, H.; Aazza, M.; Bourakhouadar, M. Kinetics and mechanism of the thermal degradation of biopolymers chitin and chitosan using thermogravimetric analysis. *Polym Degrad Stab* **2016**, *130*, 1–9, doi:10.1016/j.polymdegradstab.2016.05.016.
13. González, A.; Dasari, A.; Herrero, B.; Plancher, E.; Santarén, J.; Esteban, A.; Lim, S. Fire retardancy behavior of PLA based nanocomposites. *Polym Degrad Stab* **2012**, *97*, 248–256, doi:10.1016/j.polymdegradstab.2011.12.021.
14. Lyon, R.E.; Walters, R.N. Pyrolysis combustion flow calorimetry. *J Anal Appl Pyrolysis* **2004**, *71*, 27–46, doi:10.1016/S0165-2370(03)00096-2.

CHAPTER 9

Valorization addendum

"Technology transfer" or "knowledge valorization" are the terms used for creating social and economic impact through transfer of scientific knowledge from laboratory to the pilot and industrial scale. In this Chapter, we will elaborate, what kind of benefits this dissertation will deliver to the society, and in which way, the results and important findings of this dissertation could be implemented in real life applications. The research in this dissertation is based on the exploitation of biodegradable and biobased intumescent flame-retardants for composites and textile applications. The conventional flame-retardants that seek to protect human lives sometimes bring more hazard than the benefit they possess therefore, a right balance needs to find between the benefits one can get and the risk potential one might face when selecting a flame-retardant. For example in conventional flame-retardants there is no protection mechanism to control smoke emission that goes to the environment and statistics show that, in case of a fire accident, the major cause of death is actually the smoke inhalation, as around 37-42% of fatalities each year in Europe are attributed to smoke inhalation alone [1].

In our dissertation, we have proposed a technique through which smoke emission to the environment in case of a fire accident can be controlled by forming a char layer on the burning material therefore; fatalities due to smoke inhalation can be significantly reduced by this technique, which is a small contribution within our capacity to serve the society. Moreover, the other benefit with flame-retardants used in this dissertation is, if volatile compounds emitted from these flame-retardants anyhow manage to escape to the environment, they will not be toxic to the environment since they are based on halogen free flame-retardants and the degradability of PLA will help faster biodegradation of the compounds. Some of the findings reported in the dissertation presents very promising prospective for the industrial scale up and valorization, especially, Chapter 5 and 6 represents the novel approaches used to develop flame-retardant fibers and fabrics from intumescent technique. Particularly, in Chapter 5, flame-retardant carpet backing with novel bicomponent fibers from single polymer were produced with intumescent technique. In the following paragraphs, we will elaborate the potential valorization options for the new techniques we developed in this dissertation.

Now we will describe in what way the interesting results of this dissertation could be implemented to the industrial FR applications. One of the targeted application could be FR floor coverings, as Europe is the world's second largest market for floor coverings. Belgium, the Netherlands, and the United Kingdom are the EU's leading manufacturers, and EU manufacturing fulfils ~65% of the EU's demand for floor coverings [2]. Since, EU floor covering companies are shifting their focus towards the sustainable, renewable and biodegradable flame-retardants; therefore, findings of this dissertation would be very interesting for such companies. We are delighted that Dutch and Belgian textile companies such as Low & Bonar B.V. (Arnhem, the Netherlands) and TWE Meulebeke BVBA (Meulebeke, Belgium) are already interested to scale-up this technology for their textile products, as their pilot scale infrastructure was used during the sampling of this dissertation. Moreover, both these companies are producing nonwoven carpet backings for their national and international customers therefore, FR carpet backing made from biobased and renewable resources will be a value addition for these companies. The results obtained in this dissertation may open doors also to the other textile applications such as FR home textiles, i.e. curtains, bedding, mattresses, seat covers in automobiles etc. For such textile applications, the minimum requirement for a textile fiber is to carry LOI value up to 28%, whereas in our dissertation, we have achieved LOI value up to 32% as tested by ISO 4589 standard testing method, therefore the FR fibers we developed in this dissertation may find their application in home textiles also. A Dutch textile company HAVEP B.V. (Goirle, the Netherlands) is producing FR work wear and FR fleece vest for the firefighter clothing and the results obtained in this dissertation could be quite interesting for them as well.

Other than textiles, these flame-retardants can also be used in electrical and electronic (E&E) composite applications such as the composites made for computer and LED housing, laptop and mobile phone casings and the wire connectors in automotive. For example the company, "DSM N.V. Engineering Plastics" (Geleen, the Netherlands), found this idea very interesting for their wire connectors in automotive application. For this application, injection molded composites are produced which should possess at least V-1 rating in UL-94 vertical burning test, whereas in our dissertation we have developed composites that can achieve V-0 rating (even better) for such application as tested by ISO 9773 standard testing method. This idea was developed and tested during sample testing of some of the composite samples of this dissertation in fire testing lab of DSM N.V. Engineering Plastics in Geleen.

So far to the best of our knowledge, IFR's have not been tested in bicomponent fibers therefore, in this dissertation we described a novel technique to develop bicomponent intumescent flame-retardant fibers from single polymer composites containing reinforcement and a matrix from the same polymer but with two different grades to get uniform interface and better interfacial bonding between the components. These bicomponent flame-retardant fibers were then melted where low melting sheath material sticks with the high melting core component and form a fibrous nonwoven web, which then thermally bonded together to form a carpet backing. The ignitability test showed none of the fabric sample, produced from bicomponent fibers, was ignited after 15 (s) of flame exposure, and therefore, achieved classification of E and Efl as per the standards set for EN ISO 11925-2 method. This classification certifies that the product can be used commercially for flame-retardant floor coverings.

Finally, these biodegradable flame-retardants are very cost effective and much cheaper compared to already used intumescent flame-retardants. For example, the carbon source used in conventional intumescent flame-retardants is pentaerythritol 99% (PER 99%), which is quite expensive, as its exact price is 52.20 € per 50 grams (supplier, Sigma-Aldrich Corporation, St. Louis-Missouri, USA). Whereas the price of kraft lignin (KL) used in intumescent formulations in this dissertation is 3.00 € per 50 grams (60 € per kg) (supplier, UPM Bio-chemicals OYJ Helsinki, Finland). The cost comparison of all components that are generally used in conventional IFR's and IFR's used in this dissertation is presented in Table 9.1.

Table 9.1. Cost comparison of conventional IFR and of IFR used in the dissertation [3, 4]

Materials	**Conventional IFR's**	**Price (€) per kg**	**IFR's used in this thesis**	**Price (€) per kg**
Polymer	PP	1.20	PLA	2.60
Carbon source	PER 99%	1040.00	KL	60.00
Acid source	$Mg(OH)_2$	2.50	APP-II	2.20
Price of all components		1043.70		64.80

PLA= Polylactic acid 99% L-content, PP= Polypropylene melt grade, PER= Pentaerythritol 99%, KL= Kraft lignin, $Mg(OH)_2$= Magnesium hydroxide, APP-II= Ammonium polyphosphate form II

Moreover, lignin is aromatic polymer and after cellulose is the most abundant natural polymer obtained from renewable and biobased resources whereas PER is a petrochemical obtained from finite resources. Not only the cost, but also performance wise the efficiency of KL was even better than PER in some of the properties. For example, in Chapter 3, flammability of IFR composites containing equal wt% of KL and PER were compared. Total smoke production (TSP) value of KL composites was almost half (103 m^2/m^2) to PER composites (209 m^2/m^2) containing equal wt% that shows even better efficiency of the composites containing KL than composites containing PER. These results strengthens our claim about reduction in smoke emission to the environment of the flame-retardants used in our dissertation.

Regardless of some of the questions that still needs to be answered, for example, the washing fastness and washing durability of these intumescent flame-retardants still has to be investigated in detail. However, overall this dissertation resulted in the development of a technology, which is very useful for industrial flame-retardant applications, and has the potential to substitute conventional flame-retardants.

References

1. Zhou, R.; Ming, Z.; He, J.; Ding, Y.; Jiang, J. Effect of Magnesium Hydroxide and Aluminum Hydroxide on the Thermal Stability, Latent Heat and Flammability Properties of Paraffin/ HDPE Phase. *Polymers (Basel)* **2020**, *12*, 1–14.
2. Wilts, H. Circular Economy Potential in the Carpet Industry. J Glob Econ 2017, 5, 271–278.
3. https://www.sigmaaldrich.com/catalog/product/aldrich/236241?lang=en&region=NL
4. https://shop.upmbiochemicals.com/categories/13ee4132-9b84-4e7c-8547-53c20a3ea731

Acknowledgements

In these final pages, I would like to express my gratitude to all those people who directly or indirectly contributed to this thesis, which is the result of hard work of the past four years at Maastricht University.

First, I would like to thank Professor Gunnar Seide, for giving me an opportunity to work in his group, for the guidance and for his support throughout my PhD. I really enjoyed working under his supervision and in the "Polymer Engineering" group. I learnt a lot from his cool and calm personality, and about how to handle and overcome difficult situations in life.

During the past years, I have had the opportunity to work and collaborate with many people from different industrial organizations. I would like to thank everyone involved in the project BioTex Fieldlab consortium for the great atmosphere and feedback. I feel fortunate to be a part of such consortium and have learnt a lot from different point of views and backgrounds. Specially, I would like to thank Dr. Fabrizio Micciche and Elvira Schot from SABIC Innovative Plastics B.V. (Bergen op Zoom) for welcoming me in their fire-testing lab. Thank you for your availability and for allowing me to work in your lab as without your support my dissertation would have not been complete. Similarly, I would also like to thank Dr. Paul Steeman from DSM Engineering Plastics (Geleen) for his useful insights about the topic, the fruitful discussions we had during our meetings about my PhD and for providing help for the testing of my samples in their fire-testing lab. Rick Leuven, William Warnier and Jos Linsen from Chemelot Innovation and Learning Labs (CHILL), thank you very much for your support during my experimental work at CHILL. Special thanks to all those technicians and supporting staffs who helped me during my lab work, especially Hay Beckers (Polymer Engineering group) who not only helped me during my trials but also refreshed me with his jokes and lively friendly nature. People from ITA, RWTH Aachen University, especially Dr. Pavan Manvi, David, Gunter and Peter are also acknowledged for their support in the project.

I would also like to thank each student who I had the chance to supervise, especially Alice Buchner, thank you for your hard work in the project. The students of Maastricht Science Programme (MSP) who did not directly contribute to this dissertation but I really enjoyed supervising you also.

I would like to thank my colleagues from Polymer Engineering group and AMIBM for the good time in the lab and outside: Naveen, Stefan, Kylie, Matin, Cristina, Anna, Vahid and many others. Christian van Slagmaat thanks for your help and suggestions for assisting me in drawing the chemical structures in my dissertation. Stefan, many thanks for your help in the lab and in transporting my polymer and yarn bobbins from AMIBM to ITA and vice versa in your car. I really enjoyed the company with Naveen and his help in the early days of the project BioTex Fieldlab therefore, special thanks to you and of course, who can forget the dinners we had together with our friend Zhengwen Li.

Finally, special thanks to my beloved wife, lovely kids and caring parents whom I missed a lot in the last four years. It was not an easy decision to live thousands of miles away from your loved ones but hopefully in near future we will unite once again.

Biography

Muhammad Maqsood was born and raised in a beautiful city, Vehari in Pakistan. In the fall of 2005, he started his bachelor's degree in Textile Engineering from Bahauddin Zakariya University in Pakistan and graduated in summer 2009. After his bachelors, he worked in the textile industry in Pakistan as assistant manager for three years. In the fall of 2012, he started his Masters in Tex tile Engineering from National Textile University in Pakistan and graduated in fall 2014 with distinction (Silver Medal, with CGPA 3.80/4.00). He published three research articles from his Master thesis in peer-reviewed, impact factor journals. His dissertation for Master degree was entitled, "Modeling the stretch and recovery properties of bi-stretch woven fabrics for compression garments". After his Master's, he started teaching Textile Engineering to bachelor students in National Textile University, Pakistan from fall 2014 till spring 2016. In fall 2016, he started his doctoral studies in the "Polymer Engineering" group of Professor Gunnar Seide, at "Aachen Maastricht Institute for Biobased Materials" of Maastricht University in Geleen, the Netherlands. He gained knowledge in the field of biopolymers and Polymer Engineering in general and in biobased flame-retardants in particular during his doctoral studies. He published seven research articles in peer reviewed, impact factor journals from his PhD dissertation.

List of publications

This thesis is based on the following peer reviewed journal publications

[1] **M. Maqsood**, G. Seide, Investigation of the Flammability and Thermal Stability of Halogen-Free Intumescent System in Biopolymer Composites Containing Biobased Carbonization Agent and Mechanism of Their Char Formation, **Polymers** (Basel). 11 (2018) 1–16. doi:10.3390/polym11010048.

[2] **M. Maqsood**, F. Langensiepen, G. Seide, The Efficiency of Biobased Carbonization Agent and Intumescent Flame Retardant on Flame Retardancy of Biopolymer Composites and Investigation of their melt spinnability, **Molecules**. 24 (2019) 1–18.

[3] **M. Maqsood**, F. Langensiepen, G. Seide, Investigation of melt spinnability of plasticized polylactic acid biocomposites-containing intumescent flame retardant, **J Therm Anal Calorim.** (2019) 1–14. doi:10.1007/s10973-019-08405-3.

[4] **M. Maqsood**, G. Seide, Novel Bicomponent Functional Fibers with Sheath/Core Configuration Containing Intumescent Flame-Retardants for Textile Applications, **Materials** (Basel). 12 (2019) 1–19.

[5] **M. Maqsood**, G. Seide, Development of biobased socks from sustainable polymer and statistical modeling of their thermo-physiological properties, **J Clean Prod.** 197 (2018) 170–177. doi:10.1016/j.jclepro.2018.06.191.

[6] **M. Maqsood**, G. Seide, Statistical modeling of thermal properties of biobased compostable gloves developed from sustainable polymer, **Fibers Polym.** 19 (2018) 1094–1101. doi:10.1007/s12221-018-1126-0.

[7] **M. Maqsood,** G. Seide, Improved Thermal Processing of Polylactic Acid/Oxidized Starch Composites and Flame-Retardant Behavior of Intumescent Non-Wovens, **Coatings.** 10 (2020) 1–20

[8] **M. Maqsood,** F. Langensiepen, G. Seide, A review on biobased and halogen free flame-retardants, **(under preparation)**